

Departamento de Biología Moleculares

Facultad de Ciencias

Universidad Autónoma de Madrid



**FABRICATION OF SENSITIVE IMMUNOSENSORS:
THE SELECTION OF ANTIBODY IMMOBILIZATION
STRATEGIES AND CONJUGATION CARRIERS**

TESIS DOCTORAL

Shipeng Gao

Madrid, 2022

Departamento de Biología Moleculares

Facultad de Ciencias

Universidad Autónoma de Madrid



**FABRICATION OF SENSITIVE IMMUNOSENSORS:
THE SELECTION OF ANTIBODY IMMOBILIZATION
STRATEGIES AND CONJUGATION CARRIERS**

Shipeng Gao

Directores

Prof. José Manuel Guisan

Dr. Javier Rocha-Martin

Instituto de Catálisis y Petroleoquímica

Consejo Superior de Investigaciones Científicas (CSIC)



Acknowledgments

I have been told that this part was the only section of this dissertation that can be directly accepted without revision, so true it is! Long after that, I might have forgotten what I have done and have achieved in this dissertation, but all the memory and emotion (happiness, excitement, frustration, curiosity and worry, etc) have already been part of me. The completion of this dissertation is a “teamwork”, everyone I have met so far does do the contribution, I am the one who stands out to take the credit.

The first acknowledge would be my supervisors, Prof. Jose Manuel Guisan and Dr. Javier Rocha-Marin, for their excellent guidance during the exploitation of my “personalized” scientific research. Sincere thanks to their enthusiastic encouragement, effective and timely help when facing difficulties, full freedom when I try to do further exploration. Knowing how to think critically “outside the box” and how to head in the right direction would be the greatest gift I have received from them. The help from my tutor Filip Lim is also appreciated, thanks for his patience and kind guidance.

I also want to thank all the group members I have met since I joined the group, I cannot make it through without the help from you guys, I would send a big thanks to Roberto, Lara, Janaina, Rita, Francesca and Alejandro. Also includes Wilson, Pedro and Frederico. Everyone I have met was so kind and generous, thank you for having you people for the last three years.

I would express my sincere gratitude to Prof. Susana Campuzano Ruiz and Prof. María Pedrero Muñoz from the Complutense University of Madrid, thank you for accepting me and treating me like a member of a big family. I have benefited a lot from your excellent scientific insight and generous support. Special thanks go to Rebeca, Veronica and Maria Gamella, value lessons have been learned from your patient and generous guidance. Help and kindness received from other GEBE members also cannot be ignored, thank you Cristina, Victor, Beatriz, Eloy, Alejandro, Esther and Sara.

I also want to thank Prof. María del Puerto Morales from ICMM-CSIC, thank you for teaching me to do nanoparticles synthesis and characterization, always providing informative and clear instructions. Also, thank all the other members of the MAMBO Group members (Alvaro and Maria).

Also express my gratitude to the new friend I met here, especially for the Catata Sun.

Abstract

Immunosensors are typical biosensors using the antibody as the biorecognition element that is immobilized on a suitable transducer to qualitatively determine the antigen-antibody interaction. An ideal immunosensor with combined advantages including the high sensitivity, easy-to-operate and cost-effective, would have attributed to the rational selection of appreciating bioreceptors carriers and site-oriented antibody immobilization strategy. Achieving the site-directed immobilization only involves the fragment crystallizable (Fc) region would maximize the biofunctionality of tethered antibodies, while it would be a great challenge faced with the heterogeneous distribution of amino residues through the antibody surface. Meanwhile, the challenge still lies with the selection of bioreceptors carriers bearing desirable surface chemistries (antifouling, robustness and stability) for the irreversible conjugation of antibodies.

In this dissertation, the objective is to evaluate the analytical performance of fabricated immunosensors, in which antibody immobilization strategies and bioreceptors carrier types are primary considerations mainly in terms of the acceptable sensitivity, storage stability of fabricated immunosensors toward the low abundance of analytes and avoiding the undesirable interference dealing with clinical diagnosis.

Antibodies conjugated on the glyoxyl-agarose support results in different orientations by simply manipulating the pH of incubation conditions while the inevitable involvement of antigen-binding fragment (Fab) during the antibody/glyoxyl-agarose interaction caused the deterioration of its biofunctionality. Covalently fixing the uniform and site-directed orientation of coupled antibodies following the pre-affinity adsorption demonstrated the obvious advantage of controlling the interaction regions, over 75 % of preserved biofunctionality was observed with tethered antibodies.

Magnetic nanomaterials with adequate dextran coverage have demonstrated the equilibrium between facile magnetic recovery and sufficient colloidal stability, and magnetic nanoparticles bearing the polyaldehyde groups of $139 \mu\text{mol g}^{-1}$ nanoparticles were proven a better nanocarrier than carboxylic groups and chelate groups functionalized nanoparticles. In addition, the multifunctionality of polyaldehyde-dextran@nanoparticles was exploited as the nanoprobe and nanocarriers. Over 4-fold higher sensitivity of immunosensors was enhanced when horseradish peroxidase-streptavidin/antibody dual functionalized nanoparticles work as the nanoprobe, and the reliability of nanoparticles as the nanocarriers to detect biomarker concentration in clinical serums was confirmed by its consistency with golden standard-ELISA (enzyme-linked immunosorbent assay) analysis.

Resumen

Los inmunosensores son biosensores típicos que utilizan el anticuerpo como elemento de biorreconocimiento que se inmoviliza en un transductor adecuado para determinar cualitativamente la interacción antígeno-anticuerpo. Un inmunosensor ideal con ventajas combinadas, incluida la alta sensibilidad, fácil de operar y rentable, se habría atribuido a la selección racional de los portadores de biorreceptores apreciadores y la estrategia de inmovilización de anticuerpos orientada al sitio. Lograr la inmovilización orientada del anticuerpodirigida solo involucrando la región cristalizable (o región Fc) maximizaría la biofuncionalidad de los anticuerpos anclados. No obstante, el reto aún radica en la selección de soportes para los biorreceptores que contengan grupos reactivos en sus superficies deseables (antifouling, robustez y estabilidad) para la conjugación irreversible de anticuerpos.

En esta Tesis Doctoral, el objetivo es evaluar el rendimiento analítico de inmunosensores fabricados, en los que las estrategias de inmovilización de anticuerpos y los tipos de soportes de biorreceptores son los principales aspectos a tener en cuenta, fundamentalmente en lo que respecta a una sensibilidad aceptable, a la estabilidad de almacenamiento de inmunosensores fabricados frente a la baja abundancia de analitos y para evitar interferencias indeseables relacionadas con el diagnóstico clínico.

Los anticuerpos conjugados sobre el soporte de agarosa glioxil dieron como resultado diferentes orientaciones simplemente manipulando el pH de las condiciones de incubación del soporte-anticuerpo, mientras que la inevitable participación del fragmento de unión al antígeno (Fab) durante la interacción anticuerpo/agarosa glioxil provocó el deterioro de su biofuncionalidad. La inmovilización covalente orientada y uniforme de los anticuerpos inmovilizados previamente por afinidad sobre soportes heterofuncionales glioxil-quelato metálicos demostró la ventaja obvia de controlar las regiones de interacción, y además preservóse más del 75% de su biofuncionalidad. Los nanomateriales magnéticos con un recubrimiento adecuado de dextrano mostraron un equilibrio adecuado entre su estabilidad coloidal y la fácil recuperación magnética de los conjugados. Las nanopartículas magnéticas activadas con $139 \mu\text{mol g}^{-1}$ de grupos polialdehído demostraron ser mejores nanoportadores que las nanopartículas funcionalizadas con grupos carboxílicos y grupos quelatos. Además, se aprovechó la multifuncionalidad de las nanopartículas de polialdehído-dextrano como nanoprobetas y nanoportadores. La sensibilidad de los inmunosensores se multiplicó por 4 cuando las nanopartículas funcionalizadas con peroxidasa de rábano picante-estreptavidina/anticuerpo funcionan como las nano-sondas, y la confiabilidad de las nanopartículas como nanoportadores para detectar bajas concentraciones de biomarcadores en sueros clínicos se confirmó por su consistencia con el análisis estándar de oro-ELISA (Enzyme-Linked ImmunoSorbent Assay).

Index

Abstract	I
Resumen	II
Abbreviations	7
1. Introduction	1
1.1 Antibody as the bioreceptors – high affinity and selectivity	2
1.2 Antibody immobilization strategy	3
1.2.1 Reversible adsorption	4
1.2.2 Covalent immobilization of IgGs	5
1.3 Immobilization platforms – the selection of antibody support	7
1.3.1 Agarose-based support	8
1.3.2 Nanoparticles based support	10
1.3.2.1 Magnetic nanoparticles (MNPs)	10
1.3.2.2 Other nanoparticles with excellent characterizations	13
1.3.3 Screen-printed Electrodes	14
1.4 Functionalities of nanomaterials during the fabrication of biosensors	16
2. Objectives	20
3. Materials	21
4. Methods	24
4.1. Antibody immobilization onto the agarose beads–homofunctional and heterofunctional support	24
4.1.1 Preparation of monofunctional glyoxyl-agarose support	24
4.1.2 Immobilization of antibody on the glyoxyl-agarose support	24
4.1.3 Preparation of heterofunctional chelate-epoxy agarose support	25
4.1.4 Immobilization of antibody on the chelate-epoxy agarose support	25
4.1.5 Immunoassay determination of prepared antibody-agarose bioconjugates	26
4.1.6 Protein concentration determination	26
4.1.7 Enzyme activity determination of the immunoconjugates	26
4.1.8 Quantification of the epoxy groups density on the agarose support	27
4.1.9 Sodium dodecyl sulfate-polyacrylamide gel electrophoresis (SDS-PAGE) analysis	27
4.2. Dextran functionalization and further chemistry activation	27
4.2.1 Synthetization of the bare magnetic nanoparticles via coprecipitation	27
4.2.2 Acid treatment to achieve the γ -Fe ₂ O ₃ synthesis	28
4.2.3 Silica coating to functionalize extra SiO ₂ layer on the surface of the nanoparticles	28
4.2.4 Surface functionalization with dextran and following the crosslinking treatment (Dex@MNPs)	28

4.2.5 Evaluation of the colloidal stability and magnetic separability of surface-modified nanoparticles.....	29
4.2.6 Characterization of the Dex@MNPs with sufficient surface coverage.....	30
4.2.7 Preparation of HOOC-Dex@MNPs based on the modification with Dex@MNPs.....	31
4.2.8 Preparation of the HRP-Ab _{HRP} -Alde-Dex@MNPs nanoconjugates.....	31
4.2.9 Calculation of the functionality of Ab _{HRP} -MNPs nanoconjugates with different immobilization strategies.....	32
4.3. Alde-Dex@MNPs with optimal aldehyde density as the nanocarriers–colorimetric determination and electrochemical assays	32
4.3.1 Characterization of the Alde-Dex@MNPs.....	32
4.3.1.1. Periodate oxidation of the dextran layers on the surface of the nanoparticles	32
4.3.1.2. Antibody immobilization on the Alde-Dex@MNPs nanoparticles.....	33
4.3.1.3. Quantification of the preserved functionality of the covalently conjugated Ab _{HRP}	33
4.3.1.4. Optimization of the experimental variables for the fabrication of the immunosensor..	33
4.3.1.5. Analytical characterization of the fabricated immunosensor with the optimal conditions	34
4.3.2 Electrochemical measurements using the developed Alde-Dex@MNPs as the nanocarriers	35
4.3.2.1. Preparation of the HOOC-Dex@MNPs based on the Alde-Dex@MNPs.....	35
4.3.2.2. Immobilization of Ab _{HRP} on the surface activated carboxylated micro/nanocarriers....	35
4.3.2.3. Amperometric measurement of HRP adsorbed micro/nanoconjugates.....	36
4.4. Dual proteins functionalized Alde-Dex@MNPs–carriers of detection probes	37
4.4.1 Surface activation of the working electrodes of SPCEs	37
4.4.2 Preparation of the dual functionalized Alde-Dex@MNPs nanoprobe.....	37
4.4.3 Bioreceptors immobilization on the SPCEs	38
4.4.4 Electrochemical measurements using the developed nanocarriers.....	39
4.4.5 Analytical characterization of the fabricated immunosensor	39
4.5. Using the Alde-Dex@MNPs as the bioreceptor carriers of Ab_{CRP}.....	39
4.5.1 Preparation of the Strep-HRP-Biotin-Ab _{CRP} -CRP-Ab _{CRP} -Alde-Dex@MNPs immunosensor	39
4.5.2 Analysis of the real samples using the human serum.....	40
4.5.3 Enzyme-linked immunosorbent assay (ELISA) determination.....	40
5. Results.....	43
5.1 Heterofunctional agarose support–A better antibody carrier to control the orientation	43
5.1.1 Antibody immobilization rate on the agarose beads	44
5.1.2 The biofunctionality of immobilized antibody on the agarose beads.....	47
5.1.3 The optimization of functional groups density on the chelate-epoxy agarose support	49
5.1.4 Antigen recovery experiments from diluted human serum	52

5.2 Colloidal stability evaluation of functionalized iron oxide nanoparticles–Dextran coating improves the stability in aqueous buffer.....	53
5.2.1 Comparison of four nanoparticles with their colloidal stability and magnetic separability in distilled water	54
5.2.2 The evaluation of colloidal stability of bare MNP and Dextran@MNPs in aqueous buffer.....	57
5.2.3 The optimization of dextran coating parameters to achieve better coating efficiency	59
5.2.4 The dextran functionalization strategy: mechanical stirring or sonication.....	61
5.2.5 Quantification of remaining functionality of immobilized antibody with grafted reactive groups on the Dextran@MNPs surface	63
5.3 Magnetic nanoparticles as the bioreceptors carrier–HRP as the analytes	68
5.3.1 Colorimetric detection of HRP– The controlled oxidation extent with better analytical performance	69
5.3.1.1. Determination of the aldehyde groups density and Ab _{HRP} immobilization rate.....	69
5.3.1.2. The effect of oxidation parameters on the Ab functionality.....	71
5.3.1.3. The optimization of experimental variables to achieve better biosensing efficiency....	73
5.3.1.4. Analytical characterization of the fabricated immunosensors.....	74
5.3.2 Electrochemical detection of HRP with lower LOD – The comparison of magnetic particles size and functional groups	75
5.3.2.1. Optimization of the experimental variables to obtain Alde-Dex@MNPs with the better S/N ratio.....	76
5.3.2.2. Analytical characterization of the fabricated immunosensors using electrochemical technique.....	77
5.4 Multifunctionalities of the nanoparticles	83
5.4.1 Investigation of experimental variables effect on the analytical performance of immunosensors	85
5.4.1.1 Strep-HRP as the detection probes	85
5.4.1.2 HRP/CAb@MNPs as the probes.....	89
5.4.1.3 HRP/Streptavidin@MNPs as the detection probes	94
5.4.2 Characterization of the fabricated immunosensors with each functionalization step	96
5.4.2.1 HRP/CAb@MNPs as the detection probes	96
5.4.2.2 HRP/Streptavidin@MNPs as the detection probes	97
5.4.3 Analytical characterization of the fabricated immunosensors.....	98
5.5 Magnetic nanoparticles as the bioreceptors carrier to detect CRP in real samples	103
5.5.1 Optimization of experimental variables to achieve the immunosensor with the highest sensitivity.....	105
5.5.2 Analytical characterization of the fabricated immunosensors using Alde-Dex@MNPs as the carriers.	109
5.5.3 Determination of the CRP biomarkers in the real samples.....	111
6. Discussion	114

6.1 Antibody immobilization strategies targeting the amine groups (NH₂)	114
6.1.1 Glyoxyl and aldehyde moieties—achieving the multipoint interaction via the regions with most abundant NH ₂	115
6.1.2 Carbodiimide chemistry activated carboxylic groups—typical Ab immobilization strategy for random orientation.....	117
6.1.3. Chelate groups against histidine cluster—less stable interaction.....	118
6.2 The porous structure of supporting materials—a double-edged sword for the immunosensing	118
6.2.1 The inner surface of porous materials promotes higher antibody loading capacity while with heterogeneous distribution.....	118
6.2.2 Nonporous nanoparticles improve the response time of antigens recognition.....	120
6.3 Surface functionalization of iron oxide nanoparticles—grafting the stability and surface chemistry	121
6.3.1 Providing the colloidal stability upon sufficient coverage	121
6.3.2 Grafting the functional groups and antifouling characterization.....	123
6.4 Multifunctionalities of nanoparticles: nanocarriers and nanoprobess	124
6.4.1 Nanoprobess with high loading of reporter enzymes contribute to better sensitivity.....	124
6.4.2 Surface functionalization layers to improve the electrical properties	126
7. Conclusions	128
ANEXOS	131
References	139

Abbreviations

Ab_{HRP}: polyclonal anti-HRP antibody

Ab_{BGL}: anti-BGL antibody

AB-NTA: L-lysine disodium salt monohydrate

ABTS: 2,2'-azino-bis(3-ethylbenzothiazoline-6-sulphonic acid)

Alde-Dex@MNPs: dextran-coated iron oxide nanoparticles bearing the aldehyde groups

BCL: crosslinked beads

B-DAb: biotinylated detection antibody

BGL: β -galactosidase

BSA: bovine serum albumin

CAb: capture antibody

CB: carbon black

Chelate-epoxy support: agarose beads bearing the epoxy groups and chelate groups simultaneously

Chelate-Dex@MNPs: dextran-coated iron oxide nanoparticles bearing the chelate groups

CRP: C-reactive protein

cTnI: cardiac troponin I

cTnT: cardiac troponin T

DAb: detection antibody

DLS: dynamic light scattering

DTT: dithiothreitol

EDC: 1-ethyl-3-(3-dimethylaminopropyl) carbodiimide

(Epoxy)-Dex@MNPs: dextran-coated iron oxide nanoparticles with crosslinking

Fab: antigen-binding fragment

Fc: fragment crystallizable

FTIR: Fourier-transform infrared spectroscopy

GCE: glassy carbon electrode

GRAS: generally recognized as safe

HOOC-Dex@MNPs: dextran-coated iron oxide nanoparticles bearing the carboxylic groups

ICA: immunochromatographic assay

LFA: lateral flow assay

LOD: limit of detection

LOQ: limit of quantification

MES: 2-(*N*-morpholino)ethanesulfonic acid

MNPs: bare iron oxide nanoparticles

MWCNTs: multi-wall carbon nanotubes

NTA: nitrilotriacetic acid
NT-proBNP: N-terminal pro-B type natriuretic peptide
GO: graphene oxide
GRAS: generally recognized as safe
HOOC-Dex@MNPs: dextran-coated iron oxide nanoparticles bearing the carboxylic groups
HOOC@MBs: commercially magnetic beads bearing the carboxylic groups
HQ: hydroquinone
HRP, horseradish peroxidase
HSA: human serum albumin
IDA: iminodiacetic acid
IgG: immunoglobulin G
o-NPG: o-Nitro-phenyl- β -D-galactopyranoside
p-ABA: *p*-aminobenzoic acid
PANI: polyaniline
pI: isoelectric point
PBS: Phosphate buffered saline
PEG: polyethylene glycol
POC: point-of-care
QD: quantum dot
rGO: reduced graphene oxide
scFv: single-chain variable fragments
SiO₂@MNPs: silica layers coated iron oxide nanoparticles
S/N: signal-to-noise
Strep: streptavidin
SPCE: screen-printed carbon electrodes
SPION: superparamagnetic iron oxide nanoparticles
SPR: surface plasmon resonance
SWCNTs: single-wall carbon nanotubes
(Sulfo)-NHS: (Sulfo)-*N*-hydroxysuccinimide
TEM: transmission electron microscopy
TEOS: tetraethyl orthosilicate
TGA: thermogravimetric analysis
TMB: 3,3',5,5'-tetramethylbenzidine
UCNP: upconversion nanoparticles
VSM: vibrating-sample magnetometer

1. Introduction

Biosensors are integrated analytical devices that convert the specific interesting information of determined analytes into easily measurable signals via a signal transducer. Due to the obvious advantages of biosensors (simplicity, selectivity, cost-effective and quick response against complex matrices) than other time-consuming techniques, biosensors have been growing to be a portable alternative to the conventional analytical technique since its first appearance in the 1960s [1]. After the fast development of recent years, it has been utilized to distinct analytes (small molecules, e.g., nucleic acid and metal ions; biomarker protein; and whole cells, e.g., viruses and bacteria cells) in broad applications relating to in vitro diagnosis, food quality and safety industry, environmental and agricultural practices [2].

The precise quantification and analysis of the targeted analytes are based on the two important elements, which are “bioreceptor” and “transducer” elements (Figure 1). Bioreceptors capable of the specific recognition of analytes can be categorized into several types, typical biorecognition elements are synthetic nucleic acid (single strand DNA and selected aptamers), antibodies (Ab) (full-length Ab, Ab fragments and nanobody) and molecular imprinting polymers, etc. [3]. Signal transducers that convert the analytical response to the determination device can be categorized into electrochemical, optical, thermal and piezoelectric based on their working principles. To achieve the real-world application for point-of-care (POC) and satisfy the guidelines of the World Health Organization, which are ASSURED criteria (Affordable economically, Sensitive, Specific, User-friendly with minimal operator-training requirement, Robust and fast determination, Equipment-free and Deliverable to people in need), the smart combination and rational selection of corresponding bioreceptors and transducer elements are highly important.

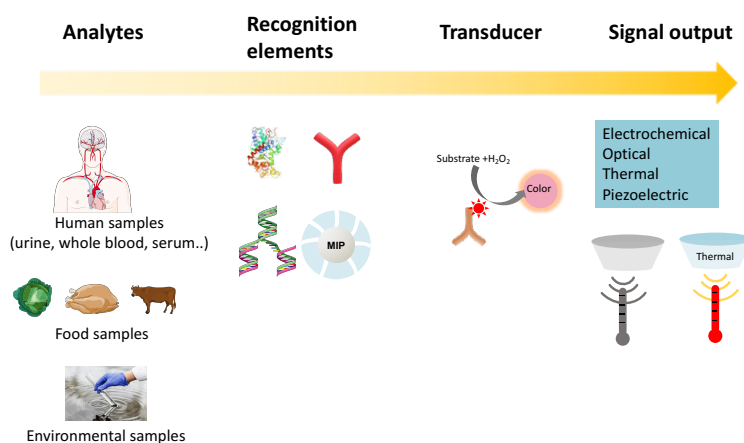


Figure 1. Scheme of the structure of the biosensor, including the recognition elements, transducer and signal output device.

1.1 Antibody as the bioreceptors – high affinity and selectivity

When selecting the bioreceptor types, different recognition elements have demonstrated distinct advantages. Aptamers have attracted the interests of researchers and have been taken as the potential great substitution for the antibodies, and aptamers can show extremely high affinities toward specific analytes even better than full-length Ab [4]. Due to the development of the SELEX (Systematic Evolution of Ligands by Exponential Enrichment) technique, high affinity aptamers with analytes can be selected via several steps screening. One of the outstanding advantages of aptamers is their small size (~1–2 nm vs. ~10 nm of full-length Ab), which endow the high functionalization density on the biosensing support to achieve higher sensitivity and a lower limit of detection (LOD) [5]. Aptamers can demonstrate outperformed LOD and response time when antibodies were randomly immobilized onto the sensing platform, while oriented conjugated antibodies can present comparable results with aptamers (dynamic range and LOD) [6]. Another advantage of aptamer over antibodies is its regeneration ability based on the morphology transformation, the reversible folding/unfolding change facilitates the facile regeneration [7].

Although aptamers have shown better performance than antibodies with certain analytes, they cannot challenge the dominant role in real-world application yet. One of the largest disadvantages of aptamer utilization is the time-cost process during the selection of aptamers with high affinity and selectivity. Further, its relatively high cost hampers the commercialization application [4].

Table 1. Comparison of antibody and aptamer as the bioreceptor

	Advantages	Disadvantages
Aptamer	Broad stability over variables; high regenerability (circulation); divided affinity strength; small size; controllable coverage density; reproductivity	Time cost for the aptamer selection; require nuclease-free condition
Antibody	Cost-effective; controllable affinity via protein engineering; different types with distinct size (scFv, Fab', nanobody)	Relative lower stability (high storage requirement); biofunctionality loss during anchoring, limited regenerability

For the efficient biofunctionalization of the biosensing platforms, antibodies are the dominant candidates so far due to their quite high sensitivity and affinity. The immunoglobulin G (IgG,

~150 kDa) is the most widely applied element, which consists of two heavy chains and two light chains, capable of capturing two analytes per IgG molecule theoretically. However, the development of antibody fragments has attracted much attention due to their smaller size with unaltered recognition capacity toward analytes [8]. Among these, the broad application of antibody fragments has been promoted by the recombinant protein engineering technique, such as single-chain Fv (scFv) fragment, antigen-binding fragment (Fab) and single-domain Ab (sdAb or nanobody) [8]

Due to the high importance of antibody orientation and coverage density onto the biosensing surface, the choice of immobilization strategy corresponding to the Ab types can significantly affect the performance.

1.2 Antibody immobilization strategy

So far, there are tremendous research have focused on the efficient immobilization of antibodies (especially IgGs) to obtain the satisfying performance of fabricated immunosensors [2, 3, 9, 10]. The IgGs are globular biomacromolecules with approximately 150 kDa molecular mass, the crystal fragment regions (Fc) are high conservation across different IgGs types while Fab fragments have diversities upon different IgGs types [11]. There are many potential anchoring points on the antibodies surface to achieve the interaction with activated support, in which amine groups, carboxyl groups, thiol groups, and *N*-glycan are the most accepted functional moieties despite the surface functionality (Figure 2A) [9]. Divided by the different orientation of bound IgGs onto the solid support, there are four types of orientation, which are “head-on”, “flat-on”, “head-on” and “end-on” orientations, in which “end-on” orientation is the most favored choice over others (Figure 2B).

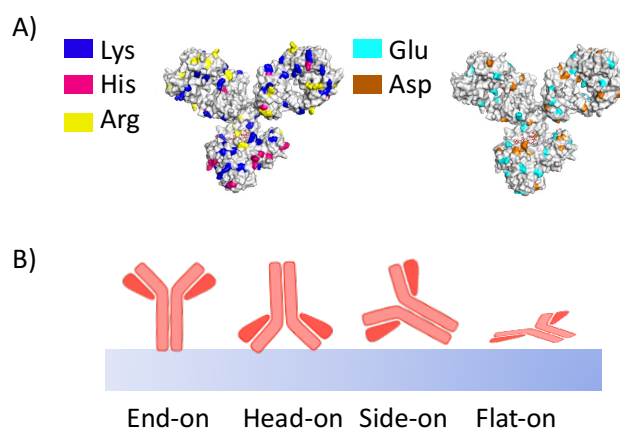


Figure 2. The available amino residues on the antibody surface contributes to the ionic interaction or covalent immobilization with surface activated support (A) and its possible

orientation (*end-on, head-on, side-on and flat-on*) upon the conjugation is affected by different parameters (*B*).

Differed from the surface functionalities of support, reactive moieties on the Ab surface and their conjugation strategies, the coupling manners have been divided as reversible interaction and covalent immobilization, and each of them also divide into two sections depending on the Ab orientation, namely random orientation and uniform orientation ([Figure 3](#)).

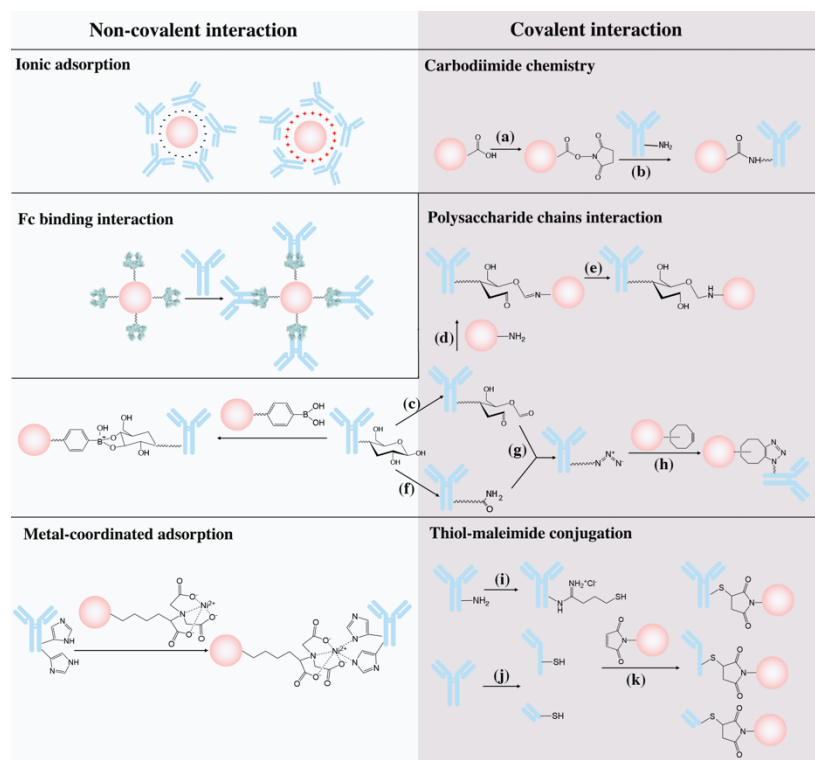


Figure 3. Common strategies to immobilize the antibodies via reversible interaction or covalent immobilization. Reprinted with permission from [2].

1.2.1 Reversible adsorption

Physical adsorption is the most classic reversible interaction technique, in which adsorption of antibodies is simple and versatile to quantify the concentration of antigens, and enzyme-linked immunosorbent assay (ELISA) is the gold standard used in the clinical analysis and reference technique [12]. Pre-adsorption of antibodies onto the nanocarriers has been reported to retain its specific antigen-recognition functionality when exposed to the plasma fluids, while the functional regions of covalently attached antibodies are prone to be shielded [13]. Although the physical adsorption may demonstrate good performance in some cases [14], lack of antibodies orientation controllability and suffering from tedious procedure make the reversible interaction to be further improved.

Therefore, oriented interaction antibodies via the Fc fragment to promise the highest exposure of Fab regions is more interesting. Boronic acid can interact with the *N*-glycan on Fc fragments to form boronate esters, but such interaction is facing competition with other (mono/poly) saccharides [15]. Protein A and G are famous IgGs-type affinity proteins derived from bacteria; they have been utilized broadly in immunosensors to link full-length antibodies due to their specificity toward the Fc fragment of many IgGs [10]. It has been reported that the combined advantages of boronic acid and protein A functionalize the biosensing surface with higher coverage density of antibodies, thus to obtain a high signal than single affinity adsorption was utilized [16].

However, to achieve the effective capture of antibodies, the homogeneously covered Ab-binding proteins on the support is another challenge faced in the real application. To allow the largest Ab adsorption capacity, derived functional domains (A, B and Z domains) instead of intact protein A show better orientation-control ability cooperation with genetic engineering techniques [17]. Tandem construction, affinity tagged (His, Cys and Halo tag), gold-binding peptides coupled domains have been well reviewed [17].

1.2.2 Covalent immobilization of IgGs

Direct immobilization of antibodies may result in better coverage density than oriented immobilization onto the sensing platforms, while the tethered antibodies may demonstrate even 10-fold lower recognition capacity [18]. However, oriented immobilization of antibodies can be obtained with much higher sensitivity with the highest Ab coverage density than physical adsorption and direct covalent interaction [19].

Amine and carboxyl groups are heterogeneously distributed on the antibodies surface, the large functional moieties population make them easy to interact with activated support [9]. Glutaraldehyde and carbodiimide chemistry (1-ethyl-3-(3-dimethylaminopropyl) carbodiimide (EDC) and *N*-hydroxysuccinimide (NHS)) are well-developed methods, their main advantages are easy-to-operation and universality across different antibody types, while the non-selective interaction results with random conjugation orientations [2].

For the oriented immobilization of antibodies, antibody fragments demonstrate better advantages to functionalize the support with higher loading density and superior orientation controllability instead of full-length antibodies due to their smaller size and better biological stability [20]. Typical antibody fragments are single-chain variable fragments (scFv) and nanobodies. The first option is to exploit the natural functional moieties of the antibody fragments, in which the hinge thiols of Fab' fragments can be coupled on the maleimide-functionalized support in a well-oriented manner. Furthermore, different tags can be inserted

into the N-/C-terminal of the fusion protein, achieved the site-directed immobilization without affecting its functionality and structure, such as Cys-tag incorporation within the terminus of the nanobodies to facilitate the covalent interaction with gold surface or maleimide activated surface [21], His-tagged nanobodies affinity interact with Co^{2+} -NTA (nitrilotriacetic acid) reversibly while the following the H_2O_2 oxidation fixed this connection [22], the site-directed biotinylation instead of random biotinylation promote the efficient interaction with streptavidin-coated microplate [23], SpyTagged nanobody achieve irreversible isopeptide bond with SpyCatcher functionalized electrical biosensor to enable the label-free detection of analytes [24, 25].

It is worth mentioning that the antibody fragments are also applicable as the detection probes when conjugated with signal generation enzymes to amplify the signal and obtain higher sensitivity, HRP linked nanobody (biotin-streptavidin interaction or SpyTag/SpyCatcher pair) [26-28] and glucose dehydrogenase linked scFv [29, 30] *via* the SpyTag/SpyCatcher pairs have substantially improved the immunosensor sensitivity.

However, the rational control of the tethering points on the full-length is a more complicated thing because the interaction residues during support-antibodies conjugation can be controlled by the surface chemistry while the involved sites are hard to predict. Developing a universal methodology suitable for various types of antibodies is quite challenging, but the conservation of Fc fragment across different IgGs can be utilized to achieve such a goal [2], and limiting the conjugation sites on the Fc fragment can also preserve the antigen-recognition capacity.

Strategies used to achieve the oriented immobilization of full-length antibodies have been summarized and published elsewhere [2]. The common characteristic of those strategies is using heterofunctional supports to achieve uniform orientation step-wisely, and two functionalized groups play different roles during antibodies conjugation. The first group works as the “bait” group, which reversibly adsorbing the antibodies with the best orientation toward analytes, this is the first while decisive step to link the Fc fragment on the support. The second group works as the “hook” group, which fixes the antibodies with their optimal orientation covalently. For the heterofunctional support, the “hook” groups have good diversity because many reactive moieties can achieve covalent bonds with amino residues. However, the selection of “bait” groups is relatively limited due to the reactive sites being restricted on the Fc fragment and the interaction condition of “bait” groups should not promote the covalent immobilization to prevent the random orientation. Boronic acid, metal chelate groups and EDC/sulfo-NHS activated carboxyl groups are the favored “bait” groups so far.

Lin's group has utilized the "bait" functionality of boronic acid to achieve site-directed immobilization [31-34]. The "hook" can be photoreactive (phenyldiazirine and alkyl diazirine) or nucleophilic substitution (S_N2) reactive type (phenylsulfonate (tosylate) ester and tosyl moieties), and such reaction has been applied in the Ab microarrays suitable for various support, including glass slides (bare and Cu_2O NPs functionalized slides) and magnetic nanoparticles.

EDC/sulfo-NHS activated carboxyl groups have obtained more attention due to its simplicity that only controlling the pH of the incubation buffer can manipulate the antibodies orientation [35]. For EDC/sulfo-NHS activated surface, the ionic adsorption happens much faster than the covalent interaction, thus the positive charged sulfo moieties can interact with negative charged Fc fragment when incubation pH is lower than the isoelectric point (pI) of IgGs [36]. This strategy is easy-to-operation and cost-effective, while its prerequisite is the known pI of used antibodies, which means the pI determination is mandatory. And the colorimetric quantification of antigens/Ab ratio is relatively less sensitive, however, the utilization of electrochemical measurement has partly solved this problem [37, 38].

Metal chelates groups also have broad applicability used as the "bait" group, that the unique His residues cluster distributed on the Fc fragment can adsorb the Ab to expose its Fab regions [39]. Tannic acid, iminodiacetic acid (IDA) and NTA are excellent metal coordination ligands, but tetradentate NTA ligands demonstrate better affinity than tridentate IDA ligands due to more interaction sites [40, 41]. The further orientation-fixing methods have many choices, such as H_2O_2 oxidation [42], glyoxyl-Lys multipoint interactions [43], photoimmobilization of benzophenone [44] and the ring-open reaction of epoxy groups [45]. Recently, the H_2O_2 oxidation reaction has been expanded with antibody fragments, such as scFv [46] and nanobody [22], further promoting its broad application and decreasing its complexity.

To conclude, there are no universally acceptable antibody immobilization strategies so far, the rational selection of conjugation techniques should take many things into consideration, such as antibody type, supporting material properties, reaction condition of the coupling and the final target of the fabricated immunosensors.

1.3 Immobilization platforms – the selection of antibody support

The immobilization strategy can affect the performance of biosensors, however, to fabricate a robust and effective biosensor upon Ab oriented functionalization is still not adequate, the rational selection of biosensing platforms and transducers are also of great importance.

Distinct materials of various origins have been used as immunosensing support for Ab conjugation, those supports are diverse with different composition, shape, size, physical

characteristics and chemical stability. To our understanding, ideal immobilization support should at least contain such advantages: chemical and physical stability, antifouling against interference biomolecules, fully inert after Ab conjugation, biocompatibility, reactive groups for anchoring points and availability with low price. While for the specific requirement of the immunosensors, one important feature of Ab-matrix conjugations is to maintain the biological activity of Fab fragment, which means the recognition sites of tethered Ab should be exposed toward analytes.

There are no universally applicable materials for the immunosensor fabrication yet, the appropriate selection of suitable matrix is directly affected by the biorecognition element and transducer. Thus, in this thesis, only several commonly used immobilization materials will be introduced.

1.3.1 Agarose-based support

Polysaccharide-based supports are popular options used in immunosensor support, the utilization of natural polymers endow such supports with many advantages, such as cost-effectiveness, biodegradability to harmless small molecules and biocompatibility for in vivo determination. The availability of functional moieties (amino and carboxyl groups) on the polymer surface facilitates their physical/covalent interaction with biomolecules, and distinct functionalities can be grafted on the backbones via the activation process [47]. In addition, due to the easy gelation to achieve stable configurations under gentle conditions, encapsulation and entrapment of biomolecules are also workable [48].

Agarose is the main composition of the agar, which is a Generally Recognized as Safe (GRAS) food additive, this neutral linear polymer consists of repeating units including α - and β -glycosidic bonds. One of its advantages and features is the reversible gelation/solution transformation upon the temperature change, which gels solution can be obtained by heating up to >80 °C, while solid gels are likely to be obtained when temperature is lower than 35 °C [49]. It also demonstrates other advantages, such as high hydrophilicity, lipophilicity, high loading capacity due to 3D porous structure, high controllability of particle and pore size and high inertness against interference molecules (complicate mediums, e.g. cell lysate and serum) [47].

Based on the hydroxyl derivatization, the surface activation and chemical functionalization of agarose beads need relatively harsh conditions, which high concentration of NaOH is necessary in most cases [47]. Monofunctional and heterofunctional supports can be obtained after several steps of activation (Figure 4). Among those grafted moieties, glyoxyl agarose has been proven with great success in enhancing the thermal stability of enzymes via achieving multipoint

covalent interaction [50]. Unlike glutaraldehyde, which achieves single point interaction with biomolecules under physiological buffer, the most possible interaction points between highly activated glyoxyl agarose and biomolecules are regions with a higher density of amino groups. Such reaction is favorable under an alkaline buffer and the whole process is quite fast upon multipoint interaction [51].

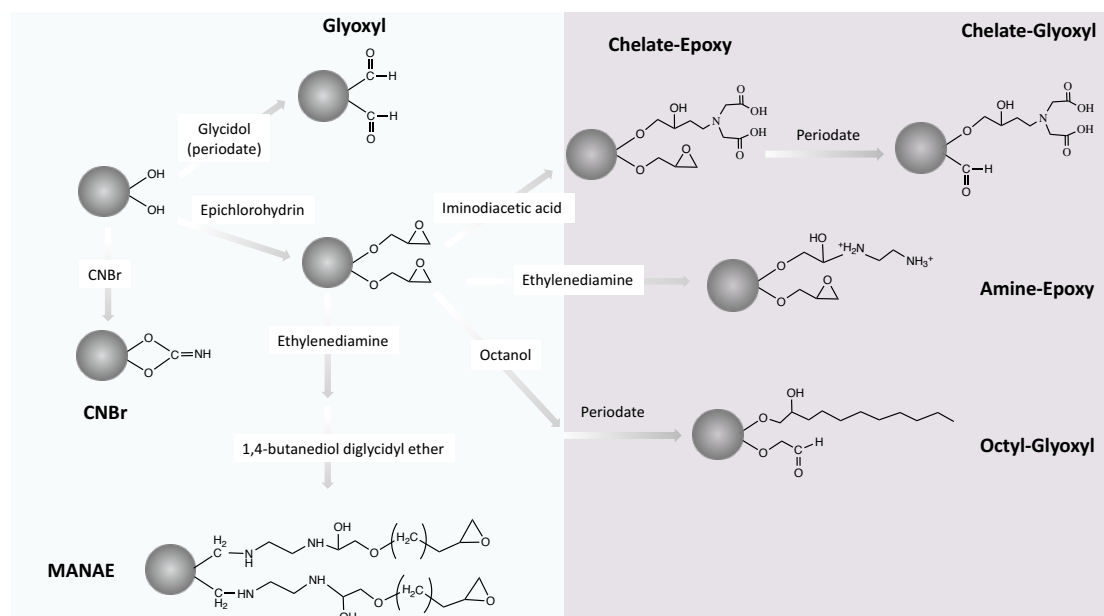


Figure 4. Agarose derivatives with different surface functionalities, include homofunctional supports (glyoxyl [51], CNBr [43] and MANAE [52]) and heterofunctional supports (chelate-epoxy [45], chelate-glyoxyl [43], amine-epoxy [53] and octyl-glyoxyl [54]).

When utilizing glyoxyl agarose as the immunosensor support, it demonstrates two characteristics: multiple points/all subunit interaction and heterogeneously diffusion in porous channels. Under the alkaline condition, the richest area in amino groups is the most potential anchoring points, which means the most abundant ϵ -Lys ($pK_a \sim 10$) are the better coupling points instead of the most reactive α -amino terminus ($pK_a \sim 7.5$). Due to the homogeneous distribution of Lys residues on the antibody surface, therefore, all the four subunits will be involved [55], which means “flat-on” is the most possible orientation after conjugation. Under this condition, the recognition capacity of the immobilized Abs is near 1 antigen per immobilized antibody, possibly due to the recognition sites being close to the support surface after antibody bound [45]. However, when polymers and reduction agents (dithiothreitol, DTT) were added as the additives, the whole immobilization procedure takes a longer time while lower capture ability was observed, which imply the “random” orientation of immobilized Abs is achieved instead of “flat-on” orientation [45]. Meantime, the distribution of biomolecules in the agarose porous channels are highly dependent on the immobilization rate. The biomolecules diffusion can be

regulated by imparting three parameters, which are surface functionality, the density of reactive groups or addition of the competitors. Thus, the tunable distribution of the biomolecules is highly controllable by rational limiting the immobilization rate [56]. Slowing down the immobilization rate causes the better uniform Ab diffusion into the porous and decreases the steric hindrances due to the crowded Ab density, almost 2-fold higher recognition capacity was observed using this strategy [43].

As an excellent and well-accepted support for immunosensing, the interaction between agarose support and biomolecules can also be affinity adsorption. A β -trefoil lectin domain LSL₁₅₀ was found with sugar-recognition ability, which is capable of binding galactose in solution with high affinity [57]. By generically incorporating the affinity domain (LSL₁₅₀) on the N-terminal of enzymes as the binding tag, such LSL₁₅₀-Enzyme-Agarose interaction is quite robust. The support materials can be unaltered agarose beads (crosslinked or un-crosslinked) and agarose functionalized magnetic nanoparticles, the bioconjugates can maintain the stability even under harsh conditions (heat up to 60 °C and 60 % acetonitrile as the incubation buffer) [58, 59].

1.3.2 Nanoparticles based support

Nanomaterials are commonly defined as particles with small size that at least one dimension ranging from 1 nm to 100 nm, and they demonstrate extraordinary physicochemical properties due to small dimensions, such as high surface-to-volume ratio and tunable surface chemistries, which endow them multiple functionalities in the biosensing application [60]. The large surface area not only provides many anchoring positions for the bioreceptor labels (e.g. aptamers, enzymes and antibodies) but also work as the multiple fluorophores/enzymes carrier to amplify the signal, thus improving the sensitivity with the low analytes appearance [61]). Furthermore, antibody–nanomaterials conjugates may demonstrate different characterization by rationally controlling the properties of the nanostructures (size, shape, surface functionality and synthesis conditions), thus it is crucial to prepare monodisperse-sized nanomaterials with distinct physicochemical properties [62]. Thus, the nanostructure morphology and properties should be taken into serious consideration to obtaining biosensing platforms with satisfying performance.

Recently, the development and application of different zero-, one-, two- and three-dimensional nanomaterials have emerged as remarkable component in the immunosensor area. In this thesis, several widely used nanomaterials will be introduced.

1.3.2.1 Magnetic nanoparticles (MNPs)

As the hot topic of MNPs application in the immunosensing application, many types of MNPs were synthesized and characterized, including single functional particles (iron, cobalt, nickel,

magnesium and platinum, etc) and multifunctional particles (core-shell-Fe₃O₄@Ag/Au, SiO₂@Fe₃O₄@AuNPs and nanohybrids-FePt, etc) [60, 63-66]. Superparamagnetic iron oxide nanoparticles (SPIONs) are the most welcomed MNPs utilized in the immunosensing application so far, including the magnetite (Fe₃O₄) and its oxidized formation maghemite (γ -Fe₂O₃).

For *in vivo* application, the superparamagnetic iron oxide nanoparticles (SPIONs) should demonstrate nontoxicity and compatibility, small size to penetrate the circulation system while high magnetization to control the movement precisely by the external magnetic field [67]. However, the restriction for the *in vitro* application is less, in which the colloidal stability in the absence of the magnetic field and the fast magnetic resonance under the applied magnetic field are highly important.

1. Synthesis of iron oxide nanoparticles

Because the properties of the MNPs are highly dependent on their dimension, thus the synthesis techniques and following surface functionalization are taken as the important variables to obtain size-dependent physicochemical properties and tailored surface functionality.

Among the many strategies to synthesize the SPIONs, top-down (physical attrition) and bottom-up (chemical synthesis) are the main choices. Instead of mechanical ball milling that hard to control the morphology of the nanocrystals, the utilization of chemical techniques (co-precipitation, hydrothermal, thermal decomposition, sol-gel and microemulsion) are more applicable to control the size and morphology of the SPIONs by manipulating the synthesis parameters [68]. The advantages of those preparation methods have been well summarized by Wu et al [69]. And the co-precipitation technique is one of the easiest and facile methods, which iron oxide MNPs can be synthesized just by adding the Fe²⁺/Fe³⁺ mixture into the alkaline solution followed by nucleation and growth, as shown as the following equation:



Although solvothermal/thermal decomposition method can obtain SPIONs with a superior uniform size distribution, co-precipitation method still plays a dominant role for the iron oxide nanoparticles preparation due to the least requirement of synthesization condition and less toxicity [70].

2. Iron oxide nanoparticles surface functionalization

The high surface area has endowed the SPIONs with excellent physicochemical properties, while they are prone to agglomerate to reduce the surface energy partly because of strong

dipole-dipole interaction. Therefore, it is quite necessary to functionalize the SPIONs to maintain its colloidal stability and contribute to better dispersibility, in which polymers, inorganic materials and bioactive molecules have been well investigated [71]. Meanwhile, the functionalized layers can also integrate unique properties to the nanoconjugates [72], limit the nonspecific interaction and serve as the anchoring points to increase the loading capacity of the target biomolecules [69].

For the application of immunosensors, one of the most important purposes of functionalization is to graft the SPIONs surface with multifunctionalities to couple the bioreceptors. Thus, natural/synthetic polymers bearing reactive moieties (or derivate moieties) are popular options. Starch [73], cellulose [74], chitosan [75], dextran [76], poly (acrylic acid) [77], alginate [78] and polyethylene glycol (PEG) [79] have been evaluated. Instead of *in situ* surface polymerization during nanoparticles synthesis, post-modification method can manipulate the grafting density and layers thickness, and multiple layers can be grafted by layer-by-layer strategy [80].

Dextran has been proven a promising organic polymer to functionalize the SPIONs due to its high solubility, biocompatibility and high stability, and it has been utilized in molecular imaging, molecular diagnostics and drug-carrier/delivery [81]. Co-precipitation with iron ions/dextran solution improves the biocompatibility of dextran–SPIONs while post-modification of dextran polymers with SPIONPs crystals result in better size distribution and monodisperse [58, 82]. For dextran coated SPIONs, covalent crosslinking is a necessary step to prevent the polymer dissociation during long-term storage and form functional moieties for the multivalent interaction. The surface functionality of dextran- SPIONs can derive from the epichlorohydrin cross linking followed by ammonia incubation to introduce the abundant primary NH₂ groups [83], or mild periodate oxidation after dextran coating [84], or use the dextran derivate polymers as the coating layers.

PEGylation of the SPIONs is one of the most favored treatments so far due to their high hydrophilicity and the grafted brush-like extensions demonstrate good repulsion against interference biomolecules in biological fluids [85, 86]. The heterobifunctional PEG terminals not only facilitate the selective interaction onto nanoparticles surface to guarantee its colloidal stability, but also activate the functional moieties to target bioreceptors. Multifunctional copolymer instead of simple monofunctional PEG polymer has been proven as a better option by N'Guyen et al. [87], which trifunctional ligand was synthesized (phosphonic moiety strongly bind with SPIONs, hydrophilic PEG polymer improves the antifouling properties and dispersibility, and coupling sites for the targets).

Silica coating is another classical functionalization technique. It can increase the colloidal stability of SPIONs, especially in acidic conditions. After functionalization, the homogeneous silica layer provides abundant Si-OH groups to activate the reactive moieties. The first classical and well proven method to prepare SPIONs@SiO₂ nanostructure is Stöber strategy [88], the hydrolysis and condensation of the sol-gel precursor (e.g., tetraethyl orthosilicate, TEOS) can tune the thickness of the silica shell. Utilizing the silanes with distinct functionalities, positive and negative moieties can be grafted simultaneously [89]. Another option is the reverse microemulsion (water-in-oil) technique, this method demonstrates better controllability with the thickness of the silica layer and avoids the appearance of the silica-free nanoparticles [90]. Similarly, organosilane ligands can graft uniform SiO₂ layer on the SPIONs surface, meanwhile tune their surface functionality, among which 3-aminopropyltriethoxysilane [91], (3-glycidyloxypropyl)trimethoxysilane [92] and 3-mercaptopropyl-trimethoxysilane [93] have been proven good application.

Several bioactive molecules can also work as the binding layer to achieve the biomolecules immobilization. The quinone groups from tannin molecules can couple the trypsin with SPIONs upon pH increment of the incubation buffer [94]. Khramtsov et al [95]. used bovine serum albumin (BSA), casein and gelatins A/B as the coating biomolecules to determine the influence of functionalization layer on its transverse relativity (R₂), results show that protein coating improves the storage stability, prevent the bioconjugates agglomeration when exposed with complex media.

1.3.2.2 Other nanoparticles with excellent characterizations

Gold nanoparticles (AuNPs) are famous noble nanoparticles used in optical biosensing application, mostly contributing to their inertness, biocompatibility, easy-of-synthesis and functionalization [96]. AuNPs demonstrate remarkable optical and electrochemical properties, such characteristics have been used in the lateral flow assay (LFA), surface plasmon resonance (SPR) and surface-enhanced Raman scattering (SERS) to promote their broad application. The spherical AuNPs are common label reporters used in the LFA due to their high extinction coefficient within the visible range [97]. Such immunoplatforms are fast, easy-of-operation and cost-effective. AuNPs and gold surface are also excellent support in the SPR, which record the refractive index change of surrounding medium, and allow the label-free detection of analytes in small quantities [98]. Further, combining the advantages of LFA and SERS can contribute even better sensitivity [99-101].

Carbon nanomaterials are important nanomaterials for the development of immunosensor, typical carbon nanomaterials including graphene, graphene oxide (GO), reduced GO (rGO),

single-wall (SWCNTs) and multi-wall carbon nanotubes (MWCNTs) and other emerging nanomaterials [102]. Though they have vast diversities, they share many common advantages, like high aspect ratios, high surface area and good electronic properties. Further, the perfect combination of excellent conductivity and good electrochemical properties promote their application as the supporting materials in electrochemical determination [103]. Decorating CNTs with other nanoparticles further improved the electrochemical activity of nanohybrids [104].

Quantum dots (QDs) are typical semiconductor materials with excellent photophysical and luminescence properties, main advantages of those QDs nanostructures are high fluorescence yields and photostability, size/shape related luminescence characterizations, with broad absorbance bands while narrow emission bands that exhibit large Stokes shift [105].

Upconversion nanoparticles (UCNPs) are typical anti-Stokes luminescent nanomaterials, that emit luminescence with near-infrared light excitation following the opposite mechanism of QDs and organic dyes [106]. The upconversion luminescence (UCL) demonstrates many interesting features, such as excellent photoexcitation and chemical stability, quite narrow emission bands, which make them well-fit applications in biosensing [107].

1.3.3 Screen-printed Electrodes

Screen-printed electrodes (SPEs) are well-known and well-proven platforms for the electrochemical determination of distinct analytes due to their easy preparation, cost-effective, disposable and excellent batch-to-batch reproducibility. In addition, the mature manufacturing techniques of relative products suit the customizable requirements from laboratory trials to commercial applications, which further promotes its broad application.

When the grafting and functionalization are directed on the working electrodes, the fabricated integrated electrochemical platforms simplify the application requirement and promote the decentralized assays [108]. To fabricate the ready-to-use biosensor based on SPEs, the surface activation of working electrodes to generate many anchoring points for the bioreceptors (aptamers, enzymes or Abs) is the first and crucial step to obtain satisfied device performance. There are three most common strategies used in this functionalization step, which are ink printing with the conductive substrates during electrode fabrication (pre-treatment), drop casting and electrochemical deposition of precursors/nanoparticles (after ink curing treatment) (Figure 5) [109].

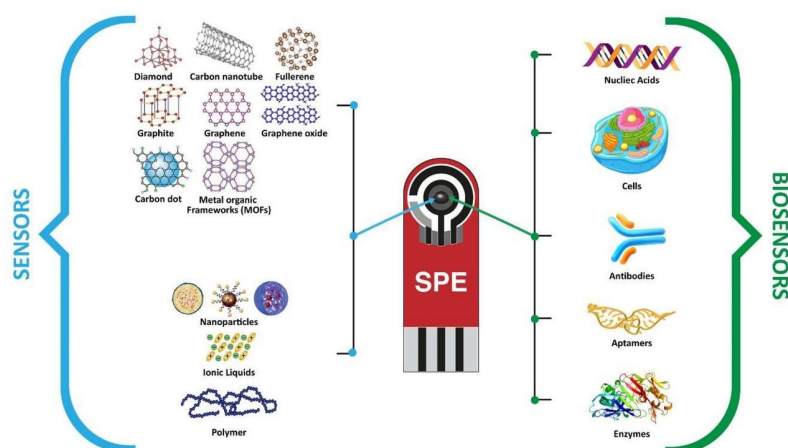


Figure 5. Common strategies to functionalize the working electrodes of SPEs. Reprinted with permission from [110].

Besides the properties of electrodes (working electrodes especially), the surface functionalization techniques can impart a strong influence on the biosensing performance, which promotes its robust application in different areas. The tremendous researches focus on efficient functionalization of electrodes have been well illustrated [108, 109, 111, 112], thus in this thesis only several typical results have been summarized, which integrated platforms can analyze varied analytes (small drug molecules, microRNA, moderate protein biomarkers and large bacteria cells or virus), and multiplexing detection is also applicable to achieve reliable results (Table S1).

One functionalization methodology is to covalently graft the reactive moieties on the working electrodes of SPEs via electrochemical reduction of diazonium salts [108]. After rational regulating the electrografting parameters, the optimal density of deposited carboxylic groups (from PB buffer activation, *p*-ABA, *p*-aminophenylacetic acid and 4-carboxyphenyl grafting) and amino groups (*p*-phenylenediamine and 4-nitrophenyl diazonium grafting) are perfect anchoring points for the bioreceptors [113-118]. This activation step is easy-to-operating and cost-effective, meanwhile, the grafted reactive moieties are highly controllable. Multiplexing determination of dual analytes can be achieved via multiple channel SPCE arrays [117, 118] or dual carbon electrodes [119], and the utilization of dual functionalized nanomaterials (HRP and Ab) have been proven with better performance to enhance the sensitivity and LOD.

Another functionalization strategy is to use AuNPs grafted SPEs, which are obtained from commercial gold electrodes [120, 121], electrochemical reduction of HAuCl₄ solution [122-126] or drop casting of AuNPs directly [127-129]. Due to its large surface area, the deposited AuNPs are promising carriers for the sulfhydrylated aptamers/peptide nucleic acid and affinity ligands (MPBA) via Au-S bonds, or antibodies via the interaction of Au-NH₂ [122]. Another

advantage is to promote the electron transfer during the electrochemical determination, and AuNPs nano hybrids with other nanostructures demonstrate even superior electrocatalysis properties and show obvious signal amplification [130-132].

Carbon nanomaterials are also welcomed functionalization materials for the SPEs. Graphene, GO and rGO are classic carbon nanostructures used in this application, which not only provide large coupling sites for the bioreceptors/AuNPs and but improve the electrical conductivity of the electrodes [97, 133, 134]. The rational combination of rGO with other nanomaterials to form multifunctional nanocomposites bearing multiple functionalities is more appealing in the real-world applications [135, 136]. Except as the support material, the carbon nanomaterials also can work as the adhesive layers to conjugate other anchoring polymers (e.g., chitosan and carboxymethylcellulose) [121, 137]. CNT-functionalized electrodes will obtain an enhanced amperometric signal, especially toward H_2O_2 and NADH, which are the common substrates in the electrochemical sensor [103]. Meanwhile, carbon black (CB) is emerging as another competitive material that demonstrates improved conductivity and enlarged protein loading capacity with better cost-effectiveness [138-140].

Polyaniline (PANI) is an intrinsically conductive polymer bears plenty of positive groups on its backbone chains, it can form a porous nanofiber structure upon electrochemically deposited onto the electrodes [141]. PANI can work as the immobilization carrier of redox enzymes due to its porosity [141] and adhesive layer to bind other nanomaterial layers exploiting its positive charged property [142, 143].

1.4 Functionalities of nanomaterials during the fabrication of biosensors

As discussed above, the application of nanomaterials is quite broad, and the performance of the biosensors has been greatly enhanced due to the unique characteristics endowed by its small dimension. To illustrate the functionalities and roles of the nanomaterials used in the biosensors, C-reactive protein (CRP) will be used as the model to be discussed.

CRP is a well-documented diagnostic biomarker for cardiovascular disease, the precise quantification of CRP concentration in human fluids is quite important to diagnose the heart attack in the early detection [144]. And the CRP level has been reported with a high correlation with the early stage of COVID-19 infection, which can work as the biomarker related to lung lesions [145].

1. Immobilization support of the capture bioreceptors

The first and most widely used functionality of nanomaterials is as the immobilization carriers of the recognition element to specifically capture the targets. Except for the antibody and

aptamer, poly(2-methacryloyloxyethyl phosphorylcholine) have also demonstrated a high binding affinity with CRP, and the easy control of the grafting density of this hydrophilic layers further promote its application [146, 147]. Meanwhile, the nanomaterial types will affect the corresponding detection techniques, thus causing the diversity of the biosensor sensitivity. AuNPs with excellent optical properties are good carriers because the nanoparticle size increase and wavelength shift can be easily monitored, however, this quantification detection method is relatively less sensitive, which LOD with $\mu\text{g mL}^{-1}$ level is observed [148-150]. The magnetic nanomaterials have broader application because of its easy magnetic separation properties facilitate the pre-purification when interact with CRP from human serum samples, which chemiluminescence, fluorescence and electrochemical detection are applicable, and LOD with ng mL^{-1} level is observed with many cases [151-157].

2. Nanocarriers of the signal probes

When nanomaterials are utilized as the carrier of the signal reporters, the large surface promotes its anchoring amount onto the surface of the nanomaterials, which is used as the signal amplifier to improve the sensitivity. HRP and detection antibody dual functionalized nanomaterials carry multiple signal molecules per nanomaterial to generate higher signal under the same analyte concentration, which makes them better detection probes instead of single enzyme molecule [144, 158]. Under this condition, improved LOD with pg mL^{-1} level was observed. When recognition aptamers and dsDNA dual coupled nanomaterials were utilized as the detection probes, DNA concatemers carry tremendous signal tags from the hybridization chain reaction and the amplification CuNPs support have been reported to greatly improve the sensitivity, which a LOD with 0.33 fg mL^{-1} was reported [159].

Colloidal AuNPs also are well-researched carriers of secondary antibodies used in the immunochromatographic assay (ICA), the density of red color facilitates the quantitation of the analytes [160, 161], and further application of gold enhancer solution demonstrate higher sensitivity [162]. Its main advantages are one-step operation, fast response speed and cost-effectiveness, while the semi-quantification and lower sensitivity hamper its application in precise determination.

When fluorescent nanomaterials were combined with the ICA technique, easy, observable quantification and improved sensitivity were reported. QDs and UCNPs are reported as excellent fluorescent nanoparticle carriers, the broad dynamic range of the ICA determination was preserved, and enhanced sensitivity was another advantage [93, 97, 163-170]. Hu et al. and Huang et al. have utilized the multiple QDs embedded nanospheres instead of single QDs to do

the CRP detection—the similar strategy like multiple HRP molecules coupled carriers—can obviously enhance fluorescence signals [171, 172].

Typical ELISA measurement can detect the CRP concentration as low as $1.06 \mu\text{g mL}^{-1}$, which is not a satisfactory option so far [173], while the combined advantages of ELISA and nanoparticles also promote higher sensitivity. The photoluminescence generated from the QDs nanoparticles cause a wide dynamic detection range [174-176], and when $\text{Ru}(\text{bpy})_3^{2+}$ was used as the photoredox, the signal was further enhanced via electrochemiluminescent (ECL) amplification [177]. When the fluorescence determination using multiple signal molecules loaded nanomaterials can obtain over 32-fold higher sensitivity than single dye loading [178], over 5 orders of dynamic range with 0.043 pg mL^{-1} LOD was achieved by this method [179].

3. Nanotracers

Noble metal nanostructures (AuNPs and AgNPs) are excellent substrates for the SERS technique due to their unique size/shape-dependent optical properties [180]. For the detection of CRP using the SERS technique, the synergic amplification effect of AuNPs and signal probes (Nile blue and methylene blue) significantly prong the detection limit which results in this main advantage with wide dynamic range and excellent sensitivity, which LOD lower than 1 pg mL^{-1} have been observed in most cases [100, 181-183].

As discussed earlier, the combination between the LFA technique and other determination methods can obviously improve the performance while maintaining easy and fast quantification. Similarly, when incorporating SERS technique with LFA method, although the detection sensitivity was not as good as the SERS determination alone, probably limited by the visualization functionality of detection probes labeled nanomaterials on the nitrocellulose membranes [184], however, the wide detection range was maintained and even lower LOD was obtained [99, 101, 180]

When immobilizing the recognition bioreceptors on the gold surface, the refractive index change of the surrounding medium is monitored by the SPR technique, and using the AuNPs labeled detection probes can even amplify the minor change [98].

4. Nanocatalysts of enzyme mimics

The enzyme-like catalytic activity of metal nanoparticles has been discovered and applied as the substitution choice of horseradish peroxidase (HRP) [185]. The nanoenzymes can catalyze the efficient oxidation of different substrates (3,3,5,5-tetramethylbenzidine (TMB), (2,2'-azinobis-(3-ethylbenzthiazolin-6-sulfonic acid)) (ABTS) and *o*-phenylenediamine) with the

appearance of H_2O_2 , and the substrate oxidation process can be monitored via colorimetric change or the electrochemical current variation.

A colorimetric reaction is the most common application of such nanoenzymes, Xie et al. [186] did very interesting research that recognition antibodies and reactive enzymes were replaced by cytidine 5'-diphosphocholine (Citicoline) and AuNP to perform the ELISA determination, which phosphorylcholine-BSA coated microplate can specifically capture the CRP analytes and lower the background signals, and their corresponding sandwich formation with aptamer coupled AuNPs simplified the operation procedure. Except for the AuNPs, AgNPs, N-/B-doped rGO, PtNPs, IrNPs and other bimetallic nanocomposites (PtRu NPs and PtAg) also demonstrate good peroxidase-like activity in sandwich formation [187-189].

When using electrochemical determination instead of colorimetric monitoring, the sensitivity can even be further improved [190]. The nanomaterials functionalized glassy carbon electrode (GCE) can improve the immobilized amount of capture bioelements, thus increase the capture capacity of analytes with low abundance, the nanoenzymes can amplify the current change and sensitive quantification of CRP level to pg mL^{-1} [191-193].

2. Objectives

The general objective of this doctoral thesis was to design and develop satisfactory immunosensing platforms for the detection of biomarkers with improved analytical effectiveness, in which rapidity, sensitivity and versatility are of great importance. The research presented in the dissertation emphasis on the exploration of site-directed bioreceptors conjugation strategy and evaluates the compatibility of diverse supporting materials.

Specifically, different objectives can be summarized as following parts:

2. Developing versatile immobilization strategies for full-length bioreceptors in terms of uniform orientation and preservation of their biofunctionality.
3. Determining the surface coating strategy and functionalization chemistries for superparamagnetic iron oxide nanoparticles on the basis of magnetic response speed and colloidal stability.
4. Evaluating and comparing different analytical techniques (optical and electrochemical analysis) with their analytical features, mainly sensitivity and applicability.
5. Exploring the multifunctionality of magnetic nanoparticles, including as the bioreceptors conjugation platform and dual-functionalized nanocarriers for signal amplification.
6. Comprising the different supporting materials in terms of immunosensing response time, cost-effectiveness, sensitivity and versatility.
7. Characterizing the analytical performance of fabricated immunosensors based on the varied supporting matrices and detection probes.

3. Materials

Provider	Products
Biomolecules (enzymes and antibodies)	
Sigma Aldrich (St. Louis, USA)	Horseradish peroxidase (HRP)
	β -galactosidase (BGL)
	Anti-HRP antibody from rabbit
	Anti-BGL antibody from chicken
	Human serum (from male AB clotted whole blood)
	Human hemoglobin
	IgG from human serum
	Human serum albumin (HSA)
	Bovine serum albumin (BSA)
	Streptavidin (Strep)
Casein	
R &D Systems (Minneapolis, USA) (Provided in CRP DuoSet ELISA kit)	Recombinant human C-Reactive Protein (CRP)
	Mouse capture antibody (cAb-CRP)
	Mouse biotin labelled antibody (B-DAb-CRP)
	N-Terminal Pro-B Type Natriuretic Peptide (NT-proBNP)
	Cardiac troponin T (cTnT)
	Cardiac troponin I (cTnI)
Roche Diagnostics GmbH (Mannheim, Germany)	Streptavidin conjugated HRP (Strep-HRP)
Antibody immobilization supports	
Agarose Bead Technologies (Madrid, Spain)	Agarose 6% crosslinked beads (BCL)
Dynal Biotech ASA (Oslo, Norway)	HOOC-MBeads (magnetic beads), 2.8 μm \varnothing , 10 mg mL ⁻¹ , Dynabeads® M-270 carboxylic acid,
Metrohm DropSens (Oviedo, Spain)	SPCEs (DRP-110, 4 mm \varnothing carbon working electrode, carbon counter electrode and Ag pseudo-reference electrode)
Chemical reagents	
Sigma Aldrich (St. Louis, USA)	Different dextran polymers from <i>Leuconostoc spp.</i> (MW ~ 10 kDa, 24.5 kDa, 40 kDa, 70 kDa)

	Sodium borohydride (NaBH ₄)
	Sodium (meta) periodate (NaIO ₄)
	2-Mercaptoethanol
	Sodium dodecyl sulfate (SDS)
	Epichlorohydrin
	Glycidol
	Ethanol
	Iron chloride (III) hexahydrate (≥98%)
	Iron chloride (II) tetrahydrate (≥99%)
	Sodium bicarbonate (NaHCO ₃)
	Ammonia solution (NH ₄ OH, 30%)
	Iminodiacetic acid (IDA)
	L-lysine disodium salt monohydrate (AB-NTA)
	<i>N</i> -hydroxysuccinimide (NHS)
	Sulfo- <i>N</i> -hydroxysuccinimide (Sulfo-NHS)
	Imidazole
	Polyethylene glycol (PEG) 600
	Dithiothreitol (DTT)
	2-(<i>N</i> -morpholino) ethanesulfonic acid (MES)
	Tris-hydroxymethyl-aminomethane-HCl (Tris-HCl)
	Hydroquinone (HQ)
	Ethanolamine
	Tetraethyl orthosilicate (TEOS)
	<i>p</i> -aminobenzoic acid (<i>p</i> -ABA) aryldiazonium salt
GE healthcare UK (Amersham, UK)	LMW calibration kit (molecular marker)
Medicell membrane Ltd (London, UK)	Dialysis membrane (12~14 kDa)
	30% Acrylamide and bis-acrylamide (N, N'-methylenebisacrylamide) mix solution
Bio-Rad (Hercules CA, USA)	TMB Liquid Substrate System for ELISA
	Quick Start™ Bradford 1x Dye Reagent
Fluka (Buchs, Switzerland)	Sodium phosphate
Novabiochem (San Diego, USA)	1-Ethyl-3-(3'-dimethylaminopropyl) carbodiimide · HCl (EDC)
	Sodium hydroxide (NaOH)

MATERIALS

PanReac Spain)	AppliChem (Barcelona, Spain)	Potassium iodide (KI) Nickel (II) sulfate hexahydrate Sulfuric acid Sodium nitrite (NaNO ₂)
Substrates of activity determination		
Sigma Aldrich (St. Louis, USA)		2,2'-azino-bis (3-ethylbenz-thiazoline-6-sulfonic acid) (ABTS) <i>o</i> -Nitro-phenyl- β -D-galactopyranoside (<i>o</i> -NPG) Hydrogen peroxide (H ₂ O ₂)
Apparatus		
Jasco (Kyoto, Japan)		UV-Vis spectrophotometer V-730
Biotek (Winooski, USA)		Epoch 2 microplate reader
Elma Schmidbauer GmbH (Singen, Germany)		S 30H Elmasonic sonicator
Malvern Instruments (Malvern, UK)		Zetasizer Nano S
CH Instruments (Austin, USA)		CHI1140A potentiostat controlled by CHI1140A software
Invitrogen–Thermo Fisher Scientific (Waltham, USA)		Magnetic separator DynaMag®2
R &D Systems (Minneapolis, USA)		Clear polystyrene microplates
TECAN (Männedorf, Switzerland)		Magellan V 7.1 microplate reader for ELISA
Homemade		Polymethylmethacrylate (PMMA) casings embed neodymium magnets (AIMAN GZ)

4. Methods

4.1. Antibody immobilization onto the agarose beads–homofunctional and heterofunctional support

4.1.1 Preparation of monofunctional glyoxyl-agarose support

The glyoxyl-agarose support was prepared by the etherification of the agarose surface, followed by the periodate oxidation [51]. Briefly, 105 g 6BCL (crosslinked) agarose beads were resuspended in mixture solution (contain 80 mL of distilled water, 3.4 g NaOH and 1.425 g NaBH₄ solid) under the gentle mechanical stirring, bulk agarose beads were dispersed before 36 mL of glycidol was added dropwise. This functionalization procedure was stirred at room temperature overnight, and adequate distilled water was used to wash the diols-activated agarose beads.

The diol groups functionalized on the agarose beads were further hydrolyzed into glyoxyl groups. Briefly, 105 g diols-activated agarose beads were pre-resuspended in 150 mL distilled water containing 3.21 g sodium periodate solid until all the bulk beads were broken. Then 1500 mL distilled water was poured into the suspension under gentle mechanical stirring, the reaction was performed at ambient temperature for 2 h. Adequate distilled water was used to wash the glyoxyl-activated agarose beads.

4.1.2 Immobilization of antibody on the glyoxyl-agarose support

Direct conjugation: 1 g of glyoxyl-agarose was incubated with 4 mg anti-HRP dissolved in 10 mL of sodium bicarbonate (25 mM, pH 10), the immobilization was performed at 25 °C for 1 h for the fast conjugation. The immobilization amount of anti-HRP at different time intervals was monitored by Bradford assay. Upon the finish of antibody immobilization, 1 mg mL⁻¹ NaBH₄ was added and reacted for 30 min to stabilize the reversible imide bonds. The antibody-glyoxyl bioconjugates were washed with phosphate buffer (PB) buffer to eliminate any impurities.

N-terminus targeted conjugation: 1 g of glyoxyl-agarose was incubated with 4 mg anti-HRP dissolved in 10 mL of sodium bicarbonate (25 mM, pH 8.5), the immobilization was performed at 25 °C for 24 h for the fast conjugation. The immobilization amount of anti-HRP at different time intervals was monitored by Bradford assay. Upon the finish of antibody immobilization, 1 mg mL⁻¹ NaBH₄ was added and reacted for 30 min to stabilize the reversible imide bonds. The antibody-glyoxyl bioconjugates were washed with PB buffer to eliminate any impurities.

Random immobilization: 1 g of glyoxyl-agarose was incubated with 4 mg anti-HRP dissolved in 10 mL of mixture 20% (w/v) PEG 600 and 50 mM DTT dissolved in 25 mM sodium bicarbonate (pH 10), the immobilization was performed at 4 °C for 6 h for the efficient conjugation. The immobilization amount of anti-HRP at different time intervals was monitored by Bradford assay. Upon the finish of antibody immobilization, 1 mg mL⁻¹ NaBH₄ was added and reacted for 30 min to stabilize the reversible imide bonds. The antibody-glyoxyl bioconjugates were washed with PB buffer to eliminate any impurities.

4.1.3 Preparation of heterofunctional chelate-epoxy agarose support

The agarose beads were first activated with epoxy groups, then epoxy groups were partly substituted by the chelate groups to achieve the heterofunctional support. Briefly, 100 g 6BCL agarose beads were resuspended in mixture solution (contain 440 mL of distilled water, 160 mL of acetone, 33 g NaOH solid and 2 g NaBH₄ solid) under the gentle mechanical stirring, bulk agarose beads were dispersed before 110 mL of epichlorohydrin was added dropwise. This functionalization procedure was stirred at room temperature overnight, and adequate distilled water was used to wash the epoxy-activated agarose beads.

The second substitution step was performed by using iminodiacetic acid to react with epoxy groups. By controlling the reaction time, different proportional epoxy groups were transformed to chelate groups. 10 g of wet epoxy activated-agarose beads were resuspended to 100 mL 0.5 M iminodiacetic acid solution (pH 11) and different time intervals were performed (2 h, 4 h, 8 h and 24 h) to obtain different heterofunctional support. Adequate distilled water was used to wash the heterofunctional agarose beads. The chelate groups on the heterofunctional supports were incoordinate with nickel sulfate (30 mg mL⁻¹, m/v) for 1 h before adequate distilled water washing.

4.1.4 Immobilization of antibody on the chelate-epoxy agarose support

Oriented immobilization: This antibody immobilization strategy was performed in a two-step manner, which are physical adsorption and covalent interaction [43]. 1 g of chelate-epoxy wet support was incubated with 4 mg anti-HRP in 25 mM sodium phosphate pH 7. The immobilization was performed at 25 °C for 1 h for the fast affinity adsorption, and the immobilization amount of anti-HRP at different time intervals was monitored by Bradford assay. Following the affinity adsorption, the supernatant was discarded by vacuum filtration, and the antibody-chelate/Ni²⁺-epoxy bioconjugations were incubated at alkaline buffer (25 mM sodium bicarbonate, pH 10) for another 24 h to achieve the irreversible covalent interaction. Thus, fully covalent conjugated antibodies were incubated with the EDTA buffer (0.5 M EDTA, 0.5 M NaCl, and pH 8) to eliminate the coordinated metal ions, affinity coupled antibodies will

be desorbed from the support. The residual epoxy groups were blocked with a 3 M glycine solution (pH 8.5).

To determine the adequate incubation time under alkaline buffer that promote the fully covalent conjugated antibodies, the antibody-agarose bioconjugates were incubated with EDTA buffer (0.5 M EDTA, 0.5 M NaCl, and pH 8) to check the ratio of irreversible connection, the bioconjugates were vacuum filtered with different time intervals. And the antibody concentration was monitored to evaluate the leaching antibody until there is no antibody detected in the supernatant.

4.1.5 Immunoassay determination of prepared antibody-agarose bioconjugates

To calculate the captured antigens per μmol immobilized antibody, proteins (HRP or BGL) with a concentration of over 20 times higher than the saturated adsorption capacity of bioconjugates was prepared, and the protein in sodium phosphate (0.1 M, pH 7) was incubated with 1 g of agarose wet support at 4 °C. After incubating for 4 h, the captured antigens were measured by the enzyme activity of bioconjugate before washing with the same buffer to eliminate the nonspecific interaction and excessive proteins.

4.1.6 Protein concentration determination

The protein concentration was determined by Bradford assay using bovine serum albumin (BSA) as standard reference protein. Briefly, 5 μL of each standard or sample was pipetted into the 96 well microplates, respectively, and 200 μL of the Quick Start™ Bradford 1x Dye Reagent was added to each well. After thoroughly mixing for 30 seconds, the mixture was incubated for another 10 minutes at 25 °C before the absorbance determination at 595 nm using a microplate reader (BioTek Instruments, Winooski, USA).

4.1.7 Enzyme activity determination of the immunoconjugates

HRP activity determination: The enzyme activity of HRP was determined following the protocol described by [194]. Sodium phosphate buffer (0.05 M, pH 6.0) was the reaction buffer, ABTS (molar extinction coefficient of ABTS^+ is $36000 \text{ M}^{-1} \text{ cm}^{-1}$) and H_2O_2 were the substrates. The equal molar concentration of ABTS and H_2O_2 (final concentration is 1 mM) were mixed in the buffer, the absorbance increases of 420 nm at 25 °C were monitored by Jasco V-730 UV-Visible spectrophotometer (Tsukuba, Japan). One enzyme unit was defined as the generated 1 μmol of ABTS^+ per min/mg enzyme under the reaction conditions. Determination experiments were performed in triplicate to calculate the mean values.

BGL activity determination: The enzyme activity of BGL was determined following the protocol described by [195]. Sodium phosphate buffer (50 mM, pH 7.0) was utilized to dissolve the *o*-NPG (molar extinction coefficient of *o*-nitrophenol is $3100 \text{ M}^{-1} \text{ cm}^{-1}$) to achieve the final concentration of 13 mM. Afterwards, the absorbance increases of 405 nm at 25 °C was monitored by Jasco V-730 UV–Visible spectrophotometer (Tsukuba, Japan). One enzyme unit was defined as the generated 1 μmol of *o*-nitrophenol per min/mg enzyme under the aforementioned condition.

4.1.8 Quantification of the epoxy groups density on the agarose support

The epoxy and aldehyde density were calculated by the decrease of the periodate amount in the supernatant solution before and after the oxidation reaction [196].

For the quantification of epoxy groups density on the agarose beads, 1 g wet agarose support bearing epoxy groups was incubated with 10 mL of 1N H_2SO_4 for 2 h to realize the ring-open reaction. The diol hydroxyl groups on the agarose support were hydrolyzed to aldehyde groups by incubating with 10 mL 100 mM NaIO_4 solution. After gentle oxidation, the supernatant of the reaction system was used to quantify the residual periodate concentration by the colorimetric reaction.

1 mL Saturated NaHCO_3 solution was pre-mixed with 1 mL 10% (w/v) potassium iodide solution, then 100 μL stock periodate solution/supernatant was added and the absorbance at 450 nm was monitored using Jasco V-730 UV–Visible spectrophotometer (Tsukuba, Japan).

4.1.9 Sodium dodecyl sulfate-polyacrylamide gel electrophoresis (SDS-PAGE) analysis

The protocol of denatured SDS-PAGE analysis was following the detail described by [197]. Soluble protein or antibody-support bioconjugates were diluted with $2\times$ lysis buffer (62.5 mM Tris-HCl, pH 6.8, 2% SDS, 5% 2-mercaptoethanol, 10 % glycerol and 0.005 % bromophenol blue) before being boiled for 5 min. 12% (w/v) polyacrylamide gel was used as the separation gel to distinguish the bands between the light chain and heavy chain of the antibody. After color development with Coomassie blue, GelQuant NET (1.7.8) was utilized to quantify the gray intensity of each band.

4.2. Dextran functionalization and further chemistry activation

4.2.1 Synthetization of the bare magnetic nanoparticles via coprecipitation

The synthesization of bare MNPs was following the protocol of Massart [198]. Briefly, 0.09 mol Fe^{3+} and 0.054 mol Fe^{2+} were dissolved in 45 mL distilled water to form a homogeneous solution with yellow color, then the mixture was gently poured into 75 mL NH_4OH solution

(30%) under vigorous stirring. The black nanoparticles appeared immediately upon the addition of ferrous solution, and the obtained nanoparticles were further heated up to 90 °C for 1h to obtain nanoparticles with larger particle size. After cooling down to room temperature, the nanocomposites were washed with ethanol and distilled water three-time and stored at 4 °C for further usage.

4.2.2 Acid treatment to achieve the γ -Fe₂O₃ synthesis

To obtain the single phase of maghemite (γ -Fe₂O₃), another oxidation treatment was performed with HNO₃ and Fe(NO₃)₃ [199]. The obtained MNPs were incubated with 2 M HNO₃ for 15 min to dissolve nanoparticles with smaller size, magnetic separation was performed to eliminate the extra HNO₃. Then 75 mL Fe(NO₃)₃ (1 M) and 130 mL distilled water were added into the above nanocomposites, heated up to 90 °C for 30 min to perform the following acid treatment, after cooling down to room temperature, the supernatant was discarded. Afterward, acid treatment was performed by incubating with 300 mL 2 M HNO₃ for 15 min. Finally, the acid-treated MNPs were washed three times with acetone and water, and a rotary evaporator was used to remove the residual acetone and concentrate the nanocomposites. To distinguish the acid-treated nanoparticles and bare nanoparticles, the acid-treated nanoparticles were defined as γ -Fe₂O₃ nanoparticles.

4.2.3 Silica coating to functionalize extra SiO₂ layer on the surface of the nanoparticles

The protective silica shell was functionalized on the bare nanoparticles by the Stöber method [88]. To achieve sufficient coating and monodispersity, 160 mg of bare MNPs were dispersed in 480 mL of a mixture of 2-isopropanol/H₂O (2 : 1, v/v) with sonication mixing, followed by the addition of 32 mL of NH₄OH (30%, v/v) to the mixture, then the addition of 0.32 mL of tetraethyl orthosilicate (TEOS) was performed via drop by drop. After 1 h ultrasound treatment to achieve the thin layer on the bare MNPs surface, the solution was changed to vigorous stirring overnight. The silica-coated nanocomposites (SiO₂@MNPs) were washed by centrifugation (14000 rpm for 30 min) with ethanol for three times and resuspended with distilled water.

4.2.4 Surface functionalization with dextran and following the crosslinking treatment (Dex@MNPs)

Mechanical stirring: The dextran coating onto the nanoparticles was based on the physical adsorption of dextran polymers onto nanoparticles surfaces under strong alkaline conditions [63]. 400 mg dextran (MW = 10 kDa, 22.5 kDa, 40 kDa or 70 kDa) was well dispersed in 2.5 mL NaOH solution (0.5 M), sonication was performed to obtain homogenous dextran solution. Under vigorous mechanical stirring (~800 rpm), 50 mg_{Fe} MNPs (dispersed in water)

resuspended in 1.6 mL NaOH solution (0.8 M concentration) were added into dextran solution drop-wisely. The dextran polymer/nanocomposites mixture solution was mechanically stirred for 24 h until there is no agglomeration observed, colloidal dispersion was obtained after sufficient coating. After finishing the polymer coating, the color of nanocomposites will change to dark brown instead of the initial black color. Dialysis membrane (12 ~ 14 kDa cutoff) was used to perform the dialysis against distilled water, several water changes for 24 h to remove the unbound dextran polymers. The polymer modified MNPs were magnetically collected with a portable magnet and resuspended in distilled water to obtain a homogeneous suspension.

Sonication: The preparation of the dextran solution and nanoparticles colloiddally suspended in alkaline condition was following the same protocol as mechanical stirring when using sonication treatment. The difference between those two methods is the mixing strategy of the dextran/nanoparticles system, in which the bare MNPs were dropped wisely added into the dextran solution under the sonication, and the mixed suspension remained under sonication treatment for another 6 h at 25 °C. The following purification and dialysis were the same as previously stated.

The dextran crosslinking was performed to strengthen the connection between nanoparticle surface and polymers, thus preventing the dissociation of polymer layers. 1 mL dextran functionalized MNPs (10 mg_{Fe}) were mixed with NaOH solution (final concentration is 2 M), sonication was performed for 10 min to get a well-dispersed mixture. Afterward, 1.5 mL epichlorohydrin liquid was added into the mixture drop wisely under vigorous stirring. The crosslinking reaction finished after 24 h reaction, after dialysis against distilled water, the modified MNPs were magnetically collected and resuspended in distilled water to obtain colloidal stabilized suspension with a concentration of 10 mg_{Fe} mL⁻¹. The crosslinked nanoparticles will be defined as Epoxy-Dex@MNPs or Dex@MNPs, the epoxy groups have been grafted on the backbone of dextran polymers during the crosslinking treatment.

4.2.5 Evaluation of the colloidal stability and magnetic separability of surface-modified nanoparticles

Evaluating the colloidal stability of nanoparticles was performed by monitoring the absorbance decline tendency in different aqueous buffers (pH range from 3 to 11), and the absorbance intensity under 400 nm wavelength was analyzed at ambient temperature.

Different aqueous buffers were prepared first, 5 types of buffer systems were corresponding to the varied pHs, namely glycine-HCl (pH 3.0), sodium acetate-acetate (pH 4.0 and 5.0), MES (pH 6.0), HEPES (pH 7.0 and 8.0) and NaHCO₃ (pH 9.0, 10.0 and 11.0). Colloidal suspension with about 5 µg_{Fe} mL⁻¹ nanoparticles (the absorbance range was 0.8–1.2) was pipetted into the

UV-transparent disposable cuvettes, then diluted to 2 mL suspension using the prepared aqueous buffer. Following the strong ultrasound treatment for 2 min to achieve the homogeneous distribution, parafilm was used to seal the cuvettes to prevent solvent evaporation. The absorbance was determined with different time intervals using the fixed wavelength (400 nm) by Jasco V-730 UV-Visible spectrophotometer (Tsukuba, Japan). The nanoparticle suspensions were stored at the ambient temperature until the absorbance determination.

When pure distilled water was used as the incubation system, highly diluted NaOH/HCl was applied to change the pH by carefully adding it into the system.

The magnetic separation capacity of the nanoparticles was quantified using the same strategy, the embedded magnets in the cell holder (Jasco STR-773) were used to quantify the absorbance variations caused by the magnetic attraction. While this determination was continuously recorded instead of periodically monitored.

4.2.6 Characterization of the Dex@MNPs with sufficient surface coverage

The particle size and morphology of the nanoparticles were determined by transmission electron microscopy (TEM, JEOL JEM 1010) operating at 100.0 keV. The diluted nanoparticles in distilled water were dried over Cu TEM grids at room temperature before performing the measurement. The size distribution of nanoparticles was determined by using ImageJ digital software to calculate the average particle size and standard deviation.

The ζ -potential, hydrodynamic size and polydispersity index of the nanoparticles were determined by dynamic light scattering (DLS, Zetasizer Nano S, Malvern Instruments), and 25 °C was selected as the experimental temperature. Nanoparticles were highly diluted in distilled water and dilute HNO₃/KOH solution was used to change the pH of nanoparticles suspension.

The nanoparticles concentration described in this thesis was the concentration of iron. The iron concentration of the nanoparticles in the colloidal state was determined by inductively coupled plasma optical emission spectroscopy (ICP-OES, ICP PERKIN ELMER mod. OPTIMA 2100 DV), 25 μ L colloids were dissolved by HNO₃/HCl mixture, 1000-fold dilution with distilled water was performed before the measurement.

Magnetic characterization was carried out in a Vibrating Sample Magnetometer (VSM, MagLabVSM, Oxford Instrument). 100 μ L nanoparticles were dropped on the cotton pellet and heat up at 50 °C dried for over 24 h to ensure the full adsorption of the solid nanomaterials. After compacted in a capsule following the standard protocol, the saturation magnetization of the samples were obtained from hysteresis loops measured at room temperature (300 K).

Fourier-transform infrared spectroscopy (FTIR, IFS66V, Bruker) was performed with solidified nanoparticles. The colloidal nanoparticle suspension was resuspended in ethanol solution, aggregated nanoparticles can be easily separated and dried for over 24 h to eliminate the distilled water in the samples. About 1 mg water-evaporated nanoparticles were mixed with 99 mg potassium bromide (spectroscopic grade) before being compressed into ~1 mm thick discs.

Thermogravimetric analysis (TGA, Q500, TA Instruments) data were recorded in nitrogen flow (10 mL min^{-1}) in a temperature range from room temperature (RT) to $800 \text{ }^\circ\text{C}$ (heating increase rate of $10 \text{ }^\circ\text{C min}^{-1}$). The solidified samples were prepared using the same strategy described in the FTIR analysis.

4.2.7 Preparation of HOOC-Dex@MNPs based on the modification with Dex@MNPs

In this part, carboxylic groups functionalized nanoparticles—HOOC-Dex@MNPs—were prepared via the reaction between epoxy groups (grafted during crosslinking treatment) and iminodiacetic acid. $10 \text{ mg}_{\text{Fe}}$ Epoxy-Dex@MNPs nanoparticles were washed three times with 10 mM NaHCO_3 (pH 10.0), then $2 \text{ mL } 0.5 \text{ M}$ iminodiacetic acid (IDA) solution prepared in NaHCO_3 solution was pipetted into the 5 mL glass tube contains the Epoxy-Dex@MNPs. Thorough sonication treatment was performed until obtains a homogeneous suspension, and the reaction time was controlled from 0.5 h to 24 h . At a specific time interval, the modified nanoparticles suspension was withdrawn from the mixture system and separated with a magnet, and further purification was performed with distilled water.

4.2.8 Preparation of the HRP-Ab_{HRP}-Alde-Dex@MNPs nanoconjugates

Before conjugating the antibody, 1 mg_{Fe} Alde-Dex@MNPs were washed with 10 mM NaHCO_3 (pH 10.0) three times to achieve the buffer exchange. Then $50 \text{ } \mu\text{L } 0.2 \text{ mg mL}^{-1}$ anti-HRP antibody dissolved in 10 mM NaHCO_3 (pH 10.0) was used to resuspend the nanoparticles, brief sonication helps to break the agglomeration caused by the magnet adsorption, the immobilization treatment was performed at $25 \text{ }^\circ\text{C}$ for 1 h . NaBH_4 dissolved in 10 mM ice-cold NaHCO_3 (pH 10.0) was freshly prepared and pipetted into the suspension with the final concentration of 1 mg mL^{-1} to stabilize the reversible imide bonds and achieve the inert surface of nanoconjugates. After washing with PB buffer (10 mM , pH 7.0) three times, the antibody-MNPs bioconjugates were kept in PB buffer before the further detection immunoassay.

4.2.9 Calculation of the functionality of Ab_{HRP}-MNPs nanoconjugates with different immobilization strategies

The remaining functionality of the immobilized Ab_{HRP} was performed by calculating the antigen-recognition capacity of the conjugated antibodies. To calculate the captured antigens per μmol immobilized antibody, an enzyme with a concentration of over 20 times higher than the saturated adsorption capacity of nanoconjugates was prepared in sodium phosphate buffer (0.01 M, pH 7.0). Then the 50 μL HRP protein was incubated with the Ab_{HRP}-Alde-Dex@MNPs (pre-separated with portable magnet), following the brief sonication to break the agglomeration, and the incubation was performed under 37 °C by a water bath. After incubated for 10 min, the HRP-Ab_{HRP}-Alde-Dex@MNPs immunoconjugates were washed with sodium phosphate buffer three times to eliminate the unspecific interaction and excessive proteins, and the enzyme activity of bioconjugate was determined as described in 4.1.7.

The calculation of the capture capacity of the immobilized Ab_{HRP} was following the protocol of [35], which means the average HRP molecule captured per immobilized Ab_{HRP} molecule.

$$\text{Ratio (capture capacity of immobilized Ab}_{\text{HRP}}) = \frac{\frac{\text{IU}_{\text{HRP}} * \text{mg MNP}^{-1}}{\text{AE}}}{\frac{\text{mg}_{\text{Ab}} * \text{mg MNP}^{-1}}{\text{MW}_{\text{Ab}}}} = \frac{\text{IU}_{\text{HRP}} * \text{mg MNP}^{-1}}{\text{AE}} \cdot \frac{\text{MW}_{\text{Ab}}}{\text{mg}_{\text{Ab}} * \text{mg MNP}^{-1}}$$

Where, $\text{IU}_{\text{HRP}} * \text{mg MNP}^{-1}$ is the enzyme unit of the HRP enzyme per mg of Ab_{HRP}-Alde-Dex@MNPs, the unit of enzyme activity has been described in 4.1.7.

AE is the specific activity of the HRP enzyme.

MW_{HRP} and MW_{Ab} are the molecular weight of the corresponding protein, respectively.

4.3. Alde-Dex@MNPs with optimal aldehyde density as the nanocarriers–colorimetric determination and electrochemical assays

4.3.1 Characterization of the Alde-Dex@MNPs

The characterization of the Alde-Dex@MNPs nanoparticles (particle size, surface charge, functional groups identification and surface coverage, etc) were following the details described in 4.2.6.

4.3.1.1. Periodate oxidation of the dextran layers on the surface of the nanoparticles

For the preparation of Alde-Dex@MNPs nanoparticles, 10 mg_{Fe} Dex@MNPs were magnetically decantated first, and 2 mL sodium periodate solution with different concentrations

(2 mM–10 mM) was pipetted into the Eppendorf tubes, briefly sonication for 1 min to break down the agglomeration and achieve the homogeneous distribution. The whole oxidation condition was performed with gentle rotation at 25 °C and protected from light by covering with aluminum foil. After reaction for different time intervals (0.5–5 h), the oxidized Dex@MNPs nanocomposites were magnetically separated by a portable magnet, and the residual generated aldehyde density was quantified by the decrease of periodate concentration by colorimetric reaction. Then the oxidized nanocomposites will be washed with 0.2 M acetic acid solution (pH 4.0) and distilled water three times, respectively.

The supernatant solution from the nanoparticles suspension upon magnetic separation was used to achieve the quantification of aldehyde groups density during the oxidation process. 1 mL saturated NaHCO₃ solution was pre-mixed with 1 mL 10% (w/v) potassium iodide solution, then 100 µL stock periodate solution/supernatant was added and the absorbance at fixed 450 nm was monitored using Jasco V-730 UV–Visible spectrophotometer (Tsukuba, Japan).

4.3.1.2. Antibody immobilization on the Alde-Dex@MNPs nanoparticles

To conjugate the Ab_{HRP} with high efficiency, 1 mg_{Fc} Alde-Dex@MNPs with different oxidation degrees were washed with 10 mM NaHCO₃ (pH 10.0) three times to achieve the buffer exchange. Then 50 µL 0.2 mg mL⁻¹ Ab_{HRP} dissolved in 10 mM NaHCO₃ (pH 10.0) was used to resuspend the Alde-Dex@MNPs nanoparticles, brief sonication was performed to break the agglomeration caused by the magnet adsorption, the immobilization treatment was performed at 25 °C for 1 h. Then NaBH₄ dissolved in 10 mM ice-cold NaHCO₃ (pH 10.0) was freshly prepared and pipetted into the suspension with the final concentration of 1 mg mL⁻¹ to stabilize the reversible imide bonds and achieve the inert surface of nanoconjugates. After washing with PB buffer (10 mM, pH 7.0) three times, the antibody-MNPs bioconjugates were kept in PB buffer before the further detection immunoassay.

4.3.1.3. Quantification of the preserved functionality of the covalently conjugated Ab_{HRP}

The quantification of the remaining functionality of Ab_{HRP}-Alde-Dex@MNPs nanoconjugates was followed by the protocol described in 4.2.9.

4.3.1.4. Optimization of the experimental variables for the fabrication of the immunosensor

Under the optimal oxidation parameters (5 mM periodate oxidation for 4 h), the generated Alde-Dex@MNPs were used as the promising carriers for antibody conjugation. Optimization of the analyte incubation parameters was performed to achieve the highest capture efficiency, which includes the incubation time, Ab_{HRP} immobilization time, Alde-Dex@MNPs concentration and

compositions of the composition. And antigen-adsorption capacity of developed Ab_{HRP}-Alde-Dex@MNPs nanoconjugates has been quantified using the enzymatic determination method.

4.3.1.5. Analytical characterization of the fabricated immunosensor with the optimal conditions

20 mg_{Fe} Alde-Dex@MNPs were first magnetic decanted and washed with 10 mM NaHCO₃ (pH 10.0) three times to equilibrium the buffer pH. Then 1000 μ L 0.2 mg mL⁻¹ Ab_{HRP} dissolved in 10 mM NaHCO₃ (pH 10.0) was pipetted into the 1.5 mL Eppendorf tube to resuspend the concentrated nanoparticles. The antibody immobilization was performed under gentle rotation mixing at 25 °C for 1 h. Then NaBH₄ dissolved in 10 mM ice-cold NaHCO₃ (pH 10.0) was freshly prepared and added into the suspension with the final concentration of 1 mg mL⁻¹ to stabilize the reversible imide bonds and achieve the inert surface of nanoconjugates. After washing with PB buffer (10 mM, pH 7.0) for three times, the antibody-MNPs bioconjugates were kept in PB buffer before the further detection immunoassay.

HRP solutions with different concentrations (range from 0–300 μ g mL⁻¹) were prepared in the PB buffer via serial dilution. Ab_{HRP}-Alde-Dex@MNPs nanoconjugates prepared earlier were divided into several aliquots that contain 1 mg_{Fe} nanoparticle of each part. The aliquot (Ab_{HRP}-Alde-Dex@MNPs nanoconjugates) in the 1.5 mL Eppendorf tube was magnetic decanted and HRP solution was pipetted into the tubes, following the brief sonication to prevent the possible nonspecific binding caused by the aggregation. Then the mixture containing HRP and Ab_{HRP}-Alde-Dex@MNPs nanoconjugates were incubated in the 37 °C (water bath for the better temperature equilibrium) for 10 min. Afterward, the HRP-Ab_{HRP}-Alde-Dex@MNPs immunoconjugates were separated by the portable magnet and washed with PB buffer for 3 times to eliminate the unabsorbed HRP molecules. Then the specific activity of the immunoconjugates was determined by monitoring the kinetic activity of the captured HRP molecules until the absorbance curve has fallen out of the linear range.

The storage stability of the nanoconjugate was also evaluated. Aliquots contain the Ab_{HRP}-Alde-Dex@MNPs nanoconjugates were stored at 4 °C in 50 μ L of filtered PB (MF-Millipore™ membrane filter with 0.45 μ m pore size), the amperometric responses in the absence or he presence of the HRP molecules were recorded.

4.3.2 Electrochemical measurements using the developed Alde-Dex@MNPs as the nanocarriers

4.3.2.1. Preparation of the HOOC-Dex@MNPs based on the Alde-Dex@MNPs

The prepared HOOC-Dex@MNPs following the protocols described in 4.2.7 resulted in low antibody coverage density, thus another functionalization strategy was selected to improve the antibody immobilization capacity on the nanoparticles.

In this part, the preparation of HOOC-Dex@MNPs was based on the reaction between Alde-Dex@MNPs and L-lysine disodium salt monohydrate (AB-NTA).

1 mL Alde-Dex@MNPs nanoparticle suspension containing 10 mg_{Fe} was pipetted into a 5 mL glass tube, followed by decantation with magnet and washing with NaHCO₃ (10 mM, pH 10.0). Then 2 mL AB-NTA solution (20 mg) prepared in the former NaHCO₃ solution was pipetted into the tube, and the pH of the Alde-Dex@MNPs suspension was adjusted to 10.5 after strong ultrasonic treatment. With the gentle rotary for 24 h at room temperature, solid NaBH₄ was added into the suspension with the final concentration of 1 mg mL⁻¹ and kept rotating for another 30 min until stable bonds were generated. Following the purification and enrichment treatment for several cycles, the prepared HOOC-Dex@MNPs were resuspended in deionized water and stored at 4 °C until further immunosensing assays.

4.3.2.2. Immobilization of Ab_{HRP} on the surface activated carboxylated micro/nanocarriers

The covalent immobilization of Ab_{HRP} on the EDC/Sulfo-NHS activated supports were following the same activation/immobilization protocol, regardless of the particle size.

HOOC-MBs as the carriers. 3 μL of HOOC-MBs (carboxylic groups) was first suspended into homogenous solution via vigorous vortexing, then 50 μL of MES buffer was used to wash the particles twice (incubating with wash buffer for 10 min). Then, HOOC-MBs microparticles resuspended in 25 μL activation solution (100 mM EDC/sulfo-NHS) prepared in MES buffer, and the activation treatment was performed for 30 min. After activation, the particles were washed twice with MES buffer to eliminate the residue activation reagents. Then the microparticles were resuspended in 25 μL of anti-HRP solution with concentration of 7.5 μg mL⁻¹, and the antibody immobilization lasted for 30 min. Following the washing steps (50 μL MES buffer), the remaining activated carboxylic groups were blocked. The blocking treatment was performed by incubating with 25 μL ethanolamine solution (prepared in 0.1 M phosphate buffer of pH 8.0 with the final concentration of 1M), and 60 min was selected to realize the full inactivation. The prepared bioconjugates were washed once with Tris-HCl (pH 7.2) and twice with Phosphate buffered saline (PBS), 50 μL of buffer was utilized, respectively.

The fabricated bioconjugates ($\text{Ab}_{\text{HRP-HOOC-MBs}}$) were incubated with 25 μL of pure HRP solution (prepared in 10 mM phosphate buffer) for 30 min to achieve the successful adsorption of HRP analytes. The fabricated HRP- $\text{Ab}_{\text{HRP-HOOC-MBs}}$ immunoassays were washed three times with 50 μL phosphate buffer to eliminate the unbound HRP molecules. To determine the storage stability of the bioconjugates ($\text{Ab}_{\text{HRP-HOOC-MBs}}$), the bioconjugates was stored in 25 μL PBS (filtered by 0.45 μm MF-Millipore™ Membrane Filter) and kept in 4 °C condition until the further immunoassays.

HOOC-Dex@MNPs as the carriers. 1 mL HOOC-Dex@MNPs nanoparticle suspension containing 10 mg_{Fe} was pipetted into a 1.5 mL Eppendorf tube, followed by decantation with magnet and washing twice with 50 μL of MES buffer. Then decanted HOOC-Dex@MNPs was resuspended in 25 μL activation solution (100 mM EDC/sulfo-NHS) prepared in MES buffer, and the activation treatment was performed for 30 min. After activation, the nanoparticles were washed twice with MES buffer to eliminate the residue activation reagents. Then the nanoparticles were resuspended in 25 μL of anti-HRP solution with concentration of 7.5 $\mu\text{g mL}^{-1}$, and the antibody immobilization lasted for 30 min. Following the washing steps (50 μL MES buffer), the remaining activated carboxylic groups were blocked. The blocking treatment was performed by incubating with 25 μL ethanolamine solution (prepared in 0.1 M phosphate buffer of pH 8.0 with the final concentration of 1M), and 60 min was selected to realize the full inactivation of reactive moieties. The prepared bioconjugates were washed once with Tris-HCl (pH 7.2) and twice with PBS, 50 μL of buffer was utilized, respectively.

The fabricated nanobioconjugates ($\text{Ab}_{\text{HRP-HOOC-Dex@MNPs}}$) were incubated with 25 μL of HRP solution (prepared in 10 mM phosphate buffer) for 30 min to achieve the successful adsorption of HRP analytes. The fabricated HRP- $\text{Ab}_{\text{HRP-HOOC-Dex@MNPs}}$ immunoassays were washed three times with 50 μL phosphate buffer to eliminate the unbound HRP molecules. To determine the storage stability of the bioconjugates ($\text{Ab}_{\text{HRP-HOOC-MBs}}$), the bioconjugates was stored in 25 μL phosphate buffer (filtered by 0.45 μm MF-Millipore™ Membrane Filter) and kept in 4 °C condition until the further immunoassays.

4.3.2.3. Amperometric measurement of HRP adsorbed micro/nanoconjugates

Commercial SPCEs were fixed on the PMMA casing assisted by the parafilm first, then the bioconjugates suspension containing analytes/ Ab /Magnetic nanomaterial were pipetted onto the working electrodes of SPCEs by the embedded neodymium magnets. The working electrode contains the analytes/ Ab /Magnetic nanomaterial bioconjugates was immersed into 10 mL reaction buffer, respectively, which consist of 50 mM PB buffer (pH 6.0) and HQ with a final concentration of 1 mM, real-time amperometric signals were starting the recording at -0.20 V

upon quick addition of 50 μL H_2O_2 solution with a concentration of 100 mM. The reaction was maintained for about 60 s before a steady-state current was observed. The difference of amperometric signal changes upon the addition of H_2O_2 was calculated, and the high reproducibility of the replicates ($n = 3$) was observed. Error bars were calculated as the standard deviation of three replicates.

4.4. Dual proteins functionalized Alde-Dex@MNPs—carriers of detection probes

4.4.1 Surface activation of the working electrodes of SPCEs

The surface functionalization of SPCEs was performed by electrical grafting of *p*-aminobenzoic acid (*p*-ABA) aryldiazonium salt on the working electrodes. To achieve the optimal carboxylic grafting density, 20 mg of *p*-ABA was dissolved in 2 mL ice pre-cold HCl (1 M) first, and NaNO_2 (2 mM) aqueous solution dissolved in distilled water was pipetted into the above-prepared *p*-ABA solution (38 μL per 200 μL) under vigorous stirring. After thorough mixing, SPCEs were immersed into 1 mL of the mixture solution for 10-round successive cyclic voltametric (CV) scans (0.0–1.0 V, $v = 200 \text{ mV s}^{-1}$). After the successful electrochemical grafting, carboxylic groups were covalently functionalized on their working electrodes, thorough washing with distilled water followed by drying in the air was performed to get ready-to-use HOOC-Phe-SPCEs.

4.4.2 Preparation of the dual functionalized Alde-Dex@MNPs nanoprobe

For the preparation of HRP and CAb_{CRP} dual functionalized **HRP/CAb@MNPs** nanoprobe, 10 mg_{Fe} Alde-Dex@MNPs were first magnetic decanted and washed with 10 mM NaHCO_3 (pH 10.0) for three times to equilibrium the buffer pH. Then 500 μL protein mixture contains 1 mg mL^{-1} HRP and 6 $\mu\text{g mL}^{-1}$ CAb_{CRP} dissolved in 10 mM NaHCO_3 (pH 10.0) was pipetted into the 1.5 mL Eppendorf tube to resuspend the concentrated nanoparticles. The antibody immobilization was performed under gentle rotation mixing at 25 $^\circ\text{C}$ for 1 h. Then NaBH_4 dissolved in 10 mM ice-cold NaHCO_3 (pH 10.0) was freshly prepared and added into the suspension with the final concentration of 1 mg mL^{-1} to stabilize the reversible imide bonds and achieve the inert surface of nanoconjugates. After washing three times with PB buffer (10 mM, pH 7.0), the HRP/CAb@MNPs bioconjugates were resuspended in 2000 μL PB buffer before the further immunoassay application.

For the preparation of HRP and Streptavidin dual functionalized **HRP/Streptavidin@MNPs** nanoprobe, a protein mixture containing 3 mg mL^{-1} HRP and 50 $\mu\text{g mL}^{-1}$ Streptavidin molecules were utilized. Other protein immobilization procedures and purification treatments were the same as the preparation of **HRP/CAb@MNPs** nanoprobe.

4.4.3 Bioreceptors immobilization on the SPCEs

After the electrochemical grafting of the carboxylic groups, the surface activation was performed to conjugate the bioreceptors.

Similar to the carboxylic activation of HOOC-MBs/HOOC-Dex@MNPs, but liquid drops were covered on the working electrodes and a humid chamber was used to maintain the humid environment. Briefly, 10 μL activation solution (0.1 M EDC/Sulfo-NHS freshly prepared in 25 mM MES buffer) was dropped on the electrodes to fully cover and activate the working electrodes after 30 min incubation. Then the electrodes were rinsed with 2 mL activation buffer and dried at room temperature, the activated electrodes are ready for bioreceptors immobilization.

When using the Strep-HRP and HRP/Streptavidin@MNPs for the detection probes, the CAb_{CRP} bioreceptors were directed on the electrodes. Namely, 5 μL 50 $\mu\text{g mL}^{-1}$ Ab_{CRP} prepared in 50 mM MES (pH 5.0) was dropped on the electrodes and kept in the humid chamber at room temperature for 60 min until the thorough rinsing with PBS buffer (10 mM, pH 7.4). A blocking step was performed by pipetting 10 μL blocking buffer (1 % (w/v) casein prepared in 10 mM PBS buffer with pH 7.4) on the electrodes and incubated for 60 min. Following the rinsing with PBS buffer, 5 μL of standard CRP solution prepared in BB buffer (1 % BSA suspended in PBS buffer) was pipetted on the electrodes and incubated for 60 min at room temperature. After rinsing with 10 mM PBS buffer again, 0.5 $\mu\text{g mL}^{-1}$ Biotin-Ab_{CRP} solution prepared in BB buffer was covering the electrodes and incubated for 30 min to achieve the antigen-recognition, the same PBS washing was performed again.

To fabricate the Strep-HRP/Biotin-Ab-CRP-CAb-Phe-SPCEs immunosensors, 5 μL of Strep-HRP with 1/5000 dilution factor was incubated with Biotin-Ab-CRP-CAb-Phe-SPCEs bioconjugates for 30 min, two successive rinsing with PBS buffer was performed before the addition of 25 μL PBS aliquots for the preservation of electrodes drying. While for the fabrication of HRP/Strep@MNPs/Biotin-Ab-CRP-CAb-Phe-SPCEs immunosensors, 5 μL of HRP/Streptavidin@MNPs (0.5 mg mL^{-1} nanoprobe prepared in 10 mM PB buffer, pH 7.0) was pipetted on the electrodes for 15 min before the thorough rinsing with PBS buffer. Two successive rinsing with PBS buffer was performed before the addition of 25 μL PBS aliquots for the preservation of electrodes drying.

When using the HRP/CAb@MNPs as the nanoprobe, streptavidin was first immobilized on the electrodes as the smart layer to conjugate the Biotin-Ab_{CRP} as the bioreceptors. Briefly, the surface activated electrodes were covered with 5 μL of streptavidin solution (prepared in 25 mM MES buffer) and the incubation was performed at room temperature for 45 min. following

the rinsing with 10 mM PBS of pH 7.4. An aliquot of Biotin-Ab solution with $5 \mu\text{g mL}^{-1}$ prepared in 10 mM PBS of pH 7.4 was pipetted on the functionalized electrodes for 30 min, followed by the washing step with PBS solution. Then a blocking step was performed by pipetting 10 μL blocking buffer (protein mixture contains 0.5 mg mL^{-1} biotin and 1 % (w/v) casein prepared in 10 mM PBS buffer with pH 7.4) on the electrodes and incubated for 90 min. After the rinsing with PBS solution, 5 μL of HRP/CAb@MNPs nanoprobe (0.5 mg mL^{-1} nanoprobe prepared in 10 mM PB buffer, pH 7.0) was pipetted on the electrodes for 60 min before the thorough rinsing with PBS buffer. Two successive rinsing with PBS buffer was performed before the addition of 25 μL PBS aliquots for the preservation of electrodes drying.

4.4.4 Electrochemical measurements using the developed nanocarriers

After the dual-functionalized MNPs were recognized by the CRP target/biotin-Ab_{CRP}, the bioconjugates composites, HRP/CAb@MNPs/CRP-Biotin-Ab-Strep-Phe-SPCEs or HRP/Strep@MNPs/Biotin-Ab-CRP-CAb-Phe-SPCEs, were fixed with the cable connector. The working electrodes contain the bioconjugates (HRP/CAb@MNPs/CRP-Biotin-Ab-Strep-Phe-SPCEs or HRP/Strep@MNPs/Biotin-Ab-CRP-CAb-Phe-SPCEs) were immersed into the reaction cells contain 10 mL of 50 mM PB (pH 6.0) and 1 mM HQ, real-time amperometric signals were monitored at -0.20 V upon addition of 50 μL of a 100 mM H₂O₂ solution. The reaction was continued for about 60 s until a steady-state current was observed. The difference of amperometric signal changes upon the addition of H₂O₂ was calculated, the high reproducibility of the replicates ($n = 3$) was observed. Error bars provided in the Figures were calculated as the standard deviation of three replicates.

4.4.5 Analytical characterization of the fabricated immunosensor

The selectivity of the prepared Ab_{HRP}-Alde-Dex@MNPs immunosensors was also determined by comparing the amperometric responses recorded with the absence or presence of the HRP analytes, but buffer contains interference proteins (human IgG, Hb, HSA) or biomarkers (cTnI, cTnT and NT-proBNP) was replaced by the pure aqueous buffer.

4.5. Using the Alde-Dex@MNPs as the bioreceptor carriers of Ab_{CRP}

4.5.1 Preparation of the Strep-HRP-Biotin-Ab_{CRP}-CRP-Ab_{CRP}-Alde-Dex@MNPs immunosensor

For the preparation of Strep-HRP-Biotin-Ab_{CRP}-CRP-Ab_{CRP}-Alde-Dex@MNPs immunosensors, 0.25 mg_{Fe} Alde-Dex@MNPs stored in 250 μL distilled water were magnetically decanted first, then washed three times with 100 μL 10 mM NaHCO₃ (pH 10.0) to equilibrium the pH of immobilization buffer. Then 200 μL $25 \mu\text{g mL}^{-1}$ CAb_{CRP} dissolved in

10 mM NaHCO₃ (pH 10.0) was pipetted into the 1.5 mL Eppendorf tube to resuspend the magnetically concentrated nanoparticles. The antibody immobilization was performed under gentle rotation mixing at 25 °C for 30 min. Then NaBH₄ dissolved in 10 mM ice-cold NaHCO₃ (pH 10.0) was freshly prepared and added into the suspension with the final concentration of 1 mg mL⁻¹ to stabilize the reversible imide bonds and achieve the inert surface of nanoconjugates. After washing three times with PB buffer (10 mM, pH 7.0), the Ab_{CRP}-Alde-Dex@MNPs bioconjugates were resuspended in 200 µL PB buffer, thoroughly vortexing and sonication were performed to obtain the homogeneously suspension. Afterwards, the bioconjugate suspensions were divided into 10 Eppendorf tubes (20 µL suspension per aliquot), following the magnetic separation and resuspended with 25 µL of 3 % (w/v) BSA solution for 60 min to prevent the unspecific binding. With thorough washing, 25 µL CRP standard prepared in BB buffer (1 % (w/v) BSA prepared in PB buffer) was incubated with blocked bioconjugates for 60 min. After three washing treatments with PB buffer, 25 µL 0.5 µg mL⁻¹ Biotin-Ab prepared in BB buffer was mixed with prepared bioconjugates for 45 min. Then Biotin-Ab_{CRP}-CRP-Ab_{CRP}-Alde-Dex@MNPs conjugates were washed three times with PB buffer, and 25 µL 1/100 Strep-HRP solution prepared in BB buffer was used to achieve the sandwich detection formation. And Strep-HRP-Biotin-Ab_{CRP}-CRP-Ab_{CRP}-Alde-Dex@MNPs immunosensors were kept in PB buffer until the further detection immunoassay.

4.5.2 Analysis of the real samples using the human serum

To explore the real-world application of the fabricated immunosensor, Ab_{CRP}-Alde-Dex@MNPs were applied for the detection of clinical samples instead of CRP standard samples prepared in aqueous buffer. The clinical samples were the human serum collected from the hospital, including the serum samples from healthy individuals and heart failure samples, and those samples were stored at -80 °C until further use.

The determination of the possible matrix effect caused by the high complexity of serum samples was performed first, in which negative samples (serum samples from healthy individuals) with different dilution factors were used to prepare CRP solution, and the amperometric responses were compared until no signal difference was observed. 1/1000 Dilution factor was selected as the optimal option to realize the CRP concentration distributed in the detection range of Ab_{CRP}-Alde-Dex@MNPs immunosensor while preventing the possible matrix effect.

4.5.3 Enzyme-linked immunosorbent assay (ELISA) determination

When CRP was the detection analyte, the results obtained from the Alde-Dex@MNPs as the immunosensing support were compared with the typical ELISA method (the golden standard), and all the reagents are the same as described, the concentration of biomolecules have changed

METHODS

according to the suggestion of the provider. Unless otherwise stated, all the operation was performed under room temperature and the Reagent Diluent solution was used as the preparation buffer of all the proteins (CAb_{CRP}, standard CRP protein, human serum samples, Biotin-Ab_{CRP} and Strep-HRP).

1. The microplate well was coated with 50 μL of a 4.0 $\mu\text{g mL}^{-1}$ capture antibody (CAb_{CRP}) per well dissolved in PBS buffer and incubated overnight at room temperature.
2. Each microplate well was washed with 400 μL of Wash Buffer (10 mM PBS, pH 7.4), followed by a blocking step to incubate with 150 μL of Reagent Diluent (10 mM PBS contains 1 % BSA, pH 7.4) solution each well for 1 h.
3. Repeated washings were performed, followed by incubation with 50 μL of CRP standard/human serum samples, 2 h of incubation time was used.
4. Repeated washings were performed, then incubated with 50 μL of 1 ng mL^{-1} Biotin-Ab_{CRP} solution for 2 h.
5. After three times washing, 1/1,000 Strep-HRP dilution was pipetted into each well and incubated for another 20 min.
6. The colorimetric reaction was performed after washing steps, 50 μL of Substrate Solution (TMB Liquid Substrate System for ELISA) was pipetted into each well and incubate for 20 min to develop the color (the colorimetric reaction was protected from light by covering with aluminum foil).
7. 25 μL of Stop Solution (1N H₂SO₄) was pipetted into each well, and the absorbance values at 450 nm of each well were measured immediately with ELISA plate reader (Magellan V 7.1, TECAN).

Results

5. Results

5.1 Heterofunctional agarose support—A better antibody carrier to control the orientation

INTRODUCTION

Crosslinked agarose beads are porous hydrogels with high controllable particle diameters and porosity, and the typical 3-dimension structures promote its application as biomolecules carriers with high loading density (enzymes and antibodies, etc) also facilitate for the chromatography matrix (size exclusion and affinity interaction, etc) [47]. Due to its hydrophilicity advantage and excellent inert surface toward non-target proteins, it has been developed with different surface chemistries (glyoxyl, maleimide, chelate, chelate-glyoxyl, and amino-epoxy, etc) to be utilized as the antibody carriers [43, 55, 159, 200].

Glyoxyl agarose supports are exceptionally promising candidates for the antibody carriers, because highly activated reactive groups can facilely achieve multipoint interaction in very short time and maintain high stability in alkaline condition [55]. While to achieve the immobilized antibodies with appreciated orientation upon covalent conjugation is not very easy, because their non-selective interaction with NH_2 groups may result in random orientation.

RESULTS

In this section, agarose beads were used as the antibody immobilization supports to evaluate the preserved biofunctionality of immobilized antibodies, which include monofunctional support (glyoxyl support) and heterofunctional support (chelate-epoxy). In addition, two analytes (horseradish peroxidase, HRP and β -galactosidase, BGL) with 10-time molecular weight differences were utilized to validate the effectiveness of developed tail-made antibody carriers.

5.1.1 Antibody immobilization rate on the agarose beads

Three antibody immobilization strategies were applied on the glyoxyl agarose supports, by controlling the pH of the incubation buffer (Figure 5.1-1). When antibody immobilization condition was controlled at pH 8.5, due to the neutral pKa of $\alpha\text{-NH}_2$ (~ 7.5) of N-terminus, only the four N-terminus on the antibody surface were reactive for the covalent conjugation, thus it took about 16 h to achieve the antibody immobilization with half of initial concentration (0.4 mg mL^{-1} anti-HRP) (Figure 5.1-2). Another consideration of antibody immobilization rate on the glyoxyl support is its weaker reactivity under less alkaline condition, which glyoxyl groups demonstrate better reactivity toward NH_2 when $\text{pH} > 10.0$ while much decreased reactivity maybe observed with pH 8.0/9.0 [201].

When controlling the antibody immobilization at pH 10.0, much higher reactivity toward nucleophilic $\epsilon\text{-NH}_2$ can be observed, and many accessible Lys residues on the outer surface of antibody promote the fast antibody-glyoxyl support interaction, thus 30 min was adequate to achieve the full conjugation of anti-HRP.

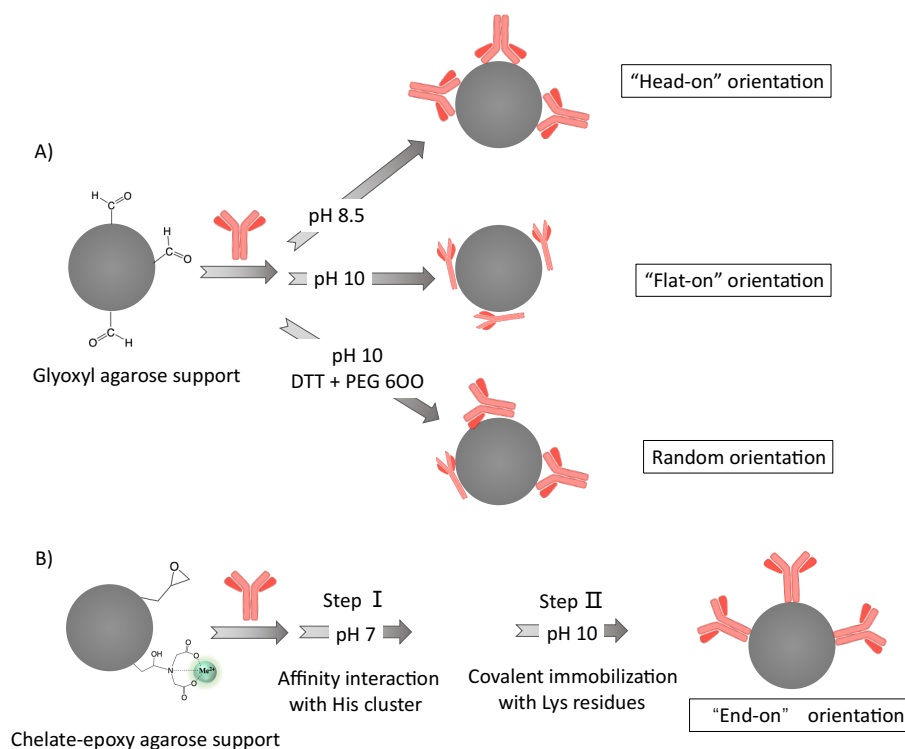


Figure 5.1-1. Scheme of antibody immobilization protocols using agarose beads as the carriers. When glyoxyl-agarose supports were utilized as the antibody carriers, antibodies with different oriented manners can be manipulated by changing the pH of the incubation buffer (A). Antibody immobilization at pH 8.5 results with "head-on" orientation, immobilization at pH 10 results with "flat-on" orientation and immobilization at pH 10 with the presence of additives (DTT and PEG polymers) results with "random" orientation. Antibody immobilization on the chelate-epoxy agarose support via two-step immobilization strategy (affinity interaction and covalent immobilization) results with "end-on" orientation (B).

While the same immobilization pH (10.0 in this case), with the presence of viscous PEG polymers suspension, the diffusion and interaction of antibody with supports will be hindered. In addition, the DTT will interact with glyoxyl groups first before conjugating with NH_2 , and "one-point" interaction was the dominant reaction instead of multipoint interaction, thus a 10-fold slower antibody immobilization rate was observed.

For the heterofunctional supports (chelate-epoxy), the antibody immobilization was performed at two steps and incubation pH exchange was performed after the previous interaction (Figure 5.1-3). The first interaction was the affinity interaction between chelate groups (Ni^{2+}) and His cluster distributed on the Fc fragment, this procedure was also achieved within a short time, and antibodies are prone to be immobilized on the outer part of the agarose beads [43].

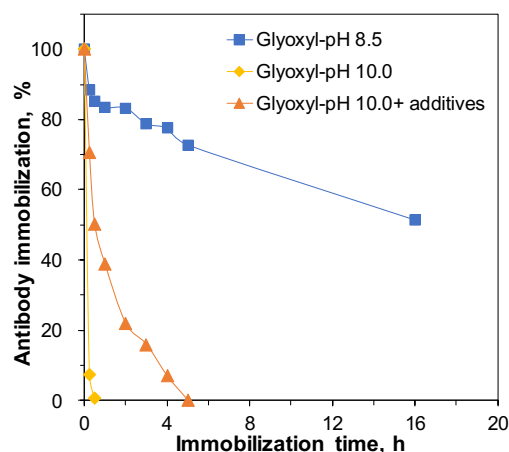


Figure 5.1-2. Antibody immobilization rate on the glyoxyl-agarose supports. By controlling the pH of antibody immobilization buffer, antibody can be immobilized on the glyoxyl support with varied rate, which “multipoint” immobilization under pH 10.0 promoted the fast immobilization rate, “one point” immobilization under pH 10.0 with the presence of additives (DTT and PEG polymers) slowed down the immobilization rate, while N-terminus oriented immobilization under pH 8.5 showed the slowest immobilization rate.

The following treatment was to realize the covalent immobilization of adsorbed antibodies on the agarose beads via the epoxy groups interacting with NH_2 groups near the His cluster. Due to the low reactivity of epoxy groups toward NH_2 , incubating for 24 h can contribute to the irreversible conjugation of antibodies on the chelate-epoxy agarose supports.

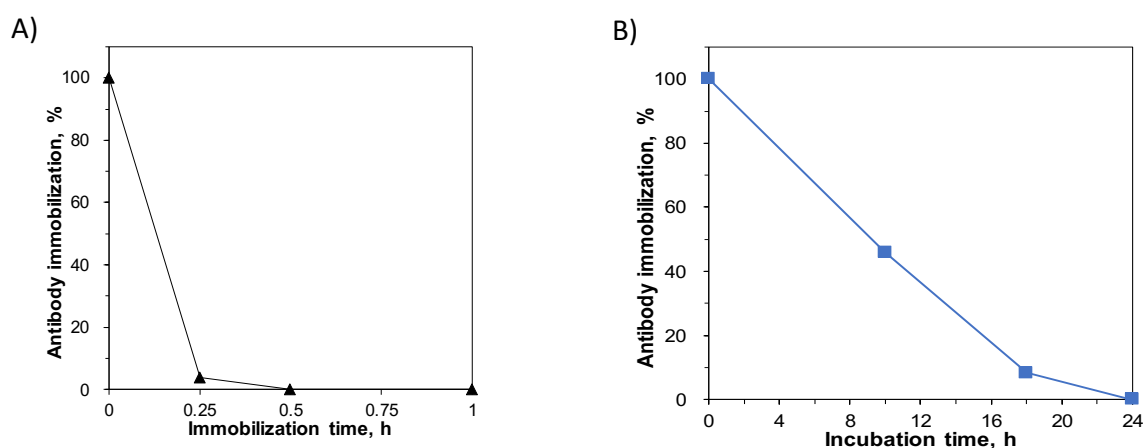


Figure 5.1-3. Antibody immobilization rate on the chelate-epoxy groups via affinity interaction (A) and the evaluation of incubation time under alkaline buffer to realize the covalent immobilization (B). The affinity interaction of chelate groups with His cluster on the Fc fragment was performed at pH 7.0, and the following covalent immobilization of Lys residues nearby the His cluster was performed at pH 10.0 to achieve the irreversible conjugation.

5.1.2 The biofunctionality of immobilized antibody on the agarose beads

By performing the antibody immobilization with different strategies, the preserved biofunctionality of tethered antibodies have demonstrated varied levels (Figure 5.1-4). In general, the remaining biofunctionality of conjugated antibodies on the chelate-epoxy agarose supports was outperformed by the glyoxyl supports.

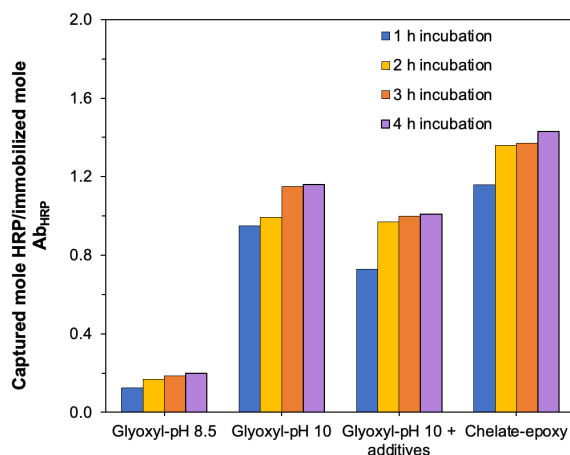


Figure 5.1-4. Determination of the antigen-binding capacity of immobilized anti-HRP using the different immobilization protocols. Four antibody immobilization protocols using the glyoxyl agarose supports and heterofunctional support (chelate-epoxy) were performed, in which pH 8.5 and pH 10.0 with and without the presence of additives (DTT and PEG polymers) were coupled with glyoxyl supports, while antibody immobilization on the chelate-epoxy supports was following the stepwise conjugation strategy. The determination of HRP analytes adsorption rate was performed under 4 °C with the presence of over 20-fold saturated HRP concentration.

Even using the carriers with the same surface chemistries—glyoxyl supports, the difference of involved NH_2 during the covalent immobilization not only affects the variation of immobilization rate but also results in antibodies with different orientation, thus obtaining varied antigen-recognition efficiency. Under pH 8.5, only the N-terminus were available for the covalent conjugation, antibody was likely to be immobilized via the “head-on” orientation. Majority of the antigen-recognition sites were blocked due to the N-terminus being close to the antigen-binding sites, and 0.2 moles HRP per mole immobilized anti-HRP was recognized.

Antibody immobilization directly under pH 10.0 using the glyoxyl support would probably results in “flat-on” orientation. Even though over 80 Lys residues distributed on the outer areas of antibody are accessible, glyoxyl groups will react with the regions bearing the highest density of Lys residues, and four subunits of the antibody are involved in the reaction simultaneously [55]. In this condition, 1.16 moles HRP was captured by per mole immobilized anti-HRP.

The addition of the PEG polymer and DTT slowed the antibody conjugation rate though with an equal amount of accessible NH_2 groups. The slower immobilization rate enhanced the interaction possibility of N-terminus with glyoxyl moieties, in case of N-terminus and Lys residues both demonstrate excellent reactivity under this condition. Thus, instead of “flat-on” orientation, the immobilized antibodies show the “random” orientation, and worse antigen-binding capacity of 1.01 moles HRP per mole Ab_{HRP} on glyoxyl agarose was calculated.

Using the stepwise immobilization of antibody on the chelate-epoxy support, the pre-adsorption of antibody with the “end-on” orientation followed by the covalent immobilization fixed the optimal orientation towards antigens. The His residues distributed on the Fc fragments and its interaction with chelate groups will not involve the Fab fragment although their interaction strength was not as strong as the His-tag/chelate groups [45]. With the adsorption, the following covalent immobilization was targeting the accessible Lys residues near to the adsorption sites instead of randomly targeting the heterogeneously distributed Lys residues. With the correct orientation, the immobilized antibody demonstrates the highest biofunctionality that 1.43 moles HRP per mole Ab_{HRP} was achieved ([Figure 5.1-4](#)).

However, different from the involvement of four subunits during the antibody conjugation on the glyoxyl agarose supports, the antibody coupling on the chelate-epoxy support was not via the simultaneous interaction of whole antibody molecules ([Figure 5.1-5](#)). Calculated from the SDS-PAGE images, 1.56-fold higher gray intensity of heavy chain/light chain was observed with soluble antibody, ratio of supernatant of Ab-agarose bioconjugates decrease to 1.32 using the room temperature immobilization protocol (room temperature at pH 10 for 24 h), and the ratio even decreased to 1.11 after immobilization at 4 °C for 7 days.

This phenomenon can be explained by the spatial selectivity of epoxy groups toward the Lys residues, that the 2nd covalent immobilization happened on the Fc fragment (close to the His cluster), thus light chains were not interacted in this procedure. However, the slower reactivity of epoxy groups is only able to covalently anchor the single heavy chain instead of multipoint interaction via glyoxyl groups [43]. Prolonged incubation under alkaline pH promoted the interaction of epoxy groups with heavy chains, but the spatial conformation of pre-fixed/rigid antibodies structure was not able to achieve the simultaneous immobilization of both heavy chains.

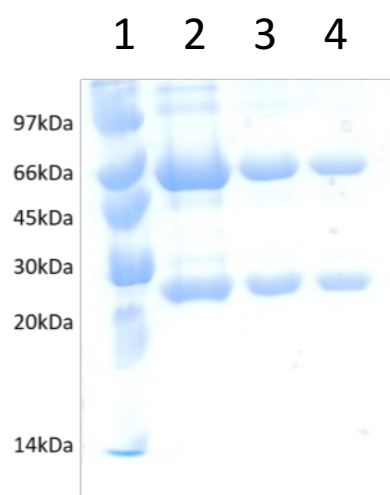


Figure 5.1-5. SDS-PAGE analysis of the supernatant of antibody-supports bioconjugates using the chelate-epoxy supports as the carriers, 12 % separation gel was used to give clear illustration of heavy chain and light chains of the antibody. Lane 1: low molecular weight protein markers, lane 2: soluble anti-HRP with 0.4 mg mL^{-1} , lane 3 and 4 are the supernatant of anti-HRP/agarose support bioconjugates with the difference of 2nd step of covalent immobilization, lane 3 was performed under $25 \text{ }^\circ\text{C}$ for 24 h to achieve the irreversible interaction while lane 4 was following the covalent immobilization under $4 \text{ }^\circ\text{C}$ for 7 days. The gray intensity of each band (heavy chains and light chains were measured, respectively) was determined with GelQuant NET (1.7.8) to calculate the ratio between heavy chain and light chain.

5.1.3 The optimization of functional groups density on the chelate-epoxy agarose support

The two functional groups on the heterofunctional support play distinct functionalities and interact with different accessible residues at controlled conditions, respectively. Chelate groups on the chelate-epoxy supports were modified from the activated epoxy groups, which means the increased density of chelate groups was accompanied with the decrease of epoxy groups (Table 5.1-1). The affinity adsorption of chelate groups with His clusters was hardly affected by the density of chelate groups, 30 min was enough to achieve the fast interaction even with 2 h modification time [45]. However, the biofunctionality of conjugated antibodies were different from the density ratio of [chelate]/[epoxy], the highest antigen-recognition capacity was obtained with 4 h modification time. Good biofunctionality of 1.53 moles HRP per mole Ab_{HRP} was achieved with $10.7\text{-}\mu\text{mol mL}^{-1}$ wet support and $24.6\text{-}\mu\text{mol mL}^{-1}$ wet support of chelate groups and epoxy groups, respectively (Figure 5.1-6).

With the optimization of the density ratio between chelate groups and epoxy groups, another larger analyte-BGL with 10-fold higher molecular weight than HRP- was determined (Figure 5.1-7). BGL is a tetramer protein that its catalytic activity can be facily determined using the o-NPG as the colorimetric substrate [202]. In theory, four-fold higher antigen-binding capacity than HRP was expected under the optimal condition (without the steric hindrance) due to its homomultimericity.

Table 5.1-1 The density of functional groups on the chelate-epoxy agarose support upon the different IDA modification time (0-24 h) with epoxy-activated support.

Modification time of IDA, h	Epoxy groups density, $\mu\text{mol mL}^{-1}$ wet support	Chelate groups density, $\mu\text{mol mL}^{-1}$ wet support	[Chelate] : [Epoxy]
0	35.29 ^a	-	-
2	31.10	4.19 ^b	0.13
4	24.56	10.73	0.43
8	13.12	22.17	1.68
24	12.51	22.78	1.82

All the data presented in the table was the average value of duplicate experiments (n = 3).

a: the density of epoxy groups was determined using the colorimetric method described in section X.X.

b: the density of chelate groups were derives from activated epoxy groups on the agarose support, its calculation was performed by subtracting the remaining epoxy groups density after the IDA functionalization.

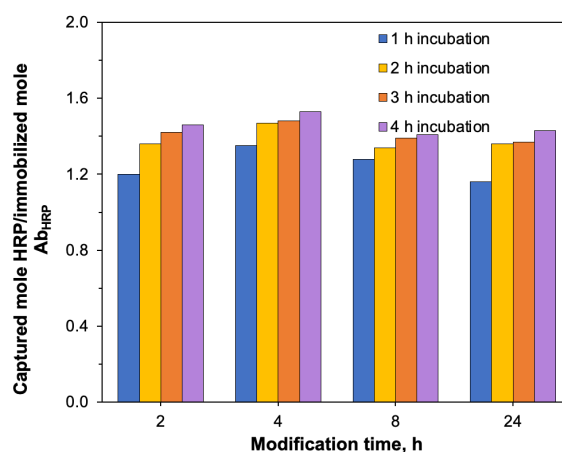


Figure 5.1-6. The effect of IDA modification time (2-24 h) on the antigen-recognition capacity

of immobilized Ab_{HRP} on the porous chelate-epoxy agarose supports. The determination of HRP analytes adsorption rate was performed under 4 °C with the presence of over 20-fold saturated HRP concentration.

In contrast, even lower biofunctionality of immobilized Ab_{BGL} was determined, in which the antigen/ Ab_{BGL} ratios were decreased for three different immobilization protocols. Fortunately, the immobilized anti-BGL on the chelate-epoxy still demonstrates the highest biofunctionality, and 2-fold higher antigen-binding capacity than the suboptimal immobilization protocol (glyoxyl agarose beads under pH 10.0 incubation).

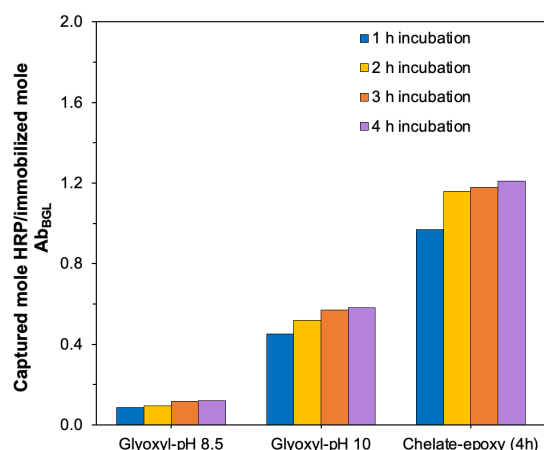


Figure 5.1-7. The antigen-recognition capacity of immobilized anti-BGL on the glyoxyl agarose support (under the pH 10.0 immobilization condition) and chelate-epoxy agarose support (two-step immobilization strategy with the IDA modification time of 4 h). The determination of BGL analytes adsorption rate was performed under 4 °C with the presence of over 20-fold saturated BGL concentration.

The possible reason for decreased biofunctionality of immobilized anti-BGL was caused by the steric hindrance of overcrowded antibodies on the outer surface of agarose beads. The antibody immobilization was too fast to realize the effective diffusion of antibodies into the agarose pores [43], and the limited distance of heterogeneously distributed antibodies caused the self-sheltering of neighboring antibodies. In this case, antigens with larger molecular weight will cause the even worse results due to the pre-adsorbed antigen would block the accessible antigen-recognition sites of antibodies. Slowing down the antibody immobilization rate would be a better strategy to achieve the free accessible antibody molecules [43].

5.1.4 Antigen recovery experiments from diluted human serum

To explore the potential application of the developed chelate-epoxy supports as the antibody carriers, the anti-HRP conjugated chelate-epoxy carriers with the optimal group density were utilized to recover the spiked HRP prepared in diluted serum samples (Table 5.1-2).

Table 5.1-2 Recovery experiments of spiked HRP analytes in the human serum by the chelate-epoxy support.

Entry	Dissolve solvent	Add concentration, mM	Detected concentration, mM	Recovery, %
1	Aqueous buffer	0.125	0.124 ± 0.011	99.4
2		0.25	0.251 ± 0.018	100.6
3		0.5	0.512 ± 0.031	102.3
4	Human serum	0.125	0.121 ± 0.006	96.8
5		0.25	0.246 ± 0.051	98.5
6		0.5	0.544 ± 0.023	108.7

The HRP recovery efficiency from aqueous buffer demonstrated good applicability, which HRP with three concentrations were successfully recovered and recovery rate of 99.4 %-102.3 % were calculated. When recovering the HRP analytes from diluted human serum, a lower recovery rate was observed with lower HRP concentration (96.8 %), while the applicability of higher concentrations validated the effectiveness of the developed chelate-epoxy supports as the promising candidates for the immunosensing carriers.

5.2 Colloidal stability evaluation of functionalized iron oxide nanoparticles–Dextran coating improves the stability in aqueous buffer

INTRODUCTION

Faced with the limited analytes diffusion ability in the porous agarose beads, antibody carriers with non-porous structures are quite appealing substitutes to solve this problem. Non-porous iron oxide nanoparticles are specifically interesting protein immobilization carriers for those unique properties endowed by their ultra-small dimension, and their fast magnetic response with a permanent magnet facilitate the purification/recovery treatment [64]. However, the colloidal stability of MNPs is a big challenge before further application, extra coating layers on the nanoparticles have been reported to significantly improve their dispersion stability [66]. When dextran–polysaccharides with excellent biocompatibility and water-solubility– is used as the functionalization layer, it has been proven to prevent the self-agglomeration, narrow the particle size distribution and enhance the physicochemical properties of bare IONPs, although saturation magnetization of coated IONPs may be decreased [203-205]. For the dextran modification treatment on the IONPs surface, the dextran molecular size and loading amount need to be taken into consideration to obtain a good equilibrium between colloidal stability and magnetic response [206].

RESULTS

As stated above, the aim of this chapter is to synthesize surface modified IONPs using varied strategies, the dispersion stability in different physiological pH and magnetic separation abilities were evaluated.

5.2.1 Comparison of four nanoparticles with their colloidal stability and magnetic separability in distilled water

Bare MNPs were first synthesized by the conventional co-precipitation method, and the surface modification treatment was performed using a post-functionalization strategy. Three surface treatment strategies were used to obtain different nanoparticles, including γ -Fe₂O₃ nanoparticles via the Fe(NO₃)₃/HNO₃ treatment, silica layer coated nanoparticles (SiO₂@MNPs) and dextran functionalized and further crosslinked nanoparticles (Dextran@MNPs) (Figure 5.2-1). The detailed surface functionalization strategies have been described in section 4.2 of “Method”, and dextran modification treatment was performed using the mechanical stirring strategy if not specifically stated.

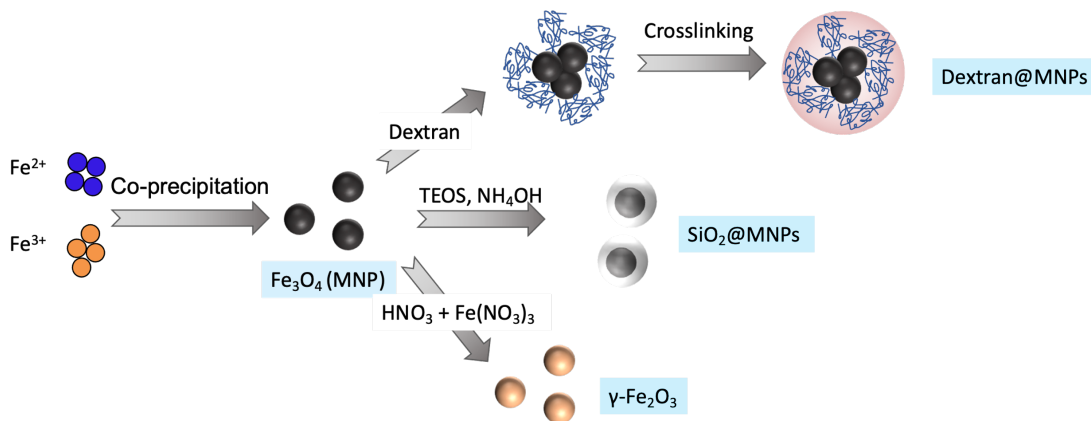


Figure 5.2-1. Scheme of synthesis and further surface functionalization of bare iron oxide nanoparticles.

The colloidal stability of different nanoparticles was evaluated by monitoring the absorbance change (400 nm) of nanoparticles suspension in the distilled water, pH of distilled water was adjusted with NaOH/HCl (Figure 5.2-2).

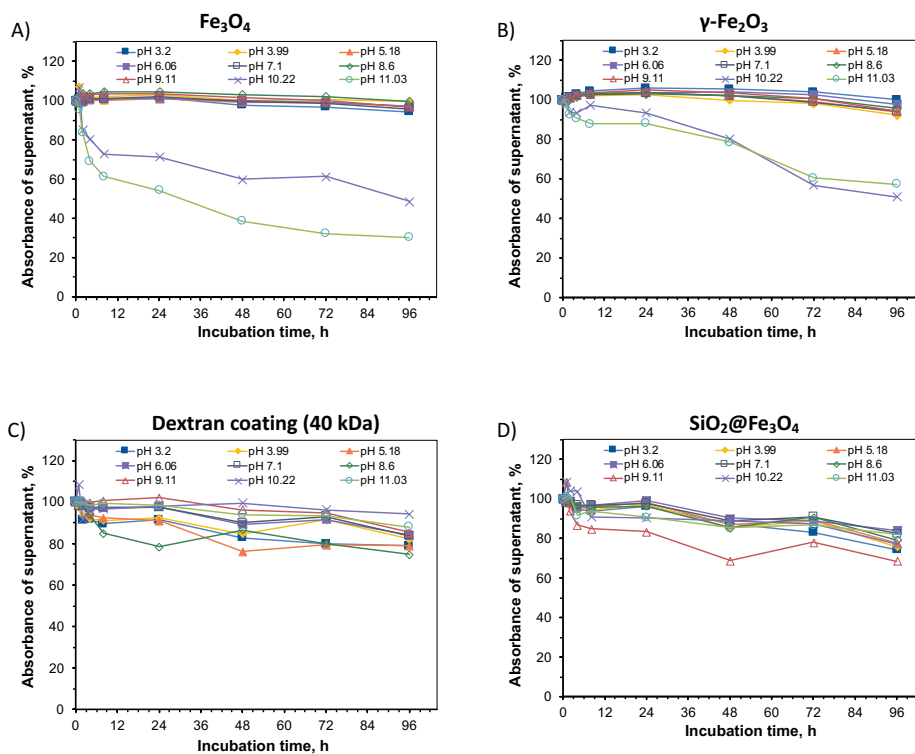


Figure 5.2-2. Colloidal stability of different nanoparticles in distilled water with different pH. The distilled water was adjusted to specific pH (3–11) with NaOH/HCl, and the absorbance values of the supernatant nanoparticle solutions were monitored under 400 nm (ambient temperature) with a spectrophotometer at different time intervals.

Bare Fe_3O_4 MNP demonstrated superior dispersion stability in the pH range of 3–9, negligible absorbance decrease was observed in this pH range. While instability was observed with alkaline pH (pH 10 and pH 11), self-agglomeration of nanoparticles caused the fast absorbance to descend in the first 3 h, afterward, the decreasing tendency was slowed down. For the $\gamma\text{-Fe}_2\text{O}_3$ nanoparticles, bare surface contributes to the quite similar performance with bare Fe_3O_4 MNP, although minor absorbance decreases with pH 3–9 and slightly improvement of stability at pH 10–11 was observed. When the bare surface was modified with dextran and silica layer, the steric repulsion force can prevent the self-agglomeration and maintain the colloidal suspension for a relatively long period (Figure 5.2-2). Although $\text{SiO}_2\text{@MNPs}$ and Dextran@MNPs demonstrated the absorbance decline in all the pH ranges, 80–90 % of absorbance in the supernatant was maintained over 96 h. In addition, the colloidal stability of $\text{SiO}_2\text{@MNPs}$ and Dextran@MNPs in the alkaline range was highly improved.

The magnetic separation ability of different nanoparticles was evaluated for the following step (Figure 5.2-3), as it is also a crucial parameter for their application as nanocarriers. Instead of the portable neodymium magnet, the integrated magnet in the spectrophotometer (Jasco STR-773) was used to record the continuous absorbance alternation. Due to the weaker magnetic attraction force of the integrated magnet, the nanoparticles separation procedure was significantly slower, but it is a useful tool to quantify the potential magnetic response ability of magnetic nanoparticles.

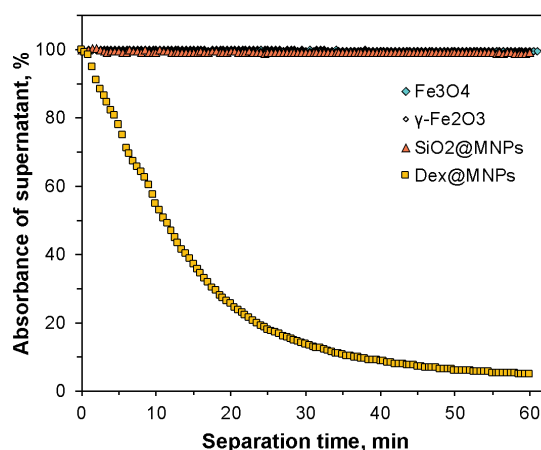


Figure 5.2-3. Evaluation of the magnetic separation ability of different nanoparticles using the integrated magnet in the spectrophotometer (Jasco STR-773). The nanoparticles suspension was prepared in distilled water without the pH adjustment (pH ~ 6.5 in this case).

Out of our expectation, there was no noticeable absorbance decrease for $\gamma\text{-Fe}_2\text{O}_3$ nanoparticles, Fe_3O_4 MNPs and $\text{SiO}_2\text{@MNPs}$, while Dextran@MNPs showed good magnetic response with the weak magnetic field. The reason may be because the small size of single nanoparticles

(~13.54 nm) is not separable with the weak magnetic field, directed magnetic forces are not comparable with randomly directed Brownian forces in such case, even with the presence of external magnet [207]. This result gives the hint that Dextran@MNPs is the cluster formation instead of individual nanoparticles like other types of nanoparticles.

5.2.2 The evaluation of colloidal stability of bare MNP and Dextran@MNPs in aqueous buffer

Although the great colloidal stability of nanoparticles was maintained in distilled water, the requirement of real-world application places great emphasis on their stability under an aqueous buffer. Thus, the anti-aggregation performance of bare Fe_3O_4 MNPs and Dextran@MNPs were monitored, respectively (Figure 5.2-4).

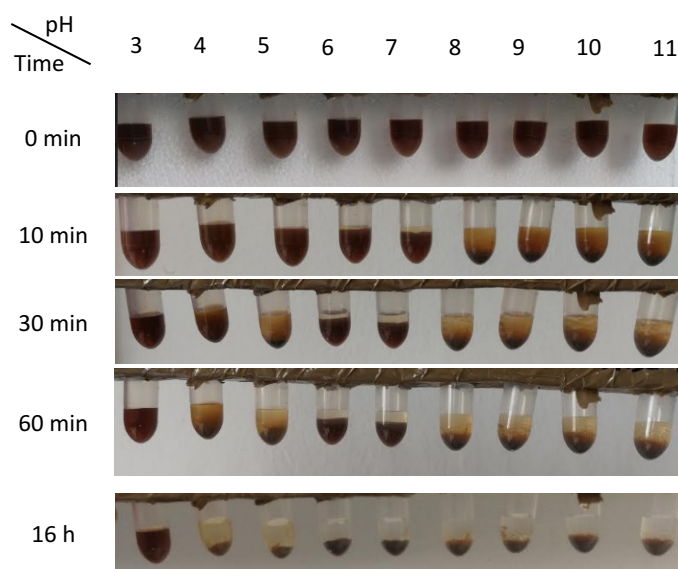


Figure 5.2-4. Colloidal stability of bare Fe_3O_4 nanoparticles (MNPs) in different aqueous buffer (pH range from 3 to 11). pH 3: 50mM Glycine-HCl; pH 4-5: 50mM NaAc-HAc; pH 6: 50mM MES; pH 7-8: 50mM HEPES; pH 9-11: 50mM NaHCO_3 . The pictures were taken at different time intervals.

When bare Fe_3O_4 MNPs were exposed to the aqueous buffer, they show different aggregation rates and sedimentation performances with varied pHs. Observed with a similar phenomenon in the distilled water, bare Fe_3O_4 MNPs showed the highest instability in the alkaline buffer (pH 8–11) that obvious aggregation and following sedimentation can be achieved within 10 min. Although slower self-agglomeration was shown in acidic conditions (pH 4–7), the bare nanoparticles were still prone to form aggregates after 30–60 min incubation, while extreme stability was observed with pH 3, probably due to the abundant protonated Fe-OH under acidic pH provide adequate negative charge for the self-repulsion against neighboring nanoparticles.

With the dextran coating, the possible self-interaction of neighboring nanoparticles was prevented by the external dextran layer, thus omitting the potential of self-agglomeration (Figure 5.2-5). Dextran@MNPs demonstrated great homogeneous dispersion across all the detected pH range, there were no observable aggregation or sedimentation for at least 16 h, which prove their better potentiality as the nanocarriers over bare nanoparticles.

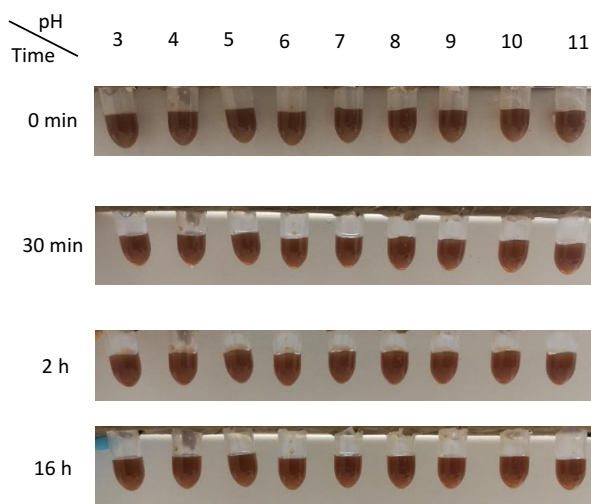


Figure 5.2-5. Colloidal stability of dextran coated Fe_3O_4 nanoparticles (Dextran@MNPs) in different aqueous buffer (pH range from 3 to 11). The dextran (40 kDa) coating was performed with 1:1 (m/m) of MNPs: Dextran. The pictures were taken at different time intervals.

Due to the presence of abundant hydrogen bonds, dextran polymers can easily interact with nanoparticles under strongly alkaline solution, the following crosslinking treatment is essential to prevent the dissociation and functionalize the epoxy groups on the surface of the nanoparticles (Figure 5.2-6) [76].

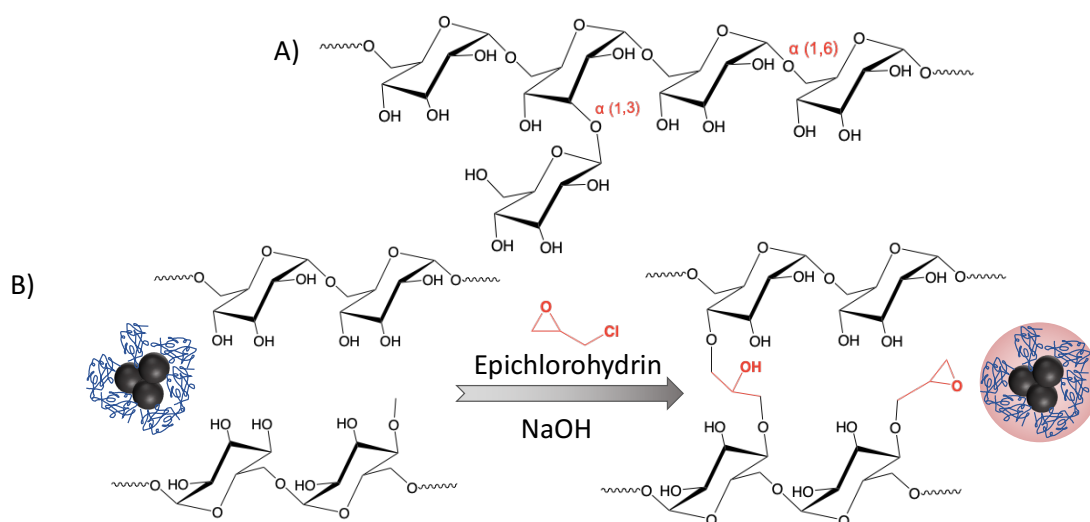


Figure 5.2-6. The simplified dextran structure (A) and crosslinking with epichlorohydrin contributes the epoxy groups functionalization on the nanoparticles surface (B).

5.2.3 The optimization of dextran coating parameters to achieve better coating efficiency

As the dextran molecular size and grafting ratio can affect the properties of coated nanoparticles [205, 208], the molecular weight of dextran and the ratio of MNP/dextran were investigated. Dextran with different sizes (10, 22.5, 40 and 70 kDa) was functionalized on the bare nanoparticles and be evaluated for their stable performance under aqueous buffers (Figure 5.2-7). Results showed that the dispersibility of Dextran@MNPs is highly related to the dextran molecular weight, dextran with larger molecular weight is likely to provide better suspension performance. For 10 kDa dextran coating, the instability was more obvious that only ~20–70 % nanoparticles were remained in the supernatant after 72 h incubation, especially for the pH range over 9.0. With 22.5 kDa dextran coating, Dextran@MNPs demonstrate better stability while 50 % nanoparticles were sedimented when prolonging the incubation time. With the even higher molecular weight of dextran (40 and 70 kDa), the stability evaluation was not significantly improved as expected, thus 40 kDa dextran was selected in this case.

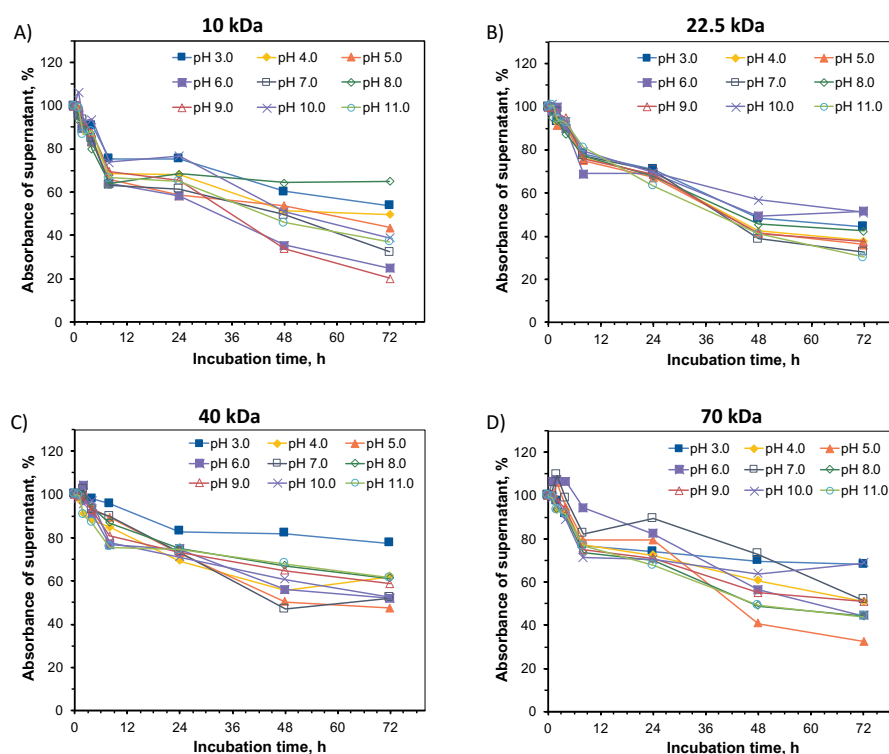


Figure 5.2-7. The influence of molecular size of dextran layers (10–70 kDa) on the colloidal stability of functionalized nanoparticles. The dextran coating was performed with 1:1 (m/m) of MNPs: Dextran and the absorbance values of the supernatant nanoparticle solutions were monitored under 400 nm (25 °C) with spectrophotometer at different time intervals.

It's worth noticing that Dextran@MNPs (40 kDa) had the best colloidal stability at pH 3.0 while demonstrating the worst stability at pH 5.0/6.0. In order to investigate the sufficient

weight ratio of dextran to magnetite, the dispersity of Dextran@MNPs (40 kDa) was compared with different MNP:Dextran ratios (from 4:1 to 1:8) under the most stable and unstable pH to determine the minimum coating amount (Figure 5.2-8). When incubating under pH 6.0, MNP:Dextran (m/m) with 4:1 was not enough to promote the sufficient coating on the nanoparticles, aggregation was observed within 10 min. With the increase of dextran coverage to 2/1, the colloidal suspension will last less than 1 day, the stabilized status able to last for ~ 5 days when the dextran coverage is higher than 1/1.

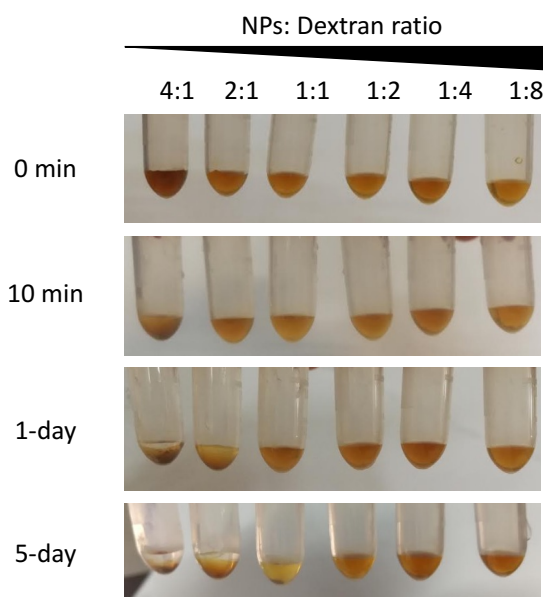


Figure 5.2-8. The stability evaluation of dextran functionalized nanoparticles (Dextran@MNPs) with controlled MNPs: Dextran ratio (40 kDa dextran with m/m from 4:1 to 1:8) during surface coating, aqueous buffer with pH 6.0 was monitored. The pictures were taken at different time intervals.

The results above showed the necessary coverage density of dextran to achieve the steric hindrance stabilization, further the absorbance change was used to quantify the stabilization index of Dextran@MNPs (Figure 5.2-9). As expected and consistent with previous results, the increased surface coverage density of dextran contributed to the less tendency of self-aggregation or sedimentation, and MNP: Dextran with a 1:8 ratio was the most positive ratio to achieve the stable colloidal suspension for at least 8 days. Therefore, dextran with 40 kDa molecular weight and 8-time loading concentration of dextran on the nanoparticles coating process were the optimized parameters.

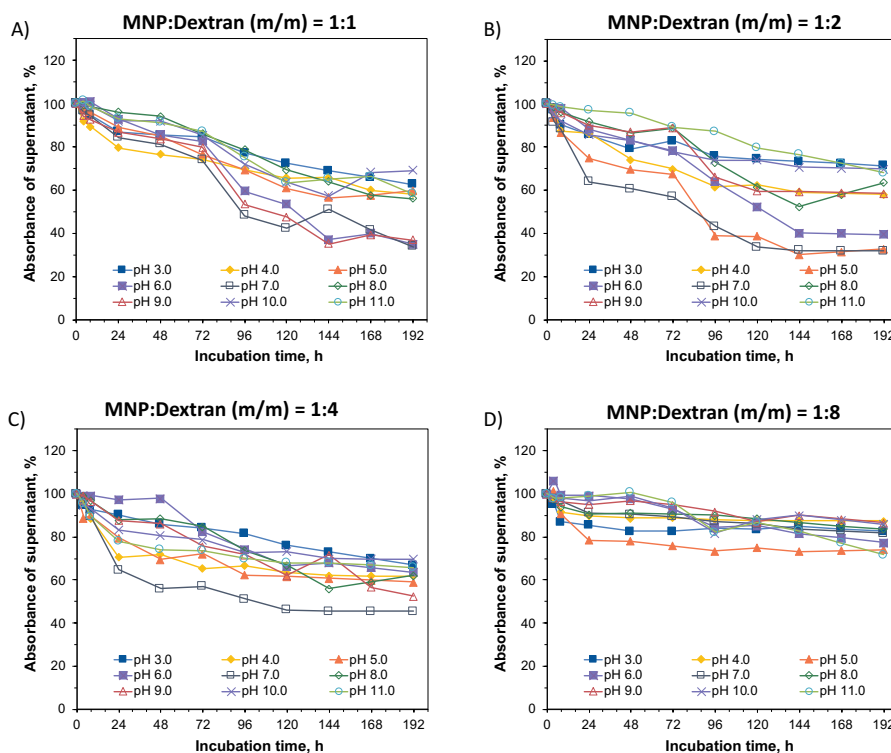


Figure 5.2-9. The stability evaluation of dextran functionalized nanoparticles (mechanical stirring) with controlled MNPs: Dextran ratio (40 kDa dextran with m/m from 1:1 to 1:8) during surface coating, the absorbance values of the supernatant nanoparticle solutions were monitored under 400 nm (ambient temperature) with spectrophotometer at different time intervals. The dextran functionalization was performed under ambient temperature with the continuous mechanical stirring treatment for 24 h.

5.2.4 The dextran functionalization strategy: mechanical stirring or sonication

Afterward, instead of using the mechanical stirring to perform the dextran functionalization, sonication treatment was utilized as another substitute and compared the performance of Dextran@MNPs (Figure 5.2-10). Results indicated that sonication functionalized nanoparticles outperformed the mechanical stirring to obviously improve its colloidal stability in all the four MNP: Dextran loading ratios (1:1 to 1:8). Four-fold of dextran loading concentration was enough to maintain the colloidal suspension of Dextran@MNPs for over 8 days that absorbance of Dextran@MNPs suspension was recorded higher than 90 % in most cases.

To satisfy the requirement of real-world and facilitate further immunosensor fabrication, the Dextran@MNPs were tested for their magnetic separability using a portable neodymium magnet (Figure 5.2-11). Though less dispersion and stability were observed with mechanical stirred Dextran@MNPs, all the Dextran@MNPs can be easily separated and recovered from the suspension with a portable neodymium magnet within 2 min. In contrast, the sonication

treatment promotes the more efficient surface coverage, while demonstrating lower magnetic separability that 2 h separation was not able to achieve sufficient recovery.

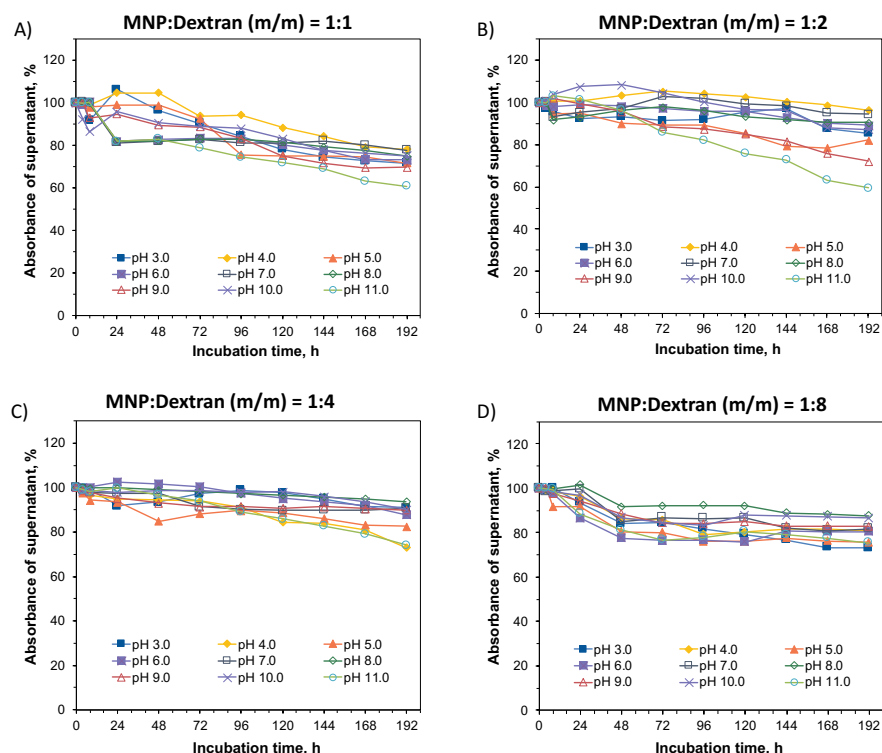


Figure 5.2-10. The stability evaluation of dextran functionalized nanoparticles (sonication) with controlled MNPs: Dextran ratio (40 kDa dextran with m/m from 1:1 to 1:8) during surface coating, the absorbance values of the supernatant nanoparticle solutions were monitored under 400 nm (ambient temperature) with spectrophotometer at different time intervals. The dextran functionalization was performed under 25 °C with the continuous sonication treatment for 6 h.

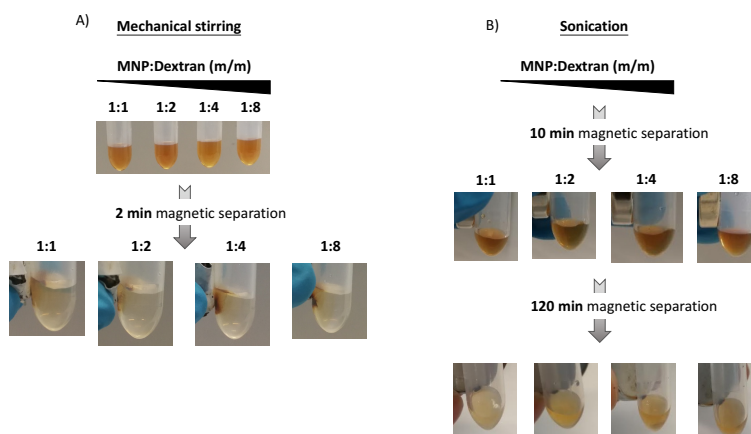


Figure 5.2-11. The evaluation of **magnetic separation ability** of Dextran@MNPs (40 kDa) with different functionalization strategies, mechanical stirring (A) and sonication (B) were compared using neodymium magnet. The pictures were taken at different time intervals.

5.2.5 Quantification of remaining functionality of immobilized antibody with grafted reactive groups on the Dextran@MNPs surface

With the optimization of the dextran functionalization parameters (coating technique, dextran molecular weight and loading ratio), the determination of the functionality of immobilized antibody was compared with different reactive groups (Figure 5.2-12). Derivate from the epoxy groups grafted via the dextran crosslinking treatment, aldehyde-Dex@MNPs, HOOC-Dex@MNPs and chelate-Dex@MNPs were fabricated, respectively.

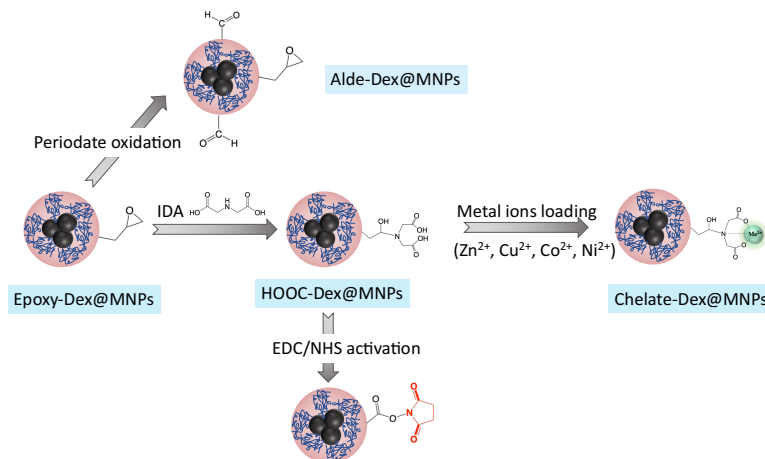


Figure 5.2-12. The scheme of surface functionalization treatment to graft different functional groups on the Dex@MNPs surface, aldehyde groups, chelate groups and carboxylic groups were grafted, respectively.

Firstly, the crosslinking parameters (concentration of NaOH, NaBH₄ and epichlorohydrin) were optimized to achieve the highest epoxy groups density on the Dextran@MNPs surface, the quantification was performed indirectly via the determination of ζ -potential value after reacting with IDA (Figure 5.2-13).

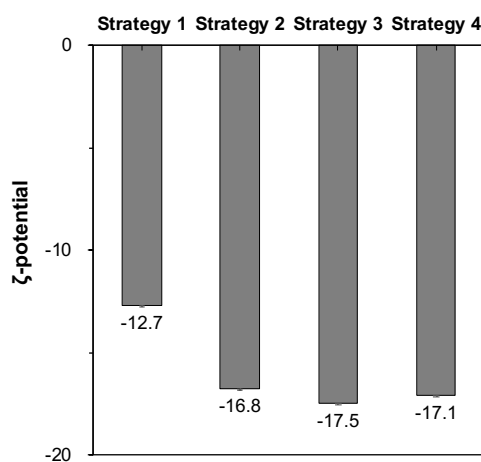


Figure 5.2-13. Optimization of crosslinking parameters (concentration of NaOH, NaBH₄ and epichlorohydrin) to achieve a higher density of epoxy groups on the Dextran@MNPs surface.

Crosslinked Dextran@MNPs (epoxy-Dextran@MNPs) were reacted with IDA to grafted carboxylic groups, and the zeta-potential of modified HOOC-Dextran@MNPs were evaluated and compared. Strategy 1 was 1M NaOH, 0.225 mL $\text{mg}_{\text{Fe}}^{-1}$ epichlorohydrin; strategy 2 was 1M NaOH, 10 mg mL^{-1} NaBH₄, 0.45 mL $\text{mg}_{\text{Fe}}^{-1}$ epichlorohydrin; strategy 3 was 1M NaOH, 0.45 mL $\text{mg}_{\text{Fe}}^{-1}$ epichlorohydrin and strategy 4 was 2M NaOH, 10 mg mL^{-1} NaBH₄, 0.225 mL $\text{mg}_{\text{Fe}}^{-1}$ epichlorohydrin.

Results indicated that epichlorohydrin concentration was a bigger influence on the epoxy density, and the optimized crosslinking condition is 1M NaOH with 0.45 mL of epichlorohydrin per mg_{Fe} .

The modification time of Epoxy-Dextran@MNPs with IDA was controlled from 0.5 h to 8 h, results revealed that 2 h modification time was likely to reach the highest carboxylic group density (Figure 5.2-14A). Ab_{HRP} was used as the model to determine the antibody immobilization capacity corresponding to the varied modified Ni²⁺-chelate-Dextran@MNPs nanocarriers (Figure 5.2-14B). Unmodified Dextran@MNPs were hardly to anchor the antibody due to the poor reactivity of epoxy groups under neutral pH [53]. With the increase of modification degree, the immobilized antibody was gradually improved while the highest antibody coverage density was achieved after 4 h functionalization with about 4 μg Ab_{HRP} per mg_{Fe} Ni²⁺-chelate-Dextran@MNPs.

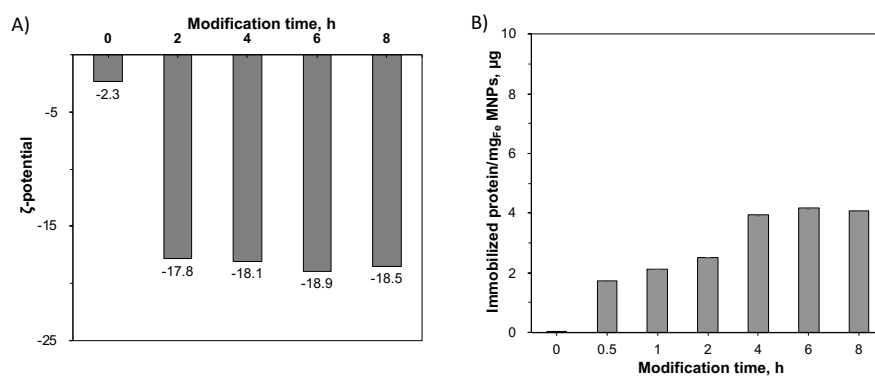


Figure 5.2-14. The effect of IDA modification time of HOOC-Dextran@MNPs on its zeta-potential (A) and immobilization capacity of antibody on Ni²⁺-chelate-Dextran@MNPs (B). The antibody immobilization condition was controlled with 10 mM HEPES, pH 7.0 for 30 min incubation time.

To explore the higher antibody coverage and better functionality of immobilized Ab_{HRP}, the effect of metal ion types and pH of the incubation buffer were investigated (Figure 5.2-15).

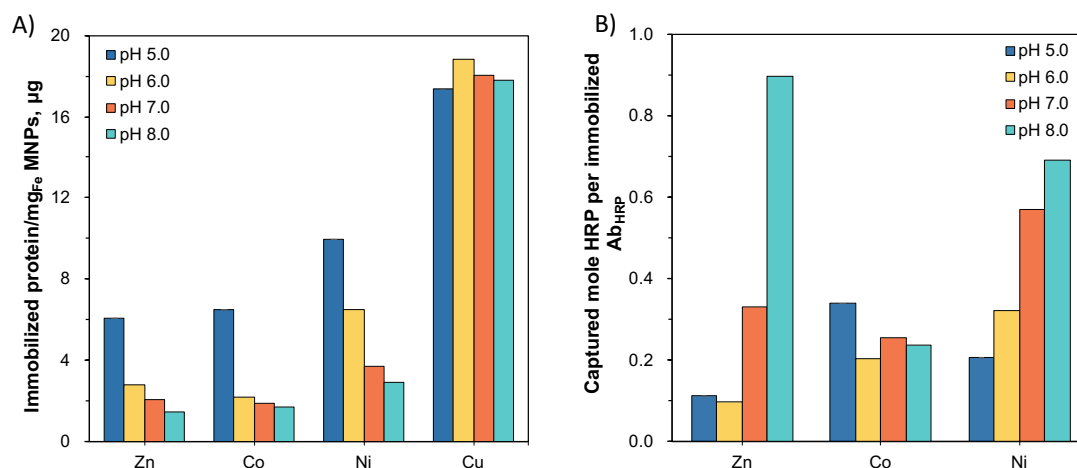


Figure 5.2-15. The antibody immobilization capacity (A) and antigen-recognition ability of immobilized anti-HRP on the *chelate-Dex@MNPs* were evaluated. IDA modification time was selected as 4 h and the antibody immobilization time was 30 min. Different incubation pHs (pH 5.0–7.0) were evaluated with four metal ions (Zn^{2+} , Cu^{2+} , Co^{2+} and Ni^{2+}), Cu^{2+} -chelate-Dex@MNP caused obvious aggregation during incubating with antibody, the abnormal concentration of adsorbed antigens was observed.

The immobilization ability of different Me^{2+} -chelate-Dextran@MNPs was varied, however, Cu^{2+} -chelate-Dextran@MNPs caused self-aggregation during the incubation with antibody, which achieved about 18 μg Ab_{HRP} per mg_{Fe} MNPs and irrational density of analytes (HRP) was absorbed via non-specific adsorption. Ni^{2+} -chelate-Dextran@MNPs outperformed other metal ions (Zn^{2+} and Co^{2+}) with all four incubation pHs, and incubation pH had a significant influence on the immobilization capacity of chelate-Dextran@MNPs that acidic pH prone to adsorb the higher antibody than neutral or alkaline pH. However, the antigen-recognition ability of immobilized Ab_{HRP} has achieved the highest remaining functionality at pH 8.0 for Zn^{2+}/Ni^{2+} -chelate-Dextran@MNPs. Unfortunately, the chelate-Dextran@MNPs was only capable of capturing 0.9-mole analyte per immobilized mole Ab_{HRP} under the optimized condition.

The carbodiimide chemistry (EDC/NHS) activated $HOOC-Dex@MNPs$ was further investigated (Figure 5.2-16). Activated $HOOC-Dex@MNPs$ immobilized with negative controls (BSA, rabbit IgG and sheep IgG) were not able to recognize the HRP analytes, which demonstrated good specificity of the Ab_{HRP} .

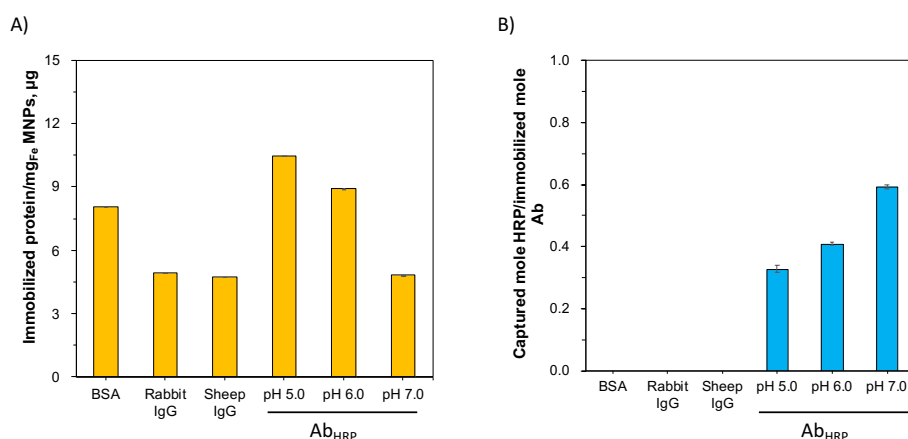


Figure 5.2-16. The protein immobilization density (A) and antigen-recognition ability of immobilized antibodies/protein on the *EDC/NHS* activated *HOOC-Dex@MNPs* (B) were evaluated. BSA, rabbit IgG and sheep IgG were used as the negative controls, the antibody immobilization time was 2 h and blocked with ethanolamine after protein immobilization. The *EDC/NHS* concentration was 1 mM (*EDC/NHS* ratio of 1:4) and the activation pH was 10 mM MES, pH 5.0, the anti-HRP immobilization condition was varied from pH 5.0 to pH 7.0.

Similar to chelate-Dextran@MNPs, pH 5.0 promoted the highest Ab_{HRP} immobilization density while resulting in the lowest antigen-recognition functionality, and the optimized functionality was observed with pH 7.0 immobilization condition that 0.9-mole analyte per immobilized mole Ab_{HRP} was captured. To facilitate the partly activated carboxylic groups to achieve the pre-physical adsorption before covalent interaction [35], the *EDC/NHS* concentration was optimized (1–50 mM) (Figure 5.2-17).

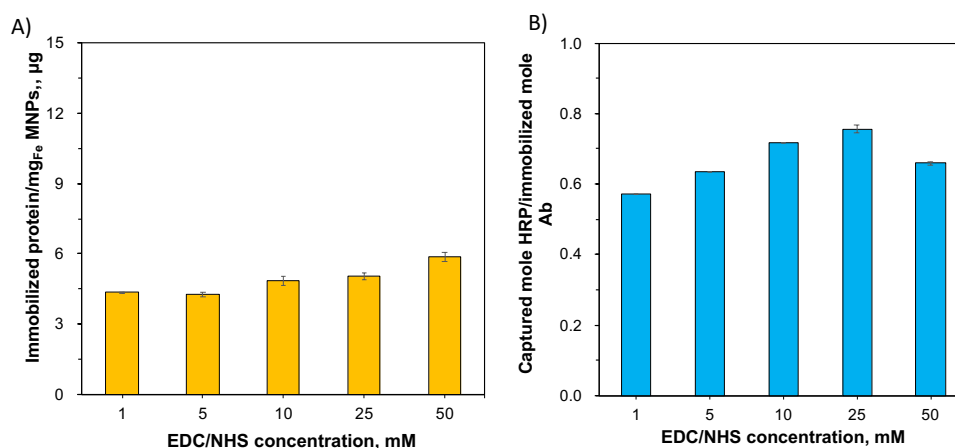


Figure 5.2-17. The effect of *EDC/NHS* concentration (fixed 1:4 ratio) on the antibody immobilization density (A) and antigen-recognition ability of immobilized antibodies/protein on the *EDC/NHS* activated *HOOC-Dex@MNPs*(B) were evaluated. The antibody immobilization time was 2 h and incubated at 10 mM HEPES, pH 7.0.

Results demonstrated that concentration of activation reagents had a minor effect on the antibody immobilization amount that 35 % higher Ab_{HRP} was tethered even EDC/NHS increased for 50-fold times. However, only 0.9-mole analyte per immobilized mole Ab_{HRP} can be recognized under the optimized condition (25 mM EDC/NHS).

The applicability of Aldehyde-Dex@MNPs as the antibody nanocarriers was examined (Figure 5.2-18). Aldehyde-Dex@MNPs demonstrated good antibody coverage with 11.4 μg Ab_{HRP} per mg_{Fe} MNPs under pH 10 incubation via the heterogeneously distributed Lys residues, while 5.4 μg Ab_{HRP} per mg_{Fe} MNPs was achieved with N-terminus under pH 8.5 incubation. And the results about the determination of remaining functionality of conjugated Ab_{HRP} showed consistency with previous outcomes [45], that Lys residues achieved better antigen-binding capacity with 1.0-mole analyte per immobilized mole Ab_{HRP} can be quantified. While N-terminus gave the worst accessibility of immobilized antibodies, only 0.36-mole analyte per immobilized mole Ab_{HRP} was applicable, and random orientation results with the presence of DTT gave moderate functionality of tethered antibody.

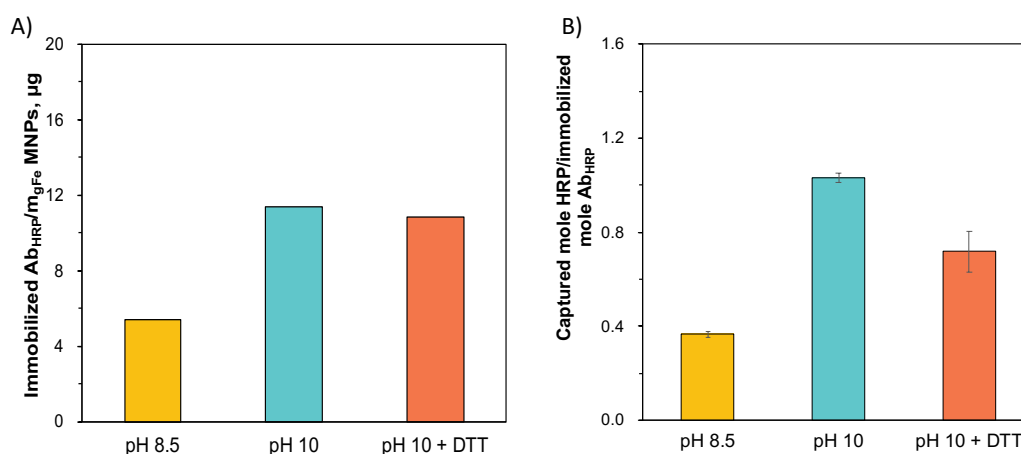


Figure 5.2-18. The protein immobilization density (A) and antigen-recognition ability of immobilized antibodies/protein on the Aldehyde-Dex@MNPs(B) were evaluated. The Aldehyde-Dex@MNPs were prepared under the controlled oxidation condition (5 mM NaIO_4 , 1 h) with protection from light. For pH 8.5 immobilization, the antibody immobilization time was 24 h and incubated at 10 mM sodium borate, pH 8.5; For pH 10.0 immobilization, the antibody immobilization time was 1 h and incubated at 10 mM sodium bicarbonate, pH 10.0; For pH 10.0+DTT immobilization, the antibody immobilization time was 6 h and incubated at 10 mM sodium bicarbonate contains 50 mM DTT.

Overall, the aldehyde-Dex@MNPs demonstrated the highest potential as the antibody nanocarriers to fabricate the immunosensor. However, the periodate oxidation parameters should be further optimized to obtain the immunosensors with optimal performance.

5.3 Magnetic nanoparticles as the bioreceptors carrier–HRP as the analytes

INTRODUCTION

Dextran aldehyde has shown broad application due to its highly controllable reactive groups density, including the drug carriers [209], fabrication of hydrogels [210], crosslinker of crosslinked enzyme aggregates (CLEAs) [211], stabilization enhancer of immobilized protein [212], co-immobilization of multiple enzymes [213] and facilitate inert surface with conserved antibody functionality [194].

The Aldehyde-Dex@MNPs demonstrated the best capacity to protect the antigen-binding functionality, while there are still many spaces for us to optimize the parameters, thus obtain immunosensor with even higher sensitivity. The antibody functionalization degree on the Aldehyde-Dex@MNPs is highly controlled via the aldehyde density on its surface, while the influence of antibody coverage and aldehyde density on the possible antibody orientation is still unknown.

RESULTS

In this chapter, the periodate oxidation conditions (periodate concentration and oxidation time) were controlled and evaluated for their antibody-conjugation amount, the functionality of conjugated antibodies was highly appreciated. With the optimized variables, the fabricated immunosensors was utilized to detect the analytes using different quantification strategies, which are colorimetric method and electrochemical techniques.

5.3.1 Colorimetric detection of HRP– The controlled oxidation extent with better analytical performance

5.3.1.1. Determination of the aldehyde groups density and Ab_{HRP} immobilization rate

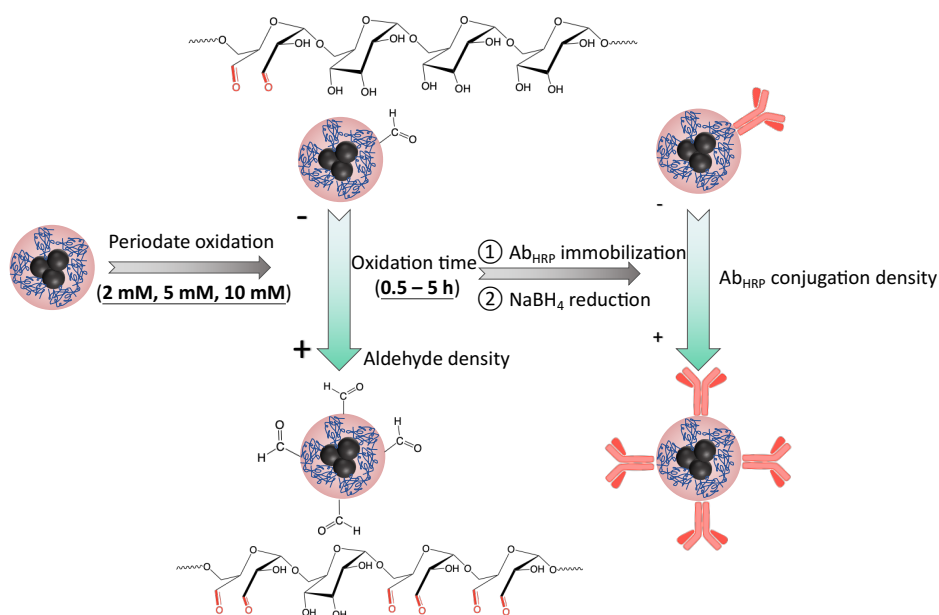


Figure 5.3-1. Scheme of the controlled oxidation of dextran layers on the MNPs surface to conjugate the Ab_{HRP} with different coverage density and orientation.

Using the optimal dextran coating strategy (mechanical stirring functionalization of 8-fold loaded dextran with 40 kDa size), the oxidation parameters of the dextran layer (time range from 0.5–5 h and $NaIO_4$ concentration range from 2–10 mM) was first investigated (Figure 5.3-1).

The generated aldehyde groups are derived from the functionalized dextran layers, thus it is highly correlated with the loading amount onto the MNP surface, and Dex@MNPs with two different loading concentrations were determined with their aldehyde density (Figure 5.3-2).

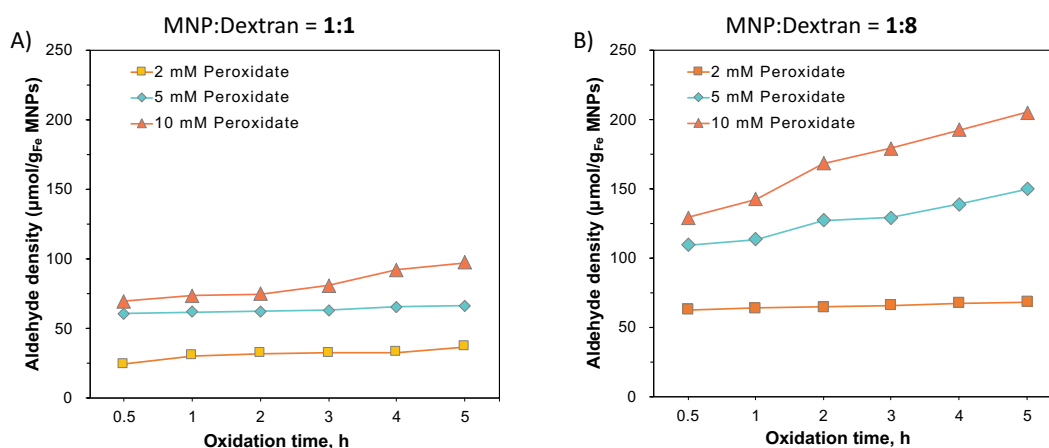


Figure 5.3-2. Controlled aldehyde groups density on the Dex@MNPs surface by changing the periodate concentration and oxidation time, lower dextran coating coverages (A) and high dextran coating coverage (B) of dextran polymer on the MNPs surface were investigated.

Results showed the clear relevance between grafted aldehyde density with initial loading amount of dextran. For Dex@MNPs with a high loading density (1:8 ratio of MNP:Dextran), 2 mM periodate oxidize for 0.5 h has produced $62.4 \mu\text{mol g}_{\text{Fe}}^{-1}$ Dex@MNPs, which is comparable with 5 mM periodate for 5 h oxidation while with lower loading density ($68.2 \mu\text{mol g}_{\text{Fe}}^{-1}$ Dex@MNPs). Furthermore, the influence of oxidation duration was not linearly related with aldehyde density, high periodate concentration (10 mM) was likely to observe a more obvious growth curve with the time proceeding, that aldehyde density in the range of 129–205 $\mu\text{mol g}_{\text{Fe}}^{-1}$ Dex@MNPs was determined for 10 mM periodate while 109–150 $\mu\text{mol g}_{\text{Fe}}^{-1}$ Dex@MNPs was calculated for 5 mM periodate.

The Ab_{HRP} immobilization rate on the Aldehyde-Dex@MNPs with different oxidation levels was determined, 5 h oxidation duration for 5 mM and 10 mM were selected to achieve the whole antibody coverage, respectively (Figure 5.3-3). Although the Ab loading amount had minor differences for low and high periodate concentrations, they shared a similar Ab immobilization rate, which 18.8 and 18.1 $\mu\text{g mg}_{\text{Fe}}^{-1}$ Aldehyde-Dex@MNPs had achieved the

full coverage, respectively. For both concentrations, the first 30 min interaction achieved about 50 % coverage, the following 30 min further promoted the surface coverage to near 65 % and 3 h incubation was enough to achieve the total coverage. To avoid the possible steric hindrance caused by the overcrowded Ab_{HRP} for following capture ratio calculation, the Ab_{HRP} immobilization time was selected as 60 min incubation for the following determination.

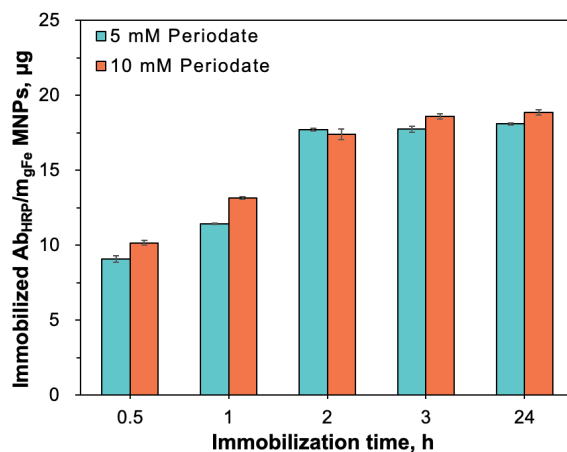


Figure 5.3-3. Ab_{HRP} immobilization rate on the Alde-Dex@MNPs, the oxidation time for both periodate concentrations (5 mM and 10 mM) was set as 5 h.

5.3.1.2. The effect of oxidation parameters on the Ab functionality

Due to the high importance of Ab functionality to fabricate highly efficient immunosensor, the Ab coverage density on the nanocarriers should not be the only consideration [6]. Thus, how the periodate concentration and oxidation time affect the antibody functionality were investigated (Figure 5.3-4).

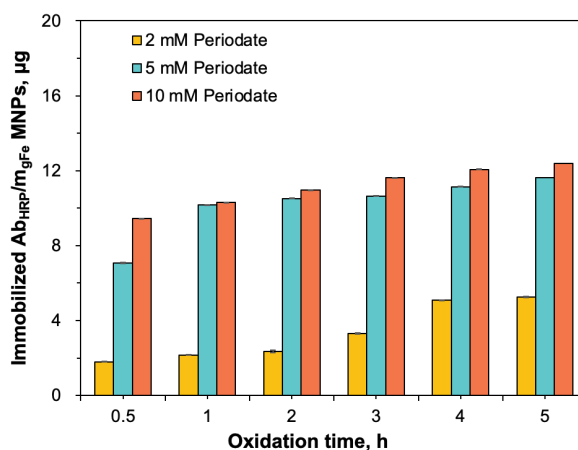


Figure 5.3-4. The Ab_{HRP} immobilization density on the Alde-Dex@MNPs with the prolonged oxidation time (0.5–5 h), the Ab_{HRP} immobilization time was set as 1 h.

Consistent with the anticipation, the Ab loading density on the Aldehyde-Dex@MNPs had shown a high correlation with generated aldehyde density that 5 h oxidation enabled 5.2, 11.6

and $12.4 \mu\text{g mg}_{\text{Fe}}^{-1}$ Alde-Dex@MNPs grafting concentration, respectively. However, the differences of Ab loading with high periodate concentration (5 mM and 10 mM) were not significant, the increase of Ab loading concentration with oxidation time was relatively slow. Taking 5 h oxidation as the reference time, they both reached over 90 % loading density after 2 h oxidation, which means aldehyde density was not the leading principle for the Ab immobilization afterward though aldehyde groups continuous substantial growth. The functionality of immobilized Ab_{HRP} was further determined and compared (Figure 5.3-5).

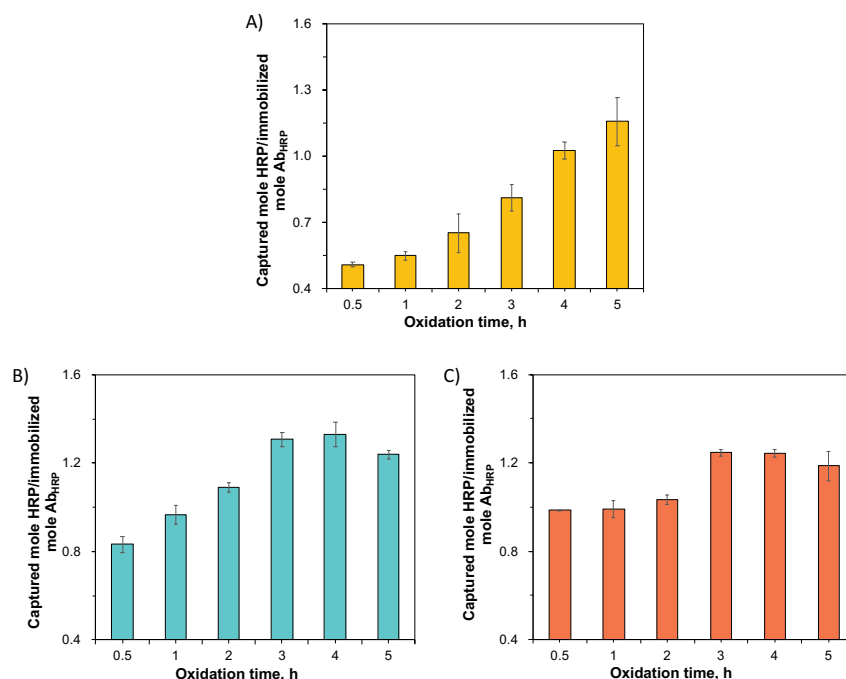


Figure 5.3-5. The capture ability of covalent immobilized Ab_{HRP} on the Alde-Dex@MNPs with different periodate concentrations: 2 mM (A), 5 mM (B) and 10 mM (C). The capture ability of fabricated immunosensors was calculated as the mole captured HRP per mole immobilized Ab_{HRP} .

Results showed the clear correlation between aldehyde density and the preserved functionality of tethered Ab, that higher aldehyde density promoted the increasing functionality retention of Ab_{HRP} . For the low periodate concentration (2 mM), this tendency was very explicit that the antigen-binding ability of immobilized Ab has increased from 0.51 to 1.16-mole analyte per immobilized mole Ab_{HRP} with the increasing of aldehyde density. The highest antigen-recognition functionality was obtained with the medium periodate concentration (5 mM), although the shortest oxidation time was observed with the lowest functionality, there was a limited increment after oxidation time reached over 2 h. The optimal oxidation time was 4 h for medium periodate concentration, longer oxidation time caused the capture ability to decrease from 1.33 to 1.24-mole analyte per immobilized mole Ab_{HRP} maybe lead by the steric hindrance of overcrowded antibody and the spatial conformation variation includes antibody orientation

changes. Similarly, high periodate concentration (10 mM) did not promote even better functionality preservation, the highest functionality of immobilized was obtained for 3 h oxidation with 1.25-mole analyte per immobilized mole Ab_{HRP} and the minor decrease was also observed after extending the oxidation time.

5.3.1.3. The optimization of experimental variables to achieve better biosensing efficiency

The oxidation parameters of dextran layers to prepare the Aldehyde-Dex@MNPs with the optimal antigen-binding functionality were defined, thus we continued to optimize the variables to capture the analytes with better efficiency (Figure 5.3-6).

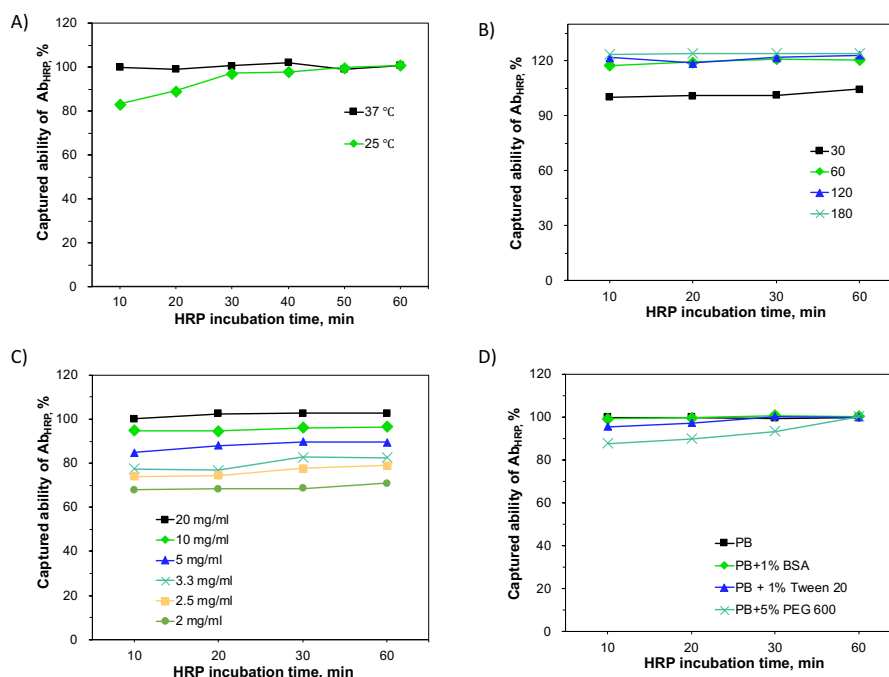


Figure 5.3-6. Optimization of experimental variables using the fabricated immunosensor with the optimal oxidation condition (5 mM periodate, 4 h oxidation time): HRP incubation temperature (A), Ab_{HRP} immobilization time (B), Alde-Dex@MNPs concentration during incubation time HRP (C) and incubation buffer composition (D) were investigated. The adsorption capacity of immunosensors with 10 min incubation was taken as the 100 % reference in all the experiments, respectively, in which 37 °C incubation temperature, 30 min incubation time, 20 mg mL^{-1} Alde-Dex@MNPs concentration and PB incubation buffer were taken as the reference parameter, respectively.

The incubation temperature (25 and 37 °C) was the first parameter to be determined, results showed a good antigen adsorption rate with the 37 °C incubation temperature that 10 min is adequate to achieve the full antigens adsorption. While it took 30 min for the Alde-Dex@MNPs to reach their saturated capacity when incubation under 25 °C, which revealed the significance of incubation temperature. Thus, 37 °C was selected for the following trials.

Followed by the optimization of antibody immobilization time (30–180 min), however, unlike the determination of antigen-recognition functionality, adequate coverage and correct orientation of conjugated antibodies are essential for the adsorption of the sufficient analyte [214]. It was good to see that immunosensors were able to achieve the full capacity within 10 min even with the relative lower Ab coverage (Ab_{HRP} immobilize for 30 min), while about 50 % surface coverage (Figure 5.3-6) limited its immunosensing capacity, that 1.2-fold capacity was observed with longer Ab incubation time. Due to the slight enhancement of antigen-adsorption capacity between 60–180 min, the Ab immobilization time was set at 60 min instead of an even longer time to find the equilibrium between functionality and cost-effectiveness.

The working concentration of Alde-Dex@MNPs was further optimized (2–20 mg_{Fe} mL⁻¹). Similarly, the nanoparticles concentration only affected the antigen-recognition capacity while the fast adsorption rate was preserved. Using the 10-fold higher nanoparticles concentration (20 mg_{Fe} mL⁻¹ vs 0.2 mg_{Fe} mL⁻¹), the immunosensing capacity was improved to 1.5-fold higher.

To determine the possible interference of additives in the incubation buffer, BSA, Tween 20 and PEG 600 were added into the incubation buffer, respectively. Results demonstrated that soluble BSA has no influence on the immunosensing performance, neither on the capture capacity or response rate, 1% Tween 20 had a minor negative effect on the immunosensing rate while over 96 % capacity was observed within 10 min incubation. However, 5 % PEG 600 caused the lower immunosensing velocity that only 88 % immunosensing capacity was achieved. Fortunately, the same adsorption capacity can be fulfilled even it takes 60 min to complete.

5.3.1.4. Analytical characterization of the fabricated immunosensors

With the optimization of experimental variables, the immunosensing performance of the immunosensor has been determined (Figure 5.3-7). Serial diluted HRP (0.3–300 µg mL⁻¹) prepared in the PB buffer was captured under the optimal condition and the immunosensing ability of Ab_{HRP}-Aldehyde-Dex@MNPs immunosensors was quantified by the specific colorimetric reaction of HRP (ABTS as the color developing substrate).

Results demonstrated clear linear relationship between increased HRP concentration and detected specific activity of nanobioconjugates in the range of 0.3–7.5 µg mL⁻¹ ($R^2=0.995$) and fitting the equation of specific activity_{nanobioconjugates} (IU g_{Fe}⁻¹) = (93.59 ± 2.68) [HRP] (IU g_{Fe} mL µg⁻¹) + (8.08 ± 0.87) (IU g_{Fe}⁻¹). The immunosensor Ab_{HRP}-Aldehyde-Dex@MNPs had an undetectable catalytic activity with the absence of analytes through light blue color can be developed after 15 min colorimetric reaction, the main reason is we have detected the kinetic catalytic activity instead of the absorbance of developed color. Therefore, the LOD value was taken as 0.3 µg mL⁻¹ using the aqueous buffer as the dissolution system.

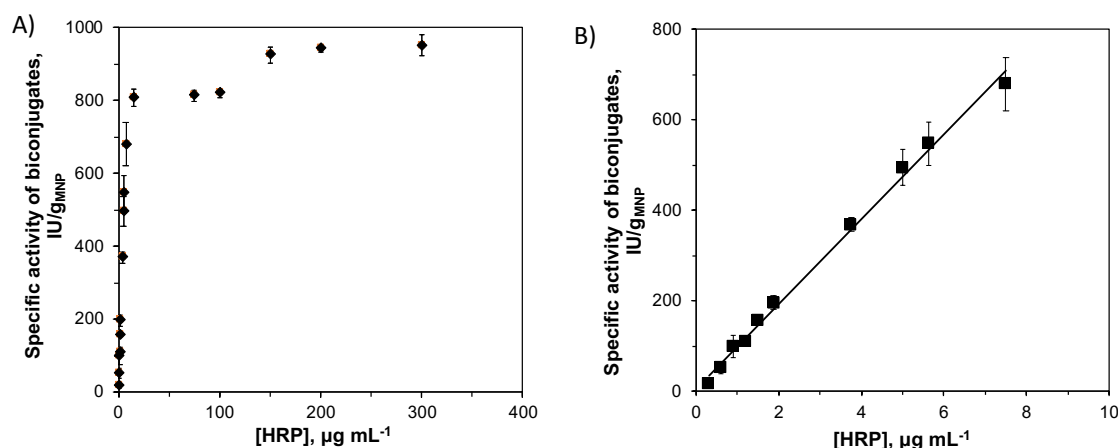


Figure 5.3-7. Analytical characterization of the fabricated immunosensor under the optimal condition for the detection of HRP. The wide range of HRP concentration ($0.3\text{--}300\ \mu\text{g mL}^{-1}$) were determined (A) and the fabricated immunosensor demonstrated a good linear relationship between $0.3\text{--}7.5\ \mu\text{g mL}^{-1}$ HRP prepared in an aqueous buffer.

To further verify the anti-interference ability of fabricated immunosensor, the recovery of the analytes experiments from diluted human serum were performed, and the information has presented in Table 5.3-1. HRP spiked in the 1 % human serum gave more “real” results, the HRP concentration detected was highly related to the spiked concentration, which revealed the credibility of the fabricated immunosensor. Results obtained from the 10 % serum demonstrated more variable data, maybe contributing to the complexity of serum solution, in which the detected concentrations were still able to reflect the “real” concentrations.

Table 5.3-1 Recovery of HRP from the diluted human serum with the fabricated immunosensors.

Spiked HRP ($\mu\text{g mL}^{-1}$)	1 % serum		10 % serum	
	Detected concentration ($\mu\text{g mL}^{-1}$)	Recovery value, %	Detected concentration ($\mu\text{g mL}^{-1}$)	Recovery value, %
1	1.06 ± 0.043	105.8	0.94 ± 0.042	93.9
2	2.01 ± 0.203	100.3	2.12 ± 0.025	106.4
5	4.95 ± 0.37	99.1	5.11 ± 0.15	102.1

5.3.2 Electrochemical detection of HRP with lower LOD – The comparison of magnetic particles size and functional groups

Instead of the colorimetric method to detect the HRP concentration, the electrochemical technique was applied for the sensitive detection of analytes with hydroquinone (HQ) as the mediator (Figure 5.3-8). In addition, three particles (Alde-Dex@MNPs, HOOC-Dex@MNPs

and HOOC@MBs) of different sizes or chemistry functionalities were determined and compared with their analytical performance.

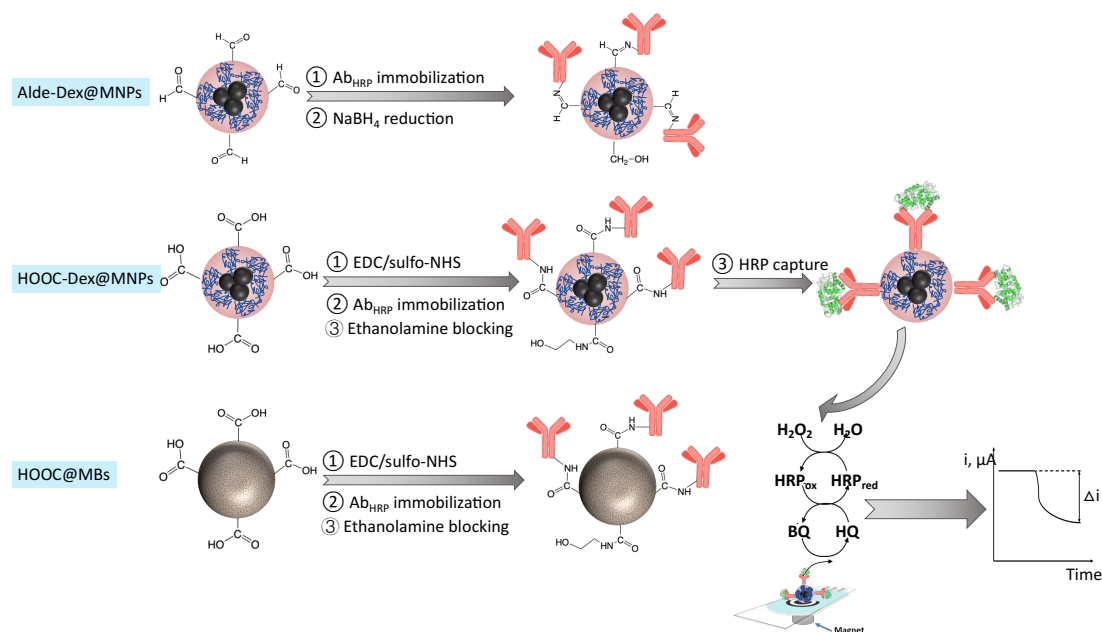


Figure 5.3-8. Scheme of the using Alde-Dex@MNPs, HOOC-Dex@MNPs and HOOC-MBs as the carriers to perform the electrochemical determination of HRP.

5.3.2.1. Optimization of the experimental variables to obtain Alde-Dex@MNPs with the better S/N ratio

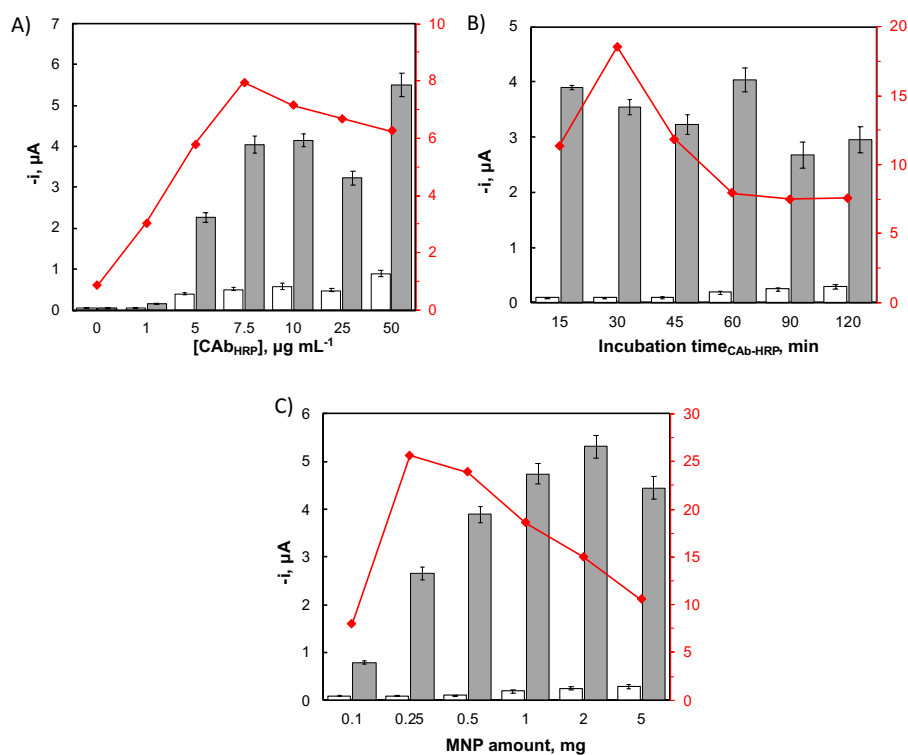


Figure 5.3-9. Effect of CAb_{HRP} loading concentration, its incubation time and MNP amount on

the amperometric responses of the immunosensors for 0 ng mL^{-1} (white bar, N) and 100 ng mL^{-1} HRP (black bars, S) and the corresponding S/N ratio (red line). $C_{Ab_{HRP}}$ loading concentration was determined with the range of $0\text{--}50 \text{ }\mu\text{g mL}^{-1}$, 60 min; $C_{Ab_{HRP}}$ incubation time was determined with the range of 15–120 min, $7.5 \text{ }\mu\text{g mL}^{-1}$ (B) and MNP amount were determined with the range of $0.1\text{--}5 \text{ mg mL}^{-1}$, $7.5 \text{ }\mu\text{g mL}^{-1}$ $C_{Ab_{HRP}}$ with 30 min incubation (C). All the error bars were calculated as the standard deviation ($n = 3$) of duplicate experiments.

Alde-Dex@MNPs was utilized as the model nanocarriers to optimize the involved parameters, including the Ab_{HRP} concentration, Ab_{HRP} immobilization time with nanocarriers and MNP amount for each electrochemical reaction (Figure 5.3-9). Taking the signal-to-noise (S/N) ratio as the primary consideration, $7.5 \text{ }\mu\text{g mL}^{-1}$ Ab_{HRP} of 30 min incubation time with Alde-Dex@MNPs gave the highest S/N ratio, and 0.25 mg per sample even promoted the higher sensitivity. The summary of optimized experimental variables is also included in Table 5.3-2.

Table 5.3-2 Optimization of the experimental variables affecting the immunosensing sensitivity of fabricated sandwich configuration on the Alde-Dex@MNPs to perform the electrochemical determination of HRP.

Experimental variables	Tested range	Selected value
$[C_{Ab_{HRP}}]$, $\mu\text{g mL}^{-1}$	1–50	7.5
$C_{Ab_{HRP}}$ incubation time, min	15–120	30
MNPs amount, mg	0.1–5	0.25

5.3.2.2. Analytical characterization of the fabricated immunosensors using electrochemical technique

Under the optimized conditions, the analytical characterization of Alde-Dex@MNPs were determined (Figure 5.3-10). The fabricated immunosensor demonstrated different calibration performance with the detected concentration range. During the HRP concentration within the $1.47\text{--}30 \text{ ng mL}^{-1}$ range, good relationship was observed ($R^2 = 0.9971$), which fitting the equation $i \text{ (nA)} = (64.67 \pm 1.73) [\text{HRP}] \text{ (nA mL ng}^{-1}) + (72.82 \pm 22.76) \text{ (nA)}$. Meanwhile, in the HRP range of $30\text{--}200 \text{ ng mL}^{-1}$ ($R^2 = 0.9915$), a much less sensitivity was determined, which fitting the equation $i \text{ (nA)} = (3.21 \pm 0.21) [\text{HRP}] \text{ (nA mL ng}^{-1}) + (1890 \pm 24.40) \text{ (nA)}$.

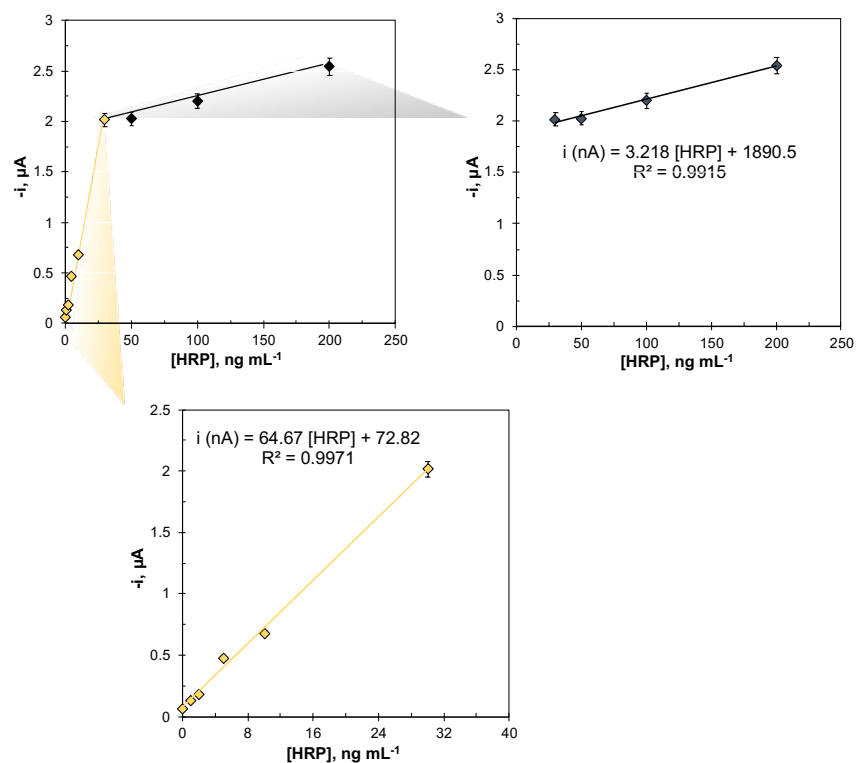


Figure 5.3-10. Analytical characterization of the immunosensor using Alde-Dex@MNPs (25 μgFe per sample) as the carriers to perform the electrochemical determination of HRP. The calibration plot demonstrates a different linear relationship with different HRP concentration ranges (0–30 ng mL^{-1} and 30–200 ng mL^{-1}).

When using higher Alde-Dex@MNPs amount as the nanocarrier (100 μg vs 25 μg), a similar analytical performance with wider linear range while less sensitivity was obtained (Figure 5.3-11). During the HRP concentration within the 1.95–100 ng mL^{-1} range, good relationship was observed ($R^2 = 0.9975$), which fitting the equation $i \text{ (nA)} = (44.68 \pm 1.46) [\text{HRP}] \text{ (nA mL ng}^{-1}) + (117.69 \pm 60.89) \text{ (nA)}$. Meanwhile, in the HRP range of 100–400 ng mL^{-1} ($R^2 = 0.9908$), a much less sensitivity was determined, which fitting the equation $i \text{ (nA)} = (5.979 \pm 0.408) [\text{HRP}] \text{ (nA mL ng}^{-1}) + (3758 \pm 111.77) \text{ (nA)}$.

Using the same Ab_{HRP} immobilization parameters with the 25 μg , HOOC-Dex@MNPs were utilized as the nanocarriers to detect its performance (Figure 5.3-12). The fabricated immunosensors with HOOC-Dex@MNPs as the nanocarriers demonstrated less sensitivity than Ab_{HRP} -Alde-Dex@MNPs, while promoting a better linear range. The calibration plot for the target HRP exhibited a linear relationship ($R^2 = 0.995$) between 0.98 ng mL^{-1} and 50 ng mL^{-1} , with slope value of $(41.42 \pm 1.16) \text{ nA mL ng}^{-1}$ and intercept value of $(96.91 \pm 22.64) \text{ (nA)}$.

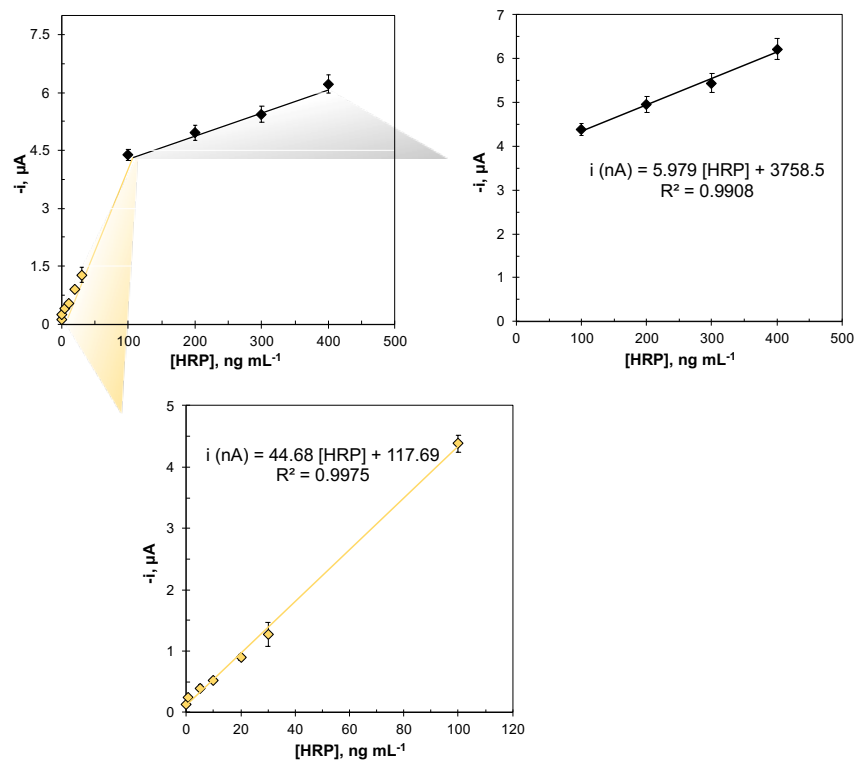


Figure 5.3-11. Analytical characterization of the immunosensor using Alde-Dex@MNPs ($100 \mu\text{g}_{\text{Fe}}$ per sample) as the carriers to perform the electrochemical determination of HRP. The calibration plot demonstrates a different linear relationship with different HRP concentration range ($0\text{--}100 \text{ ng mL}^{-1}$ and $100\text{--}400 \text{ ng mL}^{-1}$).

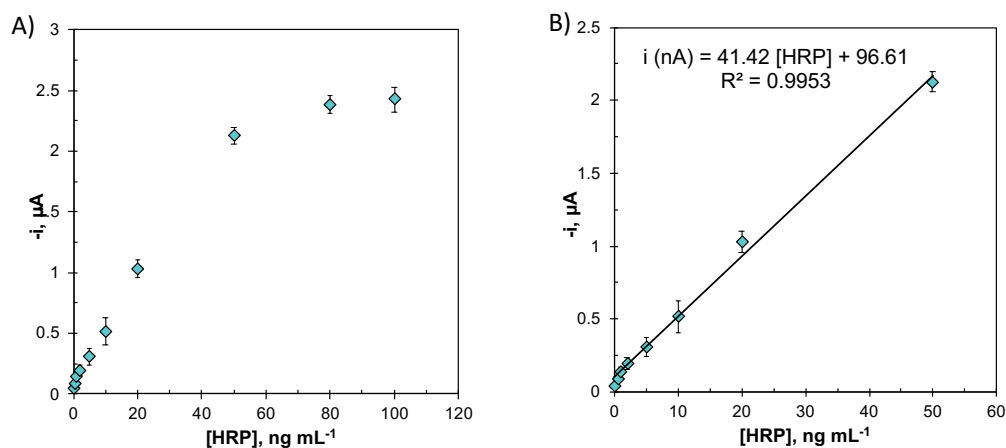


Figure 5.3-12. Analytical characterization of the immunosensor using HOOC-Dex@MNPs as the nanocarriers to perform the electrochemical determination of HRP. The amperometric response of the fabricated immunosensors during the determined HRP range (A) and its linear range (B) were demonstrated.

With the optimal conditions as previously stated, HOOC@MBs have shown as the best carriers of Ab_{HRP} , and the highest sensitivity was obtained in [Figure 5.3-13](#). In the range of $0.14\text{--}50 \text{ ng}$

mL^{-1} HRP, a linear relationship was observed ($R^2 = 0.998$), the slope and intercept values of $(109.62 \pm 2.46) \text{ nA mL ng}^{-1}$ and $(94.18 \pm 56.95) \text{ nA}$, respectively.

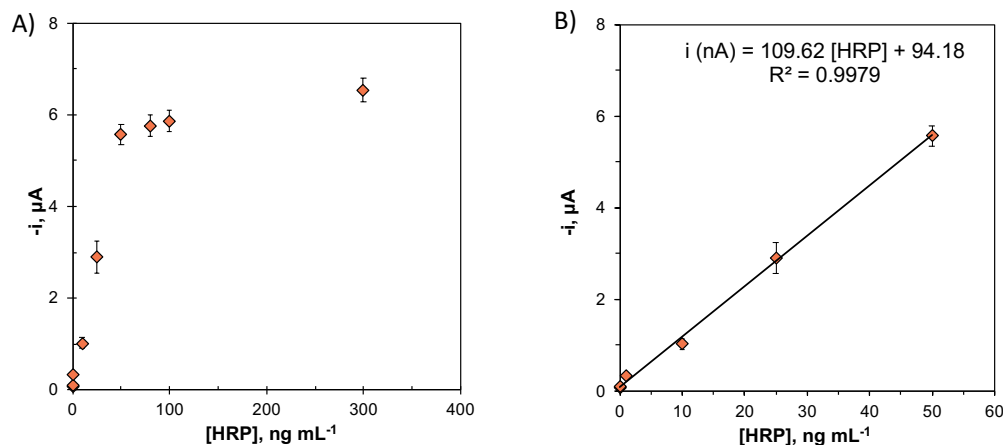
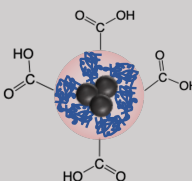
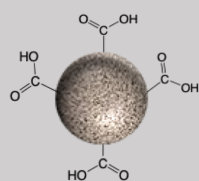


Figure 5.3-13. Analytical characterization of the immunosensor using *HOOC@MBs* as the microcarriers to perform the electrochemical determination of HRP. The amperometric response of the fabricated immunosensors during the determined HRP range (A) and its linear range (B) were demonstrated.

Limit of determination (LOD) of Alde-Dex@MNPs, HOOC-Dex@MNPs and HOOC@MBs were 0.44 ng mL^{-1} , 0.78 ng mL^{-1} and 0.14 ng mL^{-1} , respectively, following the criteria of $3 \times s_b/m$, where m is the slope of the linear calibration plot and s_b was the standard deviation of 10 amperometric measurements without the presence of the HRP analytes. In addition, the limit of quantification (LOQ) was calculated according to the $10 \times s_b/m$ criteria, which with 1.47 ng mL^{-1} , 2.59 ng mL^{-1} and 0.48 ng mL^{-1} , respectively.

Performing the amperometric measurements using the HRP concentrations described in Table 5.3-3, a relative standard deviation (RSD) value of 5.14 % – 8.76 % was obtained with those four immunosensors, respectively. Those results proved the acceptable reproducibility of the whole immunosensing procedure and confirmed the reliability of the fabricated immunosensors.

Table 5.3-2 Analytical characteristics for the determination of HRP in buffered solution using different magnetic carriers to perform the electrochemical determination.

Parameters	Alde-Dex@MNPs		HOOC-Dex@MNPs	HOOC@MBs
	0.25 mg ^c	1 mg ^d		
Linear range, ng mL ⁻¹	1.47–30	1.95–100	2.59–50	0.14–50
r	0.997	0.997	0.995	0.998
Slope, nA/ng mL ⁻¹	64.67 ± 1.73	44.68 ± 1.46	41.42 ± 1.16	109.62 ± 2.46
Intercept, nA	72.82 ± 22.76	117.69 ± 60.89	96.61 ± 22.64	94.18 ± 56.95
LOD ^a , ng mL ⁻¹	0.44	0.59	0.78	0.14
LOQ ^b , ng mL ⁻¹	1.47	1.95	2.59	0.48
RSD	8.76% ^e	5.21% ^f	6.56% ^g	5.14% ^h

a, b: calculated according to the $3 \times sb/m$ and $10 \times sb/m$ criterion, respectively, sb: standard deviation ($n = 10$) for measurements performed in the absence of HRP, m: slope value of the calibration plots.

c: the initial MNPs concentration used for the $CA_{B_{HRP}}$ immobilization amount is 0.25 mg, and the final MNPs amount for each sample is 25 μg_{Fe} MNPs.

d: the initial MNPs concentration used for the $CA_{B_{HRP}}$ immobilization amount is 1 mg, and the final MNPs amount for each sample is 100 μg_{Fe} MNPs.

e: the determination was performed with 15 ng mL⁻¹ HRP ($n = 10$).

f: the determination was performed with 50 ng mL⁻¹ HRP ($n = 10$).

g: the determination was performed with 25 ng mL⁻¹ HRP ($n = 10$).

h: the determination was performed with 30 ng mL⁻¹ HRP ($n = 10$).

It's worth mentioning that the storage stability of the Ab_{HRP} conjugated carriers was also evaluated by storing in the PB or PBS buffer at 4 °C, and the amperometric values were determined with different time intervals ([Figure 5.3-14](#)). All the prepared immunosensors have no significant decrease of the amperometric measurements, indicating the stability of immunosensor able to last at least over 26 days.

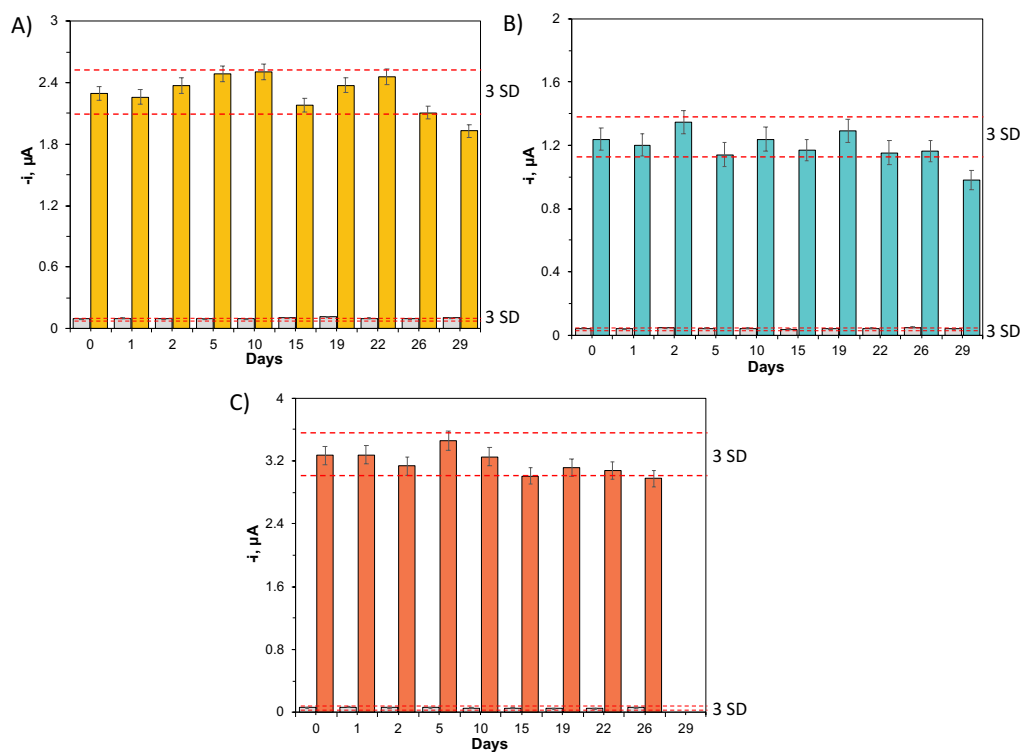


Figure 5.3-14. Storage stability of immobilized CAb_{HRP} on the MNPs or MBs for the detection of HRP, the biofunctionalized MNPs/MBs were stored in filtered PB buffer at 4 °C. The amperometric responses of the immunosensors without (gray bars) or with the presence of HRP, in which *Alde-Dex@MNPs* for 50 ng mL⁻¹ (A), *HOOC-Dex@MNPs* for 25 ng mL⁻¹ (B) and *HOOC@MBs* for 30 ng mL⁻¹ (C) were measured with the prolonged storage time.

5.4 Multifunctionalities of the nanoparticles

INTRODUCTION

The electrochemical immunoassays have been proven with good sensitivity for the analytes determination in the previous results, human C-reactive protein (CRP) was used as the target to explore the availability of the nanocarriers in different applications. For the typical sandwich-type electrochemical immunoassays, the report enzyme-Ab conjugates as the detection probes have been well accepted while multifunctional nanocarriers as the detection probe are demonstrating higher sensitivity [144, 158, 172]. The dual functionalized nanocarriers improve the performance of the immunosensors by the exploitation of signal amplification strategy, in which much lower detection limits can be obtained and enhanced sensitivity can be predicted [215, 216].

RESULTS

In this part of dissertation, CRP will be utilized as the analytes to check the analytical performance of different immunosensors, in which those immunosensors have the same bioreceptors carriers (SPCEs) while three different detection probes were utilized and compared. The surface functionalization of the working electrodes is the first step to functionalize sufficient carboxylic groups via electrochemical grafting [217], following the activation of carbodiimide chemistry (EDC/sulfo-NHS) to immobilize the bioreceptors ([Figure 5.4-1](#)). The differences of bioreceptors immobilization strategy and the compositions of those three detection probes have been demonstrated in [Table 5.4-1](#).

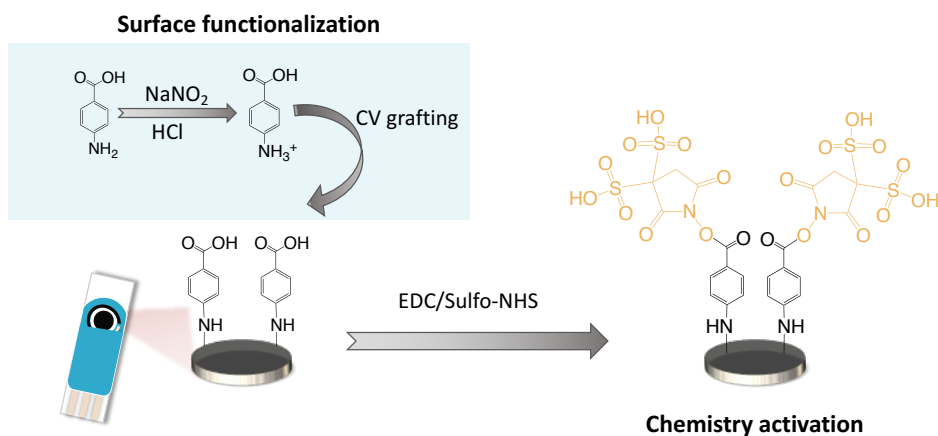


Figure 5.4-1. Illustration of the steps to sequentially achieve the surface functionalization and chemistry activation of the working electrodes on SPCEs.

Table 5.4-1 The utilization and comparison of three different detection probes in this chapter when using the SPCEs as the carriers.

SPCEs as the carriers			
	Strep-HRP ^a	HRP/CAb@MNPs ^b	HRP/Streptavidin@MNPs
Bioreceptors carrier		SPCEs	
Bioreceptors types	CAb	Biotin-Ab (B-DAb)	CAb
Bioreceptors immobilization types	Direct covalent interaction (Carbodiimide chemistry)	Affinity interaction (Streptavidin–biotin interaction)	Direct covalent interaction (Carbodiimide chemistry)
Detection probe carriers	–	Alde-Dex@MNPs	Alde-Dex@MNPs
Detection probe types	Mono-enzyme	Dual proteins (HRP + CAb)	Dual proteins (HRP + Streptavidin)

a: Strep-HRP used in this thesis is the commercially available streptavidin-HRP conjugate.

b: HRP/Streptavidin@MNPs are biofunctionalized MNPs materials with streptavidin and HRP co-immobilization.

5.4.1 Investigation of experimental variables effect on the analytical performance of immunosensors

5.4.1.1 Strep-HRP as the detection probes

Using this strategy, CAb_{HRP} will be first immobilized on the SPCEs as the antigen recognition element, and strep-HRP bioconjugates work as the detection probes ([Figure 5.4-2](#)).

The experimental variables involved in the electrochemical immunoassays will be optimized before performing the analytical determination. The CAb_{HRP} loading concentration and incubation time were first optimized, results showed that mild concentration of CAb_{HRP} (50 µg mL⁻¹) with 60 min incubation gave the best S/N ratio ([Figure 5.4-3](#)).

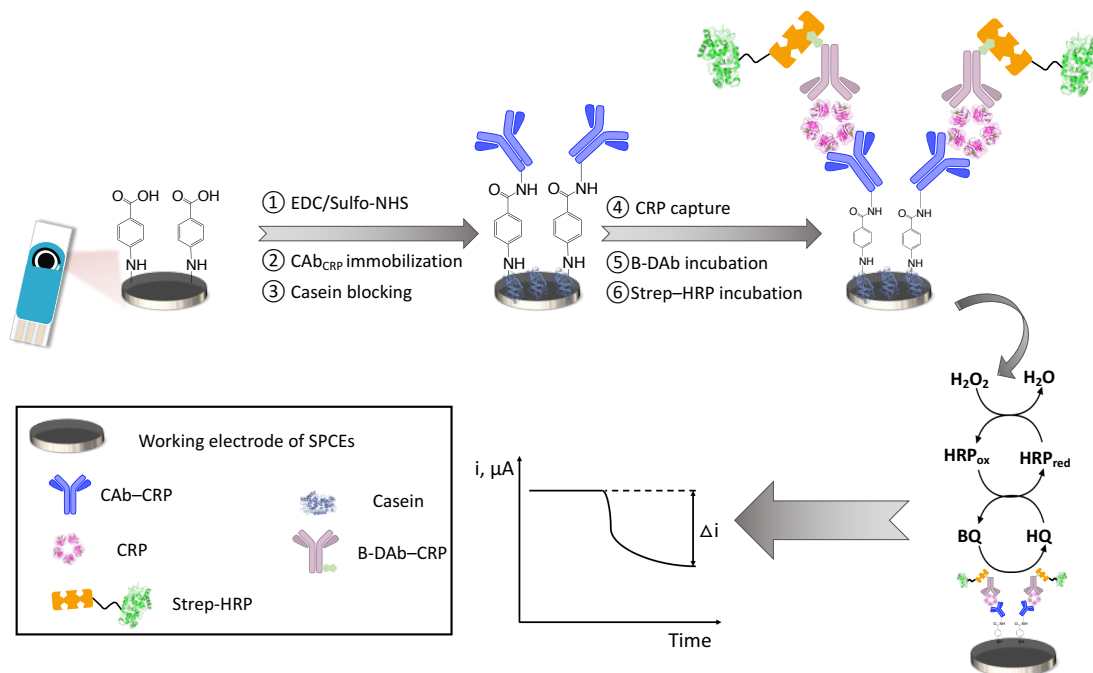


Figure 5.4-2. *Strep-HRP as the detection probes. Biofunctionalization procedures to prepare the CAB_{CRP} immobilized SPCEs as the carriers.*

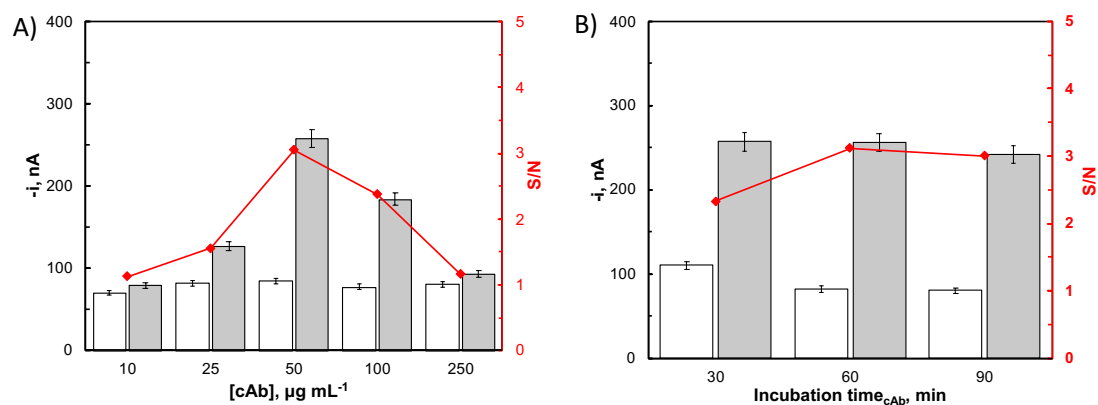


Figure 5.4-3. *Strep-HRP as the detection probes. Effect of CAB loading concentration and its incubation time on the amperometric responses of the immunosensors for 0 ng mL^{-1} (white bar, N) and 10 ng mL^{-1} CRP (gray bars, S) and the corresponding S/N ratio (red line). CAB loading concentrations were determined with the range of $10\text{--}250 \mu\text{g mL}^{-1}$ (60 min) (A) and CAB incubation time was determined with the range of $30\text{--}90 \text{ min}$ ($50 \mu\text{g mL}^{-1}$) (B). All the error bars were calculated as the standard deviation ($n = 3$) of duplicate experiments.*

The concentration and incubation time of blocking reagent was further optimized, casein has been proven with better efficiency to prevent the non-specific adsorption on the electrodes [218]. In this specific case, 1 % (w/v) casein with 60 min promised the best S/N ratio (Figure 5.4-4).

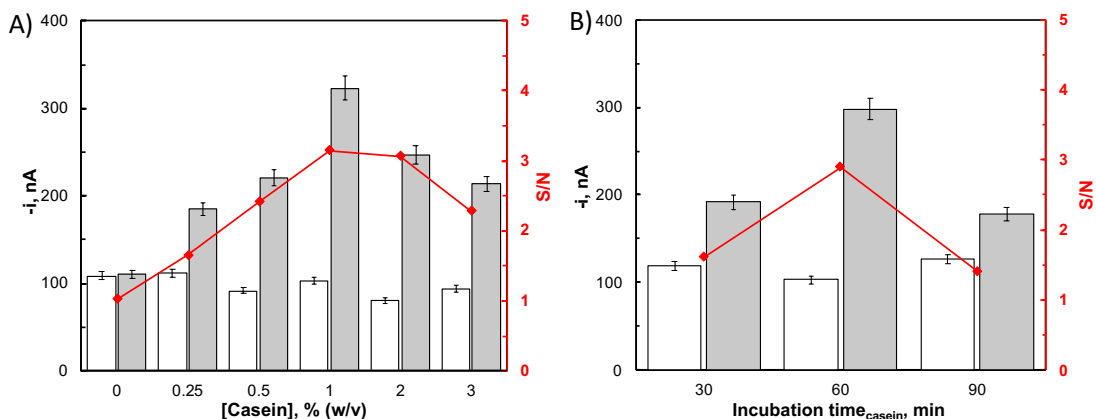


Figure 5.4-4. Strep-HRP as the detection probes. Effect of casein loading concentration and its incubation time on the amperometric responses of the immunosensors for 0 ng mL^{-1} (white bar, N) and 10 ng mL^{-1} CRP (gray bars, S) and the corresponding S/N ratio (red line). Casein loading concentration was determined with the range of 0–3 % (w/v) (60 min) (A) and casein incubation time was determined with the range of 30–90 min (1 % (w/v)) (B). All the error bars were calculated as the standard deviation ($n = 3$) of duplicate experiments.

The electrochemical signals of the immunosensors corresponding to the different Biotin-Ab_{HRP} concentration were determined (Figure 5.4-5). The results demonstrated the $0.5 \mu\text{g mL}^{-1}$ Biotin-Ab_{HRP} gave the lowest unspecific interaction with electrodes while providing a good amperometric response. Besides, 30 min incubation time promoted the best S/N ratio.

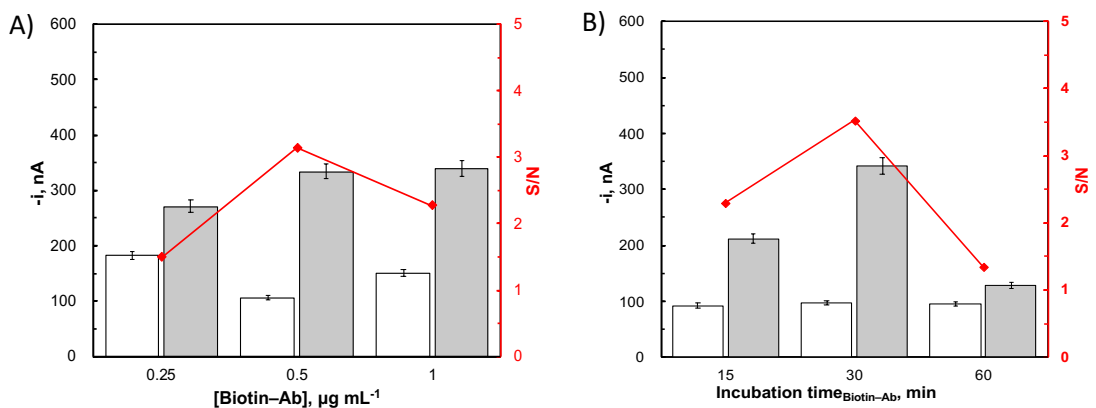


Figure 5.4-5. Strep-HRP as the detection probes. Effect of B-DAb loading concentration and its incubation time on the amperometric responses of the immunosensors for 0 ng mL^{-1} (white bar, N) and 10 ng mL^{-1} CRP (gray bars, S) and the corresponding S/N ratio (red line). B-DAb loading concentration were determined with the range of 0.25–1 % $\mu\text{g mL}^{-1}$, 30 min (A) and B-DAb incubation time were determined with the range of 15–60 min ($0.5 \mu\text{g mL}^{-1}$) (B). All the error bars were calculated as the standard deviation ($n = 3$) of duplicate experiments.

The effect of Strep-HRP concentration and incubation time were well investigated (Figure 5.4-6). Unlike the expectation, the lowest dilution of Strep-HRP did not give the best specific signal while the highest background interference was observed with 2000-fold dilution, further dilution of Strep-HRP even promotes better specificity. Although the prolongation of incubation time (15–60 min) showed higher electrochemical response, 30 min was a better option.

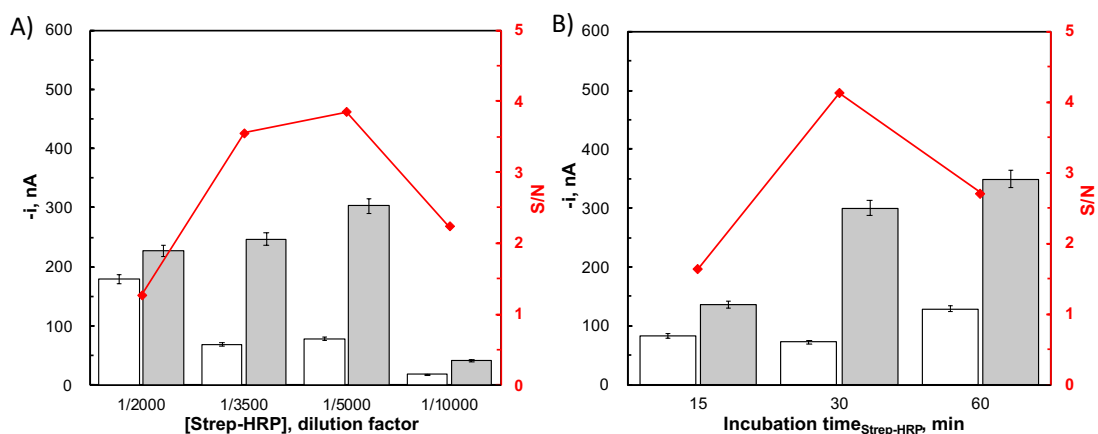


Figure 5.4-6. Strep-HRP as the detection probes. Effect of *Strep-HRP* concentration (A) and its incubation time (B) on the amperometric responses of the immunosensors for 0 ng mL^{-1} (white bar, N) and 10 ng mL^{-1} CRP (gray bars, S) and the corresponding S/N ratio (red line). *Strep-HRP* loading concentrations were determined with the range of 1/10000–1/2000 dilution factor (30 min) (A) and *Strep-HRP* incubation time was determined with the range of 15–60 min (1/5000 dilution factor) (B). All the error bars were calculated as the standard deviation ($n = 3$) of duplicate experiments.

Including all the optimized variables, the sensitivity of the fabricated immunosensor has reached the highest value, which gave the highest S/N ratio under the experimental condition described above, and optimized condition has been summarized in Table 5.4-2.

Table 5.4-2 Optimization of the experimental variables affecting the immunosensing sensitivity of fabricated sandwich configuration on the SPCEs as the carriers and *Strep-HRP* as the detection probes.

Experimental variables	Tested range	
	Tested range	Selected value
[CAb _{CRP}], $\mu\text{g mL}^{-1}$	10–250	50
CAb _{CRP} incubation time, min	30–90	60
Casein, %(w/v)	0–3	1

Casein incubation time, min	30–90	60
[B-DAb _{CRP}], $\mu\text{g mL}^{-1}$	0.25–1	0.5
B-DAb _{CRP} incubation time, min	15–60	30
[Strep-HRP], dilution factor	1/10000–1/2000	1/5000
Strep-HRP incubation time, min	15–60	30

5.4.1.2 HRP/CAb@MNPs as the probes

With the EDC/sulfo-NHS activated SPCEs as the bioreceptors carriers, there were two differences with earlier when Strep-HRP as the detection probes, namely the Biotin-Ab_{HRP} was selected as the bioreceptors, meanwhile, HRP and CAb_{HRP} dual functionalized Alde-Dex@MNPs carriers were substituted Strep-HRP for the detection probes (Figure 5.4-7).

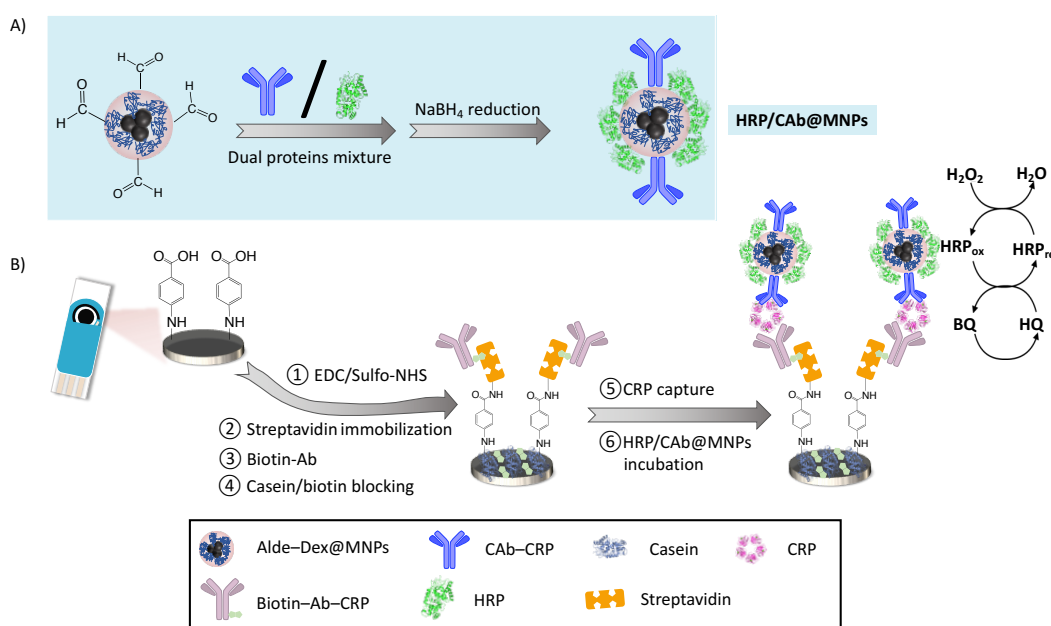


Figure 5.4-7. HRP/CAb@MNPs as the detection probes. (A) Preparation of HRP and CAb co-immobilized MNPs as the detection probes, dual protein mixtures were used. (B) Functionalization of Biotin-Ab_{CRP} on SPCEs via the pre-immobilization of streptavidin linkers.

In this strategy, the bottom-up optimization sequence was utilized. The parameters involving with the HRP/CAb@MNPs carriers were first investigated, namely the concentration of HRP and CAb_{HRP}, and the incubation time of mixtures with nanocarriers (Figure 5.4-8). Varied concentration of HRP and CAb_{HRP} did not demonstrate significant electrochemical signals in the presence of 10 ng mL^{-1} CRP, while 1 mg mL^{-1} HRP and $6 \mu\text{g mL}^{-1}$ CAb_{HRP} gave the lowest background values. Similarly, 30 min incubation time facilitated the adequate analytes adsorption. Thus 1 mg mL^{-1} HRP and $6 \mu\text{g mL}^{-1}$ CAb_{HRP} with 30 min immobilization duration were selected as the optimal condition for the preparation of HRP/CAb@MNPs probes.

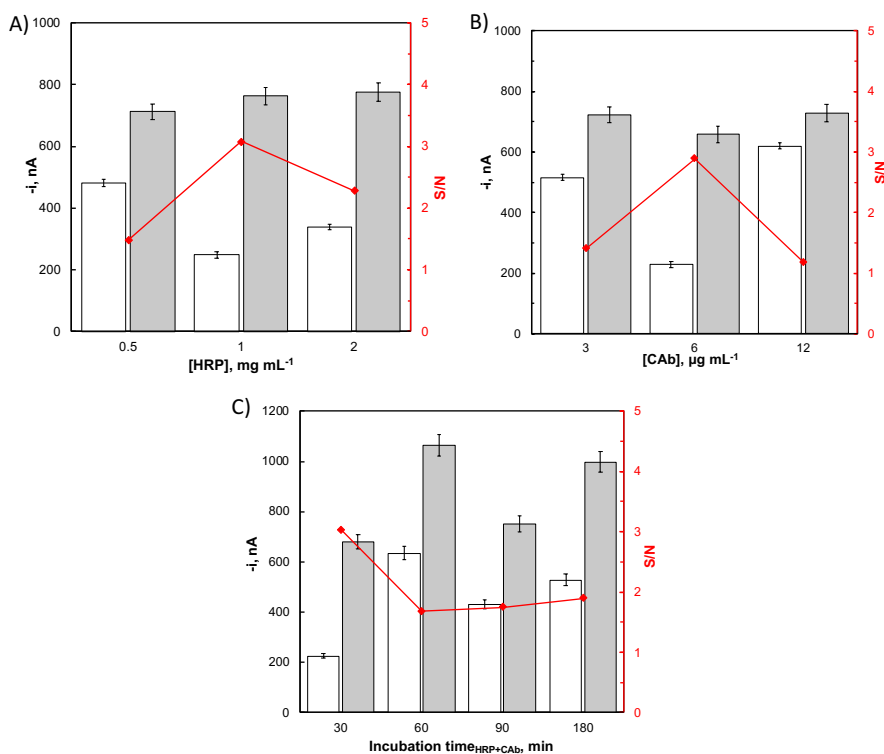


Figure 5.4-8. *HRP/Cab@MNPs as the detection probes. Effect of HRP/Cab loading concentration and their incubation time on the amperometric responses of the immunosensors for 0 ng mL⁻¹ (white bar, N) and 10 ng mL⁻¹ CRP (gray bars, S) and the corresponding S/N ratio (red line). HRP loading concentrations were determined with the range of 0.5–2 mg mL⁻¹ (6 μg mL⁻¹ CAb, 30 min incubation) (A) and CAb loading concentration were determined with the range of 3–12 μg mL⁻¹ (1 mg mL⁻¹, 30 min incubation) and incubation time of CAb/HRP mixture with MNPs were determined with the range of 30–180 min (2 mg mL⁻¹ HRP and 6 μg mL⁻¹ CAb) (C). All the error bars were calculated as the standard deviation ($n = 3$) of duplicate experiments.*

The working concentration of HRP/Cab@MNPs probes and its sufficient incubation time with analytes were further explored (Figure 5.4-9). With the increasing of HRP/Cab@MNPs nanocarriers, the S/N ratios were gradually increased, taking the lower unspecific interaction given by 0.5 mg mL⁻¹ nanoprobes, it was selected for the further study. With the incubation time consideration range between 15–120 min, 60 min showed the best S/N ratio.

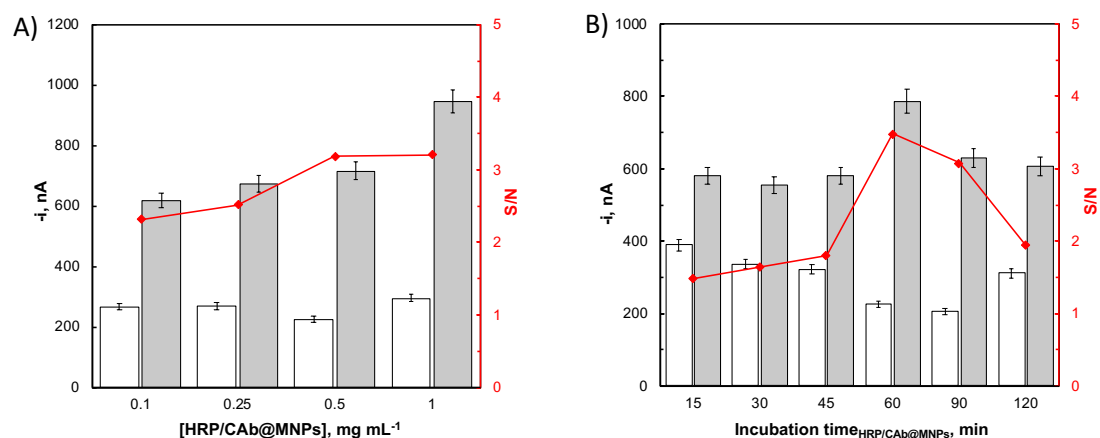


Figure 5.4-9. HRP/Cab@MNPs as the detection probes. Effect of *HRP/Cab@MNPs* loading concentration and their incubation time on the amperometric responses of the immunosensors for 0 ng mL^{-1} (white bar, N) and 10 ng mL^{-1} CRP (gray bars, S) and the corresponding S/N ratio (red line). *HRP/Cab@MNPs* conjugates loading concentration were determined with the range of $0.1\text{--}1 \text{ mg mL}^{-1}$ (30 min incubation) (A) and *HRP/Cab@MNPs* conjugates incubation time were determined with the range of $15\text{--}120 \text{ min}$ (0.5 mg mL^{-1}) (B). All the error bars were calculated as the standard deviation ($n = 3$) of duplicate experiments.

Based on the research results from earlier [119], the immobilization condition for the streptavidin was following the optimal condition without further modification. Then the optimization of bioreceptors–Biotin-Ab_{HRP} in this case– was performed (Figure 5.4-10). $5 \mu\text{g mL}^{-1}$ Biotin-Ab_{HRP} provided the highest specific signal and also the highest S/N ratio. And 30 min was adequate for the effective immobilization of the bioreceptors.

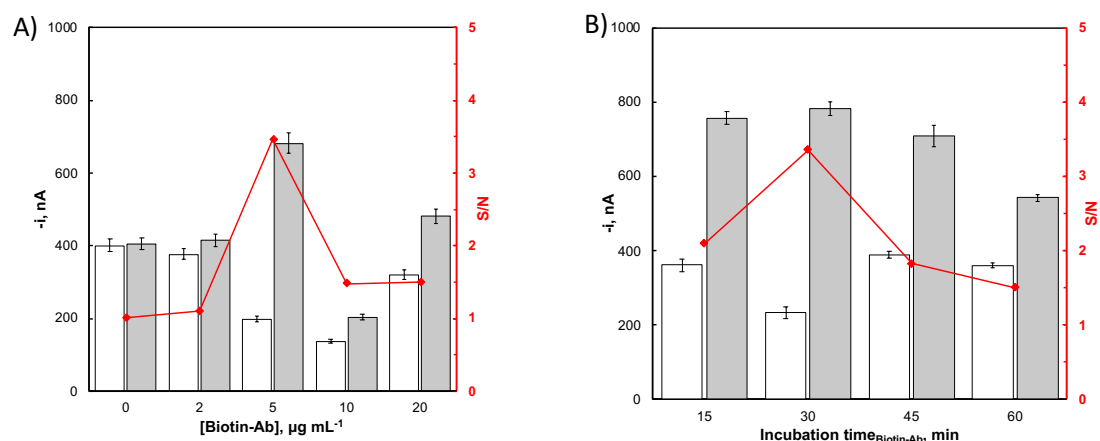


Figure 5.4-10. HRP/Cab@MNPs as the detection probes. Effect of *Biotin-Ab* loading concentration and its incubation time on the amperometric responses of the immunosensors for 0 ng mL^{-1} (white bar, N) and 10 ng mL^{-1} CRP (gray bars, S) and the corresponding S/N ratio (red line). *Biotin-Ab* loading concentration were determined with the range of $0\text{--}20 \mu\text{g mL}^{-1}$ (30 min incubation) (A) and *Biotin-Ab* incubation time were determined with the range of 15--

60 min ($5 \mu\text{g mL}^{-1}$) (B). All the error bars were calculated as the standard deviation ($n = 3$) of duplicate experiments.

The blocking reagents consist of two composites (casein and biotin) were determined to provide the suppress the unspecific interaction, due to the prevention of the cross-interaction with pre-immobilized streptavidin (Figure 5.4-11). 2 % (w/v) casein suppressed the nonspecific interaction with the highest efficiency, so was the 0.5 mg mL^{-1} biotin. The blocking effectiveness with the prolongation of incubation time (15–120 min) was evaluated, and 90 min was considered as the optimal choice to give the ideal outcome.

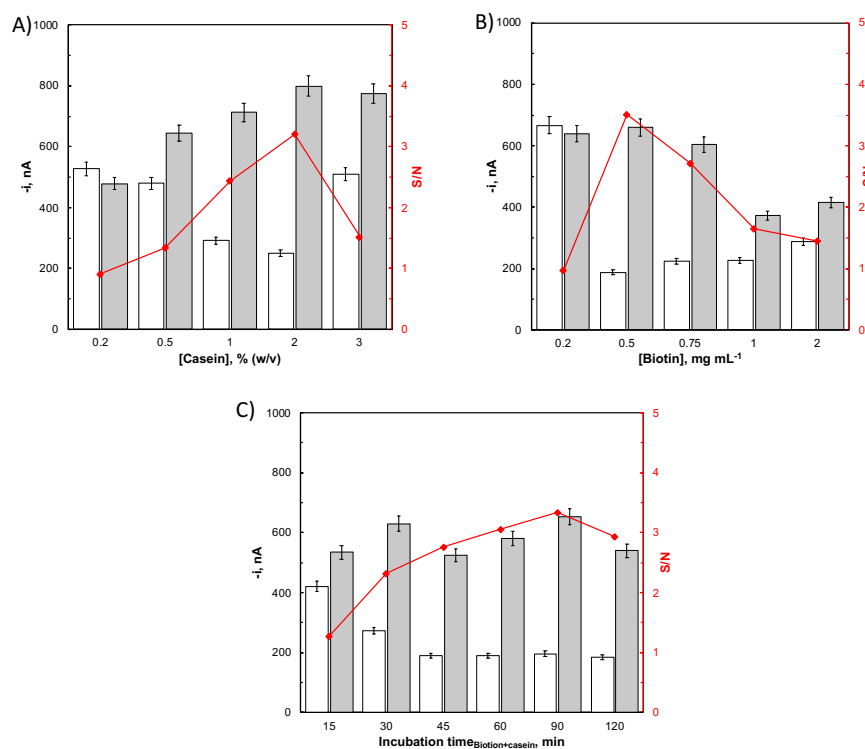


Figure 5.4-11. *HRP/CAb@MNPs as the detection probes. Effect of casein/biotin loading concentration and their incubation time on the amperometric responses of the immunosensors for 0 ng mL^{-1} (white bar, N) and 10 ng mL^{-1} CRP (gray bars, S) and the corresponding S/N ratio (red line). Casein loading concentrations were determined with the range of 0.2–3 % (w/v) (1 mg mL^{-1} biotin, 60 min incubation) (A) and biotin loading concentrations were determined with the range of 0.2–2 $\mu\text{g mL}^{-1}$ (2 % casein, 60 min incubation) and incubation time of CAb/HRP mixture with MNPs were determined with the range of 15–120 min (2 % casein and 0.5 mg mL^{-1} biotin) (C). All the error bars were calculated as the standard deviation ($n = 3$) of duplicate experiments.*

The incubation time of analytes with the immobilized bioreceptors was assessed (Figure 5.4-12). Results showed that the electrochemical signal raised with the increase of incubation time and reached the highest value with 60 min, therefore, it was selected as the optimal option.

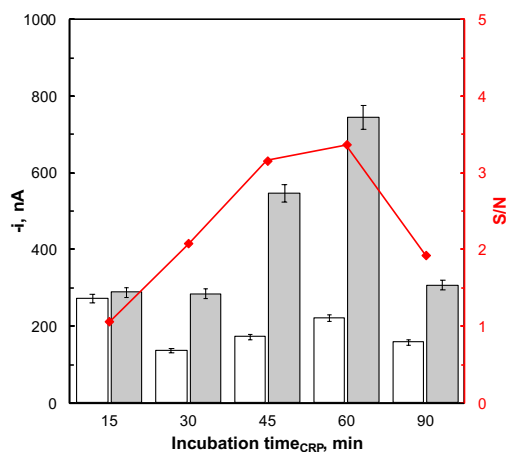


Figure 5.4-12. *HRP/CAb as the detection probes. Effect of CRP incubation time on the amperometric responses of the immunosensors for 0 ng mL⁻¹ (white bar, N) and 10 ng mL⁻¹ CRP (gray bars, S) and the corresponding S/N ratio (red line). CRP incubation time were determined with the range of 15–90 min. All the error bars were calculated as the standard deviation ($n = 3$) of duplicate experiments.*

To better illustrate the optimized condition for the immunoassays using HRP/CAb@MNPs as the detection probes, the condition was summarized in Table 5.4-3.

Table 5.4-3 *Optimization of the experimental variables affecting the immunosensing sensitivity of fabricated sandwich configuration on the SPCEs as the carriers and HRP/CAb@MNPs as the detection probes.*

Experimental variables		
	Tested range	Selected value
Biotin-Ab, $\mu\text{g mL}^{-1}$	0–20	5
Biotin-Ab incubation time, min	15–60	30
Biotin, mg mL^{-1}	0.2–2.0	0.5
Casein, % (w/v)	0.2–3.0	2.0
Incubation time of casein/biotin, min	15–120	90
CRP incubation time, min	15–90	60
[CAb], $\mu\text{g mL}^{-1}$	3–12	6
[HRP], mg mL^{-1}	0.5–2.0	1.0
Incubation of HRP/CAb mixture with MNPs, min	30–180	30

HRP/CAb@MNPs incubation time, min	15–90	60
[HRP/CAb@MNPs], mg mL ⁻¹	0.1–1	0.5

5.4.1.3 HRP/Streptavidin@MNPs as the detection probes

With the same Alde-Dex@MNPs as the nanocarriers for the detection probes, nanoparticles functionalized with HRP, and streptavidin were utilized as the detection probes. The immobilized bioreceptors were the same type when strep-HRP was used as the detection probes, and single HRP molecule were replaced by multiple HRP reporters to provide higher signals under the same condition (Figure 5.4-13).

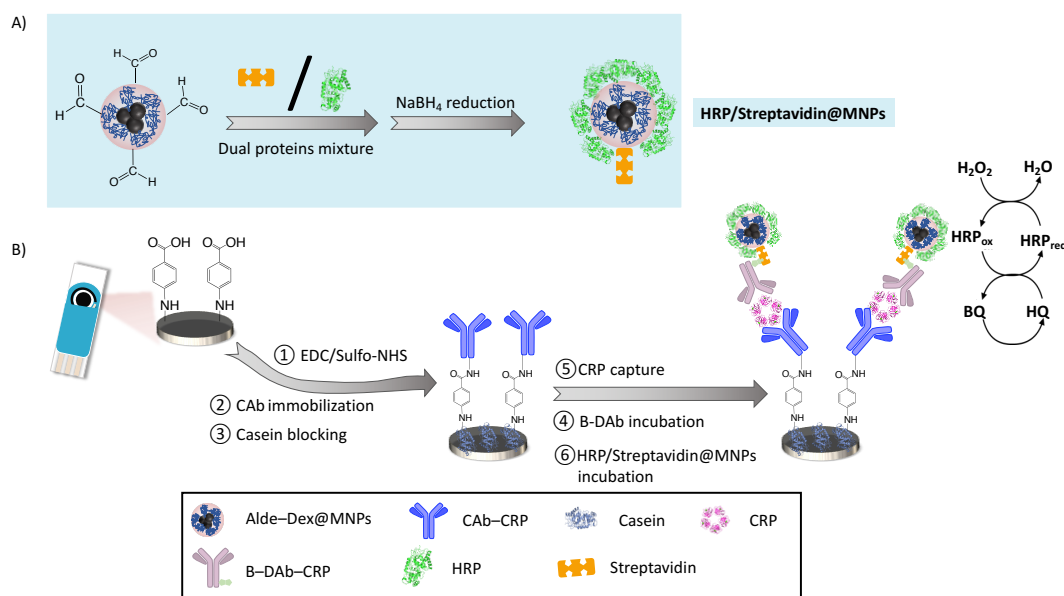


Figure 5.4-13. Biofunctionalization procedures to prepare the CAb_{CRP} immobilized SPCEs as the carriers and HRP/Streptavidin@MNPs as the detection probes.

Due to the optimal condition has been previously studied in the previous determination, only the parameters involving the variation about the HRP/Streptavidin@MNPs nanocarriers were further determined.

To develop the most appropriate nanoprobes, the concentration of HRP and streptavidin were the first of its priorities (Figure 5.4-14). Although the background signals have been increased when HRP concentration has raised from 0.5 mg mL⁻¹ to 3 mg mL⁻¹, the amperometric response also demonstrated increasing tendency, thus the S/N ratio has been pushed to its highest value. And 50 μ g mL⁻¹ streptavidin also met the high signal with the presence of 10 ng mL⁻¹ CRP.

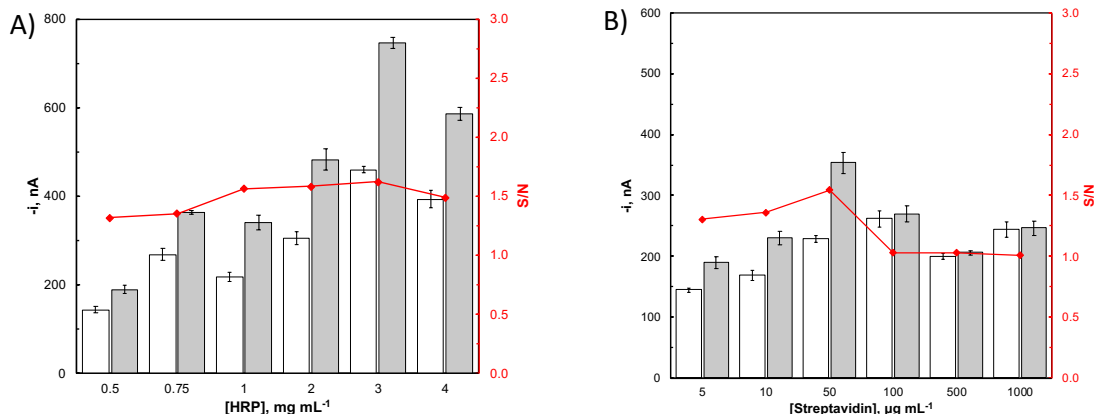


Figure 5.4-14. *HRP/Streptavidin@MNPs as the detection probes. Effect of HRP/Streptavidin loading concentration on the amperometric responses of the immunosensors for 0 ng mL⁻¹ (white bar, N) and 10 ng mL⁻¹ CRP (gray bars, S) and the corresponding S/N ratio (red line). HRP loading concentrations were determined with the range of 0.5–4 mg mL⁻¹ (10 µg mL⁻¹ Streptavidin, 60 min incubation) (A) and Streptavidin loading concentrations were determined with the range of 5–1000 µg mL⁻¹ (3 mg mL⁻¹ HRP 60 min incubation) (B). All the error bars were calculated as the standard deviation ($n = 3$) of duplicate experiments.*

The working concentration of HRP/Streptavidin@MNPs nanocarriers and its interaction time with Biotin-Ab_{CRP} revealed that 0.5 mg mL⁻¹ HRP/Streptavidin@MNPs nanocarriers gave the highest S/N ratio, and 15 min incubation also promoted the best specificity (Figure 5.4-15).

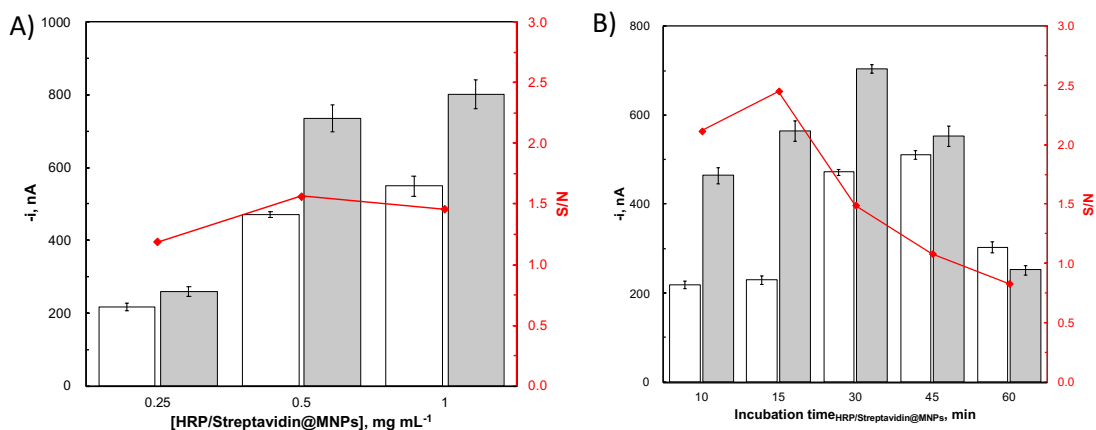
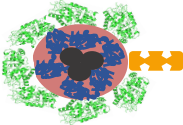


Figure 5.4-15. *HRP/Streptavidin@MNPs as the detection probes. Effect of HRP/Streptavidin@MNPs loading concentration and its incubation time on the amperometric responses of the immunosensors for 0 ng mL⁻¹ (white bar, N) and 10 ng mL⁻¹ CRP (gray bars, S) and the corresponding S/N ratio (red line). HRP/Streptavidin@MNPs loading concentrations were determined with the range of 0.25–1 mg mL⁻¹ (30 min incubation) (A) and HRP/Streptavidin@MNPs incubation time was determined with the range of 10–60 min (0.5*

mg mL⁻¹ HRP/Streptavidin@MNPs) (B). All the error bars were calculated as the standard deviation ($n = 3$) of duplicate experiments.

The listed experimental variables involved in the optimization procedure are shown as Table 5.4-4.

Table 5.4-4 Optimization of the experimental variables affecting the immunosensing sensitivity of fabricated sandwich configuration on the SPCEs as the carriers and HRP/Streptavidin@MNPs as the detection probes.

Experimental variables		
	Tested range	Selected value
Streptavidin loading, $\mu\text{g mL}^{-1}$	5–1000	50
HRP loading, mg mL^{-1}	0.5–4.0	3.0
[HRP/Streptavidin@MNPs], mg mL^{-1}	0.1–1	0.5
Incubation of HRP/CAb mixture with MNPs, min	10–60	15

5.4.2 Characterization of the fabricated immunosensors with each functionalization step

5.4.2.1 HRP/CAb@MNPs as the detection probes

Each step during the preparation of HRP/CAb@MNPs-CRP-Biotin-Ab-Streptavidin-Phe-SPCE immunosensors were characterized using electrochemical impedance spectroscopy (EIS) and cyclic voltammetry (CV) (Figure 5.4-16). Figure 5.4-15A, B revealed that the electrochemical grafting of diazonium salts hampered the electron transfer, and chemistry activation promoted the higher electron transfer efficiency (R_{ct} was 1.17 k Ω , 6.08 k Ω and 0.38 k Ω , respectively). While the immobilization of streptavidin caused the significant increase of R_{ct} due to the conformational hindrance and the reduction of the available active sites on the electrodes. The following coverage of Biotin-Ab and biotin/casein contribute to the high conductivity. The interaction between adsorbed biomolecules and nanoprobes provided higher surface area for the electron-transfer process, thus the R_{ct} was slightly decreased compared with the last step (0.28 k Ω vs 0.20 k Ω).

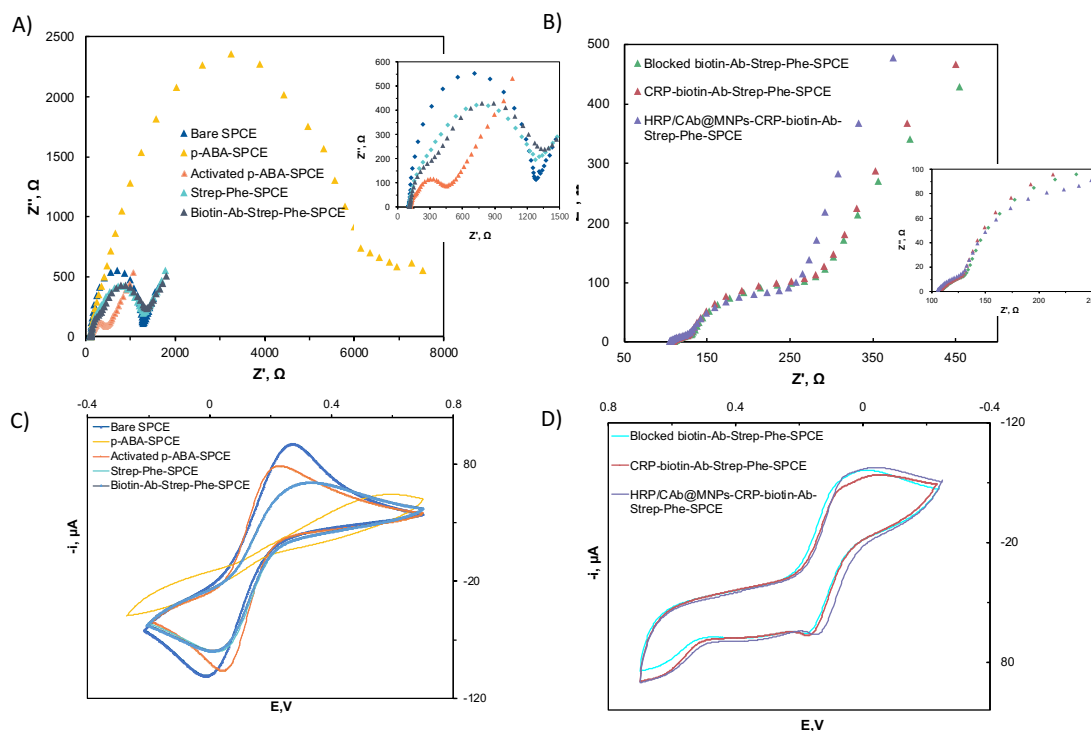


Figure 5.4-16. *HRP/Cab@MNPs as the detection probes. The validation of the sequential biofunctionalization steps during the immunosensors fabrication via cyclic voltammograms (CV) (A, B) and electrochemical impedance spectroscopy (EIS) (C, D) were monitored after each modification step. 5 mM $Fe(CN)_6^{3-/4-}$ prepared in 0.1 M KCl work as the redox probe: Bare SPCE, p-ABA/SPCE, activated p-ABA/SPCE, Streptavidin-Phe-SPCE, biotin-Ab-Streptavidin-Phe-SPCE, biotin/casein blocked Streptavidin-Phe-SPCE, CRP-Biotin-Ab-Streptavidin-Phe-SPCE and HRP/Cab@MNPs-CRP-Biotin-Ab-Streptavidin-Phe-SPCE.*

The obtained CV results (Figure 5.4-16C, D) were in good agreement with the EIS results. The determined results from EIS and CV confirm that the HRP/Cab@MNPs-CRP-Biotin-Ab-Streptavidin-Phe-SPCE immunosensors has been successfully prepared.

5.4.2.2 HRP/Streptavidin@MNPs as the detection probes

Using the same recording strategies, the layer-by-layer immobilization of different biomolecules on the EDC/NHS activated electrodes have been characterized (Figure 5.4-17). Similarly, the EIS results (Figure 5.4-17A) gave clear indication that the direct covalent conjugation of Cab_{HRP} lead to the partly hindered the electron transfer from the probes to the working electrode, and the adsorption of CRP caused a barrier on the electrodes.

Consistent with the aforementioned EIS results, the recorded CV results also confirmed the successful construction of the HRP/Streptavidin@MNPs-CRP-Biotin-Ab-Streptavidin-Phe-SPCE immunosensors.

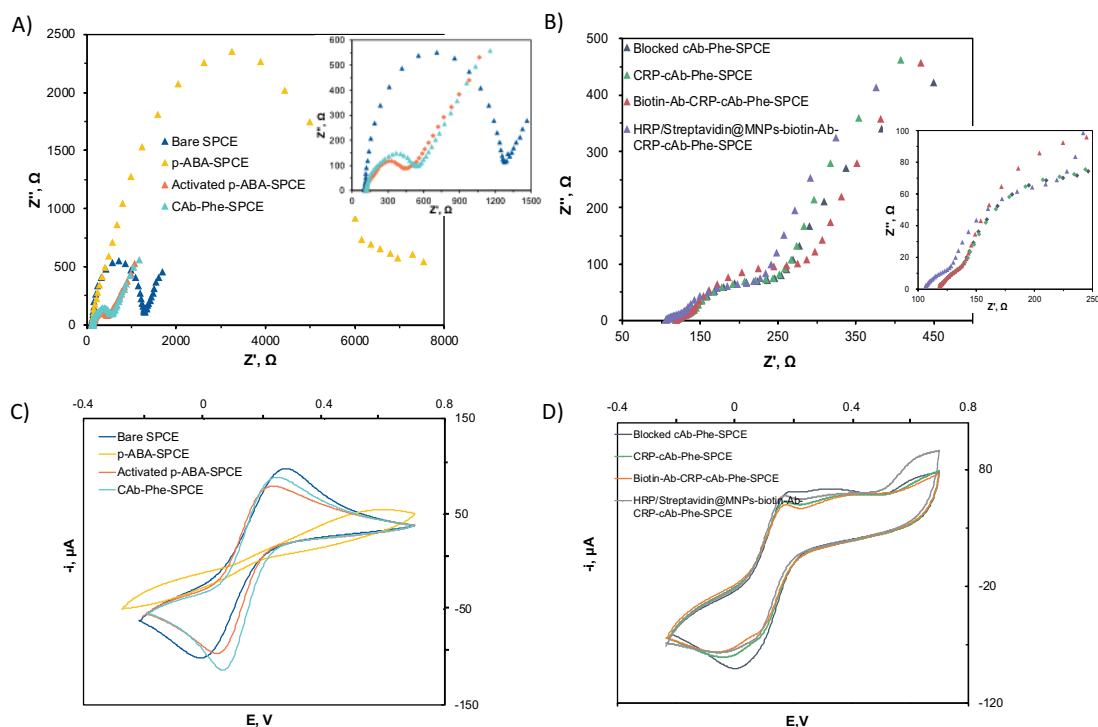


Figure 5.4-17. *HRP/Streptavidin@MNPs as the detection probes.* The validation of the sequential biofunctionalization steps during the immunosensors fabrication via cyclic voltammograms (CV) (A, B) and electrochemical impedance spectroscopy (EIS) (C, D) were monitored after each modification step. 5 mM $Fe(CN)_6^{3-/4-}$ prepared in 0.1 M KCl work as the redox probe: **Bare SPCE**, **p-ABA/SPCE**, **activated p-ABA/SPCE**, **CAb-Phe-SPCE**, **casein blocked CAb-Phe-SPCE**, **CRP-CAb-Phe-SPCE**, **Biotin-Ab-CRP-CAb-Phe** and **HRP/Streptavidin@MNPs-CRP-biotin-Ab-CRP-CAb-Phe**.

5.4.3 Analytical characterization of the fabricated immunosensors

The analytical application of the fabricated immunosensors using three different detection probes were shown in [Figure 5.4-18A](#), and the analytical curves using the nanoprobes were specifically highlighted in [Figure 5.4-18B](#) for better illustration.

For the application of Strep-HRP as the detection probe, the prepared immunosensor has been observed with gradually increased amperometric signals in the range of 0–100 ng mL⁻¹ CRP, and the recorded signals was linearly increased over a range from 2.77 to 100 ng mL⁻¹ CRP. A regression equation with i (nA) = (9.87 ± 0.1) [CRP] (nA mL ng⁻¹) + (105.07 ± 0.003) (nA) ($R^2 = 0.995$) was found, with a LOD of 0.83 and LOQ was estimated at 2.77 ng mL⁻¹, respectively (according to $3 \times s_b/m$ and $10 \times s_b/m$).

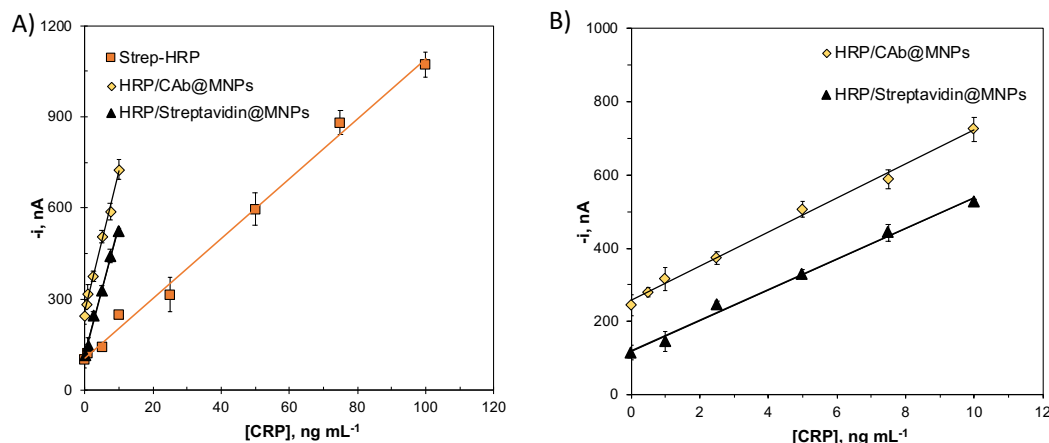


Figure 5.4-18. Analytical characterization of the immunosensor using SPCEs as the carriers. The wide range of CRP concentration (0–100 ng mL $^{-1}$) was measured when Strep-HRP as the detection probes (A), while 0–10 ng mL $^{-1}$ CRP were measured for HRP/Streptavidin@MNPs and HRP/CAb@MNPs as the detection probes (B), CRP prepared in aqueous buffer was utilized.

While for the nanoprobes (HRP/CAb@MNPs and HRP/Streptavidin@MNPs), multiple HRP reporters have been grafted on the nanocarriers instead of single reporter. Both nanoprobes demonstrated a similar dynamic range, while HRP/CAb@MNPs show higher sensitivity. For HRP/CAb@MNPs-CRP-Biotin-Ab-Streptavidin-Phe-SPCE immunosensors, the regression equation was i (nA) = (46.43 ± 0.02) [CRP] (nA mL ng $^{-1}$) + (257.17 ± 0.0006) (nA) ($R^2 = 0.996$) in the range of 0.50 to 10 ng mL $^{-1}$ CRP. When HRP/Streptavidin@MNPs were utilized, a slightly less sensitive curve was observed, which fitting the equation of i (nA) = (41.76 ± 0.024) [CRP] (nA mL ng $^{-1}$) + (118.87 ± 0.001) (nA) ($R^2 = 0.993$) in the range of 0.61 to 10 ng mL $^{-1}$. It is obvious that nanoprobes contain multiple HRP molecules significantly enhanced the LOD with at least 4.6-fold, this improved sensitivity can be ascribed to the signal-amplification of nanoprobes. The adequate aldehyde groups and higher surface area of nanocarriers improved the immobilization concentration of HRP molecules. The interaction probability between nanoprobes with CRP or Biotin-Ab had been significantly enhanced (even at very low concentration of analytes). In addition, the efficient adsorption of nanoparticles on the electrodes also improves the electron transfer efficiency, thereby leading to the enhanced sensitivity.

Storage stability and reproducibility of fabricated immunosensors was examined (Figure 5.4-19). The reproducibility of those three immunosensors were determined by recording 10 bioreceptors functionalized electrodes using the CRP concentration shown in Table 5.4-5. An acceptable reproducibility with 3.11 %, 4.15 % and 4.93 % was obtained for Strep-HRP, HRP/CAb@MNPs, and HRP/Streptavidin@MNPs, respectively. The bioreceptors conjugated

electrodes were stored at 4 °C and periodically monitored for the CRP capture, the S/N ratio of prepared immunosensors using the nanoprobes have maintained over a period of 16 days, indicating the good stability of the functionalized electrodes.

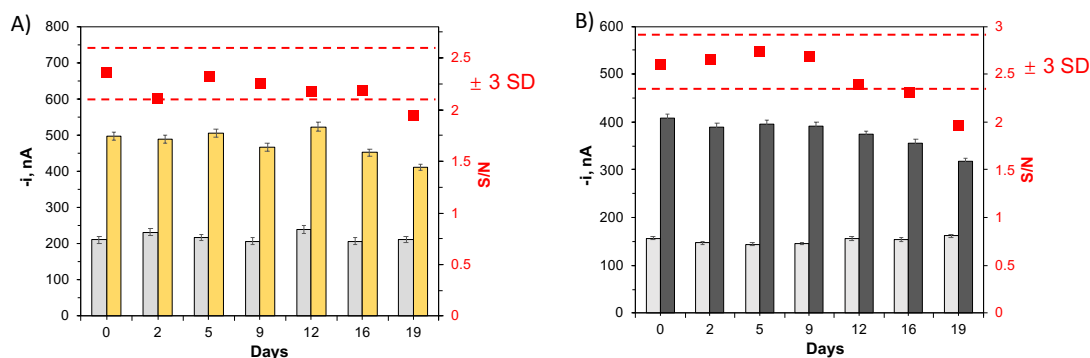


Figure 5.4-19. Monitoring the storage stability of bioreceptors of immobilized immunosensors stored in filtered PBS at 4 °C, HRP/CAb@MNPs (A) and HRP/Streptavidin@MNPs (B) were measured, respectively. The amperometric responses were measured in the absence (gray bars, N) or in the presence (yellow bars for HRP/CAb@MNPs and black bar for HRP/Streptavidin@MNPs, S) of 5 ng mL⁻¹ CRP prepared in aqueous buffer, and the corresponding S/N ratio (red line). The calculated S/N ratios are displayed as red squares.

Table 5.4-5 Analytical characteristics for the determination of CRP in buffered solution using the SPCEs as the carriers and comparison of different detection probes.

Parameters	SPCEs as the carriers		
	Strep-HRP	HRP/CAb@MNPs	HRP/Streptavidin@MNPs
Linear range, ng mL ⁻¹	2.77–100	0.50–10	0.61–10
r	0.995	0.996	0.993
Slope, nA/ng mL ⁻¹	9.87 ± 0.1	46.43 ± 0.02	41.76 ± 0.024
Intercept, nA	105.07 ± 0.003	257.17 ± 0.0006	118.87 ± 0.001
LOD ^a , ng mL ⁻¹	0.83	0.15	0.18
LOQ ^b , ng mL ⁻¹	2.77	0.50	0.61
RSD	3.11 % ^c	4.15 % ^d	4.93 % ^e
Storage stability, days	N. D ^f	19	16

Selectivity against interferents		N. D	YES ^g	YES
----------------------------------	--	------	------------------	-----

a, b: calculated according to the $3 \times sb/m$ and $10 \times sb/m$ criteria, respectively, sb: standard deviation ($n = 10$) for measurements performed in the absence of CRP, m: slope value of the calibration plots.

c: the determination was performed with 5 ng mL^{-1} CRP ($n = 10$).

d: the determination was performed with 50 ng mL^{-1} CRP ($n = 10$).

e: the determination was performed with 5 ng mL^{-1} CRP ($n = 10$).

f: Not determined.

g: BSA, HSA, human IgG, cTnI, cTnT and NT-proBNP were utilized as the interferents to measure the potential non-interference performance of the fabricated immunosensor using different detection probes.

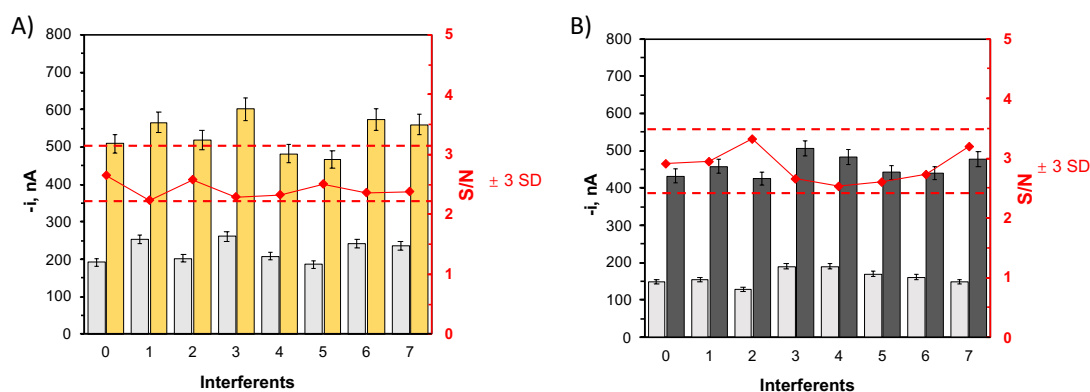


Figure 5.4-20. Determination of the potential interference effect without (0) or with the appearance of several interferents (1–7). The amperometric responses of the immunosensors for 0 ng mL^{-1} (white bar, N) and 5 ng mL^{-1} CRP and the corresponding S/N ratio (red line) were monitored. HRP/Cab@MNPs (A) and HRP/Streptavidin@MNPs (B) were determined respectively. 5.0 mg mL^{-1} BSA (1), 5.0 mg mL^{-1} HSA (3), 1.0 mg mL^{-1} human IgG (4), 500 ng mL^{-1} cTnI (5), 500 ng mL^{-1} cTnT (6) and 7.5 ng mL^{-1} NT-proBNP (7) were measured and compared, respectively. All the error bars were calculated as the standard deviation ($n = 3$) of duplicate experiments.

Selectivity of the immunosensors against other interferents was also investigated for the nanoprobes (Figure 5.4-20). The variation of the S/N ratio and amperometric responses induced by the non-specific interaction upon the addition of interferents were not obvious for both

nanoprobes, which the S/N ratios were maintained within the ± 3 SD range. Therefore, the prepared immunosensing platforms and nanoprobes have acceptable performance.

5.5 Magnetic nanoparticles as the bioreceptors carrier to detect CRP in real samples

INTRODUCTION

SPCEs as the bioreceptors carriers demonstrated great advantages with enhanced sensitivity toward CRP analytes, and both the dual-functionalized nanocarriers show better detection efficiency than single HRP enzyme reporter. While the short linear range (0–10 ng mL⁻¹ of CRP) of dual-functionalized nanocarriers limit the possible application for the possible real-samples determination. When SPCEs were replaced by magnetic beads as the carriers, the analytical performance may demonstrate diversity with different analytes. The same linear range with better sensitivity was reported for interleukin-13 receptor $\alpha 2$ [116, 219], while 100-fold enhanced dynamic range with worse sensitivity was observed for cadherin-17 [116, 220].

RESULTS

In this part, the Alde-Dex@MNPs were utilized as the nanocarriers instead of SPCEs to sensitively detect the CRP analytes (Figure 5.5-1). The differences between those two strategies are the functionality of nanoparticles (detection probes or bioreceptor nanocarriers) and the bioreceptors immobilization chemistries (activated carboxylic or aldehyde moieties).

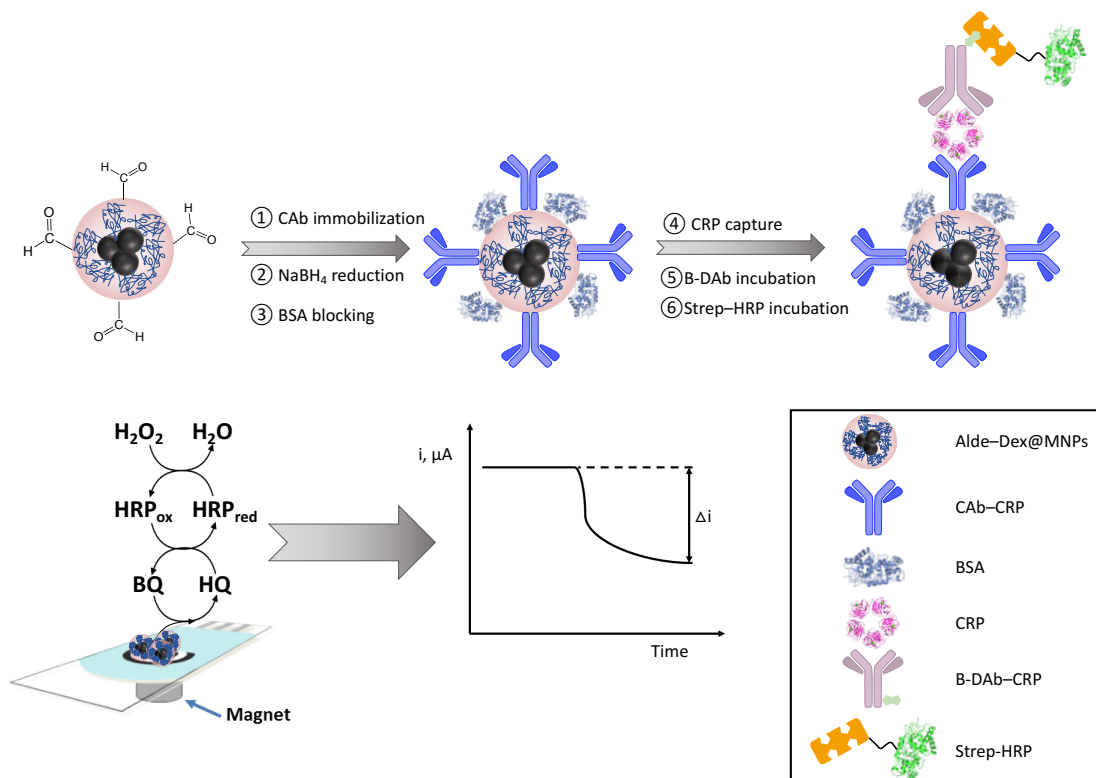


Figure 5.5-1. Illustration of the preparation and signal detection involved in the fabricated immunosensor using Alde-Dex@MNPs to perform the CRP detection.

5.5.1 Optimization of experimental variables to achieve the immunosensor with the highest sensitivity

To obtain the immunosensors with the highest sensitivity, the electrochemical signal responses against different experimental variables at the same analytes concentration were observed.

The amount of Alde-Dex@MNPs used in the CAb_{CRP} immobilization step was first evaluated from 10–200 μg per sample (Figure 5.5-2). In the range of 10–50 μg MNPs, the unspecific signals maintained minor change while specific interaction was enhanced with the increase of MNPs concentration. While the even concentrated MNP concentration caused obvious increased background signal, 25 μg was selected for the following amount when taking the S/N ratio as the major decision factor.

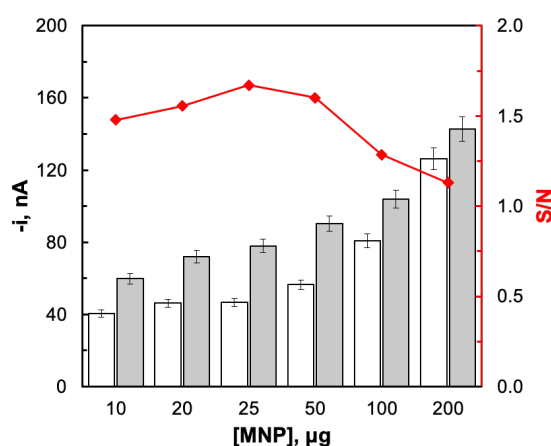


Figure 5.5-2. Effect of Alde-Dex@MNPs amount on the amperometric responses of the immunosensors for 0 ng mL⁻¹ (white bar, N) and 30 ng mL⁻¹ CRP (gray bars, S) and the corresponding S/N ratio (red line). Alde-Dex@MNPs amounts were determined with the range of 10–200 μg . All the error bars were calculated as the standard deviation ($n = 3$) of duplicate experiments.

When evaluating the CAb_{CRP} immobilization parameters on the analytical performance, its immobilization concentration and incubation time were investigated (Figure 5.5-3). The CAb_{CRP} immobilization amount did not have obvious differences in the absence of target analytes, the specific response contributed by the analytes revealed that 25 $\mu\text{g mL}^{-1}$ was the optimized option, and 30 min incubation time promoted the desired S/N ratio.

As stated in Chapter 5.2, when using the colorimetric method to evaluate the fabricated immunosensors, it was not necessary to block the unspecific interaction. However, the CRP recognition system with the sandwich format may cause the unspecific interaction with pre-immobilized biomolecules. Thus, the concentration and the corresponding incubation time of BSA was determined to suppress the unspecific binding (Figure 5.5-4). The S/N ratio reached the highest value with 3 % (w/v) BSA while even higher BSA inhibited the signal with the

presence of analytes. Similarly, the specific signals did not have an obvious increase when incubation time was over 45 min, and 60 min was selected as the best choice.

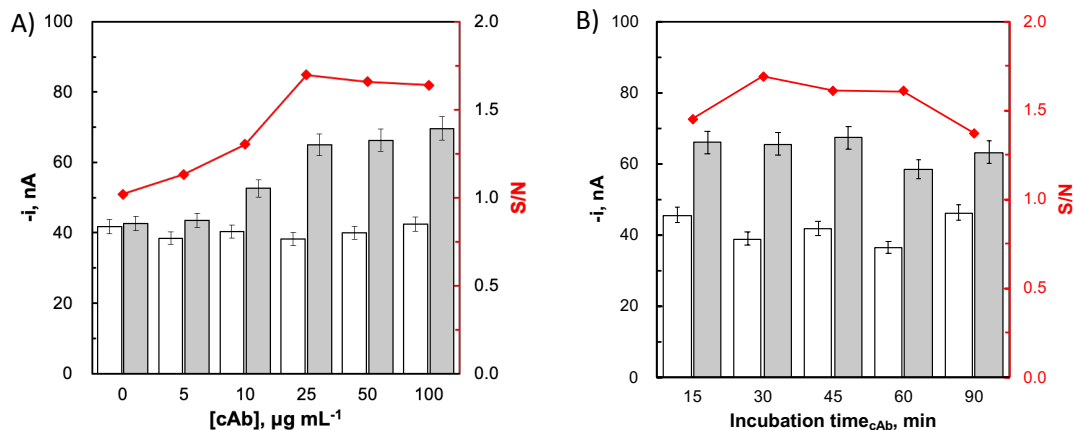


Figure 5.5-3. Effect of *CAb* loading concentration and its incubation time on the amperometric responses of the immunosensors for 0 ng mL^{-1} (white bar, *N*) and 30 ng mL^{-1} CRP (gray bars, *S*) and the corresponding *S/N* ratio (red line). *CAb* loading concentrations were determined with the range of $0\text{--}100 \mu\text{g mL}^{-1}$, 30 min (A) and *CAb* incubation time was determined with the range of $15\text{--}90 \text{ min}$, $25 \mu\text{g mL}^{-1}$ (B). All the error bars were calculated as the standard deviation ($n = 3$) of duplicate experiments.

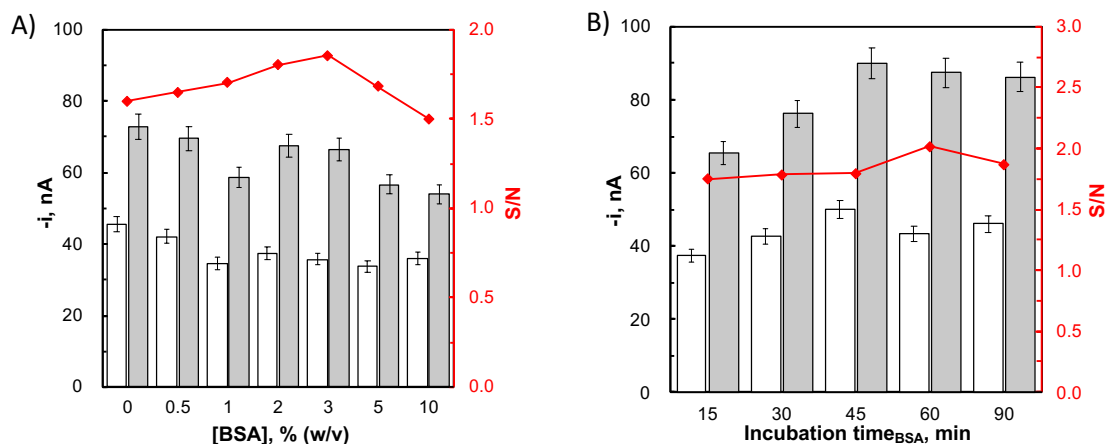


Figure 5.5-4. Effect of *BSA* loading concentration and its incubation time on the amperometric responses of the immunosensors for 0 ng mL^{-1} (white bar, *N*) and 30 ng mL^{-1} CRP (gray bars, *S*) and the corresponding *S/N* ratio (red line). *BSA* loading concentrations were determined with the range of $0\text{--}10 \%$ (w/v), 30 min (A) and *BSA* incubation time were determined with the range of $15\text{--}90 \text{ min}$, 3% (w/v) (B). All the error bars were calculated as the standard deviation ($n = 3$) of duplicate experiments.

Following the determination of CRP incubation time from 15 min to 90 min (Figure 5.5-5), results confirmed that 60 min incubation can achieve the low unspecific interaction while maintaining the high specific electrochemical signal.

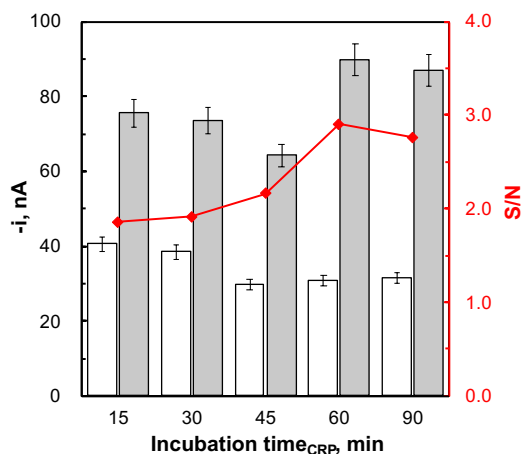


Figure 5.5-5. Effect of *CRP* incubation time on the amperometric responses of the immunosensors for 0 ng mL^{-1} (white bar, N) and 30 ng mL^{-1} CRP (gray bars, S) and the corresponding S/N ratio (red line). CRP incubation time were determined with the range of 15–90 min. All the error bars were calculated as the standard deviation ($n = 3$) of duplicate experiments.

The concentration and the incubation time of Biotin-AbCRP were investigated further (Figure 5.5-6), the S/N ratio was obviously enhanced with concentration of $0.5 \text{ } \mu\text{g mL}^{-1}$ and incubated for 45 min.

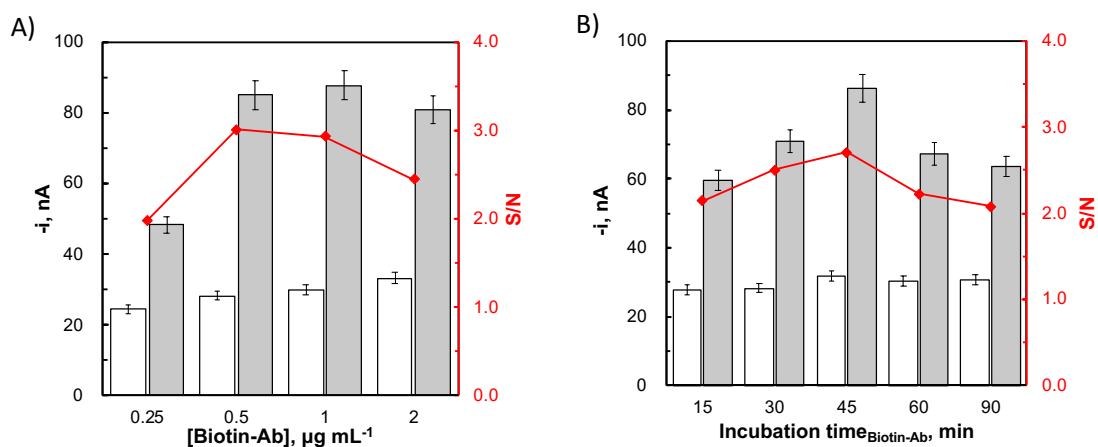


Figure 5.5-6. Effect of *B-DAb* loading concentration and its incubation time on the amperometric responses of the immunosensors for 0 ng mL^{-1} (white bar, N) and 30 ng mL^{-1} CRP (gray bars, S) and the corresponding S/N ratio (red line). *B-DAb* loading concentrations were determined with the range of $0.25\text{--}2 \text{ } \mu\text{g mL}^{-1}$, 30 min (A) and *B-DAb* incubation time were determined with the range of 15–90 min, $0.5 \text{ } \mu\text{g mL}^{-1}$ (B). All the error bars were calculated as the standard deviation ($n = 3$) of duplicate experiments.

As shown in Figure 5.5-7, the concentration of Strep-HRP had great influence on the obtained electrochemical signals, which over 1500 nA were observed when Strep-HRP was diluted with low dilution factor (≤ 250). 250-fold diluted Strep-HRP with incubation for 30 min were selected via comprehensive consideration of S/N ratio and amperometric responses.

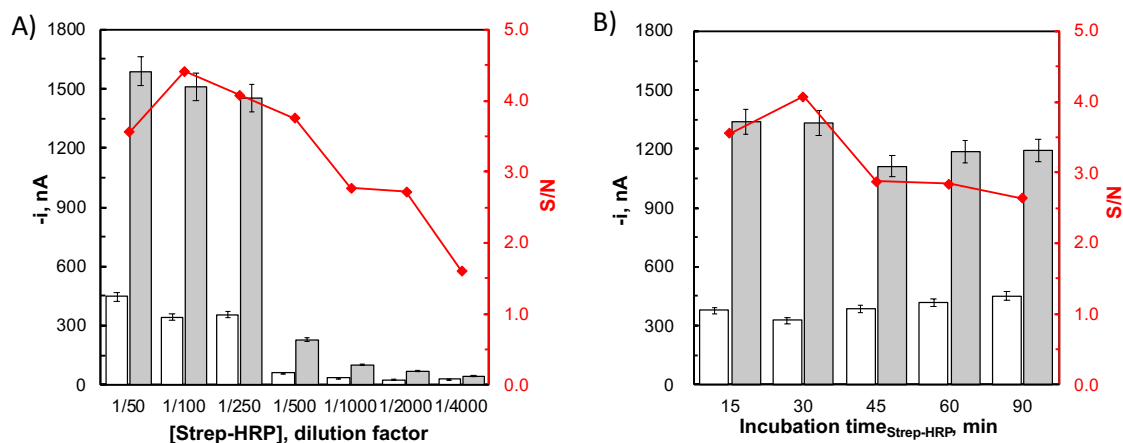


Figure 5.5-7. Effect of *Strep-HRP* concentration and its incubation time on the amperometric responses of the immunosensors for 0 ng mL^{-1} (white bar, *N*) and 30 ng mL^{-1} CRP (gray bars, *S*) and the corresponding *S/N* ratio (red line). *Strep-HRP* loading concentrations were determined with the range of 1/4000–1/50 dilution factor, 30 min (A) and *Strep-HRP* incubation time were determined with the range of 15–90 min, 1/100 dilution factor (B). All the error bars were calculated as the standard deviation ($n = 3$) of duplicate experiments.

Taking the sensitivity of the immunosensor as the key consideration, the optimal experimental variables for the fabrication of immunosensors has been summarized in Table 5.5-1.

Table 5.5-1 Optimization of the experimental variables affecting the immunosensing sensitivity of fabricated sandwich configuration on the Alde-Dex@MNPs for the detection of CRP.

Experimental variables	Tested range	Selected value
[MNP], μg	10–200	25
[CAb _{CRP}], $\mu\text{g mL}^{-1}$	0–100	25
CAb _{CRP} incubation time, min	15–90	30
CRP incubation time, min	15–90	60
BSA, %(w/v)	0–10	3
BSA incubation time, min	15–90	60
[B-DAb _{CRP}], $\mu\text{g mL}^{-1}$	0.25–2	0.5
B-DAb _{CRP} incubation time, min	15–90	45
[<i>Strep-HRP</i>], dilution factor	1/4000–1/50	1/100
<i>Strep-HRP</i> incubation time, min	15–90	30

5.5.2 Analytical characterization of the fabricated immunosensors using Alde-Dex@MNPs as the carriers.

With the optimization of experimental variables, the electrochemical responses corresponding with the different concentration of CRP prepared in the aqueous buffer have been determined (Figure 5.5-8). The CRP target with the concentration range from 0 to 500 ng mL⁻¹ have been evaluated, while a linear relationship which fitting the equation i (nA) = (42.09 ± 0.023) [CRP] (nA mL ng⁻¹) + (194.60 ± 0.006) (nA) has been observed in the range of 4.7-250 ng mL⁻¹ (R² = 0.9947). Though an even wider dynamic range was also observed in the range of 4.7-300 ng mL⁻¹, the diminished relevance between amperometric signals with CRP concentration occurred when a coefficient of determination with 0.991 was calculated in this case.

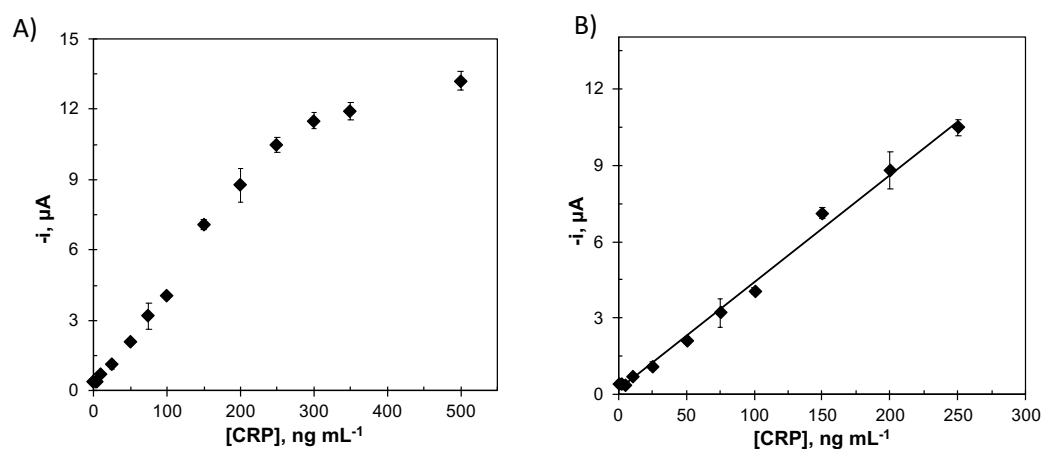


Figure 5.5-8. Analytical characterization of the immunosensor using Alde-Dex@MNPs as the carriers. The wide range of CRP concentration (0–500 ng mL⁻¹) were determined (A) and the fabricated immunosensor demonstrated a good linear relationship between 0–250 ng mL⁻¹ CRP prepared in aqueous buffer.

The anti-interference of the fabricated immunosensors was further investigated to prevent the possible influence on its analytical performance (Figure 5.5-9). The results demonstrated that the presence of human IgG and HSA in the incubation buffer entailed a reduction in the immunosensor ability of the amperometric response when 50 ng mL⁻¹ CRP was spiked in the determination system. However, the amperometric signals were also weakened with the absence of CRP analytes, therefore, the S/N ratios have been maintained in the reasonable range (± 3 SD) with the presence of all the detected interferents.

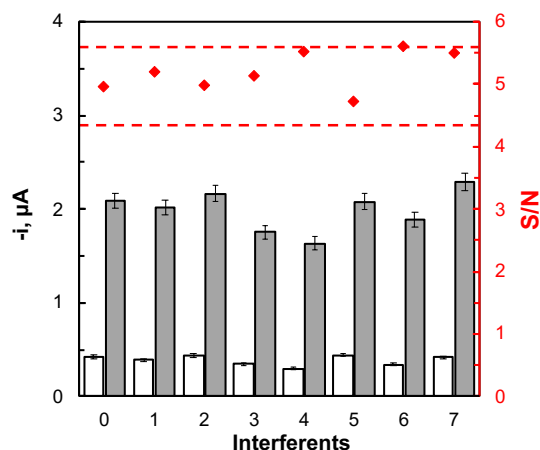


Figure 5.5-9. Determination of the potential interference effect without (0) or with the appearance of several interferents (1–7). The amperometric responses of the immunosensors for 0 ng mL^{-1} (white bar, N) and 50 ng mL^{-1} CRP (gray bars, S) and the corresponding S/N ratio (red line) were monitored. 5.0 mg mL^{-1} BSA (1), 5.0 mg mL^{-1} HSA (3), 1.0 mg mL^{-1} human IgG (4), 500 ng mL^{-1} cTnI (5), 500 ng mL^{-1} cTnT (6) and 7.5 ng mL^{-1} NT-proBNP (7) were measured and compared, respectively. All the error bars were calculated as the standard deviation ($n = 3$) of duplicate experiments.

The storage stability of the immunosensors were investigated with the long-term reservation (Figure 5.5-10). Using the amperometric response determined in the first day as the reference, the electrochemical signals with the absence of CRP have maintained the high stability after 28 days storage that all the determined signals were in the range of ± 3 SD, so as the performance with the presence of CRP analytes.

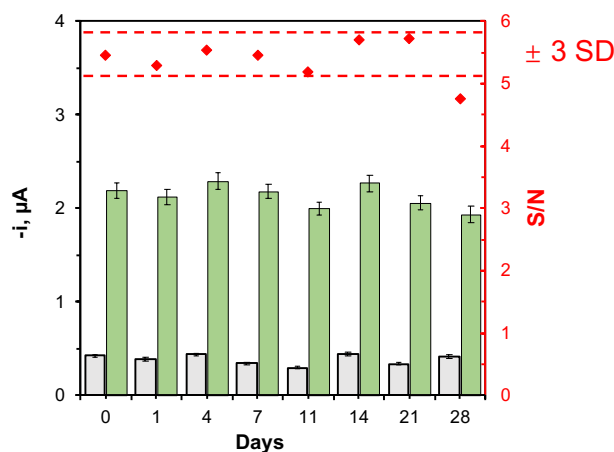


Figure 5.5-10. Storage stability of immobilized CAb_{CRP} on the Alde-Dex@MNPs for the detection of CRP, the functionalized MNPs were stored in filtered PB buffer at $4 \text{ }^{\circ}\text{C}$. The amperometric responses of the immunosensors without (gray) or with the presence of 50 ng mL^{-1} CRP (cyan) were measured with the prolonged storage time.

The reproducibility of the immunosensors determination with the presence of 50 ng mL^{-1} CRP with nice parallel measurements was tested (Table 5.5-2). The immunosensors were prepared in the same manner and the same day, and a relative standard deviation (RSD) value of 2.99 %

was calculated. These results indicated the good reproducibility of the immunosensors, and also proved the versatility of the developed protocols and experiment parameters during the preparation of immunosensors.

Table 5.5-2 Analytical characteristics for the determination of CRP in buffered solution using the Alde-Dex@MNPs as the carriers.

Parameters	Alde-Dex@MNPs
Linear range, ng mL ⁻¹	4.7–250
r	0.9947
Slope, nA/ng mL ⁻¹	42.092 ± 0.023
Intercept, nA	194.6 ± 0.006
LOD ^a , ng mL ⁻¹	1.41
LOQ ^b , ng mL ⁻¹	4.7
Relative standard deviation (RSD), %	2.99 % ^c
Storage stability, days	28
Selectivity against interferents	Yes ^d

a, b: calculated according to the $3 \times s_b/m$ and $10 \times s_b/m$ criterion, respectively, s_b : standard deviation ($n = 10$) for measurements performed in the absence of CRP, m : slope value of the calibration plots.

c: the determination was performed with 50 ng mL⁻¹ CRP ($n = 9$).

d: BSA, HSA, human IgG, cTnI, cTnT and NT-proBNP were utilized as the interferents to measure the potential non-interference performance of the fabricated immunosensor using MNPs as the carriers.

5.5.3 Determination of the CRP biomarkers in the real samples

Instead of the CRP determination in the spiked aqueous buffer, the precise quantification of the CRP concentration in the unknown real samples will be more appealing. Therefore, the developed immunosensors were tested for their potential application of CRP proteins in healthy individuals and patients have been diagnosed with heart failure.

Serial dilution of the human serum was performed and the corresponding amperometric determination were validated to prevent the possible matrix effect of the nanoparticles, 1/1000 dilution factor was proven to effectively eliminate the interference of the complex biological condition.

Results from the amperometric determination revealed the great variability of the healthy individuals and heart failure patients. All the samples from healthy individuals have been measured with the CRP concentration were in the range of 1–3 $\mu\text{g mL}^{-1}$, which are the

demarcation lines of low and moderate heart failure risk, respectively. While the samples from the heart failure patients gave strong indication of heart failure risk with the CRP range of 8.74–45.93 $\mu\text{g mL}^{-1}$ (Figure 5.5-11).

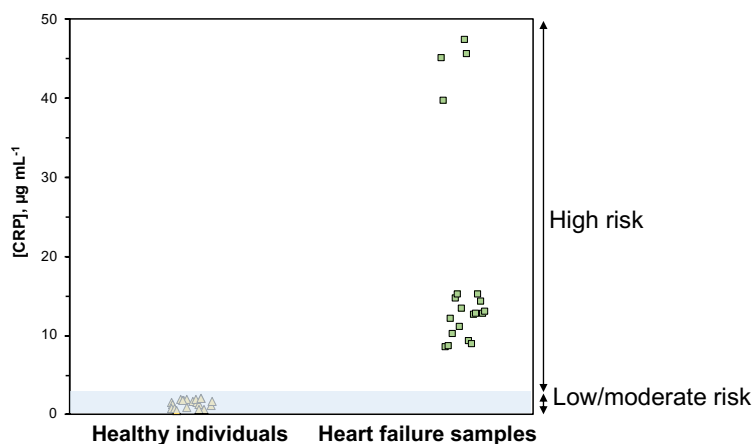


Figure 5.5-11. Application of the fabricated immunosensor for the detection of CRP in human serum samples using Alde-Dex@MNPs as the carriers. Samples from healthy individuals (orange dots) and samples from heart failure patients (cyan dots) demonstrated obvious CRP concentration in the serum samples.

To verify the versatility of the developed immunosensors, the “gold standard” determination method—ELISA—was also performed. As shown in Table 5.5-3, t_{exp} had distributed in the range of 0.33–0.99, which indicate that no significant differences have been observed with all the measures between amperometric determination and ELISA quantification.

Table 5.5-3 Measurement of the CRP concentration in real samples (human serum) with the fabricated immunosensor using Alde-Dex@MNPs as the carriers, the obtained results were compared with the results from commercial ELISA kit.

Sample types	Sample No.	ELISA (RSD)	MNPs-based immunoassay (RSD)	t_{exp}^a
Healthy individuals	1	1.04 ± 0.08 (3.68 %)	1.10 ± 0.05 (4.17 %)	0.41
	2	1.66 ± 0.18 (3.28 %)	1.74 ± 0.13 (7.68 %)	0.58
	3	1.95 ± 0.16 (2.46 %)	1.91 ± 0.12 (11.98 %)	0.70
	4	1.53 ± 0.13 (2.59 %)	1.70 ± 0.2 (6.51 %)	0.28

Heart failure patients	1	45.93 ± 3.65 (2.73 %)	44.34 ± 1.25 (7.52 %)	0.82
	2	8.74 ± 1.45 (7.88 %)	8.77 ± 0.33 (3.82 %)	0.99
	3	12.50 ± 1.79 (7.73 %)	12.31 ± 0.35 (2.81 %)	0.84
	4	14.40 ± 1.17 (4.80 %)	14.69 ± 0.49 (3.13 %)	0.84
	5	11.79 ± 1.68 (7.79 %)	12.41 ± 0.31 (8.38 %)	0.33

a: t_{exp} means student's t-test

In addition, ELISA analysis demonstrated lower standard deviation (2.46 %–7.79 %) than amperometric measurements (2.81 %–11.98 %), while the developed immunosensors can be a better option in terms of preparation time, easy-of-operation to the non-trainers and potential multiplexing determination of multiple biomarkers [221].

6. Discussion

For the fabrication of effective immunosensors with high sensitivity and good robustness against complex biofluids, the rational selection of antibody immobilization strategy and the corresponding supporting materials would promote better immunosensing performance.

While faced with the tremendous selections of supporting materials with distinct reactive functionalities, how to develop a universal strategy to achieve the site-directed antibody conjugation is the first challenge, and high versatility with the different full-length antibodies would further contribute to its attractiveness. The second challenge is to find the optimal (or suboptimal option considering the priorities and emphasis of specific immunoassay) bioreceptors carrier, which affects the antibody immobilization technique and the proper preservation of its biological functionality. In addition, it contributes to the selection of signal transmission techniques, for example, colorimetric assay or electrochemical determination.

To address those two challenges described above, in this dissertation, the following discussion will be separated into several themes:

6.1 Antibody immobilization strategies targeting the amine groups (NH₂)

Different reactive sites within the antibody structure or exposure out on the antibody surface are preferred targets for stable conjugation [222]. While taking population and accessibility of the amino residues, limited options can be selected. In addition, the distribution of accessible amino residues is highly heterogeneous, which not only affects the surface coverage density but also the interaction sites [222].

Nucleophilic NH₂ groups including the N-terminus and lysine residues are the most welcomed options, because of the large number of reactive sites (over 80 accessible sites per antibody) but also their preferable exposing characterization (Figure 1). As it can be clear seen, the front plans have the highest density of Lys residues despite of the IgG types, which means it has the most possibility to interact with reactive functionality via this side. With the quantification of the ionized residues, the front plane has the about 2-fold higher density than top planes and the bottom plane has the lowest density [35]. Moreover, different chemistry options targeting the NH₂ moieties have been developed to achieve irreversible conjugation with high efficiency and specificity [3, 9].

In this dissertation, two groups of chemistry functionalities (aldehyde/glyoxyl groups and carboxylic groups) have been grafted on the supporting materials. Moreover, the performance of fabricated immunosensors using those conjugation strategies have been compared concerning their better control ability of site-specificity and biofunctionality of immobilized antibody.

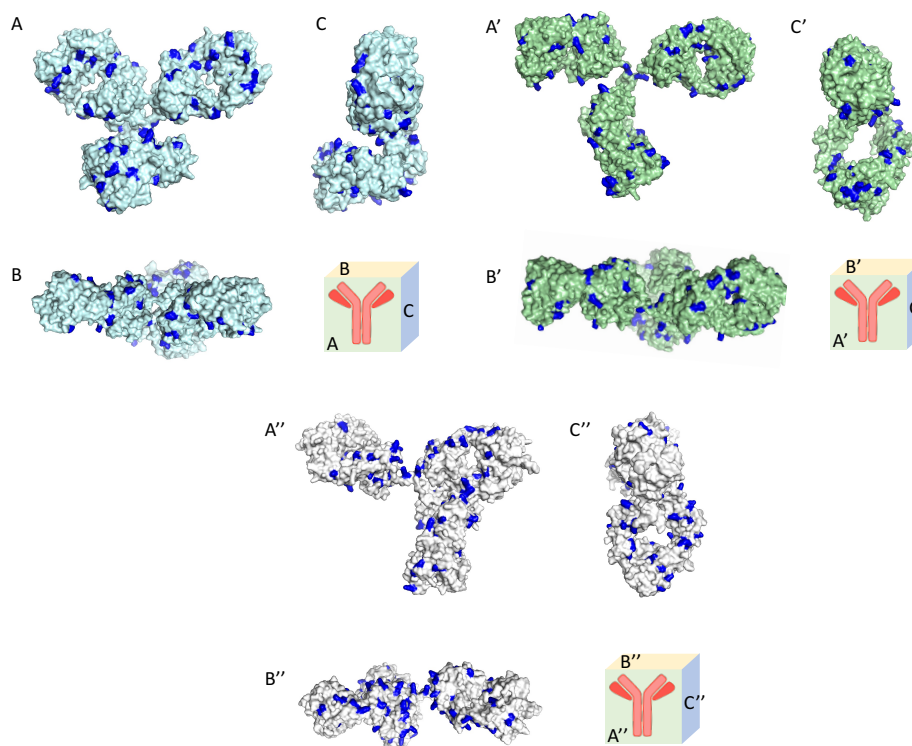


Figure 1. Three typical antibody structures (PDB ID: 1IGY for A, 1IGT for B and 1HCH for C, respectively) and their three-dimension formats. Antibody structures were generated and colored by PyMOL 2.4.1, and Lys residues were colored in blue color for the better illustration.

6.1.1 Glyoxyl and aldehyde moieties—achieving the multipoint interaction via the regions with most abundant NH_2

Highly activated glyoxyl agarose supports are likely to realize the fast multiple interactions with proteins within a very short time at suitable alkaline pH, and the reaction will be directed through the regions with the highest density of lysine residues [50]. The immobilization rate of the antibody is highly managed by the incubation pH (Figure 5.1-2), incubating at pH 10.0 has about 100-times higher immobilization rate than conjugation at pH 8.5. These distinct immobilization rates were contributed by two factors, which are the reactivity of glyoxyl groups and the accessibility of NH_2 groups. Glyoxyl groups demonstrate excellent reactivity when incubation pH > 10.0, in contrast, they may not able to immobilize the protein at lower pHs [201]. Even 1000-fold higher reactivity of amino terminus residues than Lys has been reported at the neutral condition and a much lower quantity of accessible sites (100 Lys vs 4 N-terminus) will significantly cause the much lower immobilization rate [223]. Meantime, even immobilization under the optimal pH, the presence of polymers slows down antibody conjugation due to its high viscosity of PEG solution. And the DTT are prone to react with glyoxyl groups before interacting with NH_2 groups, thus “one-point” interaction instead of

“multipoint” interaction will achieve, although the presence of DTT will not affect the functionality of glyoxyl groups [224].

Meantime, the antibody immobilization rate is not the only element affected by the incubation pH, it also determines the biorecognition functionality of immobilized antibody (Figure 5.1-4). Antibody immobilization at pH 8.5 will cause the interaction via N-terminus, the “head-on” orientation has caused the great loss of antibody biofunctionality. The fastest immobilization rate has increased the chance to interact with the Fc fragments (with the highest Lys density), however, “flat-on” rather than “end-on” due to the simultaneous conjugation of four subunits (Figure 5.1-5). Weaken antibody immobilization rate increased the interaction chance of N-terminus with glyoxyl groups and the resulting “one-point” coupling manner contributed to the unfavorable orientation of immobilized antibodies.

The polyaldehyde groups derived from the Dex@MNPs demonstrate similar characteristics with glyoxyl groups, which can achieve multipoint interaction with NH₂ residues at alkaline pH [225]. However, there are three advantages of polyaldehyde-Dex@MNPs over glyoxyl-agarose materials. The first advantage is the high controllability of aldehyde density, just regulating the oxidation parameters (periodate concentration, oxidation time or even temperature) is able to obtain activated carriers with different aldehyde densities (Figure 5.3-2). The second advantage is its high NH₂ reactivity in a wide pH range, including the neutral pHs, which facilitate its application in the preparation of cross-linked enzyme aggregates (CLEA) and surface covering linkers for multimeric proteins [47, 226]. The third advantage is the aldehyde groups are grafted from the long and flexible polymer surface, without the presence of the steric hindrance during the interaction with NH₂ groups while achieving the inert surface to prevent the unspecific adsorption after NaBH₄ reduction [225]. But the crosslinking ligand with a longer arm is not always beneficial to preserve the biofunctionality of conjugated antibody though significantly higher coverage density was observed with heterobifunctional ligand (N-γ-maleimidobutyryloxy-succinimide ester) [227].

The aldehyde groups onto the nanoparticles have been proven to affect the biofunctionality of immobilized antibodies (Figure 5.3-5), aldehyde groups of 139 μmols g_{Fe}⁻¹ MNPs were determined with the highest biofunctionality of Ab_{HRP} after covalent immobilization.

When considering the NH₂ reactive linkers, glutaraldehyde is a very important and versatile ligand to achieve stable antibody-support conjugates. Glutaraldehyde is able to immobilize proteins in a wide range of pHs (pH 6-10), and the immobilization rate is dependent on the whole aldehyde concentration in the suspension instead of the activated functional groups density on the supports [201]. While it will decrease the reactivity and stability at alkaline pH, thus in this case antibodies are prone to be site-specific immobilized via the “head-on” orientation under neutral pH.

6.1.2 Carbodiimide chemistry activated carboxylic groups—typical Ab immobilization strategy for random orientation

The carbodiimide coupling of antibodies are taken as the typical random orientation technique, due to the uncontrollability over the orientation/spatial distribution of immobilized antibodies and unsatisfied reproducibility [36]. However, even using EDC/NHS activated carriers, the oriented immobilization of full-length antibodies can be achieved by changing the immobilization pH [37]. As the isoelectric point (pI) of polyclonal anti-HRP distributed in the pH range of 5.2-6.55 (the most concentrated band shows around pH 7.0) [35, 37], the ionic interaction will happen first before the covalent interaction if the immobilization pH is lower than its pI [2].

In this dissertation, two parameters have been explored to achieve the possible ionic interaction before irreversible immobilization, which was controlling the EDC/NHS concentration and the antibody immobilization pH (Figure 5.2-16 and Figure 5.2-17). However, different from earlier research [36], immobilization of the Ab_{HRP} at pH 5.0 resulted in the highest antibody density on the nanoparticles than pH 6.0 and 7.0, but the biofunctionality of Ab_{HRP} was the best when immobilized at pH 7.0. Probably ionic interaction was the main driver when using the insufficient EDC/NHS concentration, thus adsorbed antibodies were eluted from the nanoparticles before performing the immunosensing assays. While exploring the EDC/NHS concentration can realize the equilibrium between adequate (yet partial) activation for the covalent immobilization and the remained ionized carboxylic groups for the ionic interaction on HOOC-Dex@MNPs, the optimal option was 25 mM EDC/NHS.

The preserved biofunctionality of immobilized antibodies can affect the detection sensitivity of fabricated immunosensors. When comparing the immunoassay performance of prepared immunosensors with different surface chemistries, Alde-Dex@MNPs nanocarriers demonstrated 1.8-fold lower LOD than HOOC-Dex@MNPs nanocarriers (Table 5.3-3), despite that HOOC-Dex@MNPs were modified from the Alde-Dex@MNPs (Figure 5.3-8). This result emphasizes the importance of spatial orientation of conjugated antibodies during the immunosensors fabrication, and immunosensor with higher sensitivity can be obtained with better antibody orientation.

While the antibody orientation is not the only consideration of immunosensing sensitivity, the size of spherical carriers also contributes different performance, HOOC-MBs demonstrated the highest sensitivity (2.6- and 1.7-fold than above-mentioned nanocarriers, respectively) and the lowest LOD (0.14 ng mL⁻¹) (Table 5.3-3). This result is consistent with earlier research that 3-time higher sensitivity was determined with microparticle carriers than nanoparticles with the same carboxylic chemistry [228].

6.1.3. Chelate groups against histidine cluster–less stable interaction

The interaction of His cluster distributed on Fc fragments with chelate groups will contribute uniform and site-directed antibody orientation [229], however, the lower stability of this bioconjugates interaction may suffer the possible dissociation [45].

The chelating interaction has driven reversible adsorption promise the correct orientation of immobilized antibodies, and the following the NH₂-epoxy covalent interaction further fixed the appreciated orientation (Figure 5.1-1). Though the reversible His cluster-chelate support interaction is less stable than 6×His residues-chelate support, it is enough to achieve the coupling before the epoxy-NH₂ covalent immobilization [45]. The correct orientation of the immobilized antibody on the chelate-epoxy agarose support results in the highest preserved biofunctionality (1.54 units HRP per unit Ab_{HRP}).

The types of metal ions coordinated by the chelate groups will affect the density and biofunctionality of adsorbed antibodies, Cu²⁺ seems the worst choice than other ions [43]. During the fabrication of chelate nanocarriers, the Cu²⁺ caused the unknown nanoparticles aggregation while other ions (Zn²⁺, Co²⁺ and Ni²⁺) coordinated chelate supports still have the colloidal stability.

Nevertheless, the correction immobilization of the antibody on the Epoxy-Dex@MNPs was not achieved. Due to the necessity of the simultaneous existence of epoxy groups and chelate groups, the initial epoxy should be high enough to bear the high density of chelate groups (for the fast physical interaction) while remaining enough epoxy groups for the following covalent immobilization. While the Ni-Chelate-Dex@MNPs nanocarriers only demonstrate the antibody-binding capacity of 3.7 μg mg_{Fe}⁻¹ nanoparticles at pH 7.0, in contrast, about 18 μg mg_{Fe}⁻¹ was determined with aggregated Cu-Chelate-Dex@MNPs (taken as the full adsorption capacity of antibody coverage density), which indicates the insufficient epoxy density grafted onto the nanoparticles, though the epoxy grafting strategies have been optimized (Figure 5.2-13).

6.2 The porous structure of supporting materials—a double-edged sword for the immunosensing

6.2.1 The inner surface of porous materials promotes higher antibody loading capacity while with heterogeneous distribution

Cross-linked agarose beads are classical polysaccharides-based supporting materials, the highly controllable particle size and porosity facilitate its broad application, and excellent antifouling advantage combined with easy activation makes it quite an appealing candidate for the immunosensing [47]. Thanks to the porosity, the protein binding capacity can achieve over 80 g L_{beads} (protein binding capacity provided by the manufacturer), which contributes to the well-

accepted chromatographic supports. The increasing concentration of agarose beads (2 %- 6 %) and their crosslinking degrees will cause the noticeable decrease of pores diameter (116 nm to 54 nm), over 25 % decreases of its accessibility with antibody was calculated [230].

However, the porosity of the agarose materials also causes some disadvantages in the immunosensing applications.

The antibody immobilization rate on the agarose beads is fast ([Figure 5.1-2A](#) and [Figure 5.1-3A](#)), including the IgGs-chelate-agarose interaction (pH 7.0) and IgGs-glyoxyl-agarose interaction (pH 10.0), that 30 min was able to conjugate the entire input antibody. This fast immobilization procedure facilitates the fabrication of immunosensors in a short time, however, it caused the heterogeneous distribution of antibody molecules that only the outer part of the agarose beads was visualized [43]. In this case, the accessibility of antigen-binding sites will be hindered because of the overcrowded antibody distribution, thus about 65 % antibody coverage (60 min incubation time to conjugate with Alde-Dex@MNPs) was used to prevent the steric hindrance caused by high density of antibodies.

To eliminate the steric hindrance caused by the high antibody density, controlling the antibody immobilization protocols (initial antibody concentration, immobilization time and reactive groups density on the supports) is a good strategy [56]. For the immunosensor fabrication with high antibody coverage on the carriers to improve its interaction chances with low concentration of analytes, homogeneously distributed antibodies within the porous structures is more suitable. Another alternative strategy is to slow down the antibody immobilization rate via the addition of competitive reagents. The appearance of 50 mM imidazole in the incubation buffer contributes to the over 70-fold slower immobilization time (0.25 h vs 16 h), the thoroughly distributed antibody was visualized via this strategy and near 2-fold higher antigen-recognition functionality was also improved [43].

Another interesting strategy to slow down the protein immobilization rate is through the decreased density of functional groups, 12-fold lower reactive groups density has caused the over 350-fold lower immobilization rate [56]. In both cases (lower reactive group density and addition of competitors), a more homogeneous distribution of antibodies was achieved within the agarose beads.

Another consideration is the adsorption capacity will drastically be decreased when the molecular weight of the protein is larger than 100 kDa (while it is also affected by the crosslinking degree of the agarose beads), thus the immobilization of full-length antibody (about 150 kDa in many cases) will obviously be limited, and an immobilization capacity of $< 3 \text{ g L}_{\text{beads}}$ was reported with virus-like particles ($\approx 20 \text{ nm}$) [231]. The antibody immobilization would happen on the outer side of particles followed by penetration into the inner channels via

the pore diffusion, this means the immobilization of the antibody will irreversibly narrow the diameters of the pores (Figure 3).

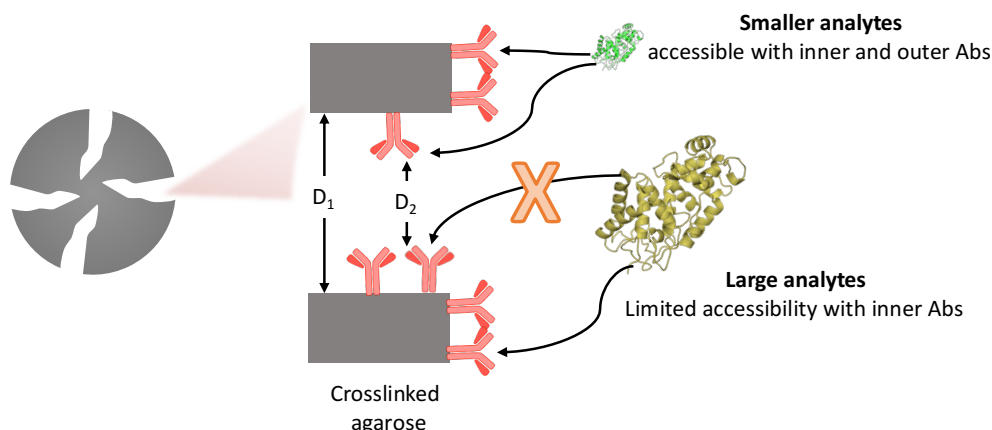


Figure 3. The dynamic change of the pores size with the biomolecules immobilization and antigen biorecognition. The initial pores size (D_1) of the crosslinked agarose supports has been narrowed because of antibody immobilization and the decreased porosity (D_2) partly hampers the efficient recognition of antigens with larger molecular size.

It is worth noting that the porous structure may help to prevent the protein inactivation during the direct and strong interaction with gas bubbles [232]. Biomolecules immobilized in the inner channels of agarose beads will not directly interact with bubbles, thus preventing the inactivation observed with proteins in soluble status or immobilized on the MNPs (non-porous). However, another coating layer of dextran derivatives (aldehyde-dextran and aspartic-aldehyde-dextran) on the immobilized enzyme/antibody will substantially improve their stability and biofunctionality [194, 232].

6.2.2 Nonporous nanoparticles improve the response time of antigens recognition

While things are different with nonporous magnetic nanoparticles, without the diffusion limitation, the antibody immobilization rate only varied with the immobilization capacity while the functional group density did not affect the immobilization rate (Figure 5.3-3). Though higher aldehyde density (5 h oxidation resulted in 150 $\mu\text{mol}/\text{g}_{\text{Fe}}$ MNPs for 5 mM periodate, 205 $\mu\text{mol}/\text{g}_{\text{Fe}}$ MNPs for 10 mM periodate) with different periodate concentrations, the antibody immobilization rate demonstrates a similar antibody coverage with 50 % and 70 % were calculated with 0.5 h and 1 h incubation with Alde-Dex@MNPs, respectively.

Although the aldehyde density did not affect the antibody immobilization rate, the antigen-binding functionality was varied with different aldehyde densities (Figure 5.3-5). The aldehyde group density is the dominant factor for the antibody immobilization coverage with low periodate concentration (2 mM), higher antibody immobilization concentration was accompanied by the increased capacity of biofunctionality. For the low periodate concentration,

steric hindrance of overcrowded antibodies will not be the problem even if oxidation time has been controlled with 5 h. However, when higher aldehyde group density did not promote the increase of antibody coverage, the conformation of immobilized antibodies may be varied. There are two properties that contribute to the conformation variation, which are flexibility and functional group density [233].

Because the reaction between aldehyde groups and antibodies is via multipoint interaction, four subunits will be involved during the immobilization, and then the binding constant would be enhanced greatly due to the increased number of interaction points [234].

For antibody immobilization with lower density, the multipoint interaction of aldehyde groups are prone to results in “flat-on” orientation, dramatically reduced binding activity happened due to the Fab fragments were restricted to twist away from the nanoparticle surface, thus loss its accessibility with antigens [235]. Antibody surface with 1 mg m^{-2} is the most appreciated density, the binding capacity dropped to <0.1 units per immobilized IgGs when antibody density was reached to 2 mg m^{-2} .

With high surface charge density, the lower ionic strength contributes to the “end-on” orientation of adsorbed antibodies, in which electrostatic interaction plays the dominant role. Oppositely, van der Waals will dominate the antibody-supports interaction and “lying-flat” orientation is predicted [236].

6.3 Surface functionalization of iron oxide nanoparticles—grafting the stability and surface chemistry

6.3.1 Providing the colloidal stability upon sufficient coverage

The development of MNPs synthesis strategies has achieved high controllability over its shapes, material types and surface multifunctionality. Stabilization characteristic is critical for the application of different fields, however, the colloidal stability (without aggregation or sedimentation) during long-term storage is still a challenge.

The typical strategies to achieve the magnetic colloidal suspension can be divided into two groups, which are electrostatic repulsion and steric hindrance. However, the addition of salts (especially with high ionic strength) would cause the break of intermolecular equilibrium, then steric hindrance via the sufficient surface coating is prone to obtain dispersible suspension and achieve the colloidal status in different kinds of media.

SiO_2 coating is a typical surface modification treatment to obtain the colloid nanoparticle suspension, and the high tunable thickness of the silica layer making it quite an appealing choice, porous structure or multiple layers can also achieve [237]. The grafting of organic silanes bearing distinct reactive groups (-SH, -epoxy, -COOH and $-\text{NH}_2$, etc) on the $\text{SiO}_2@\text{MNPs}$ would facilitate its covalent interaction with biomolecules via several exposed residues on the

antibody surface [238]. The silica functionalization was achieved with single-core coating, and the protection role of the silica layer improves its toleration against alkaline conditions (Figure 5.2-2). However, the response toward the external magnetic field still does not fit the requirement of bioseparation application, partly due to the small size of nanoparticles core (13.54 nm) is not adequate for the fast magnetic response and the silica layer (or the oxidation when exposed in the air) further contribute to the reduced magnetization [239, 240].

In contrast, the formation of small aggregates in Dex@MNPs nanocomposites during the functionalization of the nanoparticles can achieve the fast magnetism-driven separation (Figure 5.2-3). The bare spherical MNPs were agglomerated in an aqueous buffer due to the lack of external protective layers against the instability. The semi-transparent layers in the TEM image indicate the existence of polymer covering, the Dex@MNPs also appear in the agglomeration status most likely because of the self-attraction of nanoparticles during the water evaporation for the preparation of nanoparticles grafted grids. Due to the significantly increased magnetic response against the portable magnet, it is convincing that the nanoparticles were coated in the clusters form instead of monodispersed status during the preparation of Dex@MNPs. Therefore, the surface coverage density is crucial to achieving the full coating.

In addition, the surface coating parameters involved with the properties of dextran also contribute to different performance of Dex@MNPs.

Dextran polymers with varied molecular weights will demonstrate different macromolecular conformations. Dextran with small molecular weight (>10 kDa) has a fully stretched chain-like structure while larger molecular weight (> 20 kDa) promotes to achieve the random coiled status [241] and dextran polymers larger than 50 kDa will present the random-coiled conformation with spherical shape [242].

The higher adsorption of dextran on the MNPs was observed with higher initial grafting dextran concentration, evidence revealed by the lower saturated magnetism because of the higher surface coverage, and TGA values further gave more direct evidence about the increased coverage (Figure S1C of ANEXO). However, the dextran polymers higher molecular weight demonstrate higher viscosity and hindered diffusion in the dextran/nanoparticles suspension, thus higher amount of dextran adsorption with lower molecular weight (40 kDa vs.20 kDa) was reported [65]. In this case, higher water volume and vigorous stirring would help to disperse the viscous dextran into the water/nanoparticles system and improve their sufficient interaction. Cross-linked dextran polymers with longer chain length (40 kDa in this case) are prone to achieve better steric hindrance of nanoparticle core from interaction with aqueous buffer and easier to graft the functional groups than 10 kDa [243],

During the physical adsorption of dextran polymers on the surface of the nanoparticles, a slower diffusion rate caused by its high viscosity means the formation of Dex@MNPs nanocomposites

needs several hours to allow the polymer to interact with Fe-OH. It has been reported that 5 h interaction time is the minimum duration to obtain the MNPs with high coverage, while dextran desorption is also observed during this process, indicating the necessity of following crosslinking treatment to prevent the dissociation [65]. In addition, the crosslinking treatment also contributes to the alternation of polysaccharide structure to alleviate the anaphylactic reactions induced by the dextran polymer chains with higher size [243].

Different from the post-modification strategy, *in situ* synthesis of dextran-coated iron oxide nanoparticles is also appealing. With the appearance of dextran polymer during the preparation of iron oxide nanoparticles, the superparamagnetic behaviors (saturation magnetization and nanoparticles size) would be highly affected by the dextran/MNPs ratio [205]. Although the saturation magnetization of the Dex@MNPs was decreased due to the appearance of non-magnetic dextran shells and reduced nanoparticles size, a higher weight ratio of dextran/nanoparticles (2:1) can better decrease the cytotoxicity of bare MNPs and improve the stability at physiological pH (over several months) [205].

One-pot co-precipitation ($\text{Fe}^{2+}/^{3+}$ ions and dextran mixture) of Dex@MNPs was obtained with the highest stability partly because of the higher coating efficiency and larger dextran coating density on the nanoparticles [206]. Opposite with the post-modification strategy, dextran in a full extension conformation has a higher possibility to interact with Fe ions than random-coiled status, thus smaller molecular weight dextran is better to prepare larger particle size in this case [244].

6.3.2 Grafting the functional groups and antifouling characterization

Although single -OH in polysaccharide polymers is weak, the large number of repeated subunits (glucose) contribute to the high density of -OH on the dextran chains, thus obtaining with strong interaction energy with supporting materials. The large number of hydroxyl groups (Fe-OH) on the bare nanoparticles allows its surface to be readily functionalized with polysaccharides by synergy physical interactions (dextran in this case) under the strong alkaline condition. Physical grafting of dextran polymers onto the nanoparticles surface was documented by the FTIR results because the spectra of Dex@MNPs is the conjugation of dextran polymer and MNPs and no novel peaks have been detected (Figure S1E of ANEXO). Besides contributing to the higher binding energy, the grafted -OH also provides a larger number of potential functional groups that can be derived from chemical modification, such as carboxymethyl, acetal and aldehyde functionalization [245, 246].

However, the different molecular weights of the dextran polymers was reported not the dominant elements of its antifouling characterization [247], although dextran with higher molecular weight contributes to the higher stability under the same dextran/MNP ratio (Figure 5.2-8). In contrast, a oxidation level of 25 % demonstrate the highest antifouling advantage, the

main reason is the conformation transition upon the oxidation treatment that aldehyde groups favors the interaction with water molecular instead of anchoring surface, and polymer show higher extension level with higher oxidation level [247].

Instead of the physisorption of the dextran layer under alkaline condition followed by the crosslinking treatment to fulfill the stable interaction with bare nanoparticles, the covalently grafting of dextran molecules on the surface of the nanoparticles is another option. One good example is presented by Lix et al. [248] that amine-modified dextran reacts with carboxylic-activated nanoparticles upon the carbodiimide activation, partial oxidation of dextran chains with periodate followed by amination was performed in this case. Another example was demonstrated by Creixell et al. [249], carboxymethyl dextran was utilized to form irreversible bonds with aminated nanoparticles after the carbodiimide activation, and much higher stabilization than simple adsorbed Dex@MNPs was observed when incubating with cell culture media in the appearance of cells.

Another interesting materials to achieve the antifouling advantage is using the polymer brushes, the densely packed hydrophilic polymers modified on the supporting materials are especially appealing due to its controllable surface chemistry, and the zwitterionic colloids can effectively prevent the non-specific interaction and enhance the specificity and sensitivity of the immunoassays [250].

6.4 Multifunctionalities of nanoparticles: nanocarriers and nanoprobes

Detecting analytes with low abundance has placed greater demand on the sensitivity of the immunosensors, using tracer (HRP, alkaline phosphatase, etc) functionalized nanomaterials as the signal amplifier becomes a well-accepted trend (Table S1 of ANEXO).

The common characterize of this functionalized SPEs is nanomaterials can both be modified on the capture probes or used as the detection probes, which the functionalization as the capture probes can increase the anchoring density of bioreceptors and can achieve the signal amplification as the detection probes due to the high loading of signal reporters.

The nanostructures functionalization on the SPE working electrode is facile while an important strategy to improve the performance of fabricated biosensors. In addition, for the CRP determination application, nanomaterials play a not negligible role when modifying the SPEs. Their functionality can be divided into two types, which are nanocarriers of the signal probes and functionalization layers to improve the electrical properties.

6.4.1 Nanoprobes with high loading of reporter enzymes contribute to better sensitivity

When using the flat platforms as the bioreceptor carriers, which are SPCEs in this case, the commercially available detection probes (Strep-HRP or enzyme-labeled antibodies) have good accessibility toward the recognized antigens due to the firmly anchored supporting carrier. Thus,

a long detection range of 2.77-100 ng mL⁻¹ (Table 5.4-5) was found with Strep-HRP. However, due to the recognition ratio of signal probes toward analyte is 1:1, the sensitivity of the immunosensors using this probe was not satisfied. Therefore, immunosensing with multiple reporters will generate much higher signals, thus improving the sensitivity under the same analytes concentration. The co-immobilization of reporting enzymes and biorecognition elements (HRP reporters take the major proportions of bioconjugates) would contribute to linking a large number of enzymes on the nanomaterials, thus improving the catalytic performance [251].

In this dissertation, two different nanoprobe were determined and compared with their analytical performance. One is the nanoprobe with HRP with antibodies co-immobilized onto the Alde-Dex@MNPs. The antibody works as the recognition element to interact with captured CRP antigens and over 160-fold higher initial concentration of HRP over Ab (1 mg mL⁻¹ vs µg mL⁻¹) would definitely contribute to the higher HRP molecules on the nanomaterials. A 4.4-fold higher slope value demonstrated the noticeable enhancement of nanoprobe toward the sensitivity of immunosensors (Figure 5.4-18) and over 5.5-fold lower LOD further proved its functionality and advantages (LOD of 0.15 ng mL⁻¹).

The second nanoprobe are also based on the Alde-Dex@MNPs as the nanocarriers of dual proteins, which are HRP enzyme and streptavidin. The antigen-recognition function was achieved through the specific interaction between biotinylated antibodies and immobilized streptavidin molecules. It was interesting to find the sensitivity of the fabricated immunosensors without significant differences using HRP/CAb@MNPs and HRP/Streptavidin@MNPs (Figure 5.4-18). Two LODs with minor discrepancy were found (0.15 ng mL⁻¹ vs 0.18 ng mL⁻¹), the difference was the intercept of the calibration plot, which indicates the lower unspecific interaction between HRP/Streptavidin@MNPs with electrodes.

The differences between those nanoprobe may be contrite by the specificity of biorecognition elements and ionic interaction between blocking reagents (casein/biotin) with nanoprobe. The lower background signals in the absence of the CRP target were found when using strep-HRP and HRP/Streptavidin@MNPs as the detection probes, their common characteristic is to utilize the biotin-streptavidin interaction to realize the biorecognition which is one of the most specific interactions so far [252]. Owing to the higher specificity of these biorecognition elements than antibody-antigen interaction, a lower background can be expected. Meantime, when using the HRP/CAb@MNPs nanoprobe, due to the dextran layer on the nanoprobe has demonstrated a good antifouling advantage to prevent the interference of non-target protein, including the acceptable S/N ratio by the presence of BSA, HSA, human IgG and other inflammatory biomarkers.

6.4.2 Surface functionalization layers to improve the electrical properties

The first appealing property of nanomaterials functionalization is to improve the electrical properties of fabricated electrochemical biosensors, the nanostructures modification facilitates the electrons transfer during analytes determination thus obtaining lower LOD [253]. The functionalization of nanomaterials is crucial, the AuNPs is one of the most appreciated modification layers due to its unique physical and chemical properties [215, 254]. In addition, the large surface area and strong, facile Au-S bond facilitate the high-density immobilization of bioreceptors or connection ligands [253, 255-257].

Besides the single AuNPs functionalization, the hybrid nanostructures composed of several elements are of great interest, which can demonstrate synergic advantages of distinct materials. The utilization of AuNPs/carbon materials (graphene or rGO) hybrid is appealing [253, 258, 259]. There are three advantages of such hybrids, one advantage is the graphene/rGO coating obviously improves the electrical conductivity and electrons transmission, which are the most appreciated properties utilized in this application. The second advantage of the grafted carboxylic groups after surface activation treatment, this provides many anchoring points for the antibody immobilization. The third advantage is the porous structure of the graphene/rGO can adsorb many AuNPs on its surface, which further enhance the advantages of AuNP instead of functionalization of AuNPs alone on the electrode surface.

The utilization of HRP-Ab conjugates coupled AuNPs as signal amplifiers to perform the typical ELISA analysis resulted in doubled immunosensing sensitivity, while this enhancement was not obvious for low concentration of CA15-3 biomarkers [260]. While using the polymer brushes (3-dimensional structure with high flexibility) to substitute the spherical SiO₂ nanoparticles, it demonstrated better characterizations, which with 48-fold higher HRP loading and over 13-fold preserved biofunctionality upon conjugation on the nanoprobe, thus near 3-order of enhancement factor was observed [261].

Other hybrid nanostructures also demonstrate great advantages according to the distinct materials utilized [262-264]. Cheng et al. [265] have reported a dual signal amplification strategy to sensitively detect the CRP by using melamine/AuNPs composition as the immobilization carrier of electrochemical probes (ferrocene derivatives). The LOD was 56-fold lower than the chitosan and ferrocene functionalized SPE sensor, indicating the improved efficiency of such amplification strategy. Nickel sulfide/AuNPs/p-COFs composites show the combined advantages of the different part, which 2D porphyrinic COF have great photocatalytic properties and electrical conversion efficiency, and nickel sulfide has short electrons transmission due to its 2D morphology [266].

Recently, the covalent organic frameworks—highly ordered porous nanomaterials with multiple anchoring sites for the nanoparticles—have emerged as an alternative nanostructures [216]. The

DISSUSION

grafted high electronic conductivity is quite interesting for the electrochemical biosensing application. In addition, when nanomaterials as the carriers of signal reporters, high loading capacity of signal molecules is benefited from their large surface area. The typical results have been reported by Wang et al. [254] that over 5 orders of dynamic range with 1.7 pg mL^{-1} LOD was obtained after the signal amplification.

7. Conclusions

1. Glyoxyl agarose facilitates the high controllable antibody immobilization orientation via regulating the incubation pH. Immobilization of antibodies at pH 8.5 is a facile option while results in the “head-on” orientation, only 0.15 units of BGL/ unit Ab_{BGL}-Agarose were recognized. In contrast, direct conjugation under pH 10 promoted the “flat-on” orientation with 1.1 units of HRP / unit Ab_{HRP}-Agarose were captured, while the presence of polymers and thiolated reagents lead to more “random” orientation with 1.0 units and 0.6 units antigens per unit of Ab_{HRP}-Agarose and Ab_{BGL}-Agarose immunoconjugates, respectively.
2. Antibody immobilized on the heterofunctional (chelate-epoxy) agarose support maintained the highest biofunctionality via the smart regulation of incubation pH, thus managing the interacted amino residues on the antibody surface. With the regulation of the density of reactive groups (chelate and epoxy with 10 $\mu\text{mol mL}^{-1}$ and 25 $\mu\text{mol mL}^{-1}$, respectively) allows the recognition of 1.54 units HRP/ unit Ab_{HRP}-Agarose. This heterofunctional support specially demonstrates better advantages over glyoxyl agarose for larger antigens (425 kDa BGL), with 2-time biofunctionality than smaller analytes (40 kDa HRP) were observed.
3. Dextran coating (40 kDa molecular weight and 8-fold coating density) endows the hydrophilicity and antifouling characterization of iron oxide nanoparticles, promises the colloidal stability over 2-week (absorbance ≥ 80 % of initial values) against wide range of aqueous buffer (pH 3–11). Polymer functionalization using mechanical stirring instead of sonication allows the formation of small aggregates to facilitate the 100 % recovery of nanoparticles within 2 min with a portable magnet while preventing sedimentation.
4. The anchored Ab_{HRP} on the Dex@MNPs with different surface chemistries result in distinct performance. 0.89 units HRP/ unit Ab_{HRP}-Zn²⁺-IDA-Dex@MNPs was adsorbed under pH 8.0 incubation. 0.76 units HRP/ unit Ab_{HRP}-HOOC-Dex@MNPs (with EDC/NHS activation) was achieved after controlling the activation reagents concentration and conjugation pH. The highest biofunctionality performance was illustrated by Alde-Dex@MNPs with 1.03 units HRP per Ab-Alde-Dex@MNPs unit, while the oxidation condition needs to be optimized.
5. The oxidation parameters affect the aldehyde density on the Dex@MNPs and the biofunctionality of immobilized Ab_{HRP}. Aldehyde density with 139 $\mu\text{mol g}_{\text{MNPs}}^{-1}$ (5 mM sodium periodate oxidation for 4 h) promoted the optimal orientation and recognition capacity of covalently conjugated Ab_{HRP}. 1.32 Units HRP/ unit Ab_{HRP}-Alde-Dex@MNPs was achieved with antibody coverage of 11.1 $\mu\text{g mL}^{-1}$ HRP (about 70 % maximal coverage) within 10 min adsorption time at 37 °C.

CONCLUSION

6. Under the optimal parameters, colorimetric determination revealed that the prepared immunosensors–Ab_{HRP}-Alde-Dex@MNPs–have high efficiency of antigen-recognition within a wide dynamic range of 0.3–7.5 $\mu\text{g mL}^{-1}$ (LOD: 0.3 $\mu\text{g mL}^{-1}$ HRP), and also showed acceptable recovery ability from spiked serum samples (93.9 %–106.4 %) due to the inertness of grafted polymer on nanoparticles surface. However, electrochemical assays demonstrated over 500-fold higher sensitivity with a 10-fold shorter linear range using Alde-Dex@MNPs nanocarriers (LOD: 0.44 ng mL^{-1} HRP), while HOOC-Dex@MNPs nanocarriers show 1.8 times lower sensitivity under the same condition and HOOC@MBs further reached the highest sensitivity with the lowest LOD of 0.14 ng mL^{-1} HRP.

7. When surface functionalized SPCEs as the bioreceptors carriers of Ab_{CRP}, three detection probes demonstrated varied sensitivity and dynamic range. Commercial Strep-HRP probes were observed with a wide linear range (2.77–100 ng mL^{-1}) and mild sensitivity (LOD with 0.83 ng mL^{-1}). Though faced with shorter dynamic range (0.5–10 ng mL^{-1}) for dual-functionalized nanoprobe, over 4.6-fold higher sensitivity was observed due to the amplified signals by the multiple functionalized reporters (HRP) on the nanoparticles surface (LOD with 0.15 and 0.18 ng mL^{-1} , respectively).

8. Nanoparticles are more promising antibody carriers for CRP immunosensing instead of SPCEs, which achieve the longest linear range with high sensitivity. With a LOD of 1.41 ng mL^{-1} CRP, the wide linear range 4.7–250 ng mL^{-1} facilitates the accurate quantification of biomarkers in human fluids. The facile determination of CRP biomarkers concentration in human serum demonstrates the significant difference between healthy individuals and heart failure patients, and the results are highly consistent with ELISA analysis– the golden standard of clinical diagnostic technique.

ANEXOS

ANEXOS

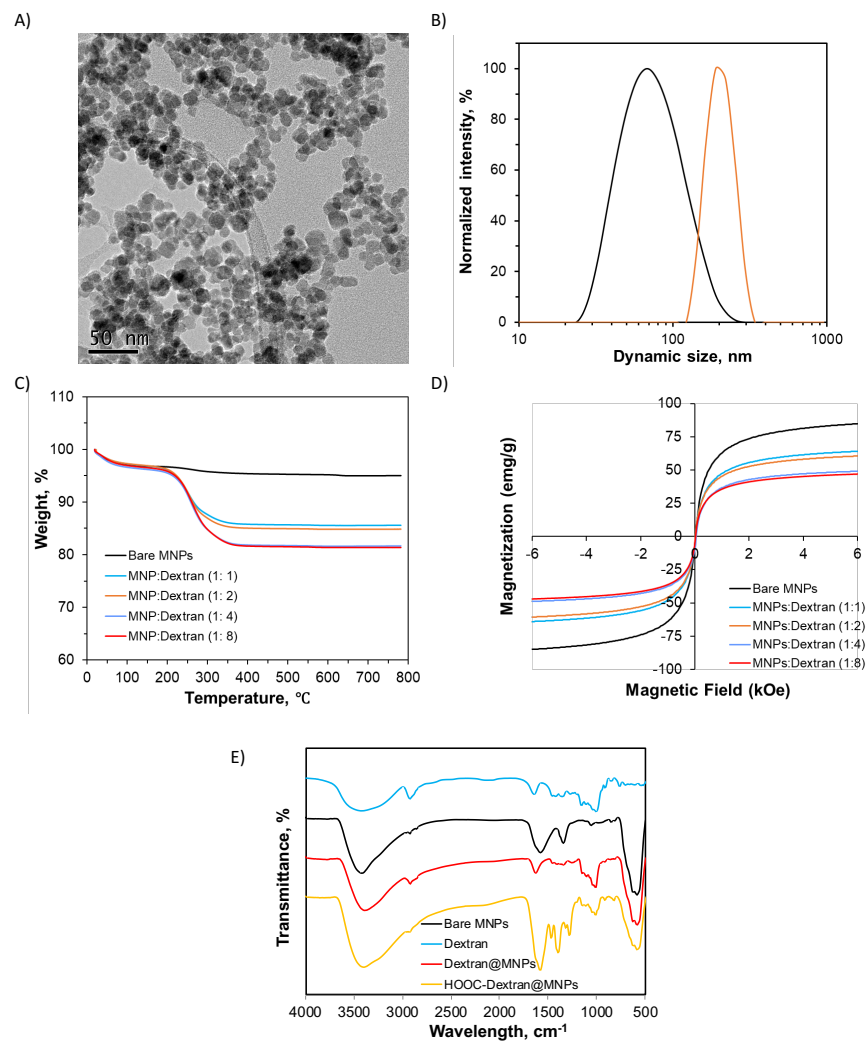


Figure S1. Characterization of the Dextran@MNPs nanoparticles. TEM image of the dextran coated nanoparticles (A), DLS data of bare nanoparticles (66 nm with PDI of 0.165) and Dex@MNPs (204 nm with PDI of 0.034), TGA curve (C) and room temperature magnetic hysteresis loops of Dextran@MNPs with different MNPs:Dextran ratios (D), FTIR spectra of the dextran and MNP derives (E).

Table S1 Various CRP detection techniques using the multifunctionalities of nanomaterials.

Biosensor type	Bioreceptors type	Immobilization support	Detection probes with nanomaterials	Signal amplification strategy	Linear range	LOD	Real sample	Ref.
Immobilization support								
Chemiluminescence	Ab	Magnetic beads	–	–	0.0125–10 $\mu\text{g mL}^{-1}$	12.5 ng mL^{-1}	Clinical human serum	[152]
Chemiluminescence	Ab	PAA-Au/Fe ₃ O ₄ NPs	–	Zwitterionic glycerophosphoryl choline blocking	1–250 ng mL^{-1}	0.26 ng mL^{-1}	Clinical human serum	[157]
Visualization–TEM	PMPC- <i>b</i> -PMAT	AuNPs	–	AuNPs aggregation upon analytes addition	–	Between 20–40 nM	–	[147]
UV/vis-spectrum	O-phosphoryle thanolamine	AuNPs	–	AuNPs aggregation upon analytes addition	50–450 ng mL^{-1}	50 ng mL^{-1}	Clinical human serum	[150]
UV/vis-spectrum	Ab	AuNPs	–	AuNPs aggregation upon analytes addition	–	–	Spiked human serum	[149]
UV/vis-spectrum	ssDNA aptamers	AuNPs	–	AuNPs aggregation upon analytes addition	0.889–20.7 $\mu\text{g mL}^{-1}$	1.23 $\mu\text{g mL}^{-1}$	–	[148]
DLS	PMPC	Fe ₃ O ₄ nanoparticles	–	–	0–600 nM (69 $\mu\text{g mL}^{-1}$)	10 nM (1.15 $\mu\text{g mL}^{-1}$)	–	[146]
CRET	Ab	Graphene	–	Graphene as the energy acceptor of chemiluminescence	1–1000 ng mL^{-1}	1.6 ng mL^{-1}	Spiked human serum	[267]

FRET	Ab	AuNPs	–	Nanomaterial-surface energy transfer effect	3.5–455 nM (0.4–52 $\mu\text{g mL}^{-1}$)	–	Clinical human serum	[268]
Fluorescence	RNA aptamer	Bio-Plex magnetic beads	–	–	0.4–100 mg L^{-1}	0.4 mg mL^{-1}	Clinical human serum	[151]
Amperometry	Ab	Dynabeads® M-280 Streptavidin	–	–	0.005–1.0 $\mu\text{g mL}^{-1}$	1.5 ng mL^{-1}	Clinical human serum/whole blood	[156]
Amperometry	Ab	rGO/Ni/PtNPs micromotors	–	–	2–100 $\mu\text{g mL}^{-1}$	0.80 $\mu\text{g mL}^{-1}$	Preterm neonate plasma	[153]
Amperometry	Ab	rGO/Ni/PtNPs micromotors	–	–	1–100 $\mu\text{g mL}^{-1}$	0.40 $\mu\text{g mL}^{-1}$	Preterm neonate plasma	[154]
Amperometry	Ab	Dynabeads M-280 Streptavidin	–	–	0.01–5 $\mu\text{g mL}^{-1}$	8 ng mL^{-1}	Clinical human serum	[155]
EIS	Ab	poly deep eutectic solvents@GO@AuNPs	–	Multiple signal molecules loading (AuNPs)	0.001–50 ng mL^{-1}	0.3 pg mL^{-1}	Spiked human serum	[269]
Nanocarriers of signal probes								
DPV	Ab	AuNPs@GCE	dsDNA@CuNPs, Ab2-aptamers	Hybridization chain reaction of aptamers	1.0 fg mL^{-1} –100 ng mL^{-1}	0.33 fg mL^{-1}	Spiked human serum	[159]
QCM	Ab	Fe_3O_4 @ SiO_2	HRP@Ab@Protein A@AuNPs	Multiple signal molecules loading (HRP)	0.001 – 100 ng mL^{-1}	0.3 pg mL^{-1}	Clinical human serum	[144]

Piezoelectric	Ab	Microtiter plate	Fe ₃ O ₄ @SiO ₂ @Au NPs@HRP	Multiple signal molecules loading (HRP)	0.01–200 ng mL ⁻¹	5 pg mL ⁻¹	Clinical human serum	[158]
Plasmonic imaging	Ab	Plasmonic gold nanohole array	AuNPs	Visualization signal generation probes	36–1E5 pg mL ⁻¹	36 pg mL ⁻¹	Clinical human serum	[270]
Photoluminescence	Ab	Microplate	CdSe/ZnS/CdZnS /ZnS core/shell QDs	Signal generation probes	0.5–1000 ng mL ⁻¹	0.41 ng mL ⁻¹	Clinical serum	[175]
FLISA– Photoluminescence	Ab	Microplate	ZnCdSeS/ZnS QDs	Signal generation probes	10–1000 ng mL ⁻¹	6.37 ng mL ⁻¹	Spiked human serum	[174]
LFISA- photoluminescence	Ab	Microplate	InP/GaP/ZnS QD @SiO ₂ nanoparticles	Signal generation probes	1–1000 ng mL ⁻¹	0.9 ng mL ⁻¹	Spiked human serum	[176]
ICA	Ab	Lateral flow test strip	AuNPs	Gold enhancer solution (NH ₂ OH·HCl)	0.1–5 µg mL ⁻¹	1 ng mL ⁻¹	Spiked human serum	[162]
ICA	Ab	Lateral flow test strip	AuNPs	Signal generation probes	119 ng mL ⁻¹ – 100 µg mL ⁻¹	43 ng mL ⁻¹	Clinical human serum	[160]
ICA	Ab	Lateral flow test strip	AuNPs	Signal generation probes	1 ng mL ⁻¹ – 500 µg mL ⁻¹	–	Clinical human serum	[161]
ICA-fluorescence	Ab	Lateral flow test strip	Tetraethylene glycol@fullerene nanoparticles	Signal generation probes	0.1–10 ng mL ⁻¹	–	Spiked human serum	[165]
ICA-fluorescence	Ab	Lateral flow test strip	Nile-red doped fluorescent nanoparticles	Signal generation probes	0.1–160 µg mL ⁻¹	0.091 µg mL ⁻¹	Clinical human plasma	[163]
ICA-fluorescence	Ab	Lateral flow test strip	Fluorescent hollow	Signal generation probes	–	1 ng mL ⁻¹ (visual)	Spiked fetal bovine serum	[97]

			ZrO ₂ @CdTe nanoparticles					
ICA-fluorescence	Ab	Lateral flow test strip	UCNPs@mSiO ₂	Signal generation probes	0.1–50 ng mL ⁻¹	0.05 ng mL ⁻¹	Clinical human serum	[164]
LFA-fluorescence	Ab	Lateral flow test strip	CdSe/ZnS QDs	Signal generation probes	0.5 ng mL ⁻¹ – 1 µg mL ⁻¹	0.3 ng mL ⁻¹	Clinical serum	[169]
LFA-fluorescence	Ab	Lateral flow test strip	CIZS/ZnS//ZnS QDs	Signal generation probes	0–800 ng mL ⁻¹	5.8 ng mL ⁻¹	–	[168]
LFA-fluorescence	Ab	Lateral flow test strip	Multiple CdSe/ZnS QDs@nanospheres	Signal generation probes and carriers multiple QDs	0.025–1.6 µg mL ⁻¹	3.89 ng mL ⁻¹	Spiked serum	[171]
LFA-fluorescence	Ab	Lateral flow test strip	QDs @ dendritic SiO ₂ spheres	Signal generation probes and carriers multiple QD	0.3–6.25 pg mL ⁻¹	90 pg mL ⁻¹	Clinical human serum	[172]
LFA-fluorescence	Ab	Lateral flow test strip	Hydrophobic CdSe/ZnS QDs	Signal generation probes	50–250 µg mL ⁻¹	1 ng mL ⁻¹	Clinical blood	[166]
LFA-fluorescence	Ab	Lateral flow test strip	QDs	Signal generation probes	556.4 nM	52.9 nM	Spiked human serum	[167]
LFA-fluorescence	Ab	Lateral flow test strip	SiO ₂ @quantum dot (QD)	Signal generation probes	0.5–10 ³ ng mL ⁻¹	0.5 ng mL ⁻¹	Clinical human serum	[170]
LFA-ECL	Ab	Lateral flow test strip	Ru(bpy) ₃ ²⁺ @AuNP	Signal generation probes	0.01–1000 ng mL ⁻¹	4.6 pg mL ⁻¹	Clinical serum	[177]
MEC	Ab	Aldehyde functionalized glass chips	Aptamer-hemin@AgNPs	Signal generation, MEC and CL signal amplification	0.7–7 × 10 ⁴ ng·mL ⁻¹	0.05 ng mL ⁻¹	Clinical human serum	[271]

Fluorescence	Ab	Magnetic beads	AgNPs	AgNPs dissolution generate signals	0.1 – 10 ng mL ⁻¹	30 pg mL ⁻¹	Clinical human serum	[272]
Fluorescence	Ab	MNPs	CdSe/ZnS@SiO ₂ NPs	Signal generation probes	1.18 ng mL ⁻¹ – 11.8 µg mL ⁻¹	1 ng mL ⁻¹	Spiked human serum	[273]
Immunofiltration assays– Fluorescence	Ab	Porous nitrocellulose membrane	PEG functionalized QDs	Signal generation probes	0.79–200 µg mL ⁻¹	0.79 µg mL ⁻¹	Clinical human blood	[274]
ELISA–Colorimetric and Fluorescence	Ab	Microplate well	PDDA@curcumin NPs	Curcumin releases generate signal	0.1 pg·mL ⁻¹ – 10 ng·mL ⁻¹	0.043 pg mL ⁻¹ (colorimetric), 0.038 pg mL ⁻¹ (fluorescence)	–	[179]
ELISA– Fluorescence	Ab	Microtiter plate	Cyanine5 doped SiO ₂ NPs	Signal generation probes and multiple signal molecules loading (Cyanine5)	0–10 µg mL ⁻¹	0.59 ng mL ⁻¹	–	[178]
Nanotracers								
SERS	Ab	Rhodamine B@ PEI@CaCO ₃ microcapsule	Porous magnetic Ni@C NP	Magnetic purification	0.1 pg mL ⁻¹ – 1 µg mL ⁻¹	0.01 pg mL ⁻¹	Spiked serum	[183]
SERS	Ab	Nanoporous anodic aluminum oxide membrane	AuNP _{su} @Nile blue A@Ag nanotags	Signal generation probes and multiple signal molecules loading	0.01–1000 ng mL ⁻¹	53.4 fg mL ⁻¹	Spiked human serum	[181]
SERS	Ab	Photonic crystal beads	PEG functionalized	Signal generation probes and multiple signal molecules loading	10 pg mL ⁻¹ –10 µg mL ⁻¹	672 fg mL ⁻¹	Clinical human serum	[100]

			Au@Nile blue A @AgNPs					
SERS	Aptamer	Au-Te nanoworm	DNA three-way junction@porous AuNPs	Signal generation probes and multiple signal molecules loading (methylene blue)	100 nM–1 pM	2.23 pM (0.51 pg mL ⁻¹)	Spiked human serum	[182]
SERS-LFA	Ab	Lateral flow test strip	Mesoporous SiO ₂ NP/AuNPs	Signal generation probes	0.5–1000 ng mL ⁻¹	0.05 ng mL ⁻¹	–	[123]
SERS-LFA	Ab	Lateral flow test strip	Fe ₃ O ₄ NP/AuNPs	Signal generation probes and magnetic pre- purification	0.01–500 ng mL ⁻¹	0.01 ng mL ⁻¹	Clinical human blood	[180]
SERS-LFA	Ab	Lateral flow test strip	AuNP@DTNB@ Ag NPs	Signal generation probes and multiple signal molecules loading	0.01 – 500 ng mL ⁻¹	0.01 ng mL ⁻¹	Monkey blood plasma	[101]
SPR	DNA Aptamer	Au surface	Ab coated AuNPs	AuNPs amplify the signal	10 pM–100 nM	10 pM	Spiked human serum	[275]
Nanocatalysts of enzyme mimics								
ELISA	Citicoline	Citicoline-BSA coated microplate	Aptamer coupled AuNP nanoenzymes	Enzyme mimics	0.1 –200 ng mL ⁻¹	8 pg mL ⁻¹	Rat blood	[186]
Pressuremeter	Ab	Magnetic beads	PtNPs nanoenzymes	Enzyme mimics	0.25–25 ng mL ⁻¹	0.2 ng mL ⁻¹	Clinical human serum	[276]
Colorimetric	Ab	SiO ₂ @Fe ₃ O ₄ NP	Bimetallic PtRu alloy NPs nanoenzymes	Enzyme mimics	0.01–180 µg mL ⁻¹	10 µg mL ⁻¹	Spiked human serum	[187]

Colorimetric	Ab	Microplate well	N- and B-codoped rGO nanoenzymes	Enzyme mimics	0.001–5 $\mu\text{g mL}^{-1}$	5 ng mL^{-1}	–	[188]
Colorimetric	Ab	Microplate well	AgNPs nanoenzymes	Enzyme mimics	1.5–25 ng mL^{-1}	1 ng mL^{-1}	Spiked human serum	[189]
Amperometry	Ab	Au NPs/ionic liquid-MoS ₂ @GCE	Ir NPs/GO-DN nanoenzymes	Enzyme mimics	0.01–100 ng mL^{-1}	3.3 pg mL^{-1}	Spiked human serum	[193]
Amperometry	Ab	Au/COF-LZUI	Bimetallic Pt/Ru/C NP nanoenzymes	Enzyme mimics	0.2–20 ng mL^{-1}	0.1 ng mL^{-1}	Spiked human serum	[190]
Amperometry	Ab	Chitosan/Au NPs/COF-TpPa-1@GCE	Co ₃ O ₄ NPs nanoenzymes	Enzyme mimics	0.05–80 ng mL^{-1}	0.017 ng mL^{-1}	Spiked human serum	[192]
Amperometry	Ab	GO/Chitosan@GCE	hollow Ag/Pt NPs nanoenzymes	Enzyme mimics	0.5–140 ng mL^{-1}	0.17 ng mL^{-1}	Spiked human serum	[191]

Abbreviations: Chemiluminescence resonance energy transfer (CRET), Covalent organic frameworks (COFs), Cytidine 5'-diphosphocholine (Citicoline), 1,5-diaminonaphthalene (DN), Differential pulse voltammetry (DPV), Dynamic light scattering (DLS), 5,5'-dithiobis (2-nitrobenzoic acid) (DTNB), Electrochemical impedance spectroscopy (EIS), Electrochemiluminescent (ECL), Fluorescence-linked immunosorbent assay (FLISA), Förster resonance energy transfer (FRET), Glassy carbon electrode (GCE), Gold nanoparticles (AuNPs), Graphene oxide (GO), Immunochromatographic assay (ICA), Metal-enhanced chemiluminescence (MEC), Molybdenum disulfide (MoS₂), poly(acrylic acid) (PAA), poly(diallyldimethylammonium chloride) (PDDA), poly(ether imide) (PEI), poly(2-methacryloyloxyethyl phosphorylcholine)-*b*-poly(N-methacryloyl-(L)-tyrosine methylester) (PMPC-*b*-PMAT), Quantum dots (QDs), Quartz crystal microbalance (QCM), reduced GO (rGO), Surface-enhanced Raman scattering (SERS), Surface plasmon resonance (SPR), Transmission electron microscopy (TEM).

References

- [1] L.C. Clark, C. Lyons, Electrode systems for continuous monitoring in cardiovascular surgery, *Ann. N. Y. Acad. Sci.* 102 (1962) 29-45.
- [2] S. Gao, J.M. Guisán, J. Rocha-Martin, Oriented immobilization of antibodies onto sensing platforms- A critical review, *Anal. Chim. Acta* (2021) 338907.
- [3] A.K. Trilling, J. Beekwilder, H. Zuilhof, Antibody orientation on biosensor surfaces: a minireview, *Analyst* 138 (2013) 1619-1627.
- [4] V. Crivianu-Gaita, M. Thompson, Aptamers, antibody scFv, and antibody Fab' fragments: An overview and comparison of three of the most versatile biosensor biorecognition elements, *Biosens. Bioelectron.* 85 (2016) 32-45.
- [5] R. Chhasatia, M.J. Sweetman, F.J. Harding, M. Waibel, T. Kay, H. Thomas, T. Loudovaris, N.H. Voelcker, Non-invasive, in vitro analysis of islet insulin production enabled by an optical porous silicon biosensor, *Biosens. Bioelectron.* 91 (2017) 515-522.
- [6] S. Arshavsky-Graham, K. Urmann, R. Salama, N. Massad-Ivanir, J.-G. Walter, T. Scheper, E. Segal, Aptamers vs. antibodies as capture probes in optical porous silicon biosensors, *Analyst* 145 (2020) 4991-5003.
- [7] K. Urmann, J.-G. Walter, T. Scheper, E. Segal, Label-free optical biosensors based on aptamer-functionalized porous silicon scaffolds, *Anal. Chem.* 87 (2015) 1999-2006.
- [8] S. Sharma, H. Byrne, Richard J. O'Kennedy, Antibodies and antibody-derived analytical biosensors, *Essays Biochem.* 60 (2016) 9-18.
- [9] N.G. Welch, J.A. Scoble, B.W. Muir, P.J. Pigram, Orientation and characterization of immobilized antibodies for improved immunoassays (Review), *Biointerphases* 12 (2017) 02D301.
- [10] M. Shen, J.F. Rusling, C.K. Dixit, Site-selective orientated immobilization of antibodies and conjugates for immunodiagnosics development, *Methods* 116 (2017) 95-111.
- [11] G. Vidarsson, G. Dekkers, T. Rispen, IgG subclasses and allotypes: From structure to effector functions, *Front. Immunol.* 5 (2014) 520.
- [12] C. Klumpp-Thomas, H. Kalish, M. Drew, S. Hunsberger, K. Snead, M.P. Fay, J. Mehalko, A. Shunmugavel, V. Wall, P. Frank, J.-P. Denson, M. Hong, G. Gulsten, S. Messing, J. Hicks, S. Michael, W. Gillette, M.D. Hall, M.J. Memoli, D. Esposito, K. Sadtler, Standardization of ELISA protocols for serosurveys of the SARS-CoV-2 pandemic using clinical and at-home blood sampling, *Nat. Commun.* 12 (2021) 113.
- [13] M. Tonigold, J. Simon, D. Estupiñán, M. Kokkinopoulou, J. Reinholz, U. Kintzel, A. Kaltbeitzel, P. Renz, M.P. Domogalla, K. Steinbrink, I. Lieberwirth, D. Crespy, K. Landfester, V. Mailänder, Pre-adsorption of antibodies enables targeting of nanocarriers despite a biomolecular corona, *Nat. Nanotechnol.* 13 (2018) 862-869.
- [14] Z. Yang, Y. Chevolut, T. Géhin, J. Solassol, A. Mange, E. Souteyrand, E. Laurenceau, Improvement of protein immobilization for the elaboration of tumor-associated antigen microarrays: Application to the sensitive and specific detection of tumor markers from breast cancer sera, *Biosens. Bioelectron.* 40 (2013) 385-392.
- [15] F. Duval, T.A. van Beek, H. Zuilhof, Key steps towards the oriented immobilization of antibodies using boronic acids, *Analyst* 140 (2015) 6467-6472.
- [16] J. Chang, N. Gao, P. Dai, Z. Zhu, H. You, W. Han, L. Li, Facile engineered polymeric microdevice via co-coupling of phenylboronic acid and Protein A for oriented antibody immobilization enables substantial signal enhancement for an enhanced fluorescence immunoassay, *Sens. Actuators B* 346 (2021) 130444.
- [17] M. Iijima, S.i. Kuroda, Scaffolds for oriented and close-packed immobilization of immunoglobulins, *Biosens. Bioelectron.* 89 (2017) 810-821.
- [18] E. de Juan-Franco, A. Caruz, J.R. Pedrajas, L.M. Lechuga, Site-directed antibody immobilization using a protein A-gold binding domain fusion protein for enhanced SPR immunosensing, *Analyst* 138 (2013) 2023-2031.

REFERENCES

- [19] C.S. Huertas, M. Soler, M.C. Estevez, L.M. Lechuga, One-step immobilization of antibodies and dna on gold sensor surfaces via a poly-adenine oligonucleotide approach, *Anal. Chem.* 92 (2020) 12596-12604.
- [20] D.A. Richards, A. Maruani, V. Chudasama, Antibody fragments as nanoparticle targeting ligands: a step in the right direction, *Chem. Sci.* 8 (2017) 63-77.
- [21] J. Goossens, H. Sein, S. Lu, M. Radwanska, S. Muyltermans, Y.G.J. Sterckx, S. Magez, Functionalization of gold nanoparticles with nanobodies through physical adsorption, *Anal. Methods* 9 (2017) 3430-3440.
- [22] L. Xu, H. Cao, C. Huang, L. Jia, Oriented immobilization and quantitative analysis simultaneously realized in sandwich immunoassay via His-tagged nanobody, *Molecules* 24 (2019) 1890.
- [23] T. Delfin-Riela, M.A. Rossotti, C. Echaides, G. González-Sapienza, A nanobody-based test for highly sensitive detection of hemoglobin in fecal samples, *Anal. Bioanal. Chem.* 412 (2020) 389-396.
- [24] I. Duznovic, A. Gräwe, W. Weber, L.K. Müller, M. Ali, W. Ensinger, A. Tietze, V. Stein, Ultrasensitive and selective protein recognition with nanobody-functionalized synthetic nanopores, *Small* (2021) 2101066.
- [25] S. Oloketuyi, E. Mazzega, J. Zavašnik, K. Pungjunun, K. Kalcher, A. de Marco, E. Mehmeti, Electrochemical immunosensor functionalized with nanobodies for the detection of the toxic microalgae *Alexandrium minutum* using glassy carbon electrode modified with gold nanoparticles, *Biosens. Bioelectron.* 154 (2020) 112052.
- [26] Y. Bae, D.G. Jang, S. Eom, T.J. Park, S. Kang, HRP-conjugated plug-and-playable IgG-binding nanobodies as secondary antibody mimics in immunoassays, *Sens. Actuators B* 320 (2020) 128312.
- [27] M. Li, M. Zhu, C. Zhang, X. Liu, Y. Wan, Uniform orientation of biotinylated nanobody as an affinity binder for detection of *Bacillus thuringiensis* (Bt) Cry1Ac Toxin, *Toxins* 6 (2014) 3208-3222.
- [28] Z. Sun, X. Wang, Z. Tang, Q. Chen, X. Liu, Development of a biotin-streptavidin-amplified nanobody-based ELISA for ochratoxin A in cereal, *Ecotoxicol. Environ. Saf.* 171 (2019) 382-388.
- [29] H. Kimura, D. Miura, W. Tsugawa, K. Ikebukuro, K. Sode, R. Asano, Rapid and homogeneous electrochemical detection by fabricating a high affinity bispecific antibody-enzyme complex using two Catcher/Tag systems, *Biosens. Bioelectron.* 175 (2021) 112885.
- [30] D. Miura, H. Kimura, W. Tsugawa, K. Ikebukuro, K. Sode, R. Asano, Rapid, convenient, and highly sensitive detection of human hemoglobin in serum using a high-affinity bivalent antibody-enzyme complex, *Talanta* 234 (2021) 122638.
- [31] A.K. Adak, K.-T. Huang, P.-J. Li, C.-Y. Fan, P.-C. Lin, K.-C. Hwang, C.-C. Lin, Regioselective SN2-type reaction for the oriented and irreversible immobilization of antibodies to a glass surface assisted by boronate formation, *ACS Appl. Bio Mater.* 3 (2020) 6756-6767.
- [32] A.K. Adak, B.-Y. Li, L.-D. Huang, T.-W. Lin, T.-C. Chang, K.C. Hwang, C.-C. Lin, Fabrication of antibody microarrays by light-induced covalent and oriented immobilization, *ACS Appl. Mater. Interfaces* 6 (2014) 10452-10460.
- [33] C.-Y. Fan, Y.-R. Hou, A.K. Adak, J.T. Waniwan, M.A.C. dela Rosa, P.Y. Low, T. Angata, K.-C. Hwang, Y.-J. Chen, C.-C. Lin, Boronate affinity-based photoactivatable magnetic nanoparticles for the oriented and irreversible conjugation of Fc-fused lectins and antibodies, *Chem. Sci.* 10 (2019) 8600-8609.
- [34] C.-Y. Fan, S.K. Kawade, A.K. Adak, C. Cho, K.-T. Tan, C.-C. Lin, Silver-coated Cu₂O Nanoparticle substrates for surface azide-alkyne cycloaddition, *ACS Appl. Nano Mater.* 4 (2021) 1558-1566.
- [35] S. Puertas, P. Batalla, M. Moros, E. Polo, P. del Pino, J.M. Guisán, V. Grazú, J.M. de la Fuente, Taking advantage of unspecific interactions to produce highly active magnetic nanoparticle-antibody conjugates, *ACS Nano* 5 (2011) 4521-4528.

REFERENCES

- [36] S. Puertas, M. de Gracia Villa, E. Mendoza, C. Jiménez-Jorquera, J.M. de la Fuente, C. Fernández-Sánchez, V. Grazú, Improving immunosensor performance through oriented immobilization of antibodies on carbon nanotube composite surfaces, *Biosens. Bioelectron.* 43 (2013) 274-280.
- [37] C. Parolo, A. de la Escosura-Muñiz, E. Polo, V. Grazú, J.M. de la Fuente, A. Merkoçi, Design, preparation, and evaluation of a fixed-orientation antibody/gold-nanoparticle conjugate as an immunosensing label, *ACS Appl. Mater. Interfaces* 5 (2013) 10753-10759.
- [38] R. Raghav, S. Srivastava, Immobilization strategy for enhancing sensitivity of immunosensors: L-Asparagine–AuNPs as a promising alternative of EDC–NHS activated citrate–AuNPs for antibody immobilization, *Biosens. Bioelectron.* 78 (2016) 396-403.
- [39] J.E. Hale, D.E. Beidler, Purification of humanized murine and murine monoclonal antibodies using immobilized metal-affinity chromatography, *Anal. Biochem.* 222 (1994) 29-33.
- [40] S. Auer, L. Azizi, F. Faschinger, V. Blazevic, T. Vesikari, H.J. Gruber, V.P. Hytönen, Stable immobilisation of His-tagged proteins on BLI biosensor surface using cobalt, *Sens. Actuators B* 243 (2017) 104-113.
- [41] W. Zhang, Q.A. Besford, A.J. Christofferson, P. Charchar, J.J. Richardson, A. Elbourne, K. Kempe, C.E. Hagemeyer, M.R. Field, C.F. McConville, I. Yarovsky, F. Caruso, Cobalt-directed assembly of antibodies onto metal–phenolic networks for enhanced particle targeting, *Nano Lett.* 20 (2020) 2660-2666.
- [42] J.E. Hale, Irreversible, oriented immobilization of antibodies to cobalt-iminodiacetate resin for use as immunoaffinity media, *Anal. Biochem.* 231 (1995) 46-49.
- [43] P. Batalla, J.M. Bolívar, F. Lopez-Gallego, J.M. Guisan, Oriented covalent immobilization of antibodies onto heterofunctional agarose supports: A highly efficient immuno-affinity chromatography platform, *J. Chromatogr. A* 1262 (2012) 56-63.
- [44] E.M. Ericsson, K. Enander, L. Bui, I. Lundström, P. Konradsson, B. Liedberg, Site-Specific and covalent attachment of his-tagged proteins by chelation assisted photoimmobilization: A strategy for microarraying of protein ligands, *Langmuir* 29 (2013) 11687-11694.
- [45] S. Gao, F. Rojas-Vega, J. Rocha-Martin, J.M. Guisán, Oriented immobilization of antibodies through different surface regions containing amino groups: Selective immobilization through the bottom of the Fc region, *Int. J. Biol. Macromol.* 177 (2021) 19-28.
- [46] J.-H. Qu, S. Horta, F. Delport, M. Sillen, N. Geukens, D.-W. Sun, K. Vanhoorelbeke, P. Declerck, J. Lammertyn, D. Spasic, Expanding a portfolio of (FO-) SPR surface chemistries with the Co(III)-NTA oriented immobilization of His6-tagged bioreceptors for applications in complex matrices, *ACS Sens.* 5 (2020) 960-969.
- [47] P. Zucca, R. Fernandez-Lafuente, E. Sanjust, Agarose and its derivatives as supports for enzyme immobilization, *Molecules* 21 (2016) 1577.
- [48] C.W. Rivero, N.S. García, J. Fernández-Lucas, L. Betancor, G.P. Romanelli, J.A. Trelles, Green production of cladribine by using immobilized 2'-Deoxyribosyltransferase from *Lactobacillus delbrueckii* stabilized through a double covalent/entrapment technology, *Biomolecules* 11 (2021) 657.
- [49] M. Ghebremedhin, S. Seiffert, T.A. Vilgis, Physics of agarose fluid gels: Rheological properties and microstructure, *Curr. Res. Food Sci.* 4 (2021) 436-448.
- [50] C. Mateo, J.M. Palomo, M. Fuentes, L. Betancor, V. Grazu, F. López-Gallego, B.C.C. Pessela, A. Hidalgo, G. Fernández-Lorente, R. Fernández-Lafuente, J.M. Guisán, Glyoxyl agarose: A fully inert and hydrophilic support for immobilization and high stabilization of proteins, *Enzym. Microb. Technol.* 39 (2006) 274-280.
- [51] J. Guisán, Aldehyde-agarose gels as activated supports for immobilization-stabilization of enzymes, *Enzym. Microb. Technol.* 10 (1988) 375-382.

REFERENCES

- [52] P. Batalla, M. Fuentes, C. Mateo, V. Grazu, R. Fernandez-Lafuente, J.M. Guisan, Covalent immobilization of antibodies on finally inert support surfaces through their surface regions having the highest densities in carboxyl groups, *Biomacromolecules* 9 (2008) 2230-2236.
- [53] C. Mateo, R. Torres, G. Fernández-Lorente, C. Ortiz, M. Fuentes, A. Hidalgo, F. López-Gallego, O. Abian, J.M. Palomo, L. Betancor, B.C.C. Pessela, J.M. Guisan, R. Fernández-Lafuente, Epoxy-amino groups: A new tool for improved immobilization of proteins by the epoxy method, *Biomacromolecules* 4 (2003) 772-777.
- [54] N. Rueda, J.C.S. dos Santos, R. Torres, C. Ortiz, O. Barbosa, R. Fernandez-Lafuente, Improved performance of lipases immobilized on heterofunctional octyl-glyoxyl agarose beads, *RSC Adv.* 5 (2015) 11212-11222.
- [55] P. Batalla, C. Mateo, V. Grazu, R. Fernandez-Lafuente, J.M. Guisan, Immobilization of antibodies through the surface regions having the highest density in lysine groups on finally inert support surfaces, *Process Biochem.* 44 (2009) 365-368.
- [56] J.M. Bolivar, A. Hidalgo, L. Sánchez-Ruiloba, J. Berenguer, J.M. Guisán, F. López-Gallego, Modulation of the distribution of small proteins within porous matrixes by smart-control of the immobilization rate, *J. Biotechnol.* 155 (2011) 412-420.
- [57] I. Angulo, I. Acebrón, B. de las Rivas, R. Muñoz, I. Rodríguez-Crespo, M. Menéndez, P. García, H. Tateno, I.J. Goldstein, B. Pérez-Agote, J.M. Mancheño, High-resolution structural insights on the sugar-recognition and fusion tag properties of a versatile β -trefoil lectin domain from the mushroom *Laetiporus sulphureus*, *Glycobiology* 21 (2011) 1349-1361.
- [58] I. Acebrón, A.G. Ruiz-Estrada, Y. Luengo, M.d.P. Morales, J.M. Guisán, J.M. Mancheño, Oriented attachment of recombinant proteins to agarose-coated magnetic nanoparticles by means of a β -Trefoil lectin domain, *Bioconjug. Chem.* 27 (2016) 2734-2743.
- [59] F. López-Gallego, I. Acebrón, J.M. Mancheño, S. Raja, M.P. Lillo, J.M. Guisán Seijas, Directed, strong, and reversible immobilization of proteins tagged with a β -trefoil lectin domain: A simple method to immobilize biomolecules on plain agarose matrixes, *Bioconjug. Chem.* 23 (2012) 565-573.
- [60] O.V. Salata, Applications of nanoparticles in biology and medicine, *J. Nanobiotechnol.* 2 (2004) 3.
- [61] C. Zhou, K. Cui, Y. Liu, S. Hao, L. Zhang, S. Ge, J. Yu, Ultrasensitive microfluidic paper-based electrochemical/visual analytical device via signal amplification of Pd@hollow Zn/Co core-shell ZIF67/ZIF8 nanoparticles for prostate-specific antigen detection, *Anal. Chem.* 93 (2021) 5459-5467.
- [62] A. Akbarzadeh, M. Samiei, S. Davaran, Magnetic nanoparticles: preparation, physical properties, and applications in biomedicine, *Nanoscale Res. Lett.* 7 (2012) 144.
- [63] M. Carmen Bautista, O. Bomati-Miguel, M. del Puerto Morales, C.J. Serna, S. Veintemillas-Verdaguer, Surface characterisation of dextran-coated iron oxide nanoparticles prepared by laser pyrolysis and coprecipitation, *J. Magn. Magn. Mater.* 293 (2005) 20-27.
- [64] A.K. Gupta, M. Gupta, Synthesis and surface engineering of iron oxide nanoparticles for biomedical applications, *Biomaterials* 26 (2005) 3995-4021.
- [65] X.Q. Xu, H. Shen, J.R. Xu, J. Xu, X.J. Li, X.M. Xiong, Core-shell structure and magnetic properties of magnetite magnetic fluids stabilized with dextran, *Appl. Surf. Sci.* 252 (2005) 494-500.
- [66] N. Zhu, H. Ji, P. Yu, J. Niu, M.U. Farooq, M.W. Akram, I.O. Udego, H. Li, X. Niu, Surface modification of magnetic iron oxide nanoparticles, *Nanomaterials (Basel)* 8 (2018).
- [67] S. Mornet, S. Vasseur, F. Grasset, P. Veverka, G. Goglio, A. Demourgues, J. Portier, E. Pollert, E. Duguet, Magnetic nanoparticle design for medical applications, *Prog. Solid State Chem.* 34 (2006) 237-247.

REFERENCES

- [68] S. Liu, B. Yu, S. Wang, Y. Shen, H. Cong, Preparation, surface functionalization and application of Fe₃O₄ magnetic nanoparticles, *Adv. Colloid Interface Sci.* 281 (2020) 102165.
- [69] W. Wu, Z. Wu, T. Yu, C. Jiang, W.-S. Kim, Recent progress on magnetic iron oxide nanoparticles: synthesis, surface functional strategies and biomedical applications, *Sci. Technol. Adv. Mater* 16 (2015) 023501.
- [70] L. Shen, B. Li, Y. Qiao, Fe₃O₄ nanoparticles in targeted drug/gene delivery systems, *Materials* 11 (2018) 324.
- [71] J. Chomoucka, J. Drbohlavova, D. Huska, V. Adam, R. Kizek, J. Hubalek, Magnetic nanoparticles and targeted drug delivering, *Pharmacol. Res.* 62 (2010) 144-149.
- [72] Y. Cao, L. Wen, F. Svec, T. Tan, Y. Lv, Magnetic AuNP@Fe₃O₄ nanoparticles as reusable carriers for reversible enzyme immobilization, *Chem. Eng. J.* 286 (2016) 272-281.
- [73] M. Ziegler-Borowska, Magnetic nanoparticles coated with aminated starch for HSA immobilization- simple and fast polymer surface functionalization, *Int. J. Biol. Macromol.* 136 (2019) 106-114.
- [74] M. Zirak, A. Abdollahiyan, B. Eftekhari-Sis, M. Saraei, Carboxymethyl cellulose coated Fe₃O₄@SiO₂ core-shell magnetic nanoparticles for methylene blue removal: equilibrium, kinetic, and thermodynamic studies, *Cellulose* 25 (2018) 503-515.
- [75] I. Khmara, M. Molcan, A. Antosova, Z. Bednarikova, V. Zavisova, M. Kubovcikova, A. Jurikova, V. Girman, E. Baranovicova, M. Koneracka, Z. Gazova, Bioactive properties of chitosan stabilized magnetic nanoparticles – Focus on hyperthermic and anti-amyloid activities, *J. Magn. Magn. Mater.* 513 (2020) 167056.
- [76] K. Vasić, Ž. Knez, M. Leitgeb, Immobilization of alcohol dehydrogenase from *Saccharomyces cerevisiae* onto carboxymethyl dextran-coated magnetic nanoparticles: a novel route for biocatalyst improvement via epoxy activation, *Sci. Rep.* 10 (2020) 19478.
- [77] M. Irfan, N. Dogan, A. Bingolbali, F. Aliew, Synthesis and characterization of NiFe₂O₄ magnetic nanoparticles with different coating materials for magnetic particle imaging (MPI), *J. Magn. Magn. Mater.* 537 (2021) 168150.
- [78] J. Li, Y. Yang, Z. Han, M. Zhao, H. Yuan, C. Ni, Degradation of tetrachloroguaiacol by an enzyme embedded in a magnetic composite cage structure of MNPs@ALG@SiO₂, *Biochem. Eng. J.* 170 (2021) 107924.
- [79] A.V. Ivanova, A.A. Nikitin, A.N. Gabashvily, D.A. Vishnevskiy, M.A. Abakumov, Synthesis and intensive analysis of antibody labeled single core magnetic nanoparticles for targeted delivery to the cell membrane, *J. Magn. Magn. Mater.* 521 (2021) 167487.
- [80] T. Tang, Y. Fu, Formation of chitosan/sodium phytate/nano-Fe₃O₄ magnetic coatings on wood surfaces via layer-by-layer self-assembly, *Coatings* 10 (2020) 51.
- [81] C. Tassa, S.Y. Shaw, R. Weissleder, Dextran-coated iron oxide nanoparticles: A versatile platform for targeted molecular imaging, molecular diagnostics, and therapy, *Acc. Chem. Res.* 44 (2011) 842-852.
- [82] H. Lee, T.-J. Yoon, J.-L. Figueiredo, F.K. Swirski, R. Weissleder, Rapid detection and profiling of cancer cells in fine-needle aspirates, *Proc. Natl. Acad. Sci.* 106 (2009) 12459-12464.
- [83] P.K. Ojha, S. Kar, K. Roy, J. Leszczynski, Toward comprehension of multiple human cells uptake of engineered nano metal oxides: quantitative inter cell line uptake specificity (QICLUS) modeling, *Nanotoxicology* 13 (2019) 14-34.
- [84] V.G. Tacias-Pascacio, C. Ortiz, N. Rueda, Á. Berenguer-Murcia, N. Acosta, I. Aranaz, C. Civera, R. Fernandez-Lafuente, A.R. Alcántara, Dextran aldehyde in biocatalysis: More than a mere immobilization system, *Catalysts* 9 (2019) 622.
- [85] S. Schöttler, G. Becker, S. Winzen, T. Steinbach, K. Mohr, K. Landfester, V. Mailänder, F.R. Wurm, Protein adsorption is required for stealth effect of poly(ethylene glycol)- and poly(phosphoester)-coated nanocarriers, *Nat. Nanotechnol.* 11 (2016) 372-377.

REFERENCES

- [86] O. Veisoh, J.W. Gunn, M. Zhang, Design and fabrication of magnetic nanoparticles for targeted drug delivery and imaging, *Adv. Drug Delivery. Rev.* 62 (2010) 284-304.
- [87] T.T.T. N'Guyen, H.T.T. Duong, J. Basuki, V. Montembault, S. Pascual, C. Guibert, J. Fresnais, C. Boyer, M.R. Whittaker, T.P. Davis, L. Fontaine, Functional iron oxide magnetic nanoparticles with hyperthermia-induced drug release ability by using a combination of orthogonal click reactions, *Angew. Chem., Int. Ed.* 52 (2013) 14152-14156.
- [88] W. Stöber, A. Fink, E. Bohn, Controlled growth of monodisperse silica spheres in the micron size range, *J. Colloid Interface Sci.* 26 (1968) 62-69.
- [89] S. Shahabi, L. Treccani, R. Dringen, K. Rezwani, Modulation of silica nanoparticle uptake into human osteoblast cells by variation of the ratio of amino and sulfonate surface groups: Effects of serum, *ACS Appl. Mater. Interfaces* 7 (2015) 13821-13833.
- [90] J. Nayeem, M.A.A. Al-Bari, M. Mahiuddin, M.A. Rahman, O.T. Mefford, H. Ahmad, M.M. Rahman, Silica coating of iron oxide magnetic nanoparticles by reverse microemulsion method and their functionalization with cationic polymer P(NIPAm-co-AMPTMA) for antibacterial vancomycin immobilization, *Colloids Surf. A Physicochem. Eng. Asp.* 611 (2021) 125857.
- [91] B. Zhang, Y. Wang, J. Zhang, S. Qiao, Z. Fan, J. Wan, K. Chen, Well-defined 3-Aminopropyltriethoxysilane functionalized magnetite nanoparticles and their adsorption performance for partially hydrolyzed polyacrylamide from aqueous solution, *Colloids Surf. A Physicochem. Eng. Asp.* 586 (2020) 124288.
- [92] S. Lyons, E.P. Mc Kiernan, G. Dee, D.F. Brougham, A. Morrin, Electrostatically modulated magnetophoretic transport of functionalised iron-oxide nanoparticles through hydrated networks, *Nanoscale* 12 (2020) 10550-10558.
- [93] C. Li, Y. Huang, Y. Yang, Coupling of an antifouling and reusable nanoplatform with catalytic hairpin assembly for highly sensitive detection of nucleic acids using zeta potential as signal readout, *Sens. Actuators B* 326 (2021) 128845.
- [94] K. Atacan, B. Çakıroğlu, M. Özacar, Efficient protein digestion using immobilized trypsin onto tannin modified Fe₃O₄ magnetic nanoparticles, *Colloids Surf. B* 156 (2017) 9-18.
- [95] P. Khramtsov, I. Barkina, M. Kropaneva, M. Bochkova, V. Timganova, A. Nechaev, I.y. Byzov, S. Zamorina, A. Yermakov, M. Rayev, Magnetic nanoclusters coated with albumin, casein, and gelatin: Size tuning, relaxivity, stability, protein corona, and application in nuclear magnetic resonance immunoassay, *Nanomaterials* 9 (2019) 1345.
- [96] L. Zhang, Y. Mazouzi, M. Salmain, B. Liedberg, S. Boujday, Antibody-gold nanoparticle bioconjugates for biosensors: Synthesis, characterization and selected applications, *Biosens. Bioelectron.* 165 (2020) 112370.
- [97] X. Liu, X. Ren, L. Chen, J. Zou, T. Li, L. Tan, C. Fu, Q. Wu, C. Li, J. Wang, Z. Huang, X. Meng, Fluorescent hollow ZrO₂@CdTe nanoparticles-based lateral flow assay for simultaneous detection of C-reactive protein and troponin T, *Microchim. Acta* 188 (2021) 209.
- [98] B. Wu, R. Jiang, Q. Wang, J. Huang, X. Yang, K. Wang, W. Li, N. Chen, Q. Li, Detection of C-reactive protein using nanoparticle-enhanced surface plasmon resonance using an aptamer-antibody sandwich assay, *Chem. Commun.* 52 (2016) 3568-3571.
- [99] Y. Li, X. Liu, J. Guo, Y. Zhang, J. Guo, X. Wu, B. Wang, X. Ma, Simultaneous detection of inflammatory biomarkers by SERS nanotag-based lateral flow assay with portable cloud Raman spectrometer, *Nanomaterials* 11 (2021) 1496.
- [100] B. Liu, H. Ni, D. Zhang, D. Wang, D. Fu, H. Chen, Z. Gu, X. Zhao, Ultrasensitive detection of protein with wide linear dynamic range based on core-shell sers nanotags and photonic crystal beads, *ACS Sens.* 2 (2017) 1035-1043.
- [101] Z. Rong, R. Xiao, S. Xing, G. Xiong, Z. Yu, L. Wang, X. Jia, K. Wang, Y. Cong, S. Wang, SERS-based lateral flow assay for quantitative detection of C-reactive protein

- as an early bio-indicator of a radiation-induced inflammatory response in nonhuman primates, *Analyst* 143 (2018) 2115-2121.
- [102] A.C. Power, B. Gorey, S. Chandra, J. Chapman, Carbon nanomaterials and their application to electrochemical sensors: a review, *Nanotechnol. Rev.* 7 (2018) 19-41.
- [103] W. Yang, K.R. Ratinac, S.P. Ringer, P. Thordarson, J.J. Gooding, F. Braet, Carbon nanomaterials in biosensors: Should you use nanotubes or graphene?, *Angew. Chem., Int. Ed.* 49 (2010) 2114-2138.
- [104] L. Qu, L. Dai, E. Osawa, Shape/size-controlled syntheses of metal nanoparticles for site-selective modification of carbon nanotubes, *J. Am. Chem. Soc.* 128 (2006) 5523-5532.
- [105] R. Freeman, I. Willner, Optical molecular sensing with semiconductor quantum dots (QDs), *Chem. Soc. Rev.* 41 (2012) 4067-4085.
- [106] N. Xin, D. Wei, Y. Zhu, M. Yang, S. Ramakrishna, O. Lee, H. Luo, H. Fan, Upconversion nanomaterials: a platform for biosensing, theranostic and photoregulation, *Mater. Today Chem.* 17 (2020) 100329.
- [107] Q. Han, X. Zhao, N. Na, J. Ouyang, Integrating near-infrared visual fluorescence with a photoelectrochemical sensing system for dual readout detection of biomolecules, *Anal. Chem.* 93 (2021) 3486-3492.
- [108] P. Yáñez-Sedeño, S. Campuzano, J.M. Pingarrón, Integrated affinity biosensing platforms on screen-printed electrodes electrografted with diazonium salts, *Sensors* 18 (2018) 675.
- [109] D. Antuña-Jiménez, M.B. González-García, D. Hernández-Santos, P. Fanjul-Bolado, Screen-Printed electrodes modified with metal nanoparticles for small molecule sensing, *Biosensors* 10 (2020) 9.
- [110] A.M. Musa, J. Kiely, R. Luxton, K.C. Honeychurch, Recent progress in screen-printed electrochemical sensors and biosensors for the detection of estrogens, *TrAC Trends Anal. Chem.* 139 (2021) 116254.
- [111] N. Baig, M. Sajid, T.A. Saleh, Recent trends in nanomaterial-modified electrodes for electroanalytical applications, *TrAC Trends Anal. Chem.* 111 (2019) 47-61.
- [112] M. Sher, A. Faheem, W. Asghar, S. Cinti, Nano-engineered screen-printed electrodes: A dynamic tool for detection of viruses, *TrAC Trends Anal. Chem.* 143 (2021) 116374.
- [113] A. Hayat, L. Barthelmebs, A. Sassolas, J.-L. Marty, An electrochemical immunosensor based on covalent immobilization of okadaic acid onto screen printed carbon electrode via diazotization-coupling reaction, *Talanta* 85 (2011) 513-518.
- [114] O. Hosu, M. Tertiş, G. Melinte, B. Feier, R. Săndulescu, C. Cristea, Mucin 4 detection with a label-free electrochemical immunosensor, *Electrochem. Commun.* 80 (2017) 39-43.
- [115] V. Serafin, R.M. Torrente-Rodríguez, A. González-Cortés, P. García de Frutos, M. Sabaté, S. Campuzano, P. Yáñez-Sedeño, J.M. Pingarrón, An electrochemical immunosensor for brain natriuretic peptide prepared with screen-printed carbon electrodes nanostructured with gold nanoparticles grafted through aryl diazonium salt chemistry, *Talanta* 179 (2018) 131-138.
- [116] V. Serafin, A. Valverde, M. Garranzo-Asensio, R. Barderas, S. Campuzano, P. Yáñez-Sedeño, J.M. Pingarrón, Simultaneous amperometric immunosensing of the metastasis-related biomarkers IL-13R α 2 and CDH-17 by using grafted screen-printed electrodes and a composite prepared from quantum dots and carbon nanotubes for signal amplification, *Microchim. Acta* 186 (2019) 411.
- [117] H. Qi, C. Ling, Q. Ma, Q. Gao, C. Zhang, Sensitive electrochemical immunosensor array for the simultaneous detection of multiple tumor markers, *Analyst* 137 (2012) 393-399.
- [118] Y. Wan, W. Deng, Y. Su, X. Zhu, C. Peng, H. Hu, H. Peng, S. Song, C. Fan, Carbon nanotube-based ultrasensitive multiplexing electrochemical immunosensor for cancer biomarkers, *Biosens. Bioelectron.* 30 (2011) 93-99.

REFERENCES

- [119] V. Serafín, A. Valverde, G. Martínez-García, E. Martínez-Periñán, F. Comba, M. Garranzo-Asensio, R. Barderas, P. Yáñez-Sedeño, S. Campuzano, J.M. Pingarrón, Graphene quantum dots-functionalized multi-walled carbon nanotubes as nanocarriers in electrochemical immunosensing. Determination of IL-13 receptor $\alpha 2$ in colorectal cells and tumor tissues with different metastatic potential, *Sens. Actuators B* 284 (2019) 711-722.
- [120] F. Hakimian, H. Ghourchian, Ultrasensitive electrochemical biosensor for detection of microRNA-155 as a breast cancer risk factor, *Anal. Chim. Acta* 1136 (2020) 1-8.
- [121] M. López Mujica, Y. Zhang, F. Gutierrez, F. Bédioui, G. Rivas, Non-amplified impedimetric genosensor for quantification of miRNA-21 based on the use of reduced graphene oxide modified with chitosan, *Microchem. J.* 160 (2021) 105596.
- [122] L. Jiang, F. Li, J. Feng, P. Wang, Q. Liu, Y. Li, Y. Dong, Q. Wei, An optionality further amplification of an sandwich-type electrochemical immunosensor based on biotin–streptavidin–biotin strategy for detection of alpha fetoprotein, *RSC Adv.* 6 (2016) 24373-24380.
- [123] L. Li, Y. Wei, S. Zhang, X. Chen, T. Shao, D. Feng, Electrochemical immunosensor based on metal ions functionalized CNSs@Au NPs nanocomposites as signal amplifier for simultaneous detection of triple tumor markers, *J. Electroanal. Chem.* 880 (2021) 114882.
- [124] N. Ma, T. Zhang, D. Fan, X. Kuang, A. Ali, D. Wu, Q. Wei, Triple amplified ultrasensitive electrochemical immunosensor for alpha fetoprotein detection based on MoS₂@Cu₂O-Au nanoparticles, *Sens. Actuators B* 297 (2019) 126821.
- [125] Z. Shi, Y. Lu, Z. Chen, C. Cheng, J. Xu, Q. Zhang, Z. Yan, Z. Luo, Q. Liu, Electrochemical non-enzymatic sensing of glycoside toxins by boronic acid functionalized nano-composites on screen-printed electrode, *Sens. Actuators B* 329 (2021) 129197.
- [126] W. Zhang, Z. Chen, Y. Guan, C. Liu, K. Zheng, X. Zou, Aptamer-functionalized screen-printed electrode coupled with graphene oxide and methylene blue nanocomposite as enhanced signal label for total arsenic determination in shellfish, *Sens. Actuators B* 335 (2021) 129383.
- [127] V.Q. Khue, T.Q. Huy, V.N. Phan, A. Tuan-Le, D.T. Thanh Le, M. Tonezzer, N.T. Hong Hanh, Electrochemical stability of screen-printed electrodes modified with Au nanoparticles for detection of methicillin-resistant *Staphylococcus aureus*, *Mater. Chem. Phys.* 255 (2020) 123562.
- [128] M. Moccia, V. Caratelli, S. Cinti, B. Pede, C. Avitabile, M. Saviano, A.L. Imbriani, D. Moscone, F. Arduini, Paper-based electrochemical peptide nucleic acid (PNA) biosensor for detection of miRNA-492: a pancreatic ductal adenocarcinoma biomarker, *Biosens. Bioelectron.* 165 (2020) 112371.
- [129] S. Sharma, J. Zapatero-Rodríguez, R. Saxena, R. O’Kennedy, S. Srivastava, Ultrasensitive direct impedimetric immunosensor for detection of serum HER2, *Biosens. Bioelectron.* 106 (2018) 78-85.
- [130] X. Mo, Z. Wu, J. Huang, G. Zhao, W. Dou, A sensitive and regenerative electrochemical immunosensor for quantitative detection of *Escherichia coli* O157:H7 based on stable polyaniline coated screen-printed carbon electrode and rGO-NR-Au@Pt, *Anal. Methods* 11 (2019) 1475-1482.
- [131] Y. Wei, X. Li, X. Sun, H. Ma, Y. Zhang, Q. Wei, Dual-responsive electrochemical immunosensor for prostate specific antigen detection based on Au-CoS/graphene and CeO₂/ionic liquids doped with carboxymethyl chitosan complex, *Biosens. Bioelectron.* 94 (2017) 141-147.
- [132] J. Zheng, H. Zhao, G. Ning, W. Sun, L. Wang, H. Liang, H. Xu, C. He, H. Zhao, C.-P. Li, A novel affinity peptide–antibody sandwich electrochemical biosensor for PSA based on the signal amplification of MnO₂-functionalized covalent organic framework, *Talanta* 233 (2021) 122520.

REFERENCES

- [133] M.R. Aflatoonian, S. Tajik, B. Aflatoonian, H. Beitollahi, K. Zhang, Q.V. Le, J.H. Cha, H.W. Jang, M. Shokouhimehr, W. Peng, A screen-printed electrode modified with graphene/Co₃O₄ nanocomposite for electrochemical detection of tramadol, *Front. Chem.* 8 (2020).
- [134] H. Xiao, S. Wei, M. Gu, Z. Chen, L. Cao, A sandwich-type electrochemical immunosensor using rGO-TEPA-Thi-Au as sensitive platform and CMK-3@AuPtNPs as signal probe for AFP detection, *Microchem. J.* 170 (2021) 106641.
- [135] M. Nodehi, M. Baghayeri, H. Veisi, Preparation of GO/Fe₃O₄@PMDA/AuNPs nanocomposite for simultaneous determination of As³⁺ and Cu²⁺ by stripping voltammetry, *Talanta* 230 (2021) 122288.
- [136] M. Zouari, S. Campuzano, J.M. Pingarrón, N. Raouafi, Femtomolar direct voltammetric determination of circulating miRNAs in sera of cancer patients using an enzymeless biosensor, *Anal. Chim. Acta* 1104 (2020) 188-198.
- [137] C.B. Arenas, E. Sánchez-Tirado, I. Ojeda, C.A. Gómez-Suárez, A. González-Cortés, R. Villalonga, P. Yáñez-Sedeño, J.M. Pingarrón, An electrochemical immunosensor for adiponectin using reduced graphene oxide-carboxymethylcellulose hybrid as electrode scaffold, *Sens. Actuators B* 223 (2016) 89-94.
- [138] V. Caratelli, A. Ciampaglia, J. Guiducci, G. Sancesario, D. Moscone, F. Arduini, Precision medicine in Alzheimer's disease: An origami paper-based electrochemical device for cholinesterase inhibitors, *Biosens. Bioelectron.* 165 (2020) 112411.
- [139] L. Fabiani, M. Saroglia, G. Galatà, R. De Santis, S. Fillo, V. Luca, G. Faggioni, N. D'Amore, E. Regalbutto, P. Salvatori, G. Terova, D. Moscone, F. Lista, F. Arduini, Magnetic beads combined with carbon black-based screen-printed electrodes for COVID-19: A reliable and miniaturized electrochemical immunosensor for SARS-CoV-2 detection in saliva, *Biosens. Bioelectron.* 171 (2021) 112686.
- [140] F.C. Vicentini, P.A. Raymundo-Pereira, B.C. Janegitz, S.A.S. Machado, O. Fatibello-Filho, Nanostructured carbon black for simultaneous sensing in biological fluids, *Sens. Actuators B* 227 (2016) 610-618.
- [141] S.P. Selvam, S.R. Chinnadayala, S. Cho, Electrochemical nanobiosensor for early detection of rheumatoid arthritis biomarker: Anti-cyclic citrullinated peptide antibodies based on polyaniline (PANI)/MoS₂-modified screen-printed electrode with PANI-Au nanomatrix-based signal amplification, *Sens. Actuators B* 333 (2021) 129570.
- [142] E.y. Jo, J.h. Lee, Polyaniline-nanofiber-modified screen-printed electrode with intermediate dye amplification for detection of endocrine disruptor bisphenol A, *Microchem. J.* 155 (2020) 104693.
- [143] A. Pangajam, K. Theyagarajan, K. Dinakaran, Highly sensitive electrochemical detection of *E. coli* O157:H7 using conductive carbon dot/ZnO nanorod/PANI composite electrode, *Sens. Bio-Sens. Res.* 29 (2020) 100317.
- [144] J. Zhou, N. Gan, T. Li, H. Zhou, X. Li, Y. Cao, L. Wang, W. Sang, F. Hu, Ultratrace detection of C-reactive protein by a piezoelectric immunosensor based on Fe₃O₄@SiO₂ magnetic capture nanoprobe and HRP-antibody co-immobilized nano gold as signal tags, *Sens. Actuators B* 178 (2013) 494-500.
- [145] L. Wang, C-reactive protein levels in the early stage of COVID-19, *Med. Mal. Infect.* 50 (2020) 332-334.
- [146] S. Iwasaki, H. Kawasaki, Y. Iwasaki, Label-Free specific detection and collection of C-reactive protein using zwitterionic phosphorylcholine-polymer-protected magnetic nanoparticles, *Langmuir* 35 (2019) 1749-1755.
- [147] Y. Iwasaki, T. Kimura, M. Orisaka, H. Kawasaki, T. Goda, S.-i. Yusa, Label-free detection of C-reactive protein using highly dispersible gold nanoparticles synthesized by reducible biomimetic block copolymers, *Chem. Commun.* 50 (2014) 5656-5658.
- [148] M. António, R. Ferreira, R. Vitorino, A.L. Daniel-da-Silva, A simple aptamer-based colorimetric assay for rapid detection of C-reactive protein using gold nanoparticles, *Talanta* 214 (2020) 120868.

REFERENCES

- [149] J.-Y. Byun, Y.-B. Shin, D.-M. Kim, M.-G. Kim, A colorimetric homogeneous immunoassay system for the C-reactive protein, *Analyst* 138 (2013) 1538-1543.
- [150] V. Raj, K. Sreenivasan, Selective detection and estimation of C-reactive protein in serum using surface-functionalized gold nano-particles, *Anal. Chim. Acta* 662 (2010) 186-192.
- [151] E.D. Bernard, K.C. Nguyen, M.C. DeRosa, A.F. Tayabali, R. Aranda-Rodriguez, Development of a bead-based aptamer/antibody detection system for C-reactive protein, *Anal. Biochem.* 472 (2015) 67-74.
- [152] W.-B. Lee, Y.-H. Chen, H.-I. Lin, S.-C. Shiesh, G.-B. Lee, An integrated microfluidic system for fast, automatic detection of C-reactive protein, *Sens. Actuators B* 157 (2011) 710-721.
- [153] Á. Molinero-Fernández, L. Arruza, M.Á. López, A. Escarpa, On-the-fly rapid immunoassay for neonatal sepsis diagnosis: C-reactive protein accurate determination using magnetic graphene-based micromotors, *Biosens. Bioelectron.* 158 (2020) 112156.
- [154] Á. Molinero-Fernández, M.Á. López, A. Escarpa, Electrochemical microfluidic micromotors-based immunoassay for C-reactive protein determination in preterm neonatal samples with sepsis suspicion, *Anal. Chem.* 92 (2020) 5048-5054.
- [155] Á. Molinero-Fernández, M. Moreno-Guzmán, L. Arruza, M.Á. López, A. Escarpa, Toward early diagnosis of late-onset sepsis in preterm neonates: Dual magnetoimmunosensor for simultaneous procalcitonin and C-reactive protein determination in diagnosed clinical samples, *ACS Sens.* 4 (2019) 2117-2123.
- [156] Á. Molinero-Fernández, M. Moreno-Guzmán, M.Á. López, A. Escarpa, An array-based electrochemical magneto-immunosensor for early neonatal sepsis diagnostic: Fast and accurate determination of C-reactive protein in whole blood and plasma samples, *Microchem. J.* 157 (2020) 104913.
- [157] Y. Xing, Q. Gao, Y. Zhang, L. Ma, K.Y. Loh, M. Peng, C. Chen, Y. Cui, The improved sensitive detection of C-reactive protein based on the chemiluminescence immunoassay by employing monodispersed PAA-Au/Fe₃O₄ nanoparticles and zwitterionic glycerophosphoryl choline, *J. Mater. Chem. B* 5 (2017) 3919-3926.
- [158] N. Gan, P. Xiong, J. Wang, T. Li, F. Hu, Y. Cao, L. Zheng, A novel signal-amplified immunoassay for the detection of C-Reactive protein using hrp-doped magnetic nanoparticles as labels with the electrochemical quartz crystal microbalance as a detector, *J. Anal. Methods Chem.* 2013 (2013) 482316.
- [159] J. Zhang, W. Zhang, J. Guo, J. Wang, Y. Zhang, Electrochemical detection of C-reactive protein using Copper nanoparticles and hybridization chain reaction amplifying signal, *Anal. Biochem.* 539 (2017) 1-7.
- [160] J. Oh, H.-A. Joung, H.S. Han, J.K. Kim, M.-G. Kim, A hook effect-free immunochromatographic assay (HEF-ICA) for measuring the C-reactive protein concentration in one drop of human serum, *Theranostics* 8 (2018) 3189-3197.
- [161] Y.K. Oh, H.-A. Joung, H.S. Han, H.-J. Suk, M.-G. Kim, A three-line lateral flow assay strip for the measurement of C-reactive protein covering a broad physiological concentration range in human sera, *Biosens. Bioelectron.* 61 (2014) 285-289.
- [162] Y. Panraksa, A. Apilux, S. Jampasa, S. Puthong, C.S. Henry, S. Rengpipat, O. Chailapakul, A facile one-step gold nanoparticles enhancement based on sequential patterned lateral flow immunoassay device for C-reactive protein detection, *Sens. Actuators B* 329 (2021) 129241.
- [163] Y. Cai, K. Kang, Y. Liu, Y. Wang, X. He, Development of a lateral flow immunoassay of C-reactive protein detection based on red fluorescent nanoparticles, *Anal. Biochem.* 556 (2018) 129-135.
- [164] J. Guo, S. Chen, S. Tian, K. Liu, X. Ma, J. Guo, A sensitive and quantitative prognosis of C-reactive protein at picogram level using mesoporous silica encapsulated core-shell up-conversion nanoparticle based lateral flow strip assay, *Talanta* 230 (2021) 122335.

REFERENCES

- [165] K.M. Park, D.J. Chung, M. Choi, T. Kang, J. Jeong, Fluorescent fullerene nanoparticle-based lateral flow immunochromatographic assay for rapid quantitative detection of C-reactive protein, *Nano Converg.* 6 (2019) 35.
- [166] X. Qi, Y. Huang, Z. Lin, L. Xu, H. Yu, Dual-quantum-dots-labeled lateral flow strip rapidly quantifies procalcitonin and C-reactive protein, *Nanoscale Res. Lett.* 11 (2016) 167.
- [167] C. Ruppert, L. Kaiser, L.J. Jacob, S. Laufer, M. Kohl, H.-P. Deigner, Duplex Shiny app quantification of the sepsis biomarkers C-reactive protein and interleukin-6 in a fast quantum dot labeled lateral flow assay, *J. Nanobiotechnol.* 18 (2020) 130.
- [168] R. Wu, T. Wang, M. Wu, Y. Lv, X. Liu, J. Li, H. Shen, L.S. Li, Synthesis of highly stable CuInZnS/ZnS//ZnS quantum dots with thick shell and its application to quantitative immunoassay, *Chem. Eng. J.* 348 (2018) 447-454.
- [169] R. Wu, S. Zhou, T. Chen, J. Li, H. Shen, Y. Chai, L.S. Li, Quantitative and rapid detection of C-reactive protein using quantum dot-based lateral flow test strip, *Anal. Chim. Acta* 1008 (2018) 1-7.
- [170] X. Yang, X. Liu, B. Gu, H. Liu, R. Xiao, C. Wang, S. Wang, Quantitative and simultaneous detection of two inflammation biomarkers via a fluorescent lateral flow immunoassay using dual-color SiO₂@QD nanotags, *Microchim. Acta* 187 (2020) 570.
- [171] J. Hu, Z.-L. Zhang, C.-Y. Wen, M. Tang, L.-L. Wu, C. Liu, L. Zhu, D.-W. Pang, Sensitive and quantitative detection of C-Reaction protein based on immunofluorescent nanospheres coupled with lateral flow test strip, *Anal. Chem.* 88 (2016) 6577-6584.
- [172] L. Huang, T. Liao, J. Wang, L. Ao, W. Su, J. Hu, Brilliant pitaya-type silica colloids with central-radial and high-density quantum dots incorporation for ultrasensitive fluorescence immunoassays, *Adv. Funct. Mater.* 28 (2018) 1705380.
- [173] O. Deegan, K. Walshe, K. Kavanagh, S. Doyle, Quantitative detection of C-reactive protein using phosphocholine-labelled enzyme or microspheres, *Anal. Biochem.* 312 (2003) 175-181.
- [174] Y. Lv, F. Wang, N. Li, R. Wu, J. Li, H. Shen, L.S. Li, F. Guo, Development of dual quantum dots-based fluorescence-linked immunosorbent assay for simultaneous detection on inflammation biomarkers, *Sens. Actuators B* 301 (2019) 127118.
- [175] Y. Lv, Y. Yuan, N. Hu, N. Jin, D. Xu, R. Wu, H. Shen, O. Chen, L.S. Li, Thick-shell CdSe/ZnS/CdZnS/ZnS core/shell quantum dots for quantitative immunoassays, *ACS Appl. Nano Mater.* 4 (2021) 2855-2865.
- [176] Y. Xu, Y. Lv, R. Wu, J. Li, H. Shen, H. Yang, H. Zhang, L.S. Li, Sensitive immunoassay based on biocompatible and robust silica-coated Cd-free InP-based quantum dots, *Inorg. Chem.* 60 (2021) 6503-6513.
- [177] D. Hong, K. Kim, E.-J. Jo, M.-G. Kim, Electrochemiluminescence-incorporated lateral flow immunosensors using Ru(bpy)₃²⁺-labeled gold nanoparticles for the full-range detection of physiological C-Reactive protein levels, *Anal. Chem.* 93 (2021) 7925-7932.
- [178] R. Nooney, V. Rebello, G. Keegan, C.L. O'Connell, D. Byrne, C. McDonagh, Highly sensitive detection of C-reactive protein using a novel dissolution approach in a dye-doped silica nanoparticle-based fluorescence immunoassay, *Anal. Methods* 9 (2017) 994-1003.
- [179] L. Chen, Y. Li, L. Miao, X. Pang, T. Li, Y. Qian, H. Li, "Lighting-up" curcumin nanoparticles triggered by pH for developing improved enzyme-linked immunosorbent assay, *Biosens. Bioelectron.* 188 (2021) 113308.
- [180] X. Liu, X. Yang, K. Li, H. Liu, R. Xiao, W. Wang, C. Wang, S. Wang, Fe₃O₄@Au SERS tags-based lateral flow assay for simultaneous detection of serum amyloid A and C-reactive protein in unprocessed blood sample, *Sens. Actuators B* 320 (2020) 128350.
- [181] R. Chen, X. Du, Y. Cui, X. Zhang, Q. Ge, J. Dong, X. Zhao, Vertical flow assay for inflammatory biomarkers based on nanofluidic channel array and sers nanotags, *Small* 16 (2020) 2002801.

REFERENCES

- [182] S.M. Kim, J. Kim, G. Yim, H.J. Ahn, M. Lee, T.-H. Kim, C. Park, J. Min, H. Jang, T. Lee, Fabrication of a surface-enhanced Raman spectroscopy-based analytical method consisting of multifunctional DNA three-way junction-conjugated porous gold nanoparticles and Au-Te nanoworm for C-reactive protein detection, *Anal. Bioanal. Chem.* (2021).
- [183] S. Wang, J. Luo, Y. He, Y. Chai, R. Yuan, X. Yang, Combining porous magnetic Ni@C nanospheres and CaCO₃ microcapsule as surface-enhanced Raman spectroscopy sensing platform for hypersensitive C-reactive protein detection, *ACS Appl. Mater. Interfaces* 10 (2018) 33707-33712.
- [184] B.G. Andryukov, Six decades of lateral flow immunoassay: from determining metabolic markers to diagnosing COVID-19, *AIMS Microbiol* 6 (2020) 280-304.
- [185] L. Gao, J. Zhuang, L. Nie, J. Zhang, Y. Zhang, N. Gu, T. Wang, J. Feng, D. Yang, S. Perrett, X. Yan, Intrinsic peroxidase-like activity of ferromagnetic nanoparticles, *Nat. Nanotechnol.* 2 (2007) 577-583.
- [186] J. Xie, M.-Q. Tang, J. Chen, Y.-H. Zhu, C.-B. Lei, H.-W. He, X.-H. Xu, A sandwich ELISA-like detection of C-reactive protein in blood by citicoline-bovine serum albumin conjugate and aptamer-functionalized gold nanoparticles nanozyme, *Talanta* 217 (2020) 121070.
- [187] P.K. Gupta, S.E. Son, G.H. Seong, Functionalized ultra-fine bimetallic PtRu alloy nanoparticle with high peroxidase-mimicking activity for rapid and sensitive colorimetric quantification of C-reactive protein, *Microchim. Acta* 188 (2021) 119.
- [188] M.S. Kim, S. Cho, S.H. Joo, J. Lee, S.K. Kwak, M.I. Kim, J. Lee, N- and B-codoped graphene: A strong candidate to replace natural peroxidase in sensitive and selective bioassays, *ACS Nano* 13 (2019) 4312-4321.
- [189] S. Sloan-Dennison, S. Laing, N.C. Shand, D. Graham, K. Faulds, A novel nanozyme assay utilising the catalytic activity of silver nanoparticles and SERRS, *Analyst* 142 (2017) 2484-2490.
- [190] T.-Z. Liu, R. Hu, Y. Liu, K.-L. Zhang, R.-Y. Bai, Y.-H. Yang, Amperometric immunosensor based on covalent organic frameworks and Pt/Ru/C nanoparticles for the quantification of C-reactive protein, *Microchim. Acta* 187 (2020) 320.
- [191] K. Dai, L. Zheng, N. Xu, Z. Yang, T. Guo, R. Hu, Y. Yang, The preparation of C-Reactive protein immunosensor based on amino graphene and hollow silver platinum nanomaterials, *J. Nanosci. Nanotechnol.* 17 (2017) 115-122.
- [192] Y. Ma, M. Lu, Y. Deng, R. Bai, X. Zhang, D. Li, K. Zhang, R. Hu, Y. Yang, The preparation of C-reactive protein immunosensor based on nano-mimetic enzyme Co₃O₄, *J. Biomed. Nanotechnol.* 14 (2018) 1169-1177.
- [193] Y. Ma, J. Yang, T. Yang, Y. Deng, M. Gu, M. Wang, R. Hu, Y. Yang, Electrochemical detection of C-reactive protein using functionalized iridium nanoparticles/graphene oxide as a tag, *RSC Adv.* 10 (2020) 9723-9729.
- [194] M. Fuentes, C. Mateo, J.M. Guisán, R. Fernández-Lafuente, Preparation of inert magnetic nano-particles for the directed immobilization of antibodies, *Biosens. Bioelectron.* 20 (2005) 1380-1387.
- [195] J.M. Bolivar, C. Mateo, V. Grazu, A.V. Carrascosa, B.C. Pessela, J.M. Guisan, Heterofunctional supports for the one-step purification, immobilization and stabilization of large multimeric enzymes: Amino-glyoxyl versus amino-epoxy supports, *Process Biochem.* 45 (2010) 1692-1698.
- [196] C. Mateo, G. Fernandez-Lorente, J. Rocha-Martin, J.M. Bolivar, J.M. Guisan, Oriented covalent immobilization of enzymes on heterofunctional-glyoxyl supports, *Immobilization of Enzymes and Cells*, Springer2013, pp. 73-88.
- [197] U.K. Laemmli, Cleavage of Structural proteins during the assembly of the head of bacteriophage T4, *Nature* 227 (1970) 680-685.
- [198] R. Massart, Preparation of aqueous magnetic liquids in alkaline and acidic media, *IEEE Trans. Magn.* 17 (1981) 1247-1248.

REFERENCES

- [199] R. Costo, V. Bello, C. Robic, M. Port, J.F. Marco, M. Puerto Morales, S. Veintemillas-Verdaguer, Ultrasmall iron oxide nanoparticles for biomedical applications: Improving the colloidal and magnetic properties, *Langmuir* 28 (2012) 178-185.
- [200] J. Yang, L. Sun, R. Guo, H. Yang, X. Feng, X. Zhang, A facile route for oriented covalent immobilization of recombinant protein A on epoxy agarose gels: In situ generation of heterofunctional amino-epoxy supports, *ChemistrySelect* 3 (2018) 10320-10324.
- [201] C. Mateo, O. Abian, M. Bernedo, E. Cuenca, M. Fuentes, G. Fernandez-Lorente, J.M. Palomo, V. Grazu, B.C.C. Pessela, C. Giacomini, G. Irazoqui, A. Villarino, K. Ovsejevi, F. Batista-Viera, R. Fernandez-Lafuente, J.M. Guisán, Some special features of glyoxyl supports to immobilize proteins, *Enzym. Microb. Technol.* 37 (2005) 456-462.
- [202] B.C.C. Pessela, C. Mateo, M. Fuentes, A. Vian, J.L. García, A.V. Carrascosa, J.M. Guisán, R. Fernández-Lafuente, Stabilization of a multimeric β -galactosidase from *Thermus* sp. Strain T2 by immobilization on novel heterofunctional epoxy supports plus aldehyde-dextran cross-linking, *Biotechnol. Prog.* 20 (2004) 388-392.
- [203] S. Dutz, W. Andrá, R. Hergt, R. Müller, C. Oestreich, C. Schmidt, J. Töpfer, M. Zeisberger, M.E. Bellemann, Influence of dextran coating on the magnetic behaviour of iron oxide nanoparticles, *J. Magn. Magn. Mater.* 311 (2007) 51-54.
- [204] S.L. Easo, P.V. Mohanan, Dextran stabilized iron oxide nanoparticles: Synthesis, characterization and in vitro studies, *Carbohydr. Polym.* 92 (2013) 726-732.
- [205] Z. Shaterabadi, G. Nabiyouni, M. Soleymani, High impact of in situ dextran coating on biocompatibility, stability and magnetic properties of iron oxide nanoparticles, *Mater. Sci. Eng. C* 75 (2017) 947-956.
- [206] A.K. Hauser, R. Mathias, K.W. Anderson, J. Zach Hilt, The effects of synthesis method on the physical and chemical properties of dextran coated iron oxide nanoparticles, *Mater. Chem. Phys.* 160 (2015) 177-186.
- [207] C.T. Yavuz, J.T. Mayo, W.W. Yu, A. Prakash, J.C. Falkner, S. Yean, L. Cong, H.J. Shipley, A. Kan, M. Tomson, D. Natelson, V.L. Colvin, Low-field magnetic separation of monodisperse Fe₃O₄ nanocrystals, *Science* 314 (2006) 964-967.
- [208] O. Strbak, I. Antal, I. Khmara, M. Koneracka, M. Kubovcikova, V. Zavisova, M. Molcan, A. Jurikova, P. Hnilicova, J. Gombos, N. Kadasova, D. Dobrota, Influence of dextran molecular weight on the physical properties of magnetic nanoparticles for hyperthermia and MRI applications, *Nanomaterials (Basel, Switzerland)* 10 (2020) 2468.
- [209] S. Oliver, D.S. Thomas, M. Kavallaris, O. Vittorio, C. Boyer, Efficient functionalisation of dextran-aldehyde with catechin: potential applications in the treatment of cancer, *Polym. Chem.* 7 (2016) 2542-2552.
- [210] A. Kirschning, N. Dibbert, G. Dräger, Chemical functionalization of polysaccharides—Towards biocompatible hydrogels for biomedical applications, *Chem. Eur. J.* 24 (2018) 1231-1240.
- [211] L. Tavernini, C. Ottone, A. Illanes, L. Wilson, Entrapment of enzyme aggregates in chitosan beads for aroma release in white wines, *Int. J. Biol. Macromol.* 154 (2020) 1082-1090.
- [212] J. Cejudo-Sanches, A.H. Orrego, A. Jaime-Mendoza, R. Ghobadi, S. Moreno-Perez, G. Fernandez-Lorente, J. Rocha-Martin, J.M. Guisan, High stabilization of immobilized *Rhizomucor miehei* lipase by additional coating with hydrophilic crosslinked polymers: Poly-allylamine/Aldehyde-dextran, *Process Biochem.* 92 (2020) 156-163.
- [213] R.O. Henriques, J.A. Bork, G. Fernandez-Lorente, J.M. Guisan, A. Furigo, D. de Oliveira, B.C. Pessela, Co-immobilization of lipases and β -d-galactosidase onto magnetic nanoparticle supports: Biochemical characterization, *Mol. Catal.* 453 (2018) 12-21.
- [214] B. Saha, T.H. Evers, M.W.J. Prins, How antibody surface coverage on nanoparticles determines the activity and kinetics of antigen capturing for biosensing, *Anal. Chem.* 86 (2014) 8158-8166.

REFERENCES

- [215] X. Tan, X. Sun, Y. Li, Y. Zeng, J. Gong, Z. Wang, Y. An, H. Li, Biomaterialized Mn₃(PO₄)₂/aptamer nanosheets for enhanced electrochemical determination of C-reactive protein, *Sens. Actuators B* 333 (2021) 129510.
- [216] T.-Z. Liu, R. Hu, X. Zhang, K.-L. Zhang, Y. Liu, X.-B. Zhang, R.-Y. Bai, D. Li, Y.-H. Yang, Metal–Organic framework nanomaterials as novel signal probes for electron transfer mediated ultrasensitive electrochemical immunoassay, *Anal. Chem.* 88 (2016) 12516-12523.
- [217] M. Moreno-Guzmán, I. Ojeda, R. Villalonga, A. González-Cortés, P. Yáñez-Sedeño, J.M. Pingarrón, Ultrasensitive detection of adrenocorticotropin hormone (ACTH) using disposable phenylboronic-modified electrochemical immunosensors, *Biosens. Bioelectron.* 35 (2012) 82-86.
- [218] V. Serafin, R.M. Torrente-Rodríguez, M. Batlle, P. García de Frutos, S. Campuzano, P. Yáñez-Sedeño, J.M. Pingarrón, Electrochemical immunosensor for receptor tyrosine kinase AXL using poly(pyrrolepropionic acid)-modified disposable electrodes, *Sens. Actuators B* 240 (2017) 1251-1256.
- [219] A. Valverde, A. ben Hassine, V. Serafin, C. Muñoz-San Martín, M. Pedrero, M. Garranzo-Asensio, M. Gamella, N. Raouafi, R. Barderas, P. Yáñez-Sedeño, S. Campuzano, J.M. Pingarrón, Dual amperometric immunosensor for improving cancer metastasis detection by the simultaneous determination of extracellular and soluble circulating fraction of emerging metastatic biomarkers, *Electroanalysis* 32 (2020) 706-714.
- [220] A. Valverde, E. Povedano, V. Ruiz-Valdepeñas Montiel, P. Yáñez-Sedeño, M. Garranzo-Asensio, N. Rodríguez, G. Domínguez, R. Barderas, S. Campuzano, J.M. Pingarrón, Determination of Cadherin-17 in tumor tissues of different metastatic grade using a single incubation-step amperometric immunosensor, *Anal. Chem.* 90 (2018) 11161-11167.
- [221] B. Arévalo, V. Serafin, J.F. Beltrán-Sánchez, J. Aznar-Poveda, J.A. López-Pastor, A.J. García-Sánchez, J. García-Haro, S. Campuzano, P. Yáñez-Sedeño, J.M. Pingarrón, Simultaneous determination of four fertility-related hormones in saliva using disposable multiplexed immunoplatforms coupled to a custom-designed and field-portable potentiostat, *Anal. Methods* 13 (2021) 3471-3478.
- [222] P. Dennler, E. Fischer, R. Schibli, Antibody conjugates: From Heterogeneous populations to defined reagents, *Antibodies* 4 (2015) 197-224.
- [223] F. López-Gallego, G. Fernandez-Lorente, J. Rocha-Martín, J.M. Bolivar, C. Mateo, J.M. Guisan, Multi-Point covalent immobilization of enzymes on glyoxyl agarose with minimal physico-chemical modification: Stabilization of industrial enzymes, in: J.M. Guisan, J.M. Bolivar, F. López-Gallego, J. Rocha-Martín (Eds.) *Immobilization of Enzymes and Cells: Methods and Protocols*, Springer US, New York, NY, 2020, pp. 93-107.
- [224] J.M. Bolivar, F. López-Gallego, C. Godoy, D.S. Rodrigues, R.C. Rodrigues, P. Batalla, J. Rocha-Martín, C. Mateo, R.L.C. Giordano, J.M. Guisán, The presence of thiolated compounds allows the immobilization of enzymes on glyoxyl agarose at mild pH values: New strategies of stabilization by multipoint covalent attachment, *Enzym. Microb. Technol.* 45 (2009) 477-483.
- [225] A.H. Orrego, R. Ghobadi, S. Moreno-Perez, A.J. Mendoza, G. Fernandez-Lorente, J.M. Guisan, J. Rocha-Martín, Stabilization of immobilized lipases by intense intramolecular cross-linking of their surfaces by using aldehyde-dextran polymers, *Int. J. Mol. Sci.* 19 (2018) 553.
- [226] M. Jannat, K.-L. Yang, Immobilization of enzymes on flexible tubing surfaces for continuous bioassays, *Langmuir* 34 (2018) 14226-14233.
- [227] R. Danczyk, B. Krieder, A. North, T. Webster, H. HogenEsch, A. Rundell, Comparison of antibody functionality using different immobilization methods, *Biotechnol. Bioeng.* 84 (2003) 215-223.

REFERENCES

- [228] V. Serafin, R.M. Torrente-Rodríguez, M. Batlle, P. García de Frutos, S. Campuzano, P. Yáñez-Sedeño, J.M. Pingarrón, Comparative evaluation of the performance of electrochemical immunosensors using magnetic microparticles and nanoparticles. Application to the determination of tyrosine kinase receptor AXL, *Microchim. Acta* 184 (2017) 4251-4258.
- [229] X. Ouyang, M. De Stefano, A. Krissanaprasit, A.L. Bank Kodal, C. Bech Rosen, T. Liu, S. Helmig, C. Fan, K.V. Gothelf, Docking of antibodies into the cavities of DNA origami structures, *Angew. Chem., Int. Ed.* 56 (2017) 14423-14427.
- [230] F. Hagemann, P. Adametz, M. Wessling, V. Thom, Modeling hindered diffusion of antibodies in agarose beads considering pore size reduction due to adsorption, *J. Chromatogr. A* 1626 (2020) 461319.
- [231] M. Yu, Y. Li, S. Zhang, X. Li, Y. Yang, Y. Chen, G. Ma, Z. Su, Improving stability of virus-like particles by ion-exchange chromatographic supports with large pore size: Advantages of gigaporous media beyond enhanced binding capacity, *J. Chromatogr. A* 1331 (2014) 69-79.
- [232] L. Betancor, M. Fuentes, G. Dellamora-Ortiz, F. López-Gallego, A. Hidalgo, N. Alonso-Morales, C. Mateo, J.M. Guisán, R. Fernández-Lafuente, Dextran aldehyde coating of glucose oxidase immobilized on magnetic nanoparticles prevents its inactivation by gas bubbles, *J. Mol. Catal. B: Enzym.* 32 (2005) 97-101.
- [233] M. Nakamoto, Y. Hoshino, Y. Miura, Effect of physical properties of nanogel particles on the kinetic constants of multipoint protein recognition process, *Biomacromolecules* 15 (2014) 541-547.
- [234] Y. Hoshino, H. Lee, Y. Miura, Interaction between synthetic particles and biomacromolecules: fundamental study of nonspecific interaction and design of nanoparticles that recognize target molecules, *Polym. J. (Tokyo, Jpn.)* 46 (2014) 537-545.
- [235] H. Xu, J.R. Lu, D.E. Williams, Effect of surface packing density of interfacially adsorbed monoclonal antibody on the binding of hormonal antigen human chorionic gonadotrophin, *J. Phys. Chem.* 110 (2006) 1907-1914.
- [236] J. Zhou, H.K. Tsao, Y.J. Sheng, S. Jiang, Monte Carlo simulations of antibody adsorption and orientation on charged surfaces, *J. Chem. Phys.* 121 (2004) 1050-1057.
- [237] J. Mosayebi, M. Kiyasatfar, S. Laurent, Synthesis, functionalization, and design of magnetic nanoparticles for theranostic applications, *Adv. Healthc. Mater.* 6 (2017) 1700306.
- [238] M. Iijima, Surface modification of nanoparticles by silane alkoxides and their application in silicone-based polymer nanocomposites, in: M. Naito, T. Yokoyama, K. Hosokawa, K. Nogi (Eds.) *Nanoparticle Technology Handbook (Third Edition)*, Elsevier 2018, pp. 705-709.
- [239] S. Sun, H. Zeng, D.B. Robinson, S. Raoux, P.M. Rice, S.X. Wang, G. Li, Monodisperse MFe₂O₄ (M = Fe, Co, Mn) Nanoparticles, *J. Am. Chem. Soc.* 126 (2004) 273-279.
- [240] L.E. Woodard, C.L. Dennis, J.A. Borchers, A. Attaluri, E. Velarde, C. Dawidczyk, P.C. Searson, M.G. Pomper, R. Ivkov, Nanoparticle architecture preserves magnetic properties during coating to enable robust multi-modal functionality, *Sci. Rep.* 8 (2018) 12706.
- [241] T. Kawaguchi, M. Hasegawa, Structure of dextran-magnetite complex: relation between conformation of dextran chains covering core and its molecular weight, *J. Mater. Sci. Mater. Med.* 11 (2000) 31-35.
- [242] F.R. Senti, N.N. Hellman, N.H. Ludwig, G.E. Babcock, R. Tobin, C.A. Glass, B.L. Lamberts, Viscosity, sedimentation, and light-scattering properties of fraction of an acid-hydrolyzed dextran, *J. Polym. Sci.* 17 (1955) 527-546.
- [243] H. Unterweger, L. Dézsi, J. Matuszak, C. Janko, M. Poettler, J. Jordan, T. Bäuerle, J. Szebeni, T. Fey, A.R. Boccaccini, C. Alexiou, I. Cicha, Dextran-coated superparamagnetic iron oxide nanoparticles for magnetic resonance imaging:

- evaluation of size-dependent imaging properties, storage stability and safety, *Int. J. Nanomedicine* 13 (2018) 1899-1915.
- [244] H. Pardoe, W. Chua-anusorn, T.G. St. Pierre, J. Dobson, Structural and magnetic properties of nanoscale iron oxide particles synthesized in the presence of dextran or polyvinyl alcohol, *J. Magn. Mater.* 225 (2001) 41-46.
- [245] J.W. Lee, D.K. Kim, Carboxymethyl group activation of dextran cross-linked superparamagnetic iron oxide nanoparticles, *J. Korean Ceram. Soc.* 58 (2021) 106-115.
- [246] J.A. Cohen, T.T. Beaudette, J.L. Cohen, K.E. Broaders, E.M. Bachelder, J.M.J. Fréchet, Acetal-Modified dextran microparticles with controlled degradation kinetics and surface functionality for gene delivery in phagocytic and non-phagocytic cells, *Adv. Mater.* 22 (2010) 3593-3597.
- [247] S. Martwiset, A.E. Koh, W. Chen, Nonfouling characteristics of dextran-containing surfaces, *Langmuir* 22 (2006) 8192-8196.
- [248] K. Lix, M.V. Tran, M. Massey, K. Rees, E.R. Sauvé, Z.M. Hudson, W.R. Algar, Dextran functionalization of semiconducting polymer dots and conjugation with tetrameric antibody complexes for bioanalysis and imaging, *ACS Appl. Bio Mater.* 3 (2020) 432-440.
- [249] M. Creixell, A.P. Herrera, M. Latorre-Estevés, V. Ayala, M. Torres-Lugo, C. Rinaldi, The effect of grafting method on the colloidal stability and in vitro cytotoxicity of carboxymethyl dextran coated magnetic nanoparticles, *J. Mater. Chem.* 20 (2010) 8539-8547.
- [250] Z. Shao, Y. Yang, H. Lee, J.W. Kim, C.O. Osuji, Synthesis and suspension rheology of titania nanoparticles grafted with zwitterionic polymer brushes, *J. Colloid Interface Sci.* 386 (2012) 135-140.
- [251] Y. Liu, Y. Liu, L. Qiao, Y. Liu, B. Liu, Advances in signal amplification strategies for electrochemical biosensing, *Curr. Opin. Electrochem.* 12 (2018) 5-12.
- [252] M. González, L.A. Bagatolli, I. Echabe, J.L.R. Arrondo, C.E. Argaraña, C.R. Cantor, G.D. Fidelio, Interaction of Biotin with Streptavidin: thermostability and conformational changes upon binding, *J. Biol. Chem.* 272 (1997) 11288-11294.
- [253] A.K. Yagati, J.-C. Pyun, J. Min, S. Cho, Label-free and direct detection of C-reactive protein using reduced graphene oxide-nanoparticle hybrid impedimetric sensor, *Bioelectrochemistry* 107 (2016) 37-44.
- [254] J. Wang, J. Guo, J. Zhang, W. Zhang, Y. Zhang, RNA aptamer-based electrochemical aptasensor for C-reactive protein detection using functionalized silica microspheres as immunoprobes, *Biosens. Bioelectron.* 95 (2017) 100-105.
- [255] S. Boonkaew, S. Chaiyo, S. Jampasa, S. Rengpipat, W. Siangproh, O. Chailapakul, An origami paper-based electrochemical immunoassay for the C-reactive protein using a screen-printed carbon electrode modified with graphene and gold nanoparticles, *Microchim. Acta* 186 (2019) 153.
- [256] C. Pinyorospatum, S. Chaiyo, P. Sae-ung, V.P. Hoven, P. Damsongsang, W. Siangproh, O. Chailapakul, Disposable paper-based electrochemical sensor using thiol-terminated poly(2-methacryloyloxyethyl phosphorylcholine) for the label-free detection of C-reactive protein, *Microchim. Acta* 186 (2019) 472.
- [257] M. Thangamuthu, C. Santschi, O. J. F. Martin, Label-Free Electrochemical Immunoassay for C-Reactive Protein, *Biosensors* 8 (2018) 34.
- [258] Y. Boonyasit, O. Chailapakul, W. Laiwattanapaisal, A folding affinity paper-based electrochemical impedance device for cardiovascular risk assessment, *Biosens. Bioelectron.* 130 (2019) 389-396.
- [259] S. Jampasa, W. Siangproh, R. Laocharoensuk, T. Vilaivan, O. Chailapakul, Electrochemical detection of c-reactive protein based on anthraquinone-labeled antibody using a screen-printed graphene electrode, *Talanta* 183 (2018) 311-319.
- [260] A. Ambrosi, F. Airò, A. Merkoçi, Enhanced gold nanoparticle based ELISA for a breast cancer biomarker, *Anal. Chem.* 82 (2010) 1151-1156.

REFERENCES

- [261] Z. Qu, H. Xu, P. Xu, K. Chen, R. Mu, J. Fu, H. Gu, Ultrasensitive ELISA using enzyme-loaded nanospherical brushes as labels, *Anal. Chem.* 86 (2014) 9367-9371.
- [262] S. Dong, D. Zhang, H. Cui, T. Huang, ZnO/porous carbon composite from a mixed-ligand MOF for ultrasensitive electrochemical immunosensing of C-reactive protein, *Sens. Actuators B* 284 (2019) 354-361.
- [263] P. Kanyong, C. Catli, J.J. Davis, Ultrasensitive Impedimetric Immunosensor for the Detection of C-Reactive Protein in Blood at Surface-Initiated-Reversible Addition-Fragmentation Chain Transfer Generated Poly(2-hydroxyethyl methacrylate) Brushes, *Anal. Chem.* 92 (2020) 4707-4710.
- [264] X. Zhang, R. Hu, K. Zhang, R. Bai, D. Li, Y. Yang, An ultrasensitive label-free immunoassay for C-reactive protein detection in human serum based on electron transfer, *Anal. Methods* 8 (2016) 6202-6207.
- [265] Y.-Y. Cheng, T. Zhan, X.-Z. Feng, G.-C. Han, A synergistic effect of gold nanoparticles and melamine with signal amplification for C-reactive protein sensing, *J. Electroanal. Chem.* 895 (2021) 115417.
- [266] X. Zhang, K.-N. Chi, D.-L. Li, Y. Deng, Y.-C. Ma, Q.-Q. Xu, R. Hu, Y.-H. Yang, 2D-porphyrinic covalent organic framework-based aptasensor with enhanced photoelectrochemical response for the detection of C-reactive protein, *Biosens. Bioelectron.* 129 (2019) 64-71.
- [267] J.S. Lee, H.-A. Joung, M.-G. Kim, C.B. Park, Graphene-based chemiluminescence resonance energy transfer for homogeneous immunoassay, *ACS Nano* 6 (2012) 2978-2983.
- [268] C. Bravin, V. Amendola, Wide range detection of C-Reactive protein with a homogeneous immunofluorimetric assay based on cooperative fluorescence quenching assisted by gold nanoparticles, *Biosens. Bioelectron.* 169 (2020) 112591.
- [269] M. Mahyari, S.E. Hooshmand, H. Sepahvand, S. Gholami, A.H. Rezayan, M.A. Zarei, Gold nanoparticles anchored onto covalent poly deep eutectic solvent functionalized graphene: An electrochemical aptasensor for the detection of C-reactive protein, *Mater. Chem. Phys.* 269 (2021) 124730.
- [270] A. Belushkin, F. Yesilkoy, J.J. González-López, J.C. Ruiz-Rodríguez, R. Ferrer, A. Fàbrega, H. Altug, Rapid and digital detection of inflammatory biomarkers enabled by a novel portable nanoplasmonic imager, *Small* 16 (2020) 1906108.
- [271] C. Zong, D. Zhang, F. Jiang, H. Yang, S. Liu, P. Li, Metal-enhanced chemiluminescence detection of C-reaction protein based on silver nanoparticle hybrid probes, *Talanta* 199 (2019) 164-169.
- [272] L.-J. Zhao, R.-J. Yu, W. Ma, H.-X. Han, H. Tian, R.-C. Qian, Y.-T. Long, Sensitive detection of protein biomarkers using silver nanoparticles enhanced immunofluorescence assay, *Theranostics* 7 (2017) 876-883.
- [273] S.F. Yang, B.Z. Gao, H.Y. Tsai, C.B. Fuh, Detection of c-reactive protein based on a magnetic immunoassay by using functional magnetic and fluorescent nanoparticles in microplates, *Analyst* 139 (2014) 5576-5581.
- [274] P. Zhang, Y. Bao, M.S. Draz, H. Lu, C. Liu, H. Han, Rapid and quantitative detection of C-reactive protein based on quantum dots and immunofiltration assay, *Int. J. Nanomedicine* 10 (2015) 6161-6173.
- [275] B. Wu, N. Chen, Q. Wang, X. Yang, K. Wang, W. Li, Q. Li, W. Liu, H. Fang, A simple label-free aptamer-based method for C-reactive protein detection, *Anal. Methods* 8 (2016) 4177-4180.
- [276] T. Ji, D. Liu, F. Liu, J. Li, Q. Ruan, Y. Song, T. Tian, Z. Zhu, L. Zhou, H. Lin, C. Yang, D. Wang, A pressure-based bioassay for the rapid, portable and quantitative detection of C-reactive protein, *Chem. Commun.* 52 (2016) 8452-8454.